Università degli Studi di Padova
Dipartimento di Ingegneria Industriale

Corso di Laurea Magistrale in Ingegneria dell'Energia Elettrica

Tesi di laurea magistrale

FE analysis in time domain of Simultaneous Double Frequency induction hardening

Candidato:
Antonio Marconi
Matricola 1068091

Relatore:
Prof. Ing Michele Forzan
Correlatore:
Ing. Mattia Spezzapria

Humana ante oculos foede cum vita iaceret in terris oppressa gravi sub religione, quae caput a caeli regionibus ostendebat horribili super aspectu mortalibus instans, primum Graius homo mortalis tollere contra est oculos ausus primisque obsistere contra; quem neque fama dum nec fulmina nec minitanti murmure compressit caelum, sed eo magis acrem inritat animi virtutem, effringere ut arta naturae primus portarm claustra cupiret.

Ergo vivida vis animi pervicit et extra processit longe flammantia moeni mundi atque omne immensum peragravit mente animoque, unde refert nobis victor quid possit oriri, quid nequeat, finita potestas denique cuique qua nam sit ragione atque alte terminus haerens. Quare religio pedibus subiecta vicissim opteritur, nos axaequat victoria caelo. - *Lucrezio, De rerum natura, Libro I*

A un certo punto non fu più la biologia a dominare il destino dell'uomo, ma il prodotto del suo cervello: la cultura. L'Universo ha elargito un grande dono all'uomo: con i suoi migliori atomi ha creato una parte di sé stesso dentro la sua mente per studiare il resto di sé. Cosicché: Le uniche leggi della materia sono quelle che la nostra mente deve architettare e le uniche leggi della mente sono architettate per essa dalla materia — James Clerk Maxwell

Dedicato alla mia famiglia, che ha reso possibile questo percorso e mi ha sorretto. Dedicato a Giulia che è stata, e sempre sarà, fonte di ispirazione. Dedicato al mio professore Michele Forzan che mi ha trasmesso l'amore per l'ingegneria e la devozione per la matematica

Contents

List of Figures

List of Tables

Sommario

La richiesta sempre maggiore di processi industriali economicamente vantaggiosi e "Environmentally friendly" rende sempre più interessante la tecnologia della tempra ad induzione. Assenza di processi di combustione, quindi di emissioni inquinanti e tempistiche di processi estremamente brevi (si parla in alcune applicazioni anche di frazioni di secondo) rappresentano gli aspetti più vantaggiosi della tempra ad induzione. A questi vanno aggiunti la capacità di progettare e controllare i processi in modo sempre più preciso.

Questo lavoro con particolare attenzione analizza lo stato dell'arte della tecnologia in un particoalre processo, quello della tempra superficiale di ruote dentate. Proprio in questa tipologia di processi industriali sempre maggior interesse suscita la tempra superficiale in doppia frequenza simultanea, che vuole, almeno teoricamente superare i limiti dei profili di tempra ottenuti sperimentalmente nell'uso di un'unica frequenza. Purtroppo oggigiorno si evidenzia ancora una discrepanza tra i profili di tempra desiderati e quelli ottenuti mediante il processo SDF (Simultaneous Double Frequency). Un aspetto chiave è rappresentato dalla difficoltà di smiulazione del processo e dalla necessità di modellizzare il problema mantenendone e non trascurando gli aspetti critici.

Riassunto

La tempra dell'acciaio consiste in una modificazione delle microstrutture dell'acciaio. In particolar modo la martensite rappresenta la struttura più dura conosciuta dell'acciaio. Settori come quello automobilistico e aereospaziale richiedono oggigiorno componenti sempre più performanti e complessi. La metallurgia dunque deve riuscire a fornire componenti ad elevato contenuto tecnologico, basti pensare agli ingranaggi delle trasmissioni, caratterizzate da geometrie molto complesse e caratteristiche superficiali molto buone. Una ruota dentata infatti dovrà resistere a sforzi meccanici nel tempo anche molto intensi. Il settore della tempra superficiale negli ultimi anni ha visto crescere l'impiego dell'induzione. Questa tecnologia infatti rispetto alla più antiche tecnologie di tempra superficiale, permette di raggiungere elevati valori di efficienza energetica di processo, richiede tempi molto ridotti, e

grande capacità di controllo, quindi risulta il non-plus ultra in un processo altamente industrializzato come per esempio quello di produzione di componenti di ingranaggi. La tempra ad induzione superficiale consente, attraverso l'alimentazione di un induttore, tipicamente costituito di rame e raffreddato ad acqua, di generare un campo magnetico alternativo, la cui frequenza è quella delle grandezze elettriche dell'alimentazione. Questo campo magnetico pulsante genera a sua volta una denistà di corrente nel pezzo da trattare. Poiché questi processi sono caratterizzati da frequenza tipicamente comprese tra 10 e 400 [kHz], in accordo con gli spessori di penetrazione, si riesce a concentrare enormi quantità di potenza, in accordo con gli spessori di penetrazione anche in sole frazioni di millimetri. Questo processo dunque permette di austenizzare piccole porzioni del corpo che si vuole trattare. Successivamente un raffreddamento brusco permette di trasformare l'austenite presente in martensite. In questo modo il pezzo viene trattato. Per capire quanto questa tecnologia sia competitiva nei settori metallurgici, basti pensare che si riesce a temprare efficacemente uno spessore di 1 [m] di una billetta di 10 [mm] di raggio e 40 [mm] di altezza in circa 0.2-0.3 secondi. Questa tecnologia negli ultimi 20 anni si è evoluta con l'introduzione di processi nuovi. Una di queste è la così definita tempra ad induzione in doppia frequenza simultanea. Questa tecnologia infatti permette da un punto di vista teorico di riuscire ad indurre differenti densità di potenza tra dente e cava. Infatti l'esperienza del settore della tempra in singola frequenza di ruote dentate ha evidenziato che per ruote dentate con modulo molto elevato, risulta molto difficile temprare in modo ottimale il dente impiegando un'unica frequenza. Infatti se si impiega la sola media frequenza (nell'ordine dei 10 [kHz]) si ottiene una tempra della sola cava del dente. Impiegando invece la sola alta frequenza (nell'ordine dei 100 [kHz]) si ottiene una tempra delle punte dei denti e non si temprano le basi. Quindi una combinazione di due frequenza (una in alta ed una in bassa) permette una tempra più uniforme del dente. Questo permetterebbe maggior prestazioni meccaniche della ruota dentata. Uno dei problemi principali di questa tecnologia è che non esiste ancora un approccio universalmente accettato, e la realizzazione del processo passa sempre per lunghi processi sperimentali, in cui si realizza un prototipo di tempra SDF e si cerca di verificare ed aggiustare tramite lunghi e spesso costosi processi sperimentali. In questo lavoro è stato modellizzato ed analizzato un processo di tempra ad induzione in doppia frequenza simultanea. A differenza di molti lavori che si trovano in letteratura, si è deciso di risolvere il processo tramite una risoluzione agli elementi finiti (FEM) risolvendo sia le equazioni di Maxwell che quelle di Fourier nel più generale dominio del tempo. Questa scelta è stata fatta poiché vista la forte non linearità del modello:

- intensità tipica dei campi elettromagnetici (10^5 [A/m])

- acciai magnetici impiegati nel processo di tempra martensitica fortemente non lineari.

Risulta impossibile ricorrere alla sovrapposizione degli effetti e sommare due distribuzioni di fmm a frequenze diverse, e ricavate tramite una risoluzione nel dominio della frequenza. Per questo motivo si è scelto di caratterizzare in modo molto preciso la curva di saturazione elettromagnetica e di risolvere il modello nel dominio del tempo. Il modello considera allora un'alimentazione in tensione imposta, dove $v(t)$

è la somma di due cosinusoidi in due frequenza distinte (f_{mf}=10 [kHz] e f_{hf}=100 [kHz]). L'accoppiamento tra le equazioni termiche e quelle elettromagnetiche è stato effettuato tramite la distribuzione delle potenze indotte nel pezzo, che provocano il riscaldamento e la temperatura della billetta. Ovvero è stato ipotizzato, che se è possibile trascurare la variazione della temperatura per un certo numero di periodi elettromagetici, è possibile considerare che in un passo temporale di risoluzione del problema termico la potenza riscaldante indotta sia costante. Quindi è possibile procedere con il seguente schema iterativo: si considera una certa ditribuzione di temperatura iniziale, si risolve un periodo elettromagnetico Tem, si ipotizza che la temperatura non vari per un certo numero intero di periodi n, e dunque si risolve il problema termico nel periodo $T_{th} = n * T_{em}$. Dalla risoluzione di un periodo elettromagnetico è possibile ricavare, per ogni elemento della mesh (o, meglio, per ogni punto di Lagrange della mesh della billetta) e per ogni istante temporale la potenza riscaldante indotta. Dunque è possibile, ricavare la potenza media riscaldante indotta (calcolata in un periodo elettromagnetico $< w(r, z) > [W/m^3]$), in ogni punto di Lagrange (o in ogni elemento della mesh), per ogni periodo elettromagnetico. Nel lavoro sono stati riportati i diversi andamenti delle grandezze elettromagnetiche e termiche più importanti all'interno dei vari periodi termici ed elettromagnetici.

Avendo risolto le equazioni elettromagnetiche nel dominio del tempo è stato possibile anche visualizzare l'andamento istantaneo della corrente, della tensione, della potenza e dei campi magnetici. Dagli andamenti delle grandezze si vede come la potenza sia composta da 5 termini principali: uno continuo, che coincide con il valore medio della potenza istantenea, e che dunque rappresenta la potenza assorbita nel periodo elettromagnetico dal pezzo. Nei risultati si vede chiaramente come varia la potenza assorbita dal carico equivalente durante il processo termico. Da questi si vede come seguono fedelmente, almeno qualitativamente, il comportamento descritto analiticamente come funzione della temperatura. E' stato possibile formularne l'andamento considerando l'effetto della temperatura sulla resistività, sulla permeabilità magnetica e sul valore della sezione della billetta magneticamente concatenata al pezzo. Questo approccio in sintesi permette di visualizzare ed analizzare l'andamento istantaneo delle principali grandezze elettriche del modello. Inoltre è stato possibile analizzare il contenuto armonico delle grandezze, cercando di attribuire un preciso significato elettrotecnico alle grandezze ricavate, come resistenze, valore RMS della corrente e della potenza. Per esempio si osserva un comportamento fortemente ondulatorio della potenza nel periodo elettromagnetico e la variazione delle sue componenti al variare della temperauta, ovvero al variare del tempo di processo.

Risolvendo nel dominio del tempo inoltre è possibile valutare molto accuratamente l'effetto della saturazione magnetica, in quanto il metodo FEM permette di ricavare per ogni istante un preciso valore della permeabilità magnetica che tiene conto del complessivo campo magnetico generato contemporaneamente dalle due correnti sinusoidali a diversa frequenza.

Tutti i risultati sono presentati nell'ultimo capitolo di questo lavoro.

Chapter 1

Introduction

In induction heating a conductive copper coil is fed by an alternative current which frequency depends on the established thickness of the hardening process. The variation of the magnetic field, generates eddy currents inside the steel pieces that has to be hardened. Electromagnetic Maxwell's equations describe induction hardening problems from the point of view of E.M. field. The PDEs system consists of four independent equations which link the depencence with time, with the spatial distribution of the physicsal quantities. Usually an induction model in which the sources are described with an unique frequency, the electromagnetic problem is studied in steady state form. This numerical simplification, that may save computational time, it's possible with the so called Steinmetz Transformation, resorting to complex numbers. It's clear that this approach loses accuracy if the problem admits for example multifrequency sources. These specific cases are, for example, industrial applications like SDF (Simultaneous Double Frequency) hardening for transmission. This technology should reach new more suitable results, in comparison with the "older" single frequency hardening tenchology that exhibits the inconvenience of a not perfect temperature profile. With this chapter I try to summarize the main theoretical aspects of induction hardening processes, and specifically, the solution of EM problems, of thermal equations and some basic aspects of metallurgy.

1.1 Metallurgy behind hardening treatments

Steels are alloy of Iron [Fe] and Carbon [C] with a certain content of carbon that is typically less than the two percent of the weight. Varying the amount of carbon it is possible to define a new classes of steels. In addition it is possible to find inside the structure of the steel other alloying elements such as Manganese, Chromium, Nickel, Tungsten, Vanadium, and so on. In many metallurgical production cycles alloying elements have been intentionally added to modify specific characteristics of the steel.

This first chapter should propose a quick look to the main phenomenas and the behaviours of steel with temperature. In metallurgy metals define certain materials that have some physical properties strictly correlated with the aggregation of atoms. In metals the aggregation of the matter is between single atoms and not between molecules. For that reason the chemical bonds between atoms are not stricted for each state of matter. The solid state of a metal is characterized by crystalline structures,

in which it is possible to find particular and repeatable geometries that represent the elementary cells. The work to break the crystal lattice, that consists of the energy to distance atoms at infinity, is essentially the internal energy of the lattice. Typically because the distances between atoms does not change significantly the crystal lattice may assume different geometries and symmetries. This phenomenon can be observed many times in the microstructure of the metals and in litterature is called Polymorphism and the various structures are defined Allotropics. The main character of this work is the iron [Fe] and it owns two most important structures: the body-centered cubic (bcc) that is stable for temperatures lower than 911℃(**Fe**α and **Fe**β) or greater than 1892℃and behind its fusion temperature (**Fe**δ) and the face-centered cubic (fcc) that is stable in the range of temperature of 911℃- 1293℃(**Fe**γ). Those two structures play a chief role in many thermal treatments.
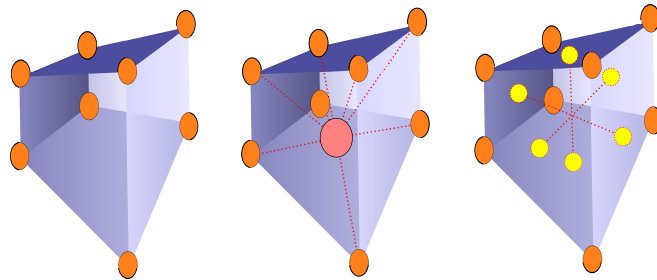
Figure 1.1: Typical crystal lattices for an Fe-C structure

Exist different thermal treatments that take advantage of allotropic transformations of metals such as the martensitic hardening. In this particular process it is possible to cause new phases where dislocations are deeply impeded. That makes possible to increase the hardness of the material that later will be better defined. To full understand the concept of hardening processes could be useful to introduce some different properties of metals

1.1.1   The Fe-C diagram

Complex phenomenas that occur throughout thermal treatments of steels are correlated with the different solubility of carbon and alloy elements in the two crystal lattices of the two allotropic forms of iron. The bases for the understanding of thermal processes are transformations that occur in steel in equilibrium, or rather where the unknown time can be neglected. That is the Fe-C phase diagram, that is represented in Figure 1.2. Later instead will be important underline what happens when the time could not be neglected.

Considering to have a pure iron material it is possible to find characteristics points, for the simultaneous existance of two phases.

- $T = 1536$ [℃] where the liquid solidifies to the form bcc: **Fe** δ;

- $T = 1392$ [℃] where the solid iron transforms from a stable form bcc to the fcc: **Fe** γ;

- $T = 768$ [℃] where the iron from its γ form transforms to the bcc one: **Fe** α;

These transformations involve internal energy changes of the closed system. Generally they may be exhotermic or endothermic. Considering a general transformation $bcc \Rightarrow fcc$ is important to note that happens a significant variation of the density of the material, in accord with a more compact structure of the lattice.

The temperature that fixes a transformation of the iron (practically a change of its characteristics) due to the heating is commonly sfecified with the letter **A**. The main temperatures A_i have been presented here:

- $A_1 = 723$ [°C]. It has sense only for a Fe-C alloy steel. This identifies the eutectoid transformation $\alpha \Rightarrow \gamma$.

- $A_3 = 911$ [°C]. This temperature identifies the allotropic transformation $\alpha \Rightarrow \gamma$. Is imporatnt to note that this temperature changes with the content of carbon from the minimum value of 723 [°C] ($\approx$ 0,8%) to the maximum value of 911 [°C] (pure iron).
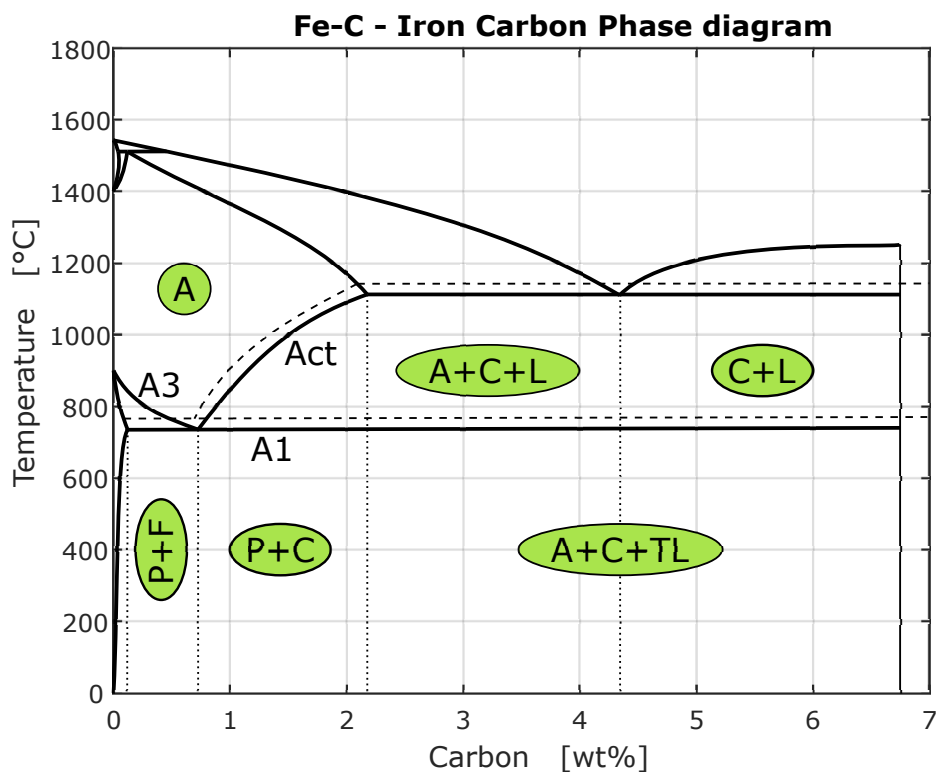
Figure 1.2: Typical crystal lattices for an Fe- structure

Fe-C alloys are characterized by the fact that carbon may exist in different forms: solid solution, graphite and cementite. Because the development of graphite occurs in conditions of extremely slow cooling, is easy to understand that graphite represents the stable form of carbon in the Fe-C diagram (continuos line), whereas cementite the meta-stable form (dashed lines). The Fe-C diagram shows which phases are to be expected at equilibrium for different concentration of carbon and temperature. Of great interest are four regions in Figure 1.2 with mixtures of two solid phases:

- ferrite + cementite, typically called pearlite.

- cementite + austenite

- ferrite + austenite.

In heat treatments of steels such as hardening or tempering usually the liquid phase is neglected. As already said before Figure 1.2 shows also important boundaries at single-phase fields:

- A_1. The eutectoid temperature, which is the minimum temperature for the existance of austenite. it is possible to observe in figure that essentially is constant with the content of carbon.

- A_3. The boundary of austenite region for low carbon steels. It varies with the concentration of carbon in the range of [0-0.8%].

- A_{cm}. The boundary for high carbon contents. As it is possible to define a eutectoid temperature exists the eutectoid carbon content at which the austenite is achievable with the minimum temperature.

   The Fe-C diagram is of experimental origin. The knowledge of the thermodynamic principles and modern thermodynamic data now permits very accurate calculations of this diagram. This is particularly useful when phase boundaries must be extrapolated and at low temperatures where the experimental equilibria are extremely slow to develop. If alloying elements are added to the iron-carbon alloy (steel), the position of the A1, A3, and Acm boundaries and the eutectoid composition are changed. Classical diagrams introduced by Bain show the variation of A1 and the eutectoid carbon content with increasing amount of a selected number of alloying elements. It suffices here to mention that all important alloying elements decrease the eutectoid carbon content, the austenite-stabilizing elements manganese and nickel decrease A1, and the ferrite-stabilizing elements chromium, silicon, molybdenum, and tungsten increase A1. These classifications relate directly to the synergisms in quench hardening as described in the articles "Quantitative Prediction of Transformation Hardening in Steels" and "Quenching of Steel" in the Volume Modern thermodynamic calculations allow accurate determinations of these shifts that affect the driving force for phase transformation (see below). These methods also permit calculation of complete ternary and higher-order phase diagrams including alloy carbides. Reference should be made to the Calphad computer system.

Transformation Diagrams

   Kinetic aspects of phase transformations are as important as equilibrium diagrams for heat treatment of steels. One can conveniently describes what happens during transformation with transformation diagrams. Two different kind of diagrams that help to describe transformation processes are:

- *IT. Isothermal transformation diagrams.* It shows what happens when a steel, with a specific content of carbon is maintained to a constant temperature for a certain time period.
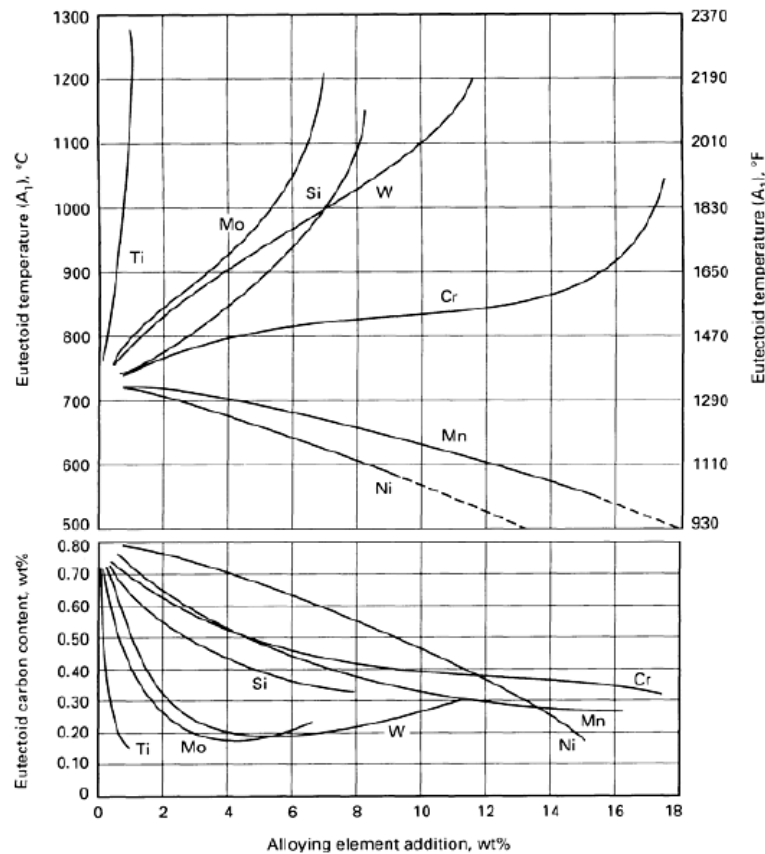
Figure 1.3: Influence of alloying element additions on eutectoid temperature and eutectoid content carbon

- *CT. Continuous transformation.* Of course performing processes with constant temperatures is unreasonable, but on the other hand is reasonable considering a transformation process as a continuous change of temperature during either cooling or heating.

Continuous transformation diagrams are obtained sperimentally and help who wants to design a specific steel treatment and reach for example a specific configuration of phases of steel. Both of them are splitted and defined for heating and cooling.

ITh - Isothermal transformation during heating

It describes the process of the formation of austenite from a pre existent micro structure of ferrite and pearlite or tempered martensite. Abscissa usually defines two different points: the start and finish time as 1% and 99% formation of austenite. In figure (ITh) A_{c1} and A_{c3} temperature are plotted. Below A_{c1} no austenite can exist. Between A_{c1} and A_{c3} there is a mixture of ferrite and austenite. It is important that the heating rate to the hold temperature be very high (in the order of thousand celsius degrees) if a true isothermal diagram is to be obtained. During the formation of austenite from an original microstructure of ferrite and pearlite or tempered

martensite, the volume decreases with the formation of the dense austenite phase. From the elongation curves, the start and finish times for austenite formation, usually defined as 1% and 99% transformation, respectively, can be derived. These times are then conveniently plotted on a tempearture-log time diagram. Notice that a considerable overheating is required to complete the transformation in a short time. The original microstructure also plays a great role. A finely distributed structure like tempered martensite is more rapdly transformed to austenite than, for insteance, a ferritic-pearlitic structure. This is particularly true for alloyed steels with carbide-forming alloying elements such as chromium and molybdenum. It is importatn that the htating rate to the hold temperature be very high if a true isothermal diagram is to be obtained.

ITc - Isothermal transformation during cooling

The procedure obviously start at a high temperature, where steel exists in a austenite homogeneuous form without undissolved carbides and follows by rapid cooling to the desired fixes temperature. Of great interest is the formation of the so called martensite, the most hard structure of steel phases. For process such as hardening that structure is the target and how it is possible to obtain it is heart of the process. Figure 1.4 shows for example different suitable areas that represent different micro-structures such as pearlite, bainite, ferrite and martensite. Above A_3 no transformation can occur. Between A_1 and A_3 only ferrite can be formed. It's important to sublined the so called "C-shaped" behaviour of the curves. This is typical for transformation curves. In figure maybe the most interesting curve is the M_s line that is the temperature at which starts the transformation of austenite to martensite.

CCT - Continuous cooling transformation diagram

Use of a constant cooling rate is very common in experimental practice, however this regime rarely occurs in practice. In Figure 1.6 is shown a CCT diagram for an AISI-4310 steel. Ferrite, pearlite and bainite regions are indicated as well as the M_s temperature, that is not constant when martensite formation is preceded by bainite formation, but typically decreases with time.

An other phenomenon that occurs during harding is that the temperatures A_{c1} and A_{c3} are functions of the heating rate. That means a good model should takes into account that temperatures A_{c1} and A_{c3} are not constant.

1.1.2 Principles and hardening techniques

Ancients blacksmiths discovered, probably accidentally that soft iron, that is extreamely malleable at ambient temperature, after heating and fast cooling changes its properties and become more hard and resistant. This process was called hardening. The practice over the centuries and the increase of the physicsal laws that explain the process allowed to get more and more accurate and controlled hardening processes. Nowadays although the "know-how" of industries specialized in this heat treatment reached very high levels. The requests for specific mechanical standards, driven by aerospatial and automotive industries, have increased interests on the theory and

ITc - Isothermal Transformation diagram (cooling)
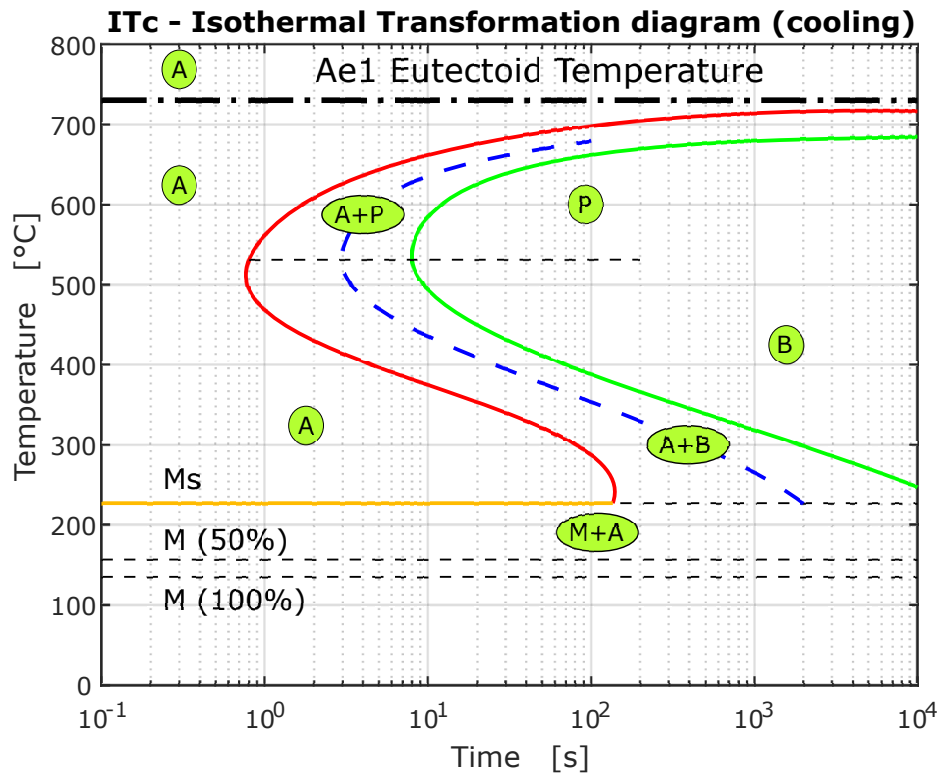
Figure 1.4: Isothermal cooling transformation (ITc) diagram for an iron-carbon alloy of eutectoid composition. In figure are included austenite-to-pearlite (A-P) and austenite-to-bainite (A-B) transformations
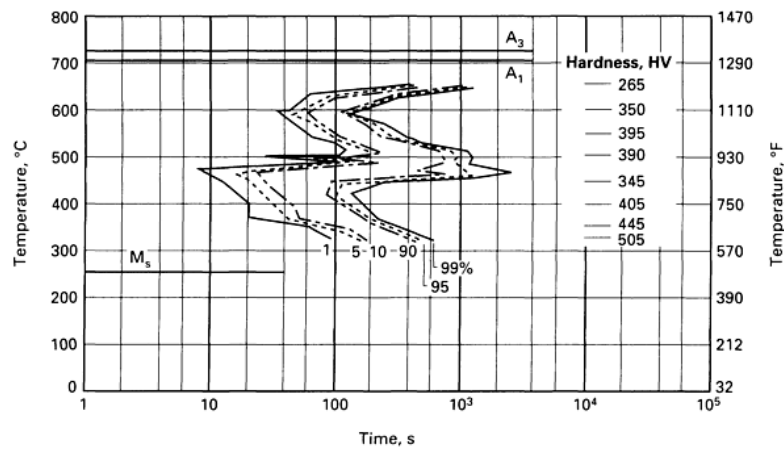
Figure 1.5: Isothermal transformation diagram for a steel with 0.39% C, 0.86% Mn, 0.72% Cr, and 0.97% Ni. The upper C-shaped curves describe transformation to pearlite; the lower C-shaped curves to bainite. Ferrite is not visible. The column on the right side of the figure indicates the hardness after completed transformation measured at room temperature.

physics behind that process. The so called surface hardening, that admit to obtain
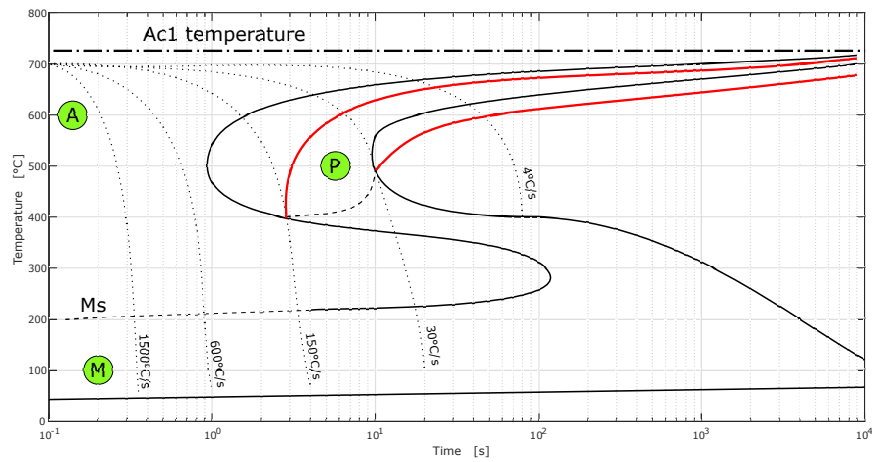
Figure 1.6: Typical Continous Cooling Transformation diagram for steel alloy
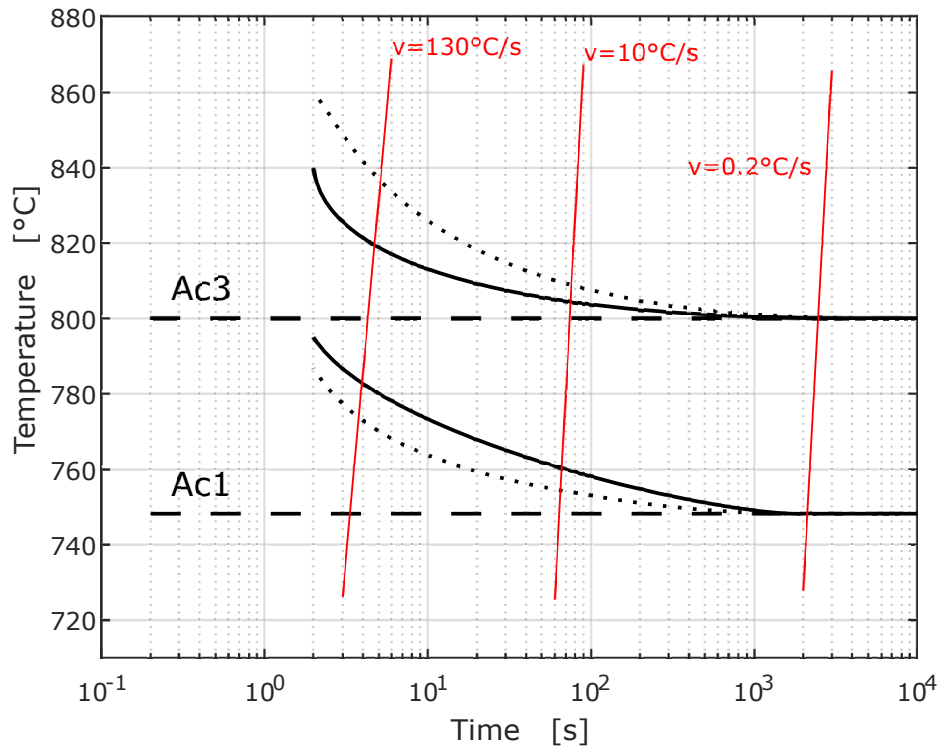
Figure 1.7: Behaviour of the temperatures A_{c1} and A_{c3} with the heating rate.

lighter and harder workpiece such as components for transmissions and toothed wheels, that are typically subjected to very heavy mechanical stresses. In this sector the use of electric energy instead of the oldest flame heating has grown in these last decades. This is motivated by several factors covering different aspects of the process: affordability, enhanced automation propensity, more respect for the environment. In

addition of these aspects there is the ability to generate thermal sources directly into the workpiece in thicknesses according to the penetration depth of the electromagnetic wave. This chapter is about the main phenomena that govern the hardening heat treatment and particularly the martensitic hardening.

Martensitic Hardening

To obtain the desired value of hardness for a steel workpiece first of all it is necessary to heat a secific zone over the austenization temperature and at the end quickly cool the workpiece, to avoid the transformation of austenite in undesidered structures such ad pearlite and bainite. The minimum quenching velocity that allows the full transformation of austenite in martensite is called critic velocity of hardening and is represented by the CCT diagram. The transformation has already said starts with the temperature M_s and finishes with the temperature M_f. Is important to note that the first is not constant for each steel, but is function of the content of its alloy elements. Is important to subline that the variation of the cooling rate with the distance from the surface, that of course starts to cool first, is particularly important and causes for example distortion inside the piece that many times are not tolerated. A process such as surface hardening, for example takes advantage of that property to obtain hardening thicknesses extremely thin. Therefore the main players to obtain the desired hardeing profile are:

- The hardenability of the steel, that is strictly function of the alloy elements that composes it.

- The mass of the workpiece.

- Hardening depth.

If a given steel does not admit to obtain a martensitic structure to a certain, requested, depth, it is necessary to choose a different steel with a higher hardenability or if it is possible to increase the cooling rate.

Quenching

The depth of hardness at a given work-piece dimension is determined by the chemical composition of the steel, the austenite grain size as established during the austenitizing treatment, and the cooling rate. The steel is normally chosen on the basis of hardenability. The choice of cooling medium, on the other hand, is less exact and crude rules are normally applied (unalloyed steel is quenched in water, alloy steels in oil, and high-alloy steels in air). Molten salt is often used for bainitic hardening of medium-carbon steels and martempering of carburized parts (salt temperature above Ms for the case). Judicious selection of cooling medium is critical for obtaining optimum mechanical properties, avoiding quench cracks, minimizing distortion (to be discussed below), and improving reproducibility in hardening. Of most interest are the liquid quenching media, and they also show the most complicated cooling process. More detailed information on cooling (quench) media can be found in the article "Quenching of Steel" in this Volume. In the chapter in which the model is developed it is shown particularly how complex is the problem of the quenching. In

literature there are a great number of different methods for evaluating quenching media. Frequently, a cylinder made of nickel-base alloy or stainless steeld is used. A thermocouple is located in the center of the testing body and is connected to a recording intrument. Figure 1.8 shows the temperature at different depths below the surface of an Inconel probe quenched in oil. This figure illustrates that the different quench stages are more pronounced closer to the specimen surface and that the resulting temperature curves differ more from either linear or natural cooling curves. The conventional CCT curves must then be used with caution.
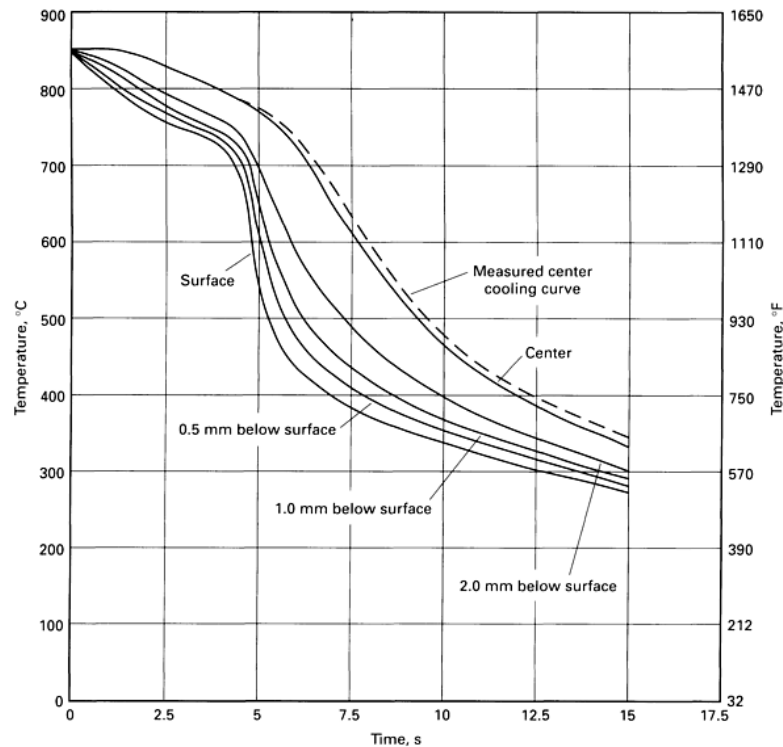
Figure 1.8: Calculated cooling curves obtained using an Alloy 600.

1.2   Induction Heating

Surface hardening is a process which includes a wide variety of tecnhique, it is used to improve the wear resistance of aprts without affecting the more soft, tough interior of the part. This combination of hard surface and resistance to breakage upon impact is useful in aprts such as a cam or ring gear that must have a very hard surface to resit wear, along with a tough interior to resist the impact that occur during normal life operation. Further, the surface hardening of steel has an advantage over through hardening because less expensive low-carbon and medium-carbon steels can be surface hardened without the problems of sistortion and cracking associated with the through hardening of thick sections. Nowadays induction heating is one of most used process to heat a conductive workpiece in industries. The main success factors have led to climb of that technology are reported here:

- Heat enanched directly inside the piece.

- The possibility to localize heat surces arbitrarily in accord with the abilities of the designer.

- Repeatability of the process: this is extreamely important for the development of that technolgy in industries, recquiring products with same characteristics throughout the inductor lifetime.

- The increase of the production capapility in accord with the reduction of the process times.

- High value of efficiency because of the extraordinary reduction of process losses.

- The automation of production cycles are made possible by the use of numerical control systems.

- The use of the electrical energy , which allows to decrease the pollutantss and break free from the price of a barrel of oil.

It is important subline that the diffusion of induction heating processes has been made possible by technological development of power electronics and particularly of the solid state converters. This work takes into account of one of the most relevant application: induction hardening, and particularly surface induction hardening, characterized by the use of high frequency converters.

The most important principles behind induction heating are:

- induction laws that explain how it is possible to transfer lectro-magnetic energy contactless (Maxwell's equations) and how Foucault's current develops inside the workpiece

- the Joule's effect taht explains the development of heat surces

- the distribution of the the induced currents appear to be non-uniform for different effects: skin effect, proximity effect, magnetic saturation and Curie's transition.

- the phenomena of conduction and thermal convection.

So from the point of view of the designer all these aspects must be taken into account to obtain a suitable preliminary plan.

The magnetic field excitation is obtained by supplying an induction coil with a current variable in time generally made of copper and cooled oppurtunely. This coil is coupled to a load , constituted by the workpiece. The choice of the frequency and the inductor design is linked with the requirments of the thermal process and with the geometry of the workpiece. it is possible to sketch an induction heating system with four main elements: a solid state converter, a capacitor battery used for power factor correction, the inductor and the coupled workpiece. Some processes such as in particular that of quenching added to this scheme a cooling system, that is not constricted with the electro-magnetic phenomena, but is equally important for the treatment.
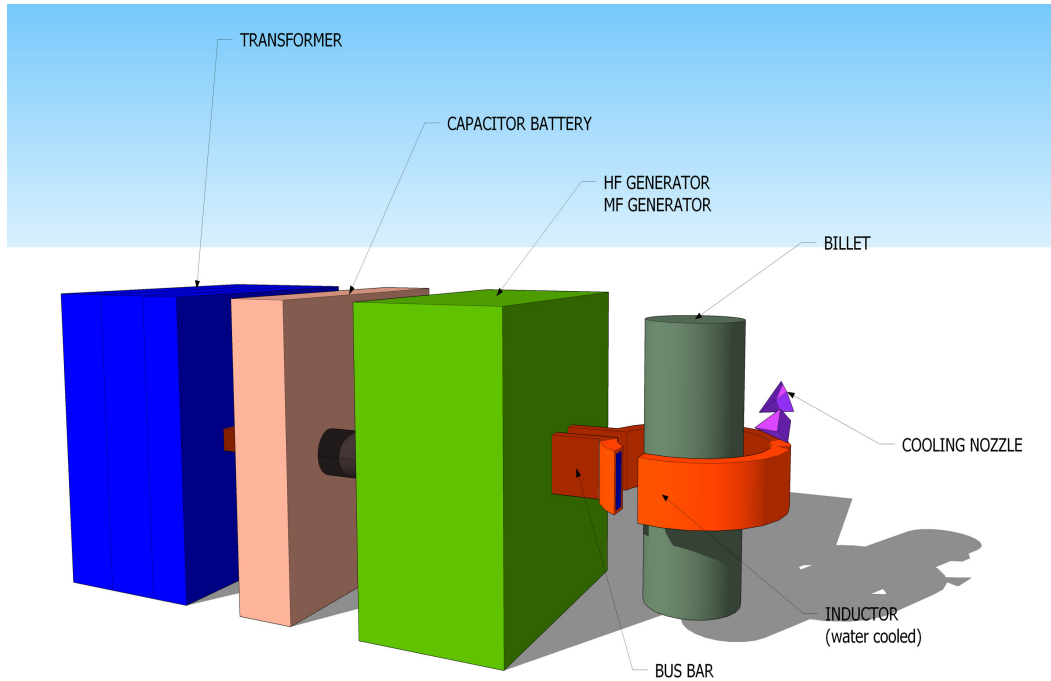
Figure 1.9: Structure of an induction heating BDF configuration

1.2.1   High Frequency surface hardening

The surface hardening represents probably the most interesting application for heat induction. The target is to hard a specified layer, which thickness depends from the application of the workpiece. It is important, as just viewed in the paragraph, that the value of the hardened layer changes the mechanical behaviour of the piece treated. Surface hardening for automotive and aerospace industries typically wants to obtain an extremely thin and hard layer and a more soft kernel. That is obtained with the use of an high frequency source that allows to heat up a surface layer above the critical temperature A_{c3} which corresponds to the transformation temperature of austenite and then cool quickly to bring the layer to a temperature lower than that of formation of martensite M_s. The main problem of this treatment is that does not exist a general law to enstablish the distribution of the heat surces, related with the distribution of the currents induced inside the piece. The same problem presents itself for the times of heating and the value of the power and frequency. The shape of the piece plays a key role in this regard. About this the hardening of gears and toothed wheels shows sperimentally that the hardened profile is not the desired.

1.2.2   Temperature Distribution

In literature exist many analytical works that shows the distribution of temperatures inside the piece during the thermal transient, supposing a time invariant power distribution. Fixed the hardening depth and the type of steel used, it is possible to obtain the process times as function of frequency and specific power. Limits of this
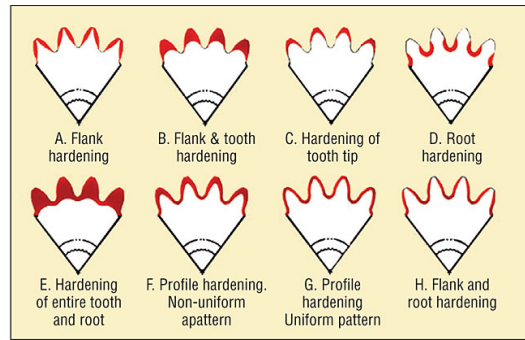
Figure 1.10: Example of different heating of the same gear wheels geometry.

approach that it does not take into account phenomena like magnetic saturation, Curie's transition, steel phase transformations and from a purely thermal point of view for example the fact that before the quenching phases thermal gradients between the kernel of the piece and the surface are so big to cause heat flows toward the center of the piece.

1.2.3 Hardening of complex geometries

Typically if the goal is to hard simple piece, such as billet or disks it is possible to obtain quite precisley the required hardened depth with a certain optimal frequency. Instead it is extreamely difficult and in some cases impossible to hard evenly complex geometries such as toothed wheels. The use of a single frequency or allows to temper only the tip of the tooth (High Frequency - 100 kHz) or only the base of the tooth (Medium Frequency - 10 kHz). To full understand the complexity of this problem we are going to subdivide the problem in two suproblems: one thermal and one electromagnetic.

1.2.4 Thermal and electric approach

Just for the geometry of the workpiece you can not get profiles of uniform quenching with power constant along the perimeter of the wheel. In these conditions in fact, the tip of the tooth and its base would be in very different conditions of heating . This is understood in the Figure 1.10 where changing the frequency we see that the surface of the tooth receveis greater power than the surface of the root. With an uniform distribution of power along the surface therefore the tip ios overheated. This occurs with high frequencies. The opposite phenomenon occurs instead in the case of the use of medium frequency , which causes the penetration of the induced currents towards the heart of the tooth and causes overheating of the base of the tooth. Therefore to heath evenly the surface it is necessary that the power transformed into heat in the tip is smaller than that in the quarry. For this reason the concept of SDF, simultaneous double frequency, might help to obtain a disomogeneous distribution of the eddy currents, and then a more uniform hardening profile along the surface of the wheel, in other words could be possible to hard in the same way the tip, the flank and the base of the tooth. From an electrical point of view, taking account that an acceptable efficiency must be reached, the choice of

the frequency is one of the most important points of the process. In the literature there are several works that compare various configurations of induction hardening of gear wheels , in particular only medium frequency , high frequency and only the combination of the two simultaneously. All these sublines that the SDF seems to be the best configuration. The influence of the choice of the frequency used in the process on the final temperature distribution is presented in figure 1.10. All these considerations are summarized in an excellent range of frequency explained by Sluhockii's formulating:

$$f_{opt} = \frac{300000 - 460000}{M^2}$$

where M is teh modulus of the wheel and it is simply defined as $M = \frac{p}{\pi}$ with p the circular pitch, that can be viewed as a concept of periodicity. Figure (LUPI PAG 318) points up the difficulty of hardening with one frequency wheel with modulus smaller than 4, because of it requires specific high frequency power over $2 - 3[kW/cm3]$ and heating times on the order of several tenths of a second. For this reasons SDF has become competitive. The complexity of processing analytical models that take into account simultaneously of all phenomena (thermal,magnetic and mechanical) and the rapid development of hardware has led to the development of specific software for numerical simulation. This work tries to model a process of induction hardening taking account of its main phenomena.

1.3   Fields theory

A realistic description of Induction Hardening must be expressed with electromagnetic fields. As already written Maxwell's Equations are the starting point of making an attempt to compute the problem. They are a set of partial differential equations that, together with the Lorentz Force and material laws, form the foundation of classical electrodynamics and electric circuits. Maxwell's equations describe how electric and magnetic fields are generated and altered by each other and by charges and currents. They can be viewed from two different point of view: The microscopic set includes charges and current in materials at the atomic scale; The macroscopic set defines instead two new auxiliary fields: Magnetic and Electric fields, where both of them generally have time and space dependence.

The four independent Maxwell's equations link each other the Magnetic field $\mathbf{H}[A/m]$, the Induction Magnetic field $\mathbf{B}[Vs/m^2]$, the Electric fiels $\mathbf{E}[V/m]$ and the Electric Displeacement field $\mathbf{D}[As/m^2]$. The sources of these fields are electric charges and electric currents, usually expressed as local densities: Charge density δ and Current density $\mathbf{J}[A/m^2]$.

$$\nabla \times \mathbf{H} = \mathbf{J} + \frac{\partial \mathbf{D}}{\partial t} \tag{1.1}$$

$$\nabla \times \mathbf{E} = -\frac{\partial \mathbf{B}}{\partial t} \tag{1.2}$$

$$\nabla \cdot \mathbf{B} = 0 \tag{1.3}$$
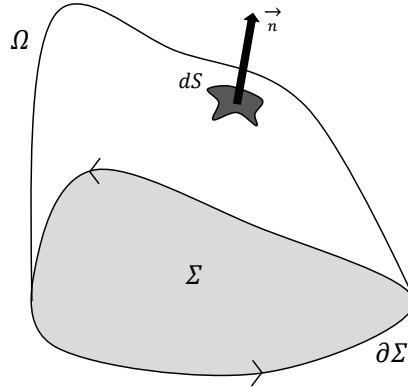
Figure 1.11: Domain Ω and surface Σ

$$\nabla \cdot \mathbf{D} = \delta \tag{1.4}$$

It's easy to add another equation that can be written as a linear combination of (1.1) and (1.4):

$$\nabla \cdot \mathbf{J} = -\frac{\partial \delta}{\partial t} \tag{1.5}$$

Punctual formulations are not the only possibile. With the help of Stokes and Green theorems it is possible to express Maxwell's equations in their integral form.

The Maxwell Induction Law (1.2) indeed is usually written as follow:
After have defined an arbitrary surface Σ whose support is the closed path $\partial\Sigma$, the surface integral of the curl of the electric field:

$$\int_{\Sigma} \nabla \times \mathbf{E} \, dV = \oint_{\partial\Sigma} \mathbf{E} \cdot d\mathbf{l} = -\frac{\partial}{\partial t} \int_{\Sigma} \mathbf{B} \cdot \mathbf{n} \, dS$$

that is many times written in litterature as:

$$fem = -\frac{\partial \Phi}{\partial t} \tag{1.6}$$

where $\Phi[Tm^2]$ is the Magnetic Flux throughout the surface Σ.

As just done before the same integration metohd can be implemented for the Ampere-Maxwell Law (1.1) and achieve the integral expression:

$$\oint_{\partial\Sigma} \mathbf{H} \cdot d\mathbf{l} = \int_{\Sigma} \mathbf{J} \cdot \mathbf{n} \, dS + \frac{\partial}{\partial t} \int_{\Sigma} \mathbf{D} \cdot \mathbf{n} \, dS$$

Magnetic Gauss Law (1.3) is usually known as the impossible of the existance of sources and shafts. For the Green integration method it can be expressed as:

$$\int_{\Omega} \nabla \cdot \mathbf{B} \, dV = \int_{\partial\Omega} \mathbf{B} \cdot \mathbf{n} \, dS = 0$$

This last equation says that the Magnetic Flux through the closed surface $\partial\Omega$ that includes the volume region Σ must be zero:

$$\Phi_{\partial\Omega} = 0 \tag{1.7}$$

The last integral form that must be defined is the Conservation of the Electric Charge. The integration of divergence of electric current, implementing Green's law, in the same way as the last step, admits to obtain the following relation among the total current and the total electrical charge:

$$\int_{\partial\Omega} \mathbf{J} \cdot d\mathbf{s} = -\frac{\partial}{\partial t} \int_{\Omega} \delta\, dV$$

and at the last is possibile to rewrite the formulation as:

$$I = -\frac{\partial Q}{\partial t} \tag{1.8}$$

where $Q[C]$ is the total elctric charge inside the volume Ω and $I[A]$ is the total current through the surface $\partial\Omega$

1.3.1   Boundary Conditions

The integral formulations just defined, allow to understand what, for example, happens across and through interfaces of different materials. For example it is possible to find in a domain Ω two or more materials that are characterized from completely various behaviour of the fields.
In litterature is commonly defined as normal or tangent component conservation of fields, and it depends from the kind of the field that we want study.

B-Normal Conservation

The conservation of the normal component of $\mathbf{B}$ is proved from the divergence of the magnetic induction field. On the plane $\partial\Omega$ that is the interface between two diferrent regions, characterized from two different materials, for example μ_1 and μ_2 it is possible to build a flattened cylinder as it is possible to observe in figure. This button is defined from a radius that is more and more large than its height. Therefore is possibile to integrate in the total surface of the object Σ and neglecting the second order terms:

$$\oint_{\Sigma} \mathbf{B} \cdot d\mathbf{S} = \mathbf{B_1} \cdot \mathbf{n_1} S_1 + \mathbf{B_2} \cdot \mathbf{n_2} S_2 = 0$$

and finally this entails the conservation of the normal component of the magnetic induction field through boundaries.

$$\mathbf{B_1} \cdot \mathbf{n} = \mathbf{B_2} \cdot \mathbf{n} \tag{1.9}$$
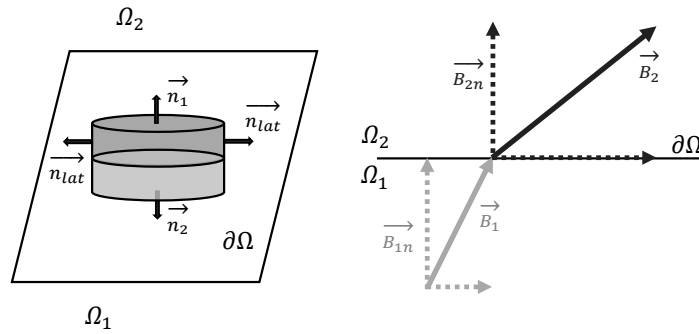
Figure 1.12: Conservation of the normal component of a vector. In figure there is an infinitesimal cylinder which height is smaller than its radius. The interface $\partial Omega$ separates two regions with different material parameters. In that case the two regions Ω_1 and Ω_2 have different relative permeabilities.

D-Normal Conservation

In the same way has just done, is possibile to integrate the divergence of the electric displeacement vector on the same flattened cylinder.

$$\oint_{\Sigma} \mathbf{D} \cdot d\mathbf{S} = \mathbf{D_1} \cdot \mathbf{n_1} S_1 + \mathbf{D_2} \cdot \mathbf{n_2} S_2 = 0$$

that implicates the conservation of the normal component of $\mathbf{D}$

$$\mathbf{D_1} \cdot \mathbf{n} = \mathbf{D_2} \cdot \mathbf{n} \tag{1.10}$$

J-Normal Conservation

From the equaiton (1.5) is easy to understand that the conservation of the normal component of the current density vector depends strictly on the dependence of the charge density with the time. In the more general case that $\frac{\partial \delta}{\partial t} \not\equiv 0$:

$$\mathbf{J_1} \cdot \mathbf{n} = \mathbf{J_2} \cdot \mathbf{n} - \frac{\partial Q}{\partial t} \tag{1.11}$$

That means there is a jump due to the total electric charge inside the button.

E-Tangent Conservation

In the same way like before in the genaral case of time-variation of the magnetic induction vector ($\frac{\partial \mathbf{B}}{\partial t} \not\equiv 0$) it is possible to integrate on a surface Σ, as it is possible to view in figure, the curl of the electric field. The geometry taken into account in this different case is a rectangle Σ, whose height is smaller and smaller than its width. For this reason it is possible to neglect the superior order therms, in other words

the integrals along the height. The rectangle structure passes through the boundary
between the two different regions Ω_2 and Ω_2.

$$\int_{\Sigma} \nabla \times \mathbf{E} \cdot d\mathbf{S} = \oint_{\partial\Sigma=l} \mathbf{E} \cdot d\mathbf{l} = -\frac{\partial\Phi}{\partial t}$$

and finally it is possible to obtain the conservation of the tangentl component unless
the jump due to the variation of the magnetic induction vector

$$\mathbf{E_1} \cdot \mathbf{t} = \mathbf{E_2} \cdot \mathbf{t} - \frac{\partial\Phi}{\partial t} \tag{1.12}$$
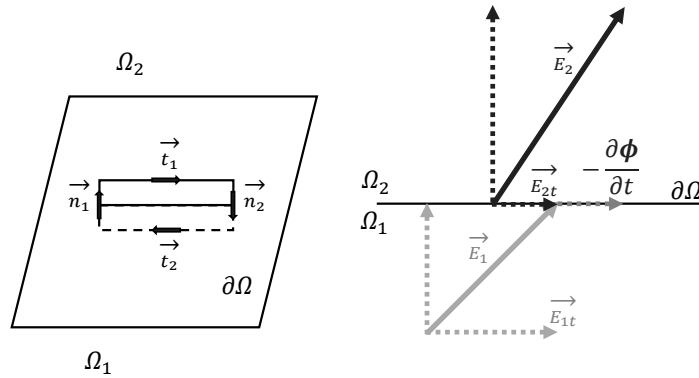
Figure 1.13: Conservation of the tangent component of a vector like the Electric Field.
In figure there is a rectangular closed path which height is smaller than its
width. The interface $\partial Omega$ separates two regions with different material
parameters. In that case the two regions Ω_1 and Ω_2 . because the therm
$-\frac{\partial\mathbf{B}}{\partial t}$ is not equal to zero, exits a jump on the tangent component of the
Electric field $\mathbf{E}$.

H-Tangent Conservation

If there is the presence of a Current density $\mathbf{J}$ from the equation (1.1) it is possible
to understand that the curl of the magnetic vector is not zero, so as just done it is
possible to integrate along the rectangle Σ and obtain the conservation of the tangent
component of the Magnetic Field, below the hypothesis that the time derivattive of
the Electric Displeacement field must be negligible,or rather $\frac{\partial\mathbf{D}}{\partial t} \approx 0$

$$\mathbf{H_1} \cdot \mathbf{t} = \mathbf{H_2} \cdot \mathbf{t} + \int_{\Sigma} \mathbf{J} \cdot \mathbf{n} \, dS \tag{1.13}$$

The jump between the current density in the first and in the second region is due to
the current through the surface.

1.3.2 Constitutive Laws

To solve the problem it is necessary to add to the model the Constitutive Laws that connect different fields each other and represent the coefficients of the PDEs.

$$\mathbf{B} = \mu \mathbf{H} \tag{1.14}$$

$$\mathbf{J} = \sigma \mathbf{E} \tag{1.15}$$

$$\mathbf{D} = \epsilon \mathbf{D} \tag{1.16}$$

Where $\mu = \mu_r \mu_0$ expresses the magnetic permeability $[H/m]$ prodct of vacuum magnetic permeability μ_0 and relative amgnetic permeability μ_r.

$$\mu_0 = 4\pi 10^{-7} [H/m] \tag{1.17}$$

The electric conductivity $\sigma[S/m]$ can be seen as $\sigma = \frac{1}{\rho}$ where $\rho[\Omega/m]$ is the electric resistivity, while electric permittivity is $\epsilon = \epsilon_r \epsilon_0$ where ϵ_0 is the vacuum electric permittivity:

$$\epsilon_0 = 8.85 * 10^{-12} [F/m] \tag{1.18}$$

For the applications considered in this work, and usually used in the induction hardening processes it is possible to neglect the derivative of the electric displeacement field Is easily to demonstrate thath circumstance for a model in wich the sources are sinusoidal and in which it is possible to assume avarage values for the material parameters:

$$\mathbf{D} = \epsilon_0 \epsilon_r \mathbf{E} + \mathbf{P}$$

where $\mathbf{P}$ is the electric polarization vector. For conductive materials : $\mathbf{P} \ll \epsilon_0 \mathbf{E}$ therefore the displeacement electric field is approximately $\mathbf{D} \approx \epsilon_0 \mathbf{E}$. Therefore it is possible to study the problem with the Steinmetz Transformer:

$$\nabla \times \mathbf{H} = \mathbf{J} + \frac{\partial \mathbf{D}}{\partial t} = \sigma_e l \mathbf{E} + j\omega \epsilon_0 \mathbf{E} = (\sigma_e l + j\omega_r \omega_0)\mathbf{E}$$

and considering an inductor coupled with a simple steel billet:

$$\sigma_{Steel} \approx 10^6 [S/m]$$

$$\epsilon_{Steel} \approx 10^{-11} [F/m]$$

$$\omega_{alim} \approx 10^5 [rad/s]$$

where it is possible to understand that the imaginary part of the complex number $Im(\nabla \times \mathbf{H}) = j\omega_r \omega_0 \mathbf{E}$ is negligible. Therefore it is possible to don't consider the contribution of the displeacement electric field $\frac{\partial \mathbf{D}}{\partial t}$.

At he end it is possible to write the Magneto Quasi Static Model of the induction problem (MQS):

$$\nabla \times \mathbf{H} = \mathbf{J} \tag{1.19}$$

$$\nabla \times \mathbf{E} = -\frac{\partial \mathbf{B}}{\partial t} \tag{1.20}$$

$$\nabla \cdot \mathbf{B} = 0 \tag{1.21}$$

$$\nabla \cdot \mathbf{J} = 0 \tag{1.22}$$

Adding constitutive laws to the previous set of equations it is possible to combine them and achieve an only equation that describes entirely the electromagnetic problem with two different unknows: the magnetic vector potential $\mathbf{A}$ and the electric scalar potential V.

Because the divergence of the induction magnetic field must be zero from the equation (1.19) than exists a magnetic vector potential $\mathbf{A}$ whose curl can totally build the induction magnetic field $\mathbf{B}$:

$$\mathbf{B} = \nabla \times \mathbf{A} \tag{1.23}$$

It is important to understand that the equation (1.23) doesen't fix an only magnetic vector potential. Indeed exist infinite vector potential that solve the equation $\nabla \cdot \mathbf{B} = \nabla \cdot \nabla \times \mathbf{A} = 0$ for every $\mathbf{A} = \mathbf{A}' + \nabla \Lambda$. To find an only solution it is possible to difine cerain gauge techinque that I am going to introduce and describe later, like Coulomb gauge and Lorenz gauge. From the equation (1.20) it is possible to find a new formulation for the electric field $\mathbf{E}$, in other words describe it like effect of both the potential:

$$\mathbf{E} = -\nabla V - \frac{\partial \mathbf{A}}{\partial t} \tag{1.24}$$

where V is the electric scalar potential.

Combining both the formulation for electric and magnetic fields in to the (1.19) and considering constitutive laws for elecrtic and magnetic field $\mathbf{J} = \sigma \mathbf{E}$ and $\mathbf{H} = \frac{1}{\mu}\mathbf{B}$

$$\nabla \times \mathbf{H} = \mathbf{J} = \sigma \mathbf{E}$$

$$\nabla \times \frac{1}{\mu} \nabla \times \mathbf{A} = -\sigma \nabla V - \sigma \frac{\partial \mathbf{A}}{\partial t}$$

The same thing can be done for the equation (1.22):

$$\nabla \cdot \mathbf{J} = \nabla \cdot \sigma \mathbf{E}$$

$$\nabla \cdot \sigma \nabla V = -\nabla \cdot \sigma \frac{\partial \mathbf{A}}{\partial t}$$

Those two equations describe the MQS complitely. The final system of equation with the Coulomb gauge, that is necessary to have one only solution is:

$$\nabla \times \frac{1}{\mu} \nabla \times \mathbf{A} + \sigma \nabla V + \sigma \frac{\partial \mathbf{A}}{\partial t} = 0 \tag{1.25}$$

$$\nabla \cdot \sigma \nabla V = 0 \tag{1.26}$$

1.3.3   Solution of several problems

Once out in its full complexity the electromagnetic problem is critical to the resolution of the set equations which is reached. In literature (Bessel) you can find a careful analytical resolution of the electromagnetic problem with particular their attention to the study of an ideal system of electromagnetic coupling between an inductor ideally toroidal and a billet full, always with cylindrical symmetry. Although this approach are excellent results for geometries and physicsal relatively simple, unfortunately it should not overlook aspects particularly critical as not linearity of the materials involved or broken symmetries, geometric or field. The development and optimization in the last decades of numerical solution techniques such as FDM and FEM later, in agree with the significant increase in performance of the hardware simulation has enabled the achievement of simulations numerical increasingly accurate and complex. With particular attention to the problem analyzed in this work, the finite element simulation for tempering toothed wheels is still a topic of concern both at the experimental research. The complexity of the geometries often treated in the process of surface hardening, hardening thicknesses required by companies contractors and powers brought into play to achieve attractive returns and achieve the desired economy They force you to treat models often extremely complicated and to limit the overall timescale simulation push to consider simplifications in the model analyzed. Still of major interest from the point of view of the modeling nuemrica is a new type of quenching Surface: the simultaneous dual frequency (SDF), which although has a good response to industrial level (There are already several machines on the market), it is still difficult to model. From the numerical point of view, not to vitiate the goodness of the results is excessively fact forces us to having to solve the whole problem coupled simultaneously, and this of course involves a huge computational burden.

Particularly, a resolution in the time domain, makes it possible to observe and try to understand more, the main phenomena that occur during different processes. But to succeed in doing what is necessary to first define uniquely the geometry of the problem, physics, materials, and only finally solve the model using appropriate numerical methods.

1.3.4   Boundary Conditions

In mathematics, in the field of differential equations, a boundary value problem is a differential equation together with a set of additional constraints, called the boundary conditions. A solution to a boundary value problem is a solution to the differential equation which also satisfies the boundary conditions. Boundary value problems arise in several branches of physics as any physicsal differential equation will have them. Problems involving the wave equation, such as the determination of normal modes, are often stated as boundary value problems. A large class of important boundary value problems are the Sturm–Liouville problems. The analysis of these problems involves the eigenfunctions of a differential operator. To be useful in applications, a boundary value problem should be well posed. This means that given the input to the problem there exists a unique solution, which depends continuously on the input. Much theoretical work in the field of partial differential equations is devoted to proving that boundary value problems arising from scientific and

engineering applications are in fact well-posed. Among the earliest boundary value problems to be studied is the Dirichlet problem, of finding the harmonic functions (solutions to Laplace's equation).

Dirchlet boundary condition

In mathematics, the Dirichlet (or first-type) boundary condition is a type of boundary condition, named after Peter Gustav Lejeune Dirichlet (1805–1859). When imposed on an ordinary or a partial differential equation, it specifies the values that a solution needs to take on along the boundary of the domain.

$$\nabla^2 y + y = 0 \tag{1.27}$$

The Dirichlet BC on a domain Ω takes the form:

$$y(\mathbf{x}) = f(\mathbf{x}) \tag{1.28}$$

where f is a fixed function on the boundary.

Neumann boundary condition

In mathematics, the Neumann (or second-type) boundary condition is a type of boundary condition, named after Carl Neumann. When imposed on an ordinary or a partial differential equation, it specifies the values that the derivative of a solution is to take on the boundary of the domain. In engineering applications, the following would be considered Neumann boundary conditions. For a PDE:

$$\nabla^2 y + y = 0 \tag{1.29}$$

The Neumann BC on a domain Ω takes the form:

$$\frac{\partial y}{\partial \mathbf{n}}(\mathbf{x}) = f(\mathbf{x}) \tag{1.30}$$

for each $\mathbf{x}$ on the boundary Ω, and $\mathbf{n}$ is the normal to the boundary and f(x) is a given scalar function. Homogeneous Neumann boundary condition impoes that

$$f(\mathbf{x}) = 0 \tag{1.31}$$

The question of finding solutions to such equations is known as the Dirichlet problem. In engineering applications, a Dirichlet boundary condition may also be referred to as a fixed boundary condition.

1.3.5   Magnetic Saturation and Curie Temperature

One of the main challenge is describe the complex behaviour that the magnetic induction field $\mathbf{B}$ manifests with the increasing of the magnetic field $\mathbf{H}[A/m]$ and the material temperature $\Theta[K]$. An accurate simulation must take account of magnetic saturation and phase transition due to Curie temperature. Saturation is a characteristic of ferromagnetic materials, such as iron, nickel, cobalt and their alloys. Saturation is most clearly seen in the magnetization curve, also usually called

BHcurve. It underlines that as magnetic field increases, the induction magnetic field tends to a maxium value asymptotically. This upper limit is defined the saturation level for the material, $B_s[T]$. The relation between the magnetizing field $\mathbf{H}$ and the magnetic field $\mathbf{B}$ is usually expressed as a function product of the magnetic permeability $\mathbf{B} = \mu(|\mathbf{H}|)\mathbf{H}$ where is easy to understand that the magnetic permeability, which is the product of relative permeability μ_r and the constant vaccum permeability μ_0, is not constant. In saturable materials as those that are used for hardening processes the qualitative curve of μ_r is the derivative of curves that are plotted in Figure 1.14. It is possible to distinguish two different behaviour the first, for small magnetic field $\mathbf{H}$, is a linear dependence and the relative permeability can be assumed constant, the second starts on the curve knee and represents the saturation. In litterature exists an analytical function that describes quite good that behaviour:

$$|\mathbf{B}| = \mu_0|\mathbf{H}| + \frac{2B_s}{\pi} \arctan\left[\frac{\pi(\mu_{r0} - 1)|\mathbf{H}|}{2B_s}\right] \tag{1.32}$$

where B_s [T] is the saturation level and μ_{r0} is the initial relative permeability.
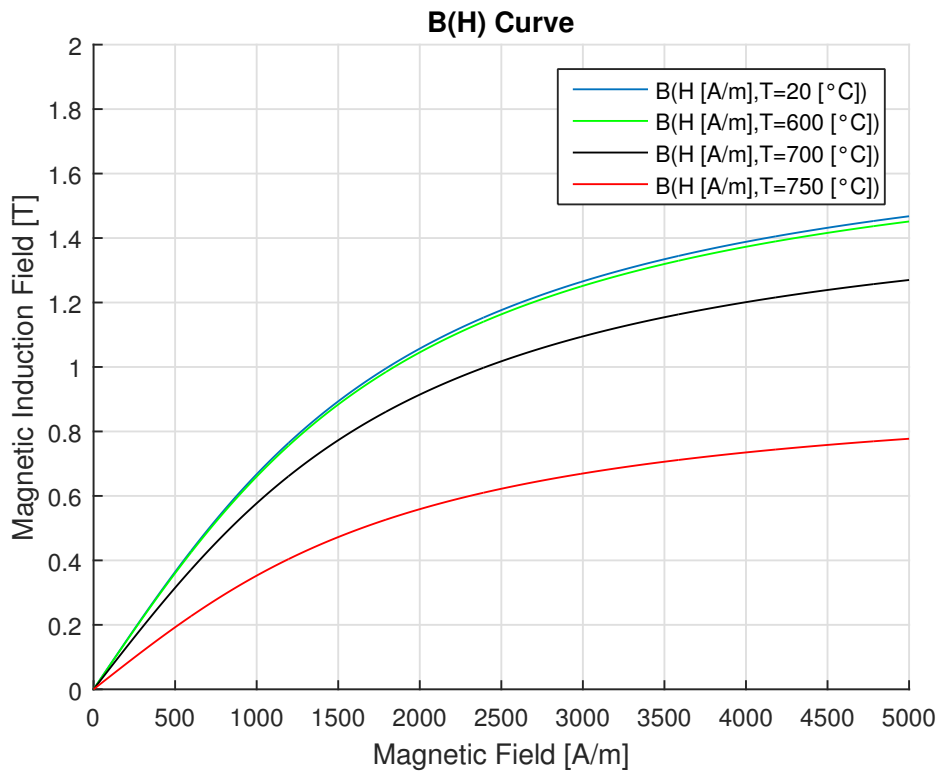
Figure 1.14: Behaviour of the Induction Field [T] function of the Magnetic Field for a particular low alloy steel. In the figure it is possible to see the saturation behaviour.

The other phenomena that must be taken into acount for the non linear behaviour of the magnetic permeability is the transition phase that occurs in steels at the

Curie Temperature. Adding those consideration to the last equation, it's possible to describe the absolute value of the induction field as follow:

$$|\mathbf{B}| = \mu_0 |\mathbf{H}| + \frac{2B_s}{\pi} \arctan\left[\frac{\pi(\mu_{r0} - 1)|\mathbf{H}|}{2B_s}\right] \cdot \left(1 - \exp\left(\frac{\theta - \theta_c}{C}\right)\right) \tag{1.33}$$

where θ_c is the Curie Temperature at which the relative permeability falls to zero. C $[C]$ instead is a temperature constant.

it is possible to combine what just said about the behaviour of the induction field with the temperature and the magnetic field and plot a three dimensional curve that summarize the magnetic saturation and the phase transition of the magnetic steel that causes the loss of its magnetic properties. The curves presented in this section consider the following parameters:

Constant	Value	Unit
μ_0	$4\pi \cdot 10^{-7}$	$[H/m]$
B_s	1.8	$[T]$
μ_{r0}	600	$[-]$
θ_c	780	$[C]$
C	40	$[C]$

Table 1.1: Paramaters of the formulation of the induction field, function of temperature and mangetic field.

1.4   Fourier's Equation

In the heating processes of isotropic solids temperature of each element of the body is a function of spatial coordinates and time.

$$\theta = \theta(x, y, z, t)$$

Thinking about a heating process it is possible, for each instant, to define the isotherms inside the body, whose time evolution describes how temperature distributions change inside the body. The heat equation is a parabolic partial differential equation that describes the distribution of heat and the variation with the temperature in a given region over the time. The heat equation is derived from Fourier's law and conservation of Energy [Cannon 1984]. By Forurier's law, the rate of flow of heat energy per unit aera through a surface is proportional to the negative temperature gradient across the surface: The Fourier's equation defines the relation for each point P of the body, between the specific thermal flux $\mathbf{p}$ $[W/m^2]$ and the temperature gradient.

$$\mathbf{p} = -\lambda \frac{\partial \theta}{\partial n} = -\lambda \nabla \theta \tag{1.34}$$

where n is the normal vector of the surface, oriented to the direction of increasing temperatures, and λ $[W/(mK)]$ the thermal conductivity. The thermal flux may be
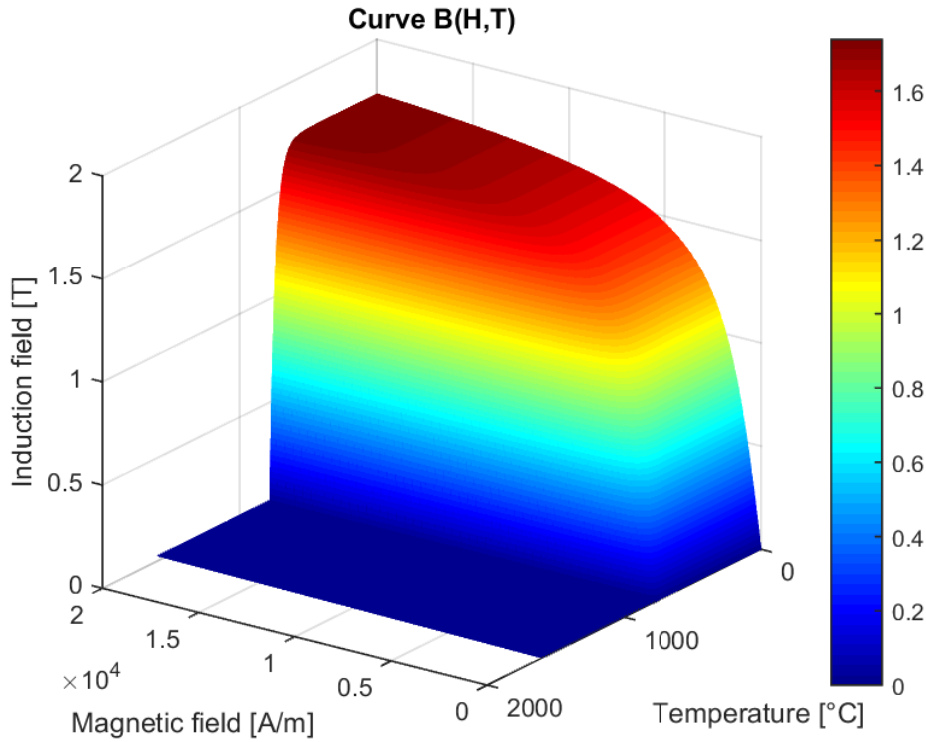
Figure 1.15: 3D figure of the Induction Magnetic Field function of Temperature and Magnetic Field $[A/m]$

written as the sum of its components $\mathbf{u_x},\mathbf{u_y},\mathbf{u_z}$, in a three dimensional coordinate system.

$$\mathbf{p} = p_x\mathbf{u_x} + p_y\mathbf{u_y} + p_z\mathbf{u_z} \tag{1.35}$$

that means it posible to write again the thermal flux as:

$$\mathbf{p} = -\lambda\frac{\partial\theta}{\partial x}\mathbf{u_x} - \lambda\frac{\partial\theta}{\partial y}p_y\mathbf{u_y} - \lambda\frac{\partial\theta}{\partial z}p_z\mathbf{u_z} \tag{1.36}$$

The general equation of conduction expresses the energy balance of an infinitesimal element of the body dV. This means that the sum of thermal fluxes throughout the lateral surface Thermal fluxes through the lateral surfaces:

$$dP_s = \sum_{i\in\mathbb{N}} dP_i = \sum_i P_i dA_i = -\nabla \cdot \mathbf{p}dV$$

Energy that is transformed in heat inside the solid piece is

$$dP_w = w(P,t)dV$$

where w $[W/m^3]$ is the specific power inside the piece Increase of internal energy of the piece is

$$dP_c = c\gamma\frac{\partial\theta}{\partial t}dV$$
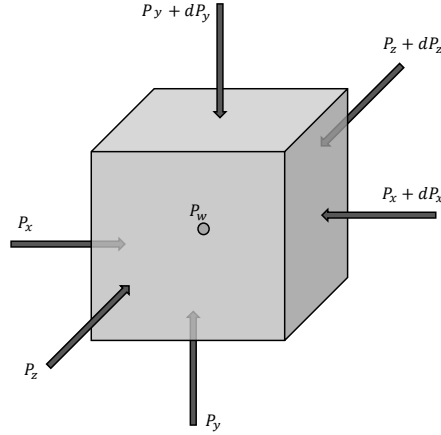
Figure 1.16: Thermal energy conservation for an infinitesimal cube of volume dV.

where c $[J/kgK]$ is the specific heat capacity and γ $[kg/m^3]$ is the mass density. At this point it is possible to impose the conservation of energy and power for the whole system:

$$dP_c = dP_s + dP_w$$

and finally it is possible to obtain the more known Fourier's equation:

$$c\gamma \frac{\partial \theta}{\partial t} = -\nabla \cdot \lambda \nabla \theta + w(P, t) \tag{1.37}$$

As already done for Maxwell's equations it is possible to rewrite the PDE of the thermal problem in an axial symmetrical coordinate system:

$$c\gamma \frac{\partial \theta}{\partial t} = \frac{1}{r}\frac{\partial}{\partial r}(r\lambda\frac{\partial \theta}{\partial r}) + \frac{1}{r}\frac{\partial}{\partial \varphi}(\frac{1}{r}\lambda\frac{\partial \theta}{\partial \varphi}) + \frac{\partial}{\partial z}(\lambda\frac{\partial \theta}{\partial z}) + w(r, z, t) \tag{1.38}$$

If the material is isotropic and homogeneous it is possible to rewrite the equation as:

$$\frac{\partial \theta}{\partial t} = \frac{\lambda}{c\gamma}(\frac{\partial^2 \theta}{\partial r^2} + \frac{1}{r}\frac{\partial \theta}{\partial r} + \frac{1}{r^2}\frac{\partial^2 \theta}{\partial \varphi^2} + \frac{\partial^2 \theta}{\partial z^2}) + \frac{w(r, z, t)}{c\gamma} \tag{1.39}$$

where $k = \frac{\lambda}{c\gamma}$ $[m^2/s]$ is the thermal diffusivity of the material.

1.4.1   Boundary conditions

For a process such as induction hardening it is necessary to consider during the problem, also if the time of the treatment is extremely short, all the thermal losses of the problem, such as convection and radiation. So you need to define these two heat flows outward. Then exist boundaries of the body on which can be defined heat flowsof the types:

$$p_{conv} = \lambda \nabla \theta = \alpha(\theta_a - \theta) \tag{1.40}$$

This boundary condition is defined on each boundary on which exists a convective loss: this is so called Robin's Boundary. In the same way it is possible to define the rafiation lossess as:

$$p_{rad} = \frac{5,67 \cdot 10^{-12}}{\frac{1}{\varepsilon} + \frac{S}{S_a}(\frac{1}{\varepsilon_a} - 1)}(\theta^4 - \theta_a^4) \tag{1.41}$$

where ε ad ε_a are respectively the emissivity of the surface of the material, in other words is its effectiveness in emitting energy as thermal radiation, and the absorption coefficient. S and S_a are the radiating surface and the absorbing surface. Typically you can neglect the radiating surface than the absorbent, then you can approximate the formulation of radiation losses as:

$$P_{rad} = 5,67 \cdot 10^{-12}\varepsilon(\theta^4 - \theta_a^4) \tag{1.42}$$

1.4.2 Thermal material properties

To solve the thermal problem there is, also in this case, the necessity of defining the cofficients of the corrispondent PDE. The physicsal properries of steel are first of all a function of its chemical composition: althought carbon content and alloying elements are responsible for mechanical properties, in some case they could affect its thermal behaviour. Moreover, prior metallurgical structure is found to have big influence on the material's response to heat treatment. In the particular case of surface inudction hardening there is the necessity of suitable formulation for material properties, because they dramatically change in the course of the heat treatment, mainly due to the effect of temperature θ. The coefficients that are necessary to describe and solve the thermal problem are:

- Thermal Conductivity λ $[W/m/C]$

- Heat Capacity c_p $[J/m^3/C]$

- Density γ $[kg/m^3]$

Thermal Conductivity

it is a thermo-physicsal material property, which expresss the quantity of heat that a specific material can transfer through an unit surface area in an unit time when exists a gradient temperature between two different points. In other words it establishes the ability of the material to transfer heat. In literature it is possible to find a suitable formulation for thermal conductivity, that expresses it as function of temperature θ:

$$\lambda(\theta) = \lambda_a + (\lambda_b - \lambda_a) \cdot (1 - \exp{(-\frac{\theta - \theta_b}{\tau})}) \tag{1.43}$$

where θ_b $[C]$ is the reference temperature, λ_a $[W/m/C]$ is the asymptotic steady conductivity value, in other words it is the limit value that thermal conductivity assumes when the temperature gradient becomes extremely big. λ_b instead is the residual conductivity value at the reference temperature, in other words it is the value of λ that a material shows also if does not exist a temperature gradient. Finally τ $[C]$ is a temperature constant. In the simulation model of this work , avaible experimentally-determined data has been used.

Constant	Value	Unit
λ_a	22	[W/m/°C]
λ_b	45	[W/m/°C]
θ_b	770	[°C]
τ	260	[°C]

Table 1.2: Parameters of the exponential formulation of thermal conductivity.
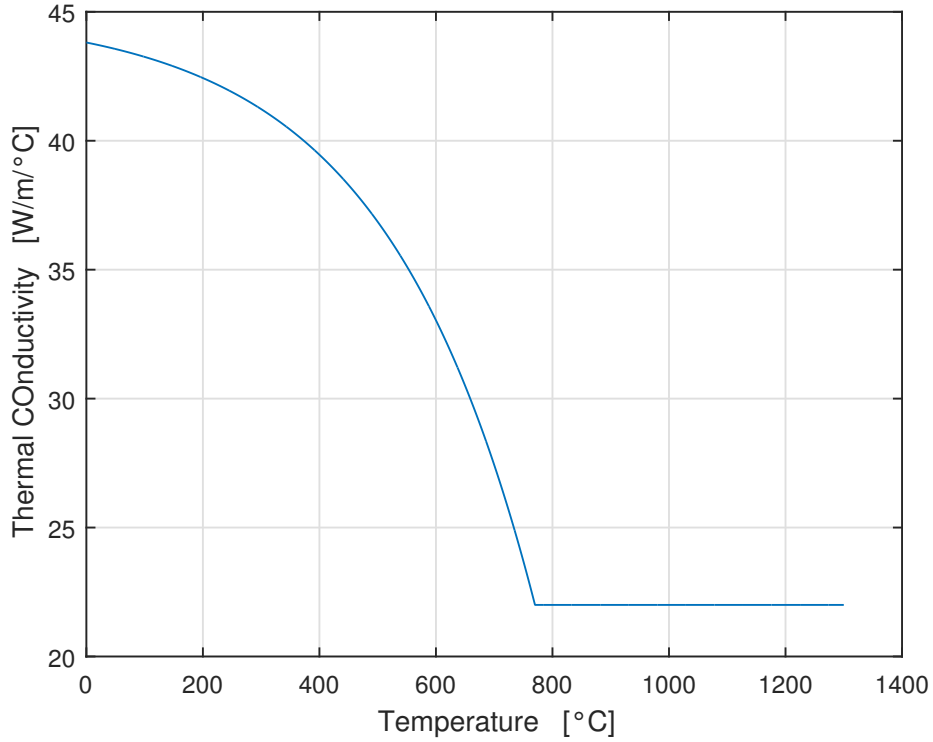
Figure 1.17: Thermal Conductivity $\lambda(\theta)$ function of the temperature.

Heat Capacity

The heat capacity of a material is the heat quantity (that is dimensionally an energy) that must be applyed to raise its temperature by one Celsius degree (or equally by one Kelvin degree). It makes possible to evaluate the amount of energy exchanged by a body during a process characterized by a temperature variation in time. The volumetric heat capacity is extremely important for exampke in a hardening process, because itb behaviour is function of phase transition. Typically it is expressed as the simultaneous combination of an exponential function and a Gaussian function of temperature θ:

$$\gamma C_P(\theta) = \gamma C_{Pi} + (\gamma C_{P0} - \gamma C_{Pi}) \exp\left(-\frac{\theta}{\tau}\right) + E \cdot G(\theta) \qquad (1.44)$$

$$G(\theta) = \frac{1}{\sigma_{dev}\sqrt{2\pi}} \exp\left(-\frac{1}{2}\left(\frac{\theta - \theta_{ph}}{\sigma_{dev}}\right)^2\right) \tag{1.45}$$

where the first term γ $[kg/m^3]$ is the material density, γC_{Pi} $[J/m^3/C]$ is the heat "asymptotic" capacity of the material, in other words for $\theta \Rightarrow \infty$, γC_{P0} instead is the initial heat capacity, at the initial zero temperature. E $[J/m^3]$ is the energy necessary to obtain the phase transition, σ_{dev} $[C]$ is a sperymentally obtained Gaussian standard deviation. θ_{ph} $[C]$ is the phase transition temperature. It is important subline, as already done, that this value is function of heating rate and might vary for different heat treatment that use the same material. Finally τ $[C]$ is the temperature constant of the exponential function, that fixes the temperature interval of the Gaussian spike. Under that considerations it is possible to full describe heat capacity of a particular kind of material, such as AISI 4340:

Constant	Value	Unit
γ	7800	$[kg/m^3]$
γC_{P0}	$3{\cdot}10^6$	$[J/m^3/C]$
γC_{Pi}	$6{\cdot}10^6$	$[J/m^3/C]$
E	$850{\cdot}10^6$	$[J/m^3]$
σ_{dev}	50	$[C]$
τ	300	$[C]$
θ_{ph}	870	$[C]$

Table 1.3: Parmater of the Gaussian-exponential formulation of the volumetric heat capacity (AISI 4340).
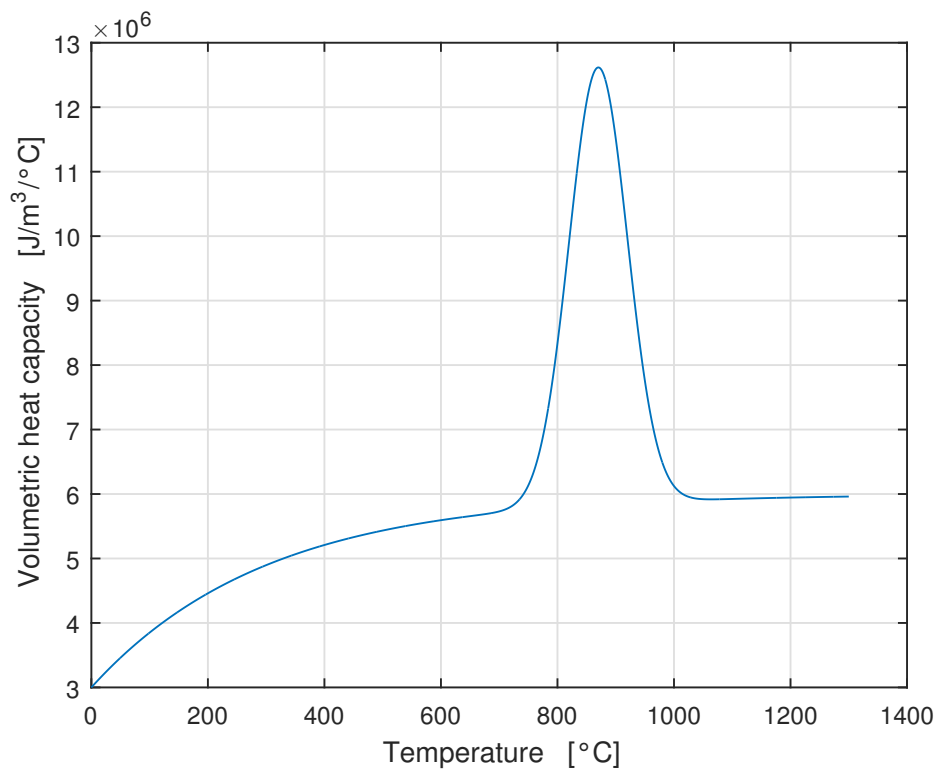
Figure 1.18: Heat Capacity $\gamma C_P(\theta)$ function of the temperature.

Chapter 2

Electrical Analysis

SInce of the target of our problem is to fully hard a thin layer of material, carefully following the teeth profile, the use of SDF allows to produce power distribution inside the piece and teorically heat equally the tip and the base of the teeth. From a pure electrical point of view the double frequency system consist in supplying a load with a combination of two sinusoidal wave form at different frequencies f_1 and f_2.

2.1 Purely Inductive case

If it is possible to suppose an ideal model, linear and purely inductive, the model can be viewed as two voltage generators connented in series and closed to a load, that consists of the inductor coupled with the piece that must be heated. At this point is possible, instead of using Steinmetz' transformation and phasorial representiation, to represent analtically the physical quantities $v(t),i(t)$ and $p(t)$ in the time domain. In this way, the voltage imposed is

$$v(t) = V_1 \cos(\omega_1 t) + V_2 \cos(\omega_2 t) \tag{2.1}$$

where V_1 [V] is the high frequency amplitude, V_2 [V] is the medium frequency amplitude, $\omega_1 = 2\pi f_1$ and $\omega_2 = 2\pi f_2$ [Hz] are respectively the pulsations of high and medium frequency. As already said if the load is describable as a pure inductance L [mH] then the current that flows in the circuit is:

$$i(t) = \int_0^t \frac{1}{L} v(t)\, dt = \frac{1}{L}(\frac{V_1}{\omega_1} \sin(\omega_1 t) + \frac{V_2}{\omega_2} \sin(\omega_2 t)) \tag{2.2}$$

The istant power that the system absorbs is the istant product of voltage and current, so

$$p(t) = v(t)i(t) = \frac{1}{L}(V_1 \cos(\omega_1 t) + V_2 \cos(\omega_2 t))(\frac{V_1}{\omega_1} \sin(\omega_1 t) + \frac{V_2}{\omega_2} \sin(\omega_2 t)) \tag{2.3}$$

Now the power can be viewed as the sum of four therms $p(t) = p_1(t) + p_2(t) + p_3(t) + p_4(t)$ Taking advantage of Prosthaphaeresis Formulas

$$\sin(\alpha) + \sin(\beta) = 2 \sin(\frac{\alpha + \beta}{2}) \cos(\frac{\alpha - \beta}{2})$$
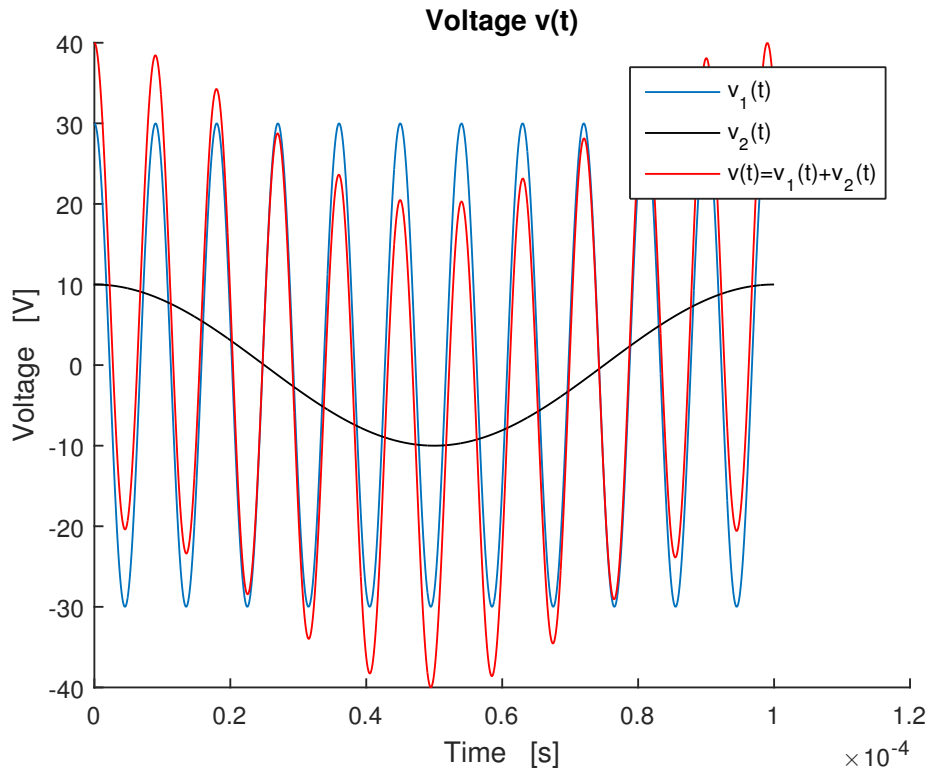
Figure 2.1: Voltage $v(t) = v_1(t) + v_2(t)$. The circuit is voltage supplied
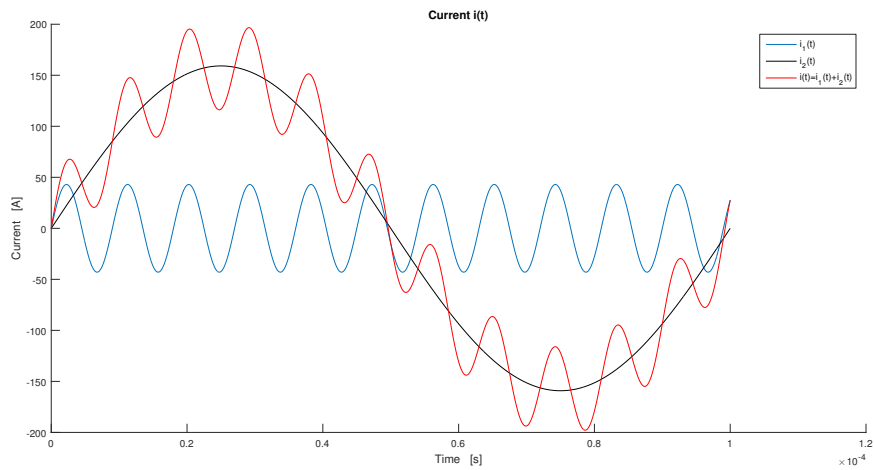
Figure 2.2: Current that flows in the circuit can be view as the sum of two terms
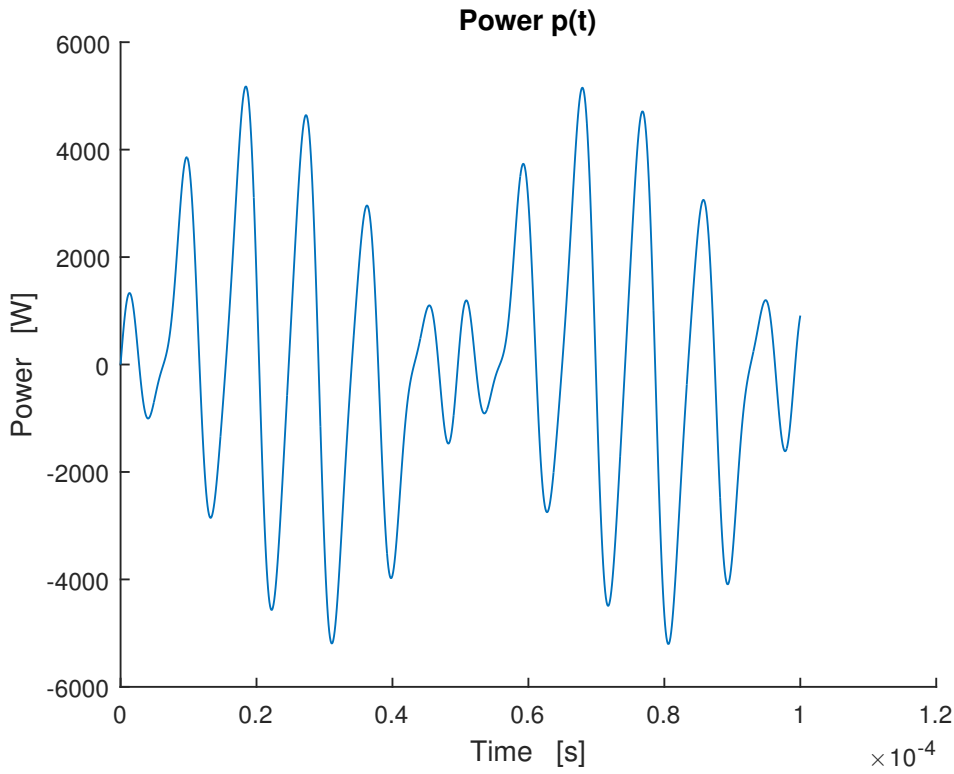
Figure 2.3: Power absorbed from the purely inductive circuit

$$\sin(\alpha) - \sin(\beta) = 2\cos(\frac{\alpha+\beta}{2})\sin(\frac{\alpha-\beta}{2})$$

is possible to completely rewrite the power as:

$$p_1(t) = \frac{V_1^2}{2\omega_1 L}\sin(2\omega_1 t) \tag{2.4}$$

$$p_2(t) = \frac{V_2^2}{2\omega_2 L}\sin(2\omega_2 t) \tag{2.5}$$

$$p_3(t) = \frac{V_1 V_2}{2L}\frac{\omega_1+\omega_2}{\omega_1\omega_2}\sin((\omega_1+\omega_2)t) \tag{2.6}$$

$$p_4(t) = -\frac{V_1 V_2}{2L}\frac{\omega_1-\omega2}{\omega_1\omega_2}\sin((\omega_1-\omega_2)t) \tag{2.7}$$

In this way is possible to view the istant power as the sum of four powers that evolve in time with four different frequencies.

What is the average power in a period $T = \frac{1}{f_2}$? Since there is no resistance R in the circuit under analysis it is zero everytime and for every choice of freqeuncies.

After have splitted the power as the sum of four terms $< p(t) >=< p_1(t) > + < p_2(t) > + < p_3(t) > + < p_4(t) >$ it is possible to compute the average value of each:

$$< p(t) >= \int_0^T p(t)\,dt = \int_0^{\frac{1}{f_2}} p(t)\,dt \tag{2.8}$$
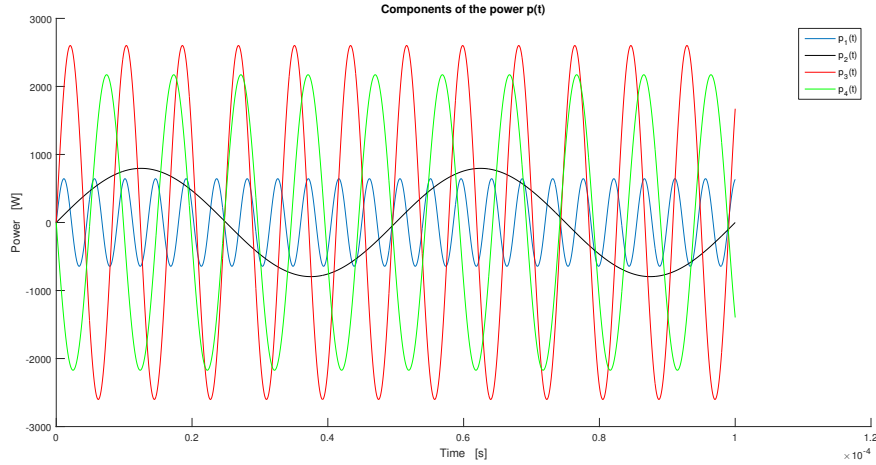
Figure 2.4: Scomposition of power absorbed from the inductive system in its main four therms

Starting from the second therm wich evolves with the frequency $2f_2$:

$$< p_2(t) >= \frac{1}{T} \int_0^T p_2(t)\, dt = 0 \tag{2.9}$$

It is clear that all other terms are equal to zero for every possible choice. For simplicity we consider the sum of the average powers $< p_3(t) > + < p_4(t)$

$$< p_3(t) > + < p_4(t) >= \frac{V_1 V_2}{4\pi^2 f_1 L}(2 - \cos(\frac{\omega_1 + \omega_2}{\omega_2} 2\pi) - \cos(\frac{\omega_1 - \omega_2}{\omega_2} 2\pi)) = 0 \tag{2.10}$$

If now we suppose that the two frequencies are in a general ratio $r = \frac{f_1}{f_2} > 1$ and $r \in \mathbb{R}$ it is possible to rewrite again the last equation and obtain:

$$< p_3(t) > + < p_4(t) >= \frac{V_1 V_2}{2\pi f_2 L}(1 - \cos(2\pi r)) = 0 \tag{2.11}$$

The same approach can be done for the average power of $p_1(t)$:

$$< p_1(t) >= -\frac{\omega_2}{\omega_1} \frac{V_1^2}{4\pi L}(\cos(4\pi \frac{\omega_1}{\omega_2}) - 1) = -\frac{V_1^2}{16\pi f_2 L} \frac{1}{r^2}(\cos(4\pi r) - 1) \tag{2.12}$$

Also in this case the average power $< p_1(t) >$ is equal to zero only if the ratio $r \in \mathbb{Z}$.

So if it possible to study the purely inductive case, the avarage power is every time equal to zero, because a resistive component does not exist. This means that all the power transferred is accumulated in the magnetic field. This means that of cours

$$< p >= 0 \tag{2.13}$$

The analysis of a purely inductive model is not interesting computationally, but instead it allows us to introduce the study of the more complex real model (series RL). So it is possible, with a similar approach, analyze the more complex case, in which a SDF voltage feeds an RL load, in which inductance and resistance are supposed constant and unique.

2.2 Beats

Tecnically beats are the product of a sinusoidal wave form that evolves with a frequency α superimposed to a second sinusoidal wave form evolving with a frequencyβ. The condition to have a beat is that the two frequency must be very similar and the two wave forms must have the same amplitude. In our case the power shows exactly that condition:

$$p(t) = v(t)i(t) = (V_1\cos(\omega_1 t) + V_2\cos(\omega_2 t))(\frac{V_1}{L\omega_1}\sin(\omega_1 t) + \frac{V_2}{L\omega_2}\sin(\omega_2 t)) = \quad (2.14)$$

if now we suppose that the frequecies and the voltages are in the same ratio, that means:

$$\frac{\omega_1}{\omega_2} = \frac{V_1}{V_2} = r$$

is possible to better view beats of the wave form:

$$p(t) = \frac{2V_1^2}{L\omega_1}(\cos(\omega_1 t) + \frac{1}{r}\cos(\omega_2 t))(\sin(\frac{\omega_1 + \omega_2}{2}t)\cos(\frac{\omega_1 - \omega_2}{2}t) \qquad (2.15)$$

In this last equation the term $\frac{1}{r}\cos(\omega_2 t)$ is much smaller than the term $\cos(\omega_1 t)$ for values of $r = \frac{\omega_1}{\omega_2}$ sufficiently big. This supposition is in agreement with a heat treatment such as simultaneous double frequency induction hardening of teethed wheels. With this hypotesis then is possible to better view beats of the wave form of the power:

$$p(t) \approx \frac{2V_1^2}{L\omega_1}\cos(r\omega_2 t)\sin(\omega_1\frac{r+1}{2}t)\cos(\omega_1\frac{r-1}{2}t) \qquad (2.16)$$

2.3 Fourier's Analysis

The Fourier transform of a periodic function, $s(t)$, with period T, becomes a Dirac comb function, modulated by a sequence of complex coefficients. The integral over any interval of length P:

$$S(k) = \frac{1}{T}\int_T s(t) \cdot \exp\left(-i2\pi\frac{k}{T}\right)dt \qquad (2.17)$$

The inverse transform, known as Fourier series, is a representation of $s(t)$ in terms of a summation of a potentially infinite number of harmonically related sinusoids or complex exponential functions, each with an amplitude and phase specified by one of the coefficients:

$$s(t) = \sum_{k=-inf}^{inf} S(k) \cdot e^{i2\pi\frac{k}{T}t} \qquad (2.18)$$

To represent a generic periodic signal, Dirichlet's criterion must be respected, this means that:

- $f(t)$ must be absolutely integrable on the period T.
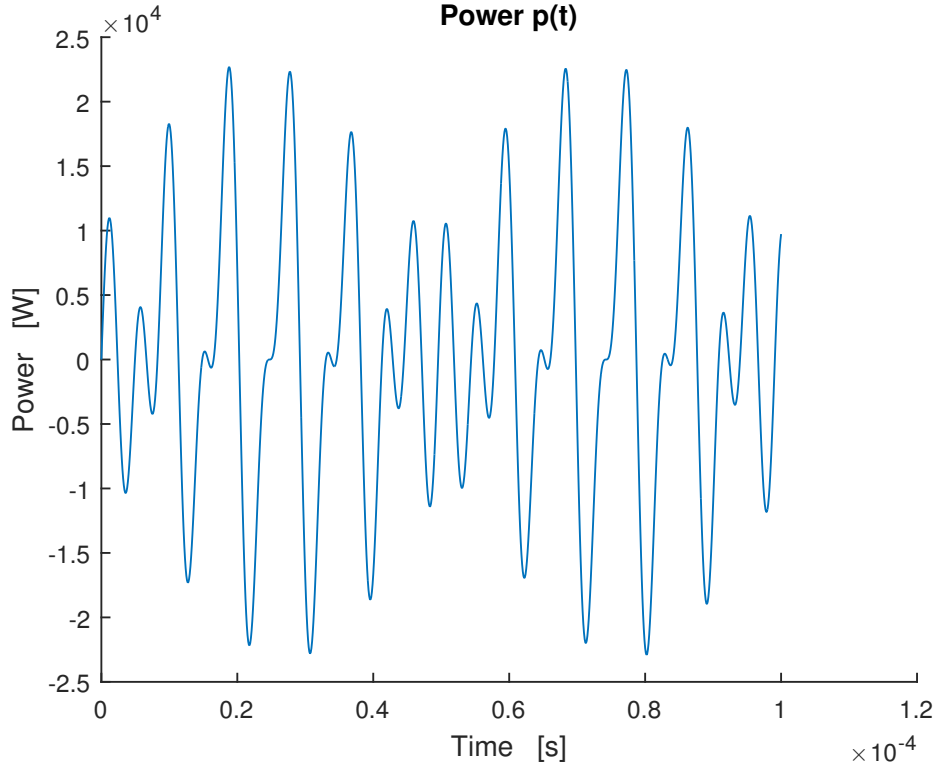
Figure 2.5: Beats that occur in the power wave form. It is possible to view the passeges
to the zero

- $f(t)$ must be continuous or have at least a finished number of discontinuites.

- $f(t)$ must be derivable in time on the period.

- $f(t)$ must be bounded.

It easy understand that the wave forms taken into occunt respect all these
criteria. This means that Fourier's Analyssis can be an extremely usefull tool for
SDF supplying. The trigonometric form of Fourier's transform is:

$$f(t) = a_0 + \sum_{k=1}^{N} \left(a_k \cos\left(\frac{2\pi}{T}kt\right) + b_k \sin\left(\frac{2\pi}{T}kt\right) \right) \qquad (2.19)$$

where a_0, a_k, b_k are coefficients of Fourier's components.

$$a_0 = \frac{2}{T} \int_{-\frac{T}{2}}^{\frac{T}{2}} f(t)\, dt \qquad (2.20)$$

$$a_k = \frac{2}{T} \int_{-\frac{T}{2}}^{\frac{T}{2}} f(t) \cdot \cos\left(\frac{2\pi}{T}kt\right) dt \qquad (2.21)$$

$$b_k = \frac{2}{T} \int_{-\frac{T}{2}}^{\frac{T}{2}} f(t) \cdot \sin\left(\frac{2\pi}{T}kt\right) dt \qquad (2.22)$$

With this approach it is possible to study electrical sources of the inductor. The voltage is imposed and this means that exist only two frequencies components:

$$V_{10kHz} = V_{mf} \tag{2.23}$$

$$V_{100kHz} = V_{hf} \tag{2.24}$$

For an ideal inductive load the current that flows through voltage generators is

$$I_{10kHz} = \frac{V_{mf}}{2\pi f_{mf}} \frac{1}{L} \tag{2.25}$$

$$I_{100kHz} = \frac{V_{hf}}{2\pi f_{hf}} \frac{1}{L} \tag{2.26}$$

This means that the current shows two components that evolve with the two imposed frequencies. Therefore also generated magnetic field shows the same waveform. Now it is possible to analyze the istantaneous absorbed power in the same way as done for current and voltage.

$$P_{20kHz} = \frac{V_{mf}^2}{2L} 2\pi f_{mf} \tag{2.27}$$

$$P_{200kHz} = \frac{V_{hf}^2}{2L} 2\pi f_{hf} \tag{2.28}$$

$$P_{90kHz} = \frac{V_{hf}V_{mf}}{2L} \frac{f_{hf} - f_{mf}}{2\pi f_{hf}f_{mf}} \tag{2.29}$$

$$P_{110kHz} = \frac{V_{hf}V_{mf}}{2L} \frac{f_{hf} + f_{mf}}{2\pi f_{hf}f_{mf}} \tag{2.30}$$

Then the power shows four main frequencies. Particularly interesting is to the understand the amplitudes of the different components.

You can define, a general relationship between the frequencies

$$K = \frac{f_{hf}}{f_{mf}}$$

and a general relationship between voltages:

$$S = \frac{V_{hf}}{V_{mf}}$$

This makes it possible to obtain a relationship between the various components of the instantaneous power, varying the ratios of voltages and frequencies. Than the four power components are:

$$P_{2MF} = \frac{V_{mf}^2}{4\pi L f_{mf}} \tag{2.31}$$

$$P_{2HF} = \frac{V_{mf}^2}{4\pi L f_{mf}} \cdot \frac{S^2}{K} \tag{2.32}$$

$$P_{HF-MF} = \frac{V_{mf}^2}{4\pi L f_{mf}} \cdot \frac{S(K+1)}{K} \tag{2.33}$$
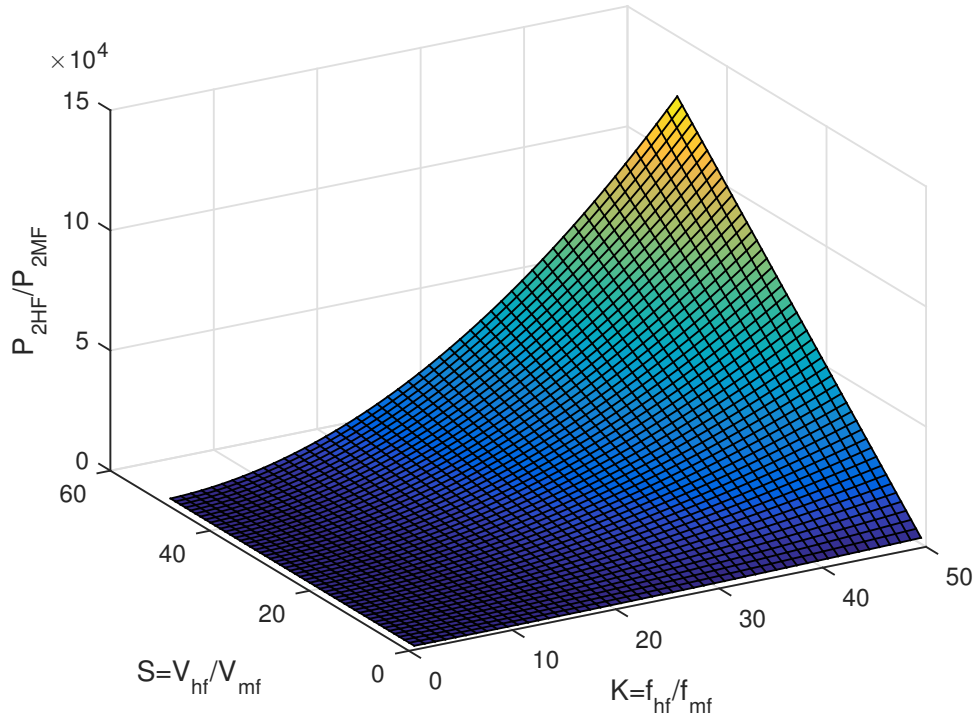
Figure 2.6: Power in high frequency normalized with respect to that evolves with the double of the medium frequency. It is function of both the parameters $K = \frac{f_{hf}}{f_{mf}}$ and $S) = \frac{V_{hf}}{V_{mf}}$

$$P_{HF+MF} = \frac{V_{mf}^2}{4\pi L f_{mf}} \cdot \frac{S(K-1)}{K} \qquad (2.34)$$

In this way you can see how varied the harmonic content of the power , by varying the two fundamental parameters S and K.

With this approach it is possible to understand how changes accordingly the harmonic spectrum of power. It is clear from the figure that the component of the power that evolves with the double of the high frequency tends to decrease with increasing ratio K , ie the higher the difference between high frequency and medium frequency. Instead varying the ratio S and maintaining frequencies fixed ,it is clear that, with an equal power component which evolves with the frequency equal to twice the medium $(2f_{mf})$, the component P_{2HF} tends to increase in a very marked way with respect to the components to lower frequencies.

RL series

The problem can be generalized further, with an equivalent model that also contains a resistive component. This model is more in accord with the true physics of the problem. The pattern then consists of a RL series, where the inductance and the electrical resistance are equivalent parameters of the coupled model (inductor and billet). For simplicity it is possible to consider to feed, instead of in voltage, in
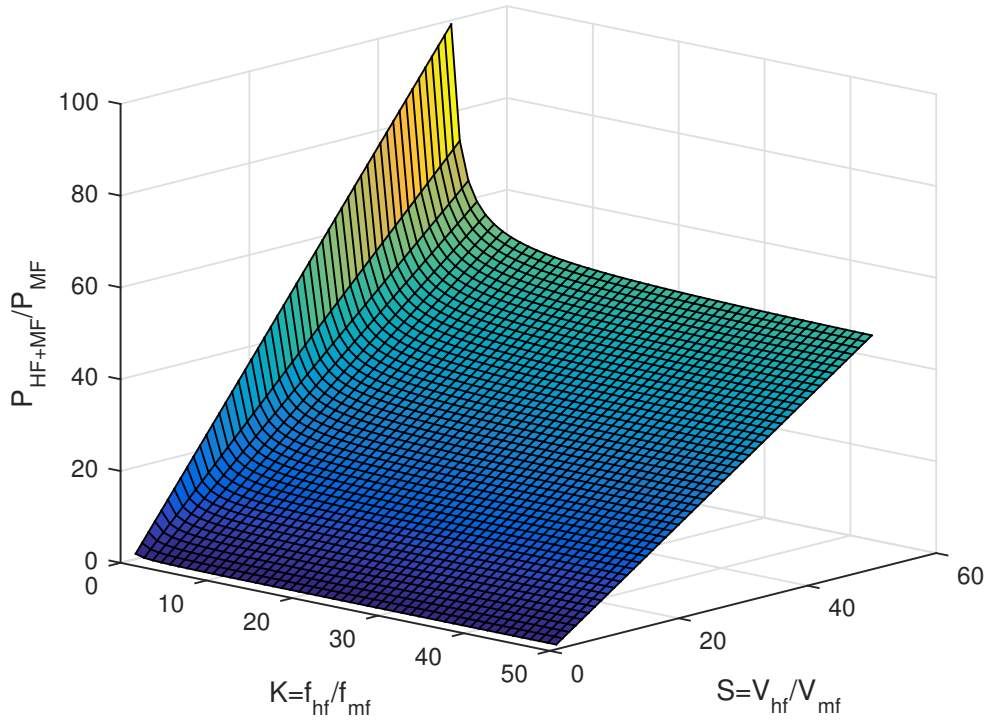
Figure 2.7: Power that evolves with the sum between high and medium frequency normalized with respect to that evolves with the double of the medium frequency.

current the system. This means that now the source of the model is a current:

$$i(t) = I_{hf} \sin(\omega_{hf}t) + I_{mf} \sin(\omega_{mf}t) \tag{2.35}$$

The voltage equation than is

$$v(t) = Ri(t) + L\frac{\partial i(t)}{\partial t} \tag{2.36}$$

Then you can write the voltage across the series as:

$$\begin{aligned} v(t) = &RI_{hf} \sin(\omega_{hf}t) + RI_{mf} \sin(\omega_{mf}t) + \\ &+ L\omega_{hf}I_{hf} \cos(\omega_{hf}t) + L\omega_{mf}I_{mf} \cos(\omega_{mf}t) \end{aligned} \tag{2.37}$$

As seen previously, the instantaneous power absorbed by the model is the product of voltage and current, this means that

$$\begin{aligned} p(t) = &v(t) \cdot i(t) = p_0(t) + p_{2HF}(t) + p_{2MF}(t) + p_{HF+MF} + p_{HF-MF} + \\ &+ q_{2HF}(t) + q_{2MF}(t) + q_{HF+MF}(t) + q_{HF-MF}(t) \end{aligned} \tag{2.38}$$

The instantaneous power is seen to be formed from four basic terms , which are closely related respectively to the active and reactive power absorbed by the hardening system.
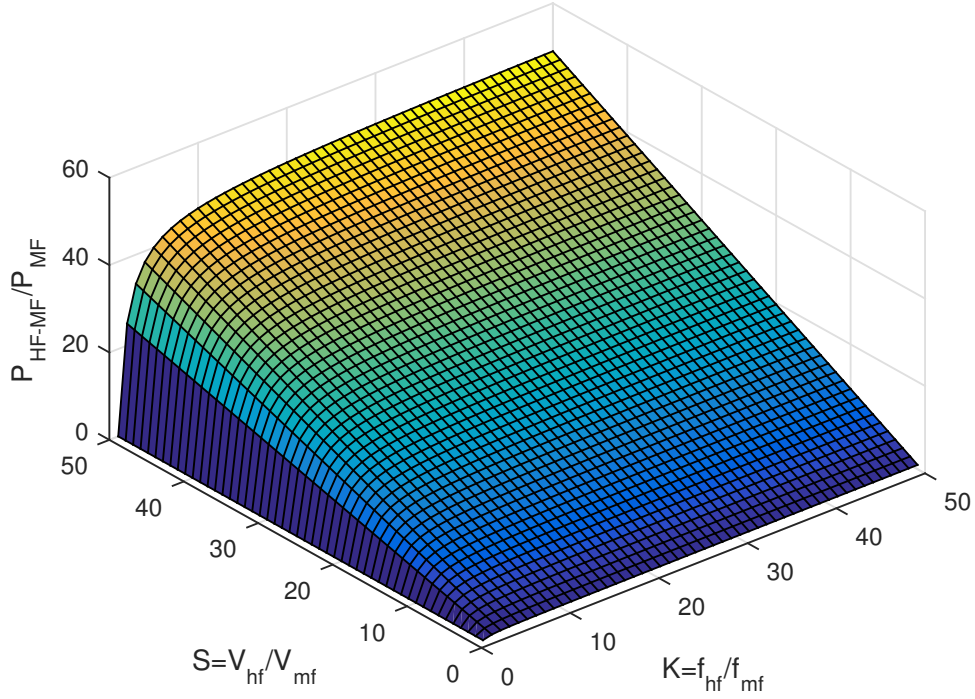
Figure 2.8: Power that evolves with the difference between high and medium frequency normalized with respect to that evolves with the double of the medium frequency.

So it is interesting to explain the various terms, with the help of Prosthaphaeresis and Bisection rules respectively as:

$$P_0 = \frac{R}{2} \left(I_{hf}^2 + I_{mf}^2 \right) \tag{2.39}$$

$$p_{2HF}(t) = -\frac{R}{2} I_{hf}^2 \cos\left(2\omega_{hf}\right) \tag{2.40}$$

$$p_{2MF}(t) = -\frac{R}{2} I_{mf}^2 \cos\left(2\omega_{mf}\right) \tag{2.41}$$

$$p_{HF+MF}(t) = -R I_{hf} I_{mf} \cos\left(\omega_{hf} + \omega_{mf}\right) \tag{2.42}$$

$$p_{HF-MF}(t) = R I_{hf} I_{mf} \cos\left(\omega_{hf} - \omega_{mf}\right) \tag{2.43}$$

$$q_{2HF}(t) = \frac{L I_{hf}^2 \omega_{hf}}{2} \sin\left(2\omega_{hf}t\right) \tag{2.44}$$

$$q_{2MF}(t) = \frac{L I_{mf}^2 \omega_{mf}}{2} \sin\left(2\omega_{mf}t\right) \tag{2.45}$$

$$q_{HF+MF}(t) = \frac{L I_{hf} I_{mf}}{2} \left(\omega_{hf} + \omega_{mf}\right) \sin\left((\omega_{hf} + \omega_{mf})t\right) \tag{2.46}$$

$$q_{HF-MF}(t) = \frac{L I_{hf} I_{mf}}{2} \left(\omega_{hf} - \omega_{mf}\right) \sin\left((\omega_{hf} - \omega_{mf})t\right) \tag{2.47}$$
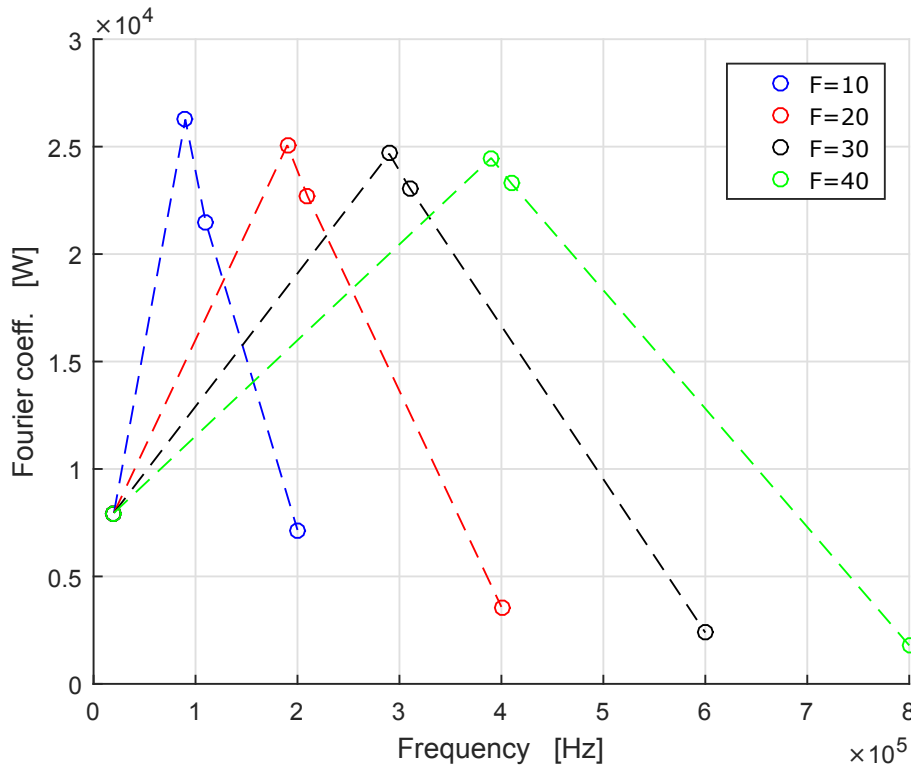
Figure 2.9: Fourier's harmonic distribution. It is possible understand how different the harmonic spectrum , varying the frequency of the sources.

As for the case of purely inductive model, it is possible to try to make explicit the average power in a period electromagnetic. With simple mathematical manipulations you obtain the following formulas for the average powers.

$$< p_0(t) > = \frac{1}{T} \int_0^T p_0(t)\, dt = \frac{R}{2} \left(I_{hf}^2 + I_{mf}^2 \right) \tag{2.48}$$

$$< p_{2HF} > = < p_{2MF} > = 0 \tag{2.49}$$

$$< p_{HF+MF} > = -\frac{1}{T} \frac{R I_{hf} I_{mf}}{\omega_{hf} + \omega_{mf}} \sin\left(2\pi \frac{f_{hf} + f_{mf}}{f_{mf}} T\right) \tag{2.50}$$

$$< p_{HF-MF} > = \frac{1}{T} \frac{R I_{hf} I_{mf}}{\omega_{hf} + \omega_{mf}} \sin\left(2\pi \frac{f_{hf} - f_{mf}}{f_{mf}} T\right) \tag{2.51}$$

This means that these two terms that evolves with the sum and difference of the two main frequencies have a non zero avarage power only if the two frequencies are not in an integer ratio. This phenomenon is due to the appearance of two terms in power that evolve with the sum and difference of the two carrier frequencies of the supply (voltage or current). The remaining terms which have the inductance as coefficient are omitted , as they have a shape essentially similar to that seen in the previous paragraph. it is clear that it is possible to achieve the same result, if instead of the full development of the terms, you try to get the true RMS value of
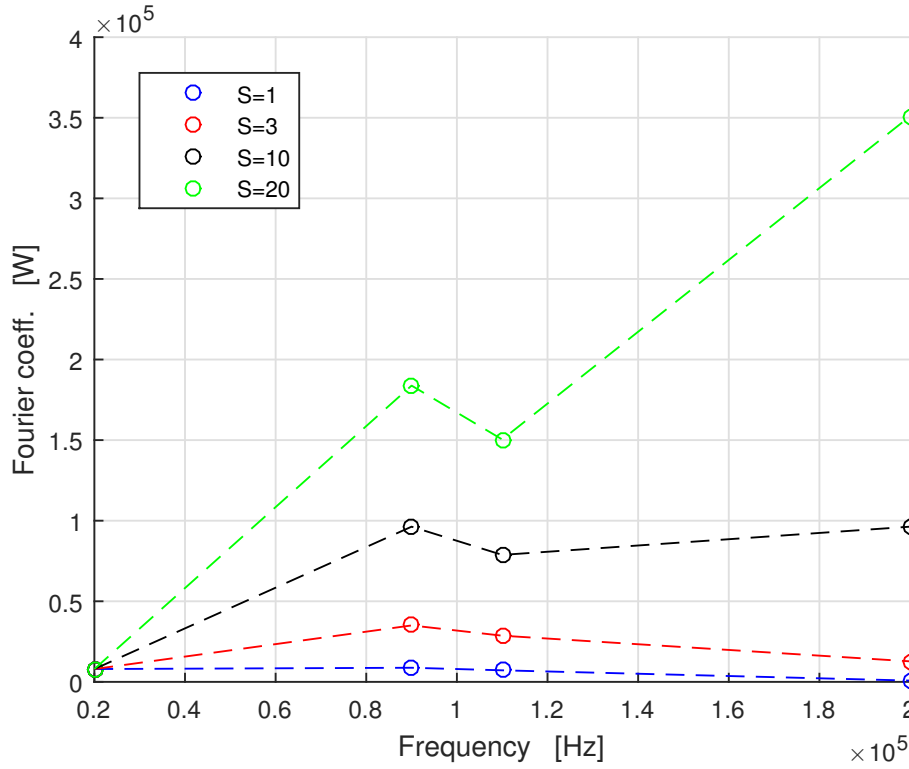
Figure 2.10: Fourier's harmonic distribution. It is possible understand how different the harmonic spectrum , varying the voltage amplitudes of the sources.

the current, from which it is then possible to derive the active power.

$$P_{AVG} = R \cdot I_{RMS}^2 = R \cdot \left(\sqrt{\frac{1}{T} \int_0^T i^2(t) \, dt} \right)^2 \tag{2.52}$$

where I_{RMS} $[A]$ is the true rms value of the current waveform. and this therm is exactly the same of Equation 2.39

The model that has been solved by the FEM software has as its source a voltage generator which imposes a specific waveform on the inductor. So it is more interesting to try to complicate the model, analyzing the response of the series RL considering a voltage source instead of a current source. This means that the generator requires the electrical circuit a waveform of the type:

$$v(t) = V_{hf} \cos (\omega_{hf} t) + V_{mf} \cos (\omega_{mf} t) \tag{2.53}$$

Then if it is possible to write the current in a general form as:

$$i(t) = I_{hf} \sin (\omega_{hf} t + \delta_{hf}) + I_{mf} \sin (\omega_{mf} t + \delta_{mf}) \tag{2.54}$$

Then it is possible to simplify the formulation by means of simple steps, whereas the general form of the voltage imposed to the generator as:

$$v(t) = Ri(t) + L \frac{\partial i(t)}{\partial t} \tag{2.55}$$

Then the instantaneous current can be expressed as also:

$$i(t) = \frac{\omega_{hf} L V_{hf}}{(L\omega_{hf})^2 + R^2} \sin(\omega_{hf}t) + \frac{\omega_{mf} L V_{mf}}{(L\omega_{mf})^2 + R^2} \sin(\omega_{mf}t) +$$
$$+ \frac{R V_{hf}}{(L\omega_{hf})^2 + R^2} \cos(\omega_{hf}t) + \frac{R V_{mf}}{(L\omega_{mf})^2 + R^2} \cos(\omega_{mf}t)$$
(2.56)

Then in the same way as done in the previous paragraph it is then possible to define the instantaneous value of the power supplied by the generator. In this way you get eight terms which constitute the instantaneous power . One of these terms is continuous and corresponds to the average power absorbed by the load P_0 [W], four co-sinusoidal terms within which evolve with the four frequencies previously views: A_{2HF},A_{2MF},A_{HF+MF},A_{HF-MF}, and four sinusoidal terms always that evolve with the same frequencies B_{2HF},B_{2MF},B_{HF+MF},B_{HF-MF}. Of particular interest is the constant term , which reconstructs the power absorbed by the total system . Recall that the resistance and inductance into account both the billet and the inductor. So within this term they are also kept count dellle inductor losses . The power is dissipated by Joule losses on the inductor load system must be dissipated by the cooling system of the inductor itself.

$$P_0 = <p> = \frac{1}{T} \int_0^T p(t)\, dt =$$
$$= \frac{R}{2} \left(\frac{V_{hf}^2}{(L\omega_{hf})^2 + R^2} + \frac{V_{mf}^2}{(L\omega_{mf})^2 + R^2} \right)$$
(2.57)

If you try to isolate the various terms that make up the power, you can effectively isolate the various factors that make up the Fourier series of power. The term $\P_0$ in fact is precisely the constant term of the Fourier series. Similarly it is possible to define all the components of the various terms that make the istantaneous power. Through simple mathematical it easy to get the eight terms:

$$A_{2HF} = \frac{1}{2} \frac{R}{(L\omega_{hf})^2 + R^2} V_{hf}^2$$
(2.58)

$$A_{2MF} = \frac{1}{2} \frac{R}{(L\omega_{mf})^2 + R^2} V_{mf}^2$$
(2.59)

$$A_{HF+MF} = A_{HF-MF} = \frac{1}{2} R \left(\frac{1}{(L\omega_{mf})^2 + R^2} + \frac{1}{(L\omega_{hf})^2 + R^2} \right) V_{hf} V_{mf}$$
(2.60)

$$B_{2HF} = \frac{1}{2} \frac{\omega_{hf} L}{(L\omega_{hf})^2 + R^2} V_{hf}^2$$
(2.61)

$$B_{2MF} = \frac{1}{2} \frac{\omega_{mf} L}{(L\omega_{mf})^2 + R^2} V_{mf}^2$$
(2.62)

$$A_{HF+MF} = \frac{1}{2} \left(\frac{\omega_{hf} L}{(L\omega_{hf})^2 + R^2} + \frac{\omega_{mf} L}{(L\omega_{mf})^2 + R^2} \right) V_{hf} V_{mf}$$
(2.63)

$$A_{HF-MF} = \frac{1}{2} \left(\frac{\omega_{hf} L}{(L\omega_{hf})^2 + R^2} - \frac{\omega_{mf} L}{(L\omega_{mf})^2 + R^2} \right) V_{hf} V_{mf}$$
(2.64)

where the various terms in function of time are:

$$a_{2HF} = A_{2HF} \cos\left(2\omega_{hf}\right) \tag{2.65}$$

$$a_{2MF} = A_{2MF} \cos\left(2\omega_{mf}\right) \tag{2.66}$$

$$a_{HF+MF} = A_{HF+MF} \cos\left(\omega_{hf} + \omega_{mf}\right) \tag{2.67}$$

$$a_{HF-MF} = A_{HF-MF} \cos\left(\omega_{hf} - \omega_{mf}\right) \tag{2.68}$$

$$b_{2HF} = B_{2HF} \sin\left(2\omega_{hf}\right) \tag{2.69}$$

$$b_{2MF} = B_{2MF} \sin\left(2\omega_{mf}\right) \tag{2.70}$$

$$b_{HF+MF} = B_{HF+MF} \sin\left(\omega_{hf} + \omega_{mf}\right) \tag{2.71}$$

$$b_{HF-MF} = B_{HF-MF} \sin\left(\omega_{hf} - \omega_{mf}\right) \tag{2.72}$$

After developed all the terms it is still possible try to find a more compact formulation, trying to write the instantaneous power as the sum of a constant term plus four cosine terms that evolve with the four main frequencies. It is possible to do that, considering the relationship:

$$A \cos\left(x\right) + B \sin\left(x\right) = \sqrt{A^2 + B^2} \cos(x - \delta) \tag{2.73}$$

where δ is the phase shift $[rad]$

$$\delta = \tan^{-1}\left(\frac{B}{A}\right) \tag{2.74}$$

If you make that transformation for all terms of the power, you may understand how the istantaneous power evolwes in time. It is clearly made by four terms that evolve with the four frequencies $2 \cdot f_{hf}$, $2 \cdot f_{mf}$, $f_{hf} + f_{mf}$, $f_{hf} - f_{mf}$ $[Hz]$. Then it is possible to define four coefficients:

$$W_{2HF} = \sqrt{A_{2HF}^2 + B_{2HF}^2} \tag{2.75}$$

$$W_{2MF} = \sqrt{A_{2MF}^2 + B_{2MF}^2} \tag{2.76}$$

$$W_{HF+MF} = \sqrt{A_{HF+MF}^2 + B_{HF+MF}^2} \tag{2.77}$$

$$W_{HF-MF} = \sqrt{A_{HF-MF}^2 + B_{HF-MF}^2} \tag{2.78}$$

and finally the four phase shift:

$$\delta_{2HF} = \arctan\left(\frac{B_{2HF}}{A_{2HF}}\right) \tag{2.79}$$

$$\delta_{2MF} = \arctan\left(\frac{B_{2MF}}{A_{2MF}}\right) \tag{2.80}$$

$$\delta_{HF+MF} = \arctan\left(\frac{B_{HF+MF}}{A_{HF+MF}}\right) \tag{2.81}$$

$$\delta_{HF-MF} = \arctan\left(\frac{B_{HF-MF}}{A_{HF-MF}}\right) \tag{2.82}$$

Thanks to this rewriting of the istantaneous power is finally possible try to plot the distribution of the coefficient of the varoius terms as function of the frequency. Initially with a fixed value of voltages, and then trying to vary the ratio between high frequency voltage and medium frequency voltage. To understand the various waveforms and the typical behavior of the system SDF in the final part of this chapter contains several charts that summarize when called and processed.
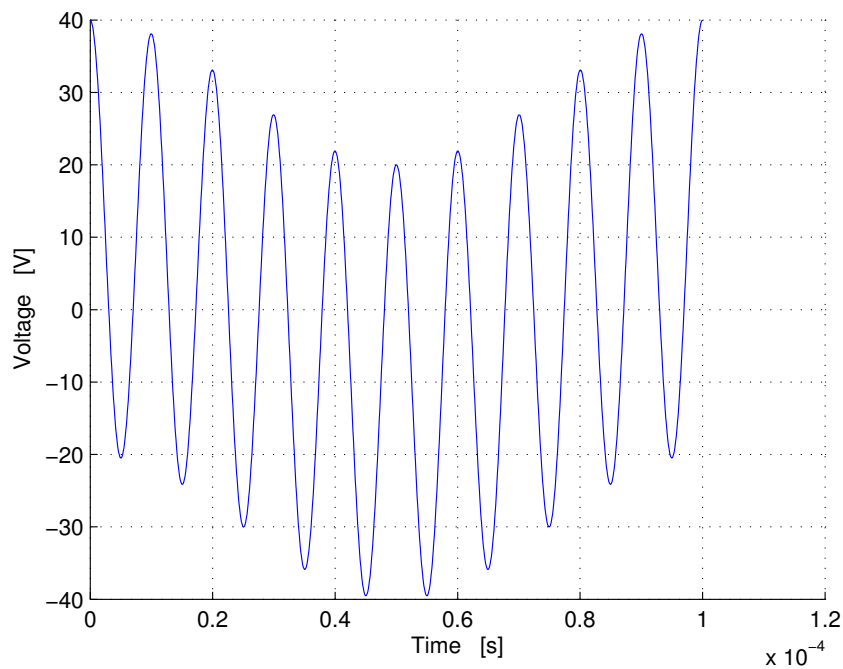
Figure 2.11: Istantaneous voltage delivered by the generator $v(t)$ $[V]$
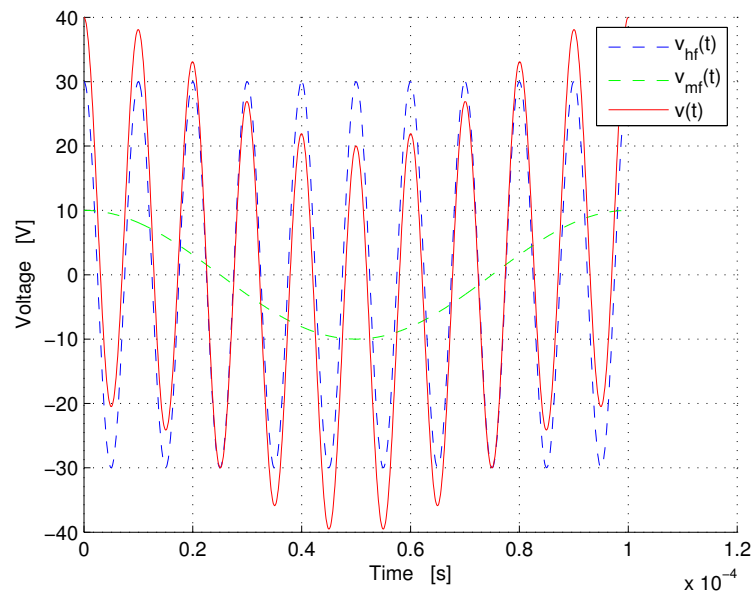
Figure 2.12: Two components of the voltage $v_{hf}(t)$ and $v_{mf}(t)$ $[V]$
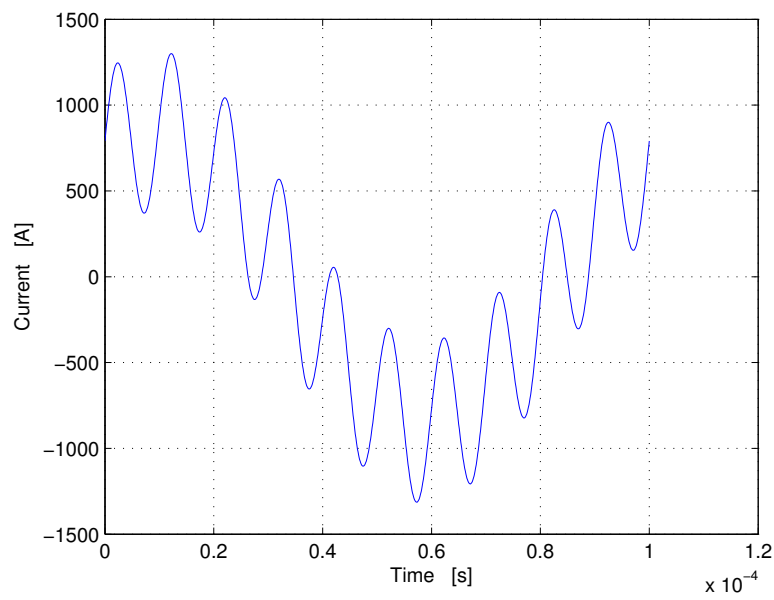
Figure 2.13: Istantaneous current absorbed by the load $i(t)$ $[A]$
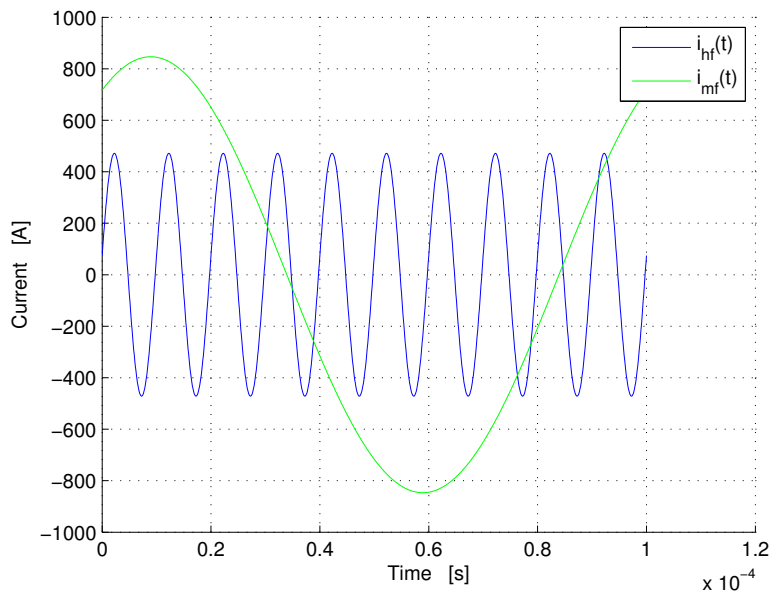
Figure 2.14: Two components of the current $i_{hf}(t)$ and $i_{mf}(t)$ [A]
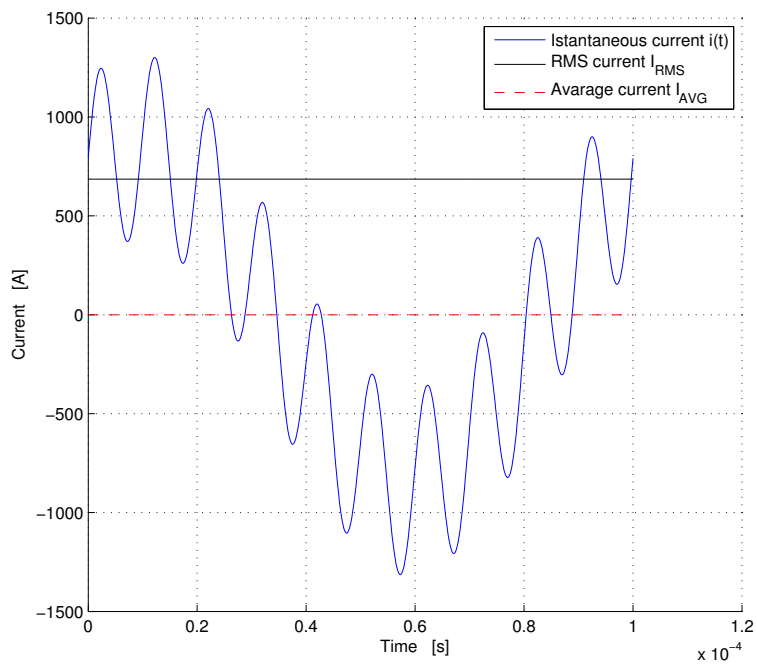
Figure 2.15: Istantaneous current absorbed by the load $i(t)$ [A] and its avarage and RMS values
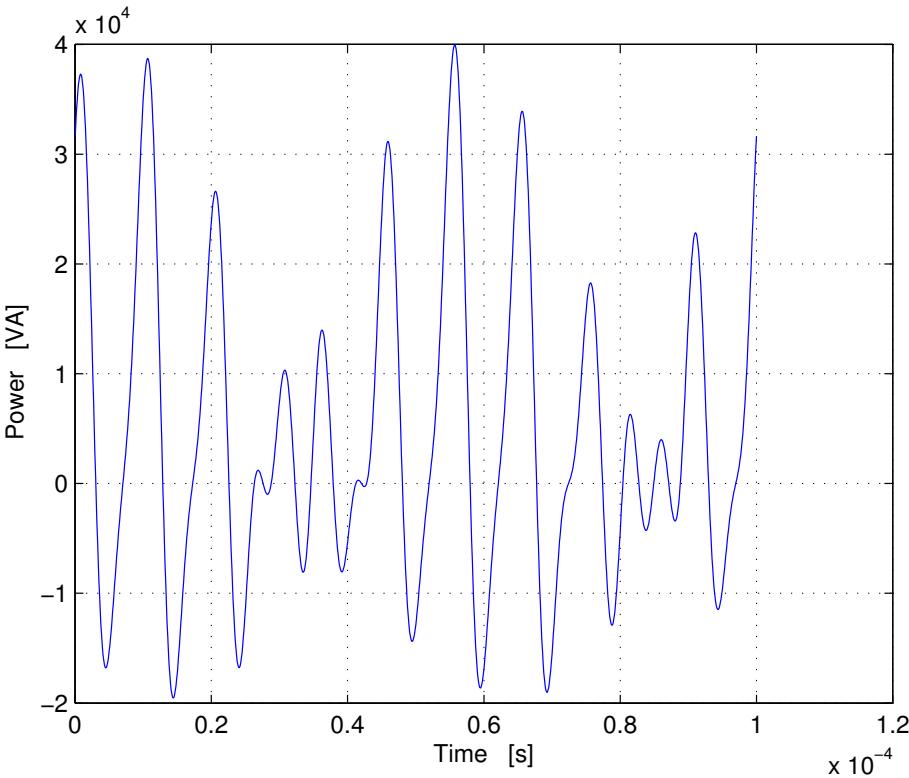
Figure 2.16: Istantaneous power absorbed by the load $p(t)$ $[VA]$
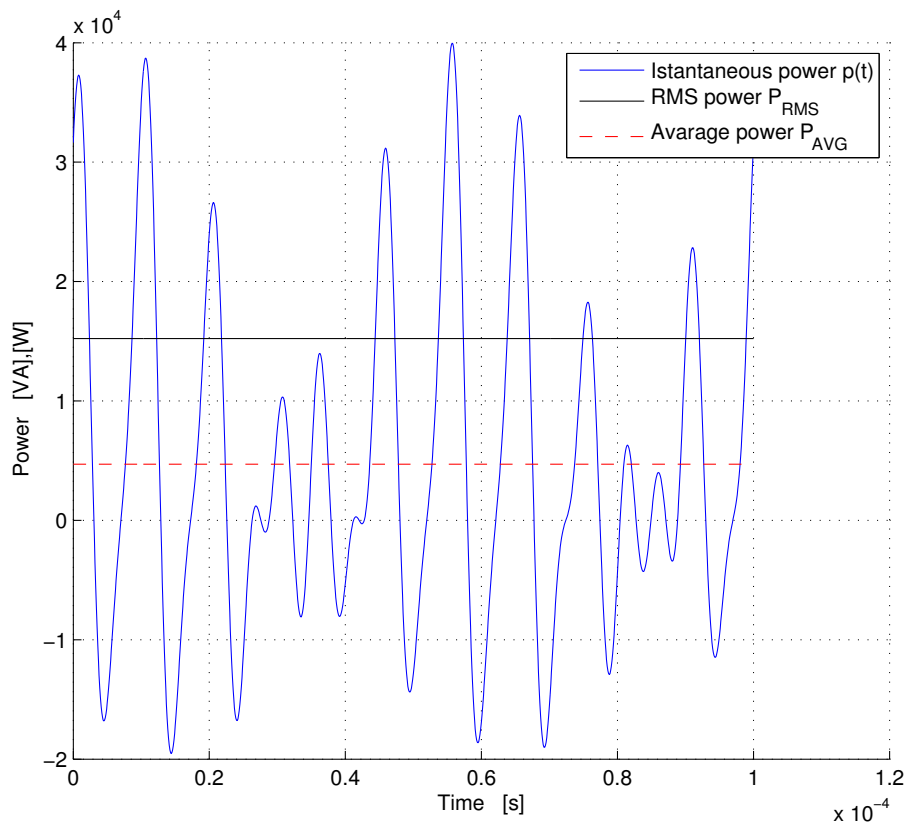
Figure 2.17: Power $p_{(}t)$ and $P_{AVG}(t)$ $[W]$ and P_{RMS} $[VA]$

Finally also in this case it is interesting have a look of the distribution of voltage, current and power in the frequency plane. This means that the Fourier's coefficients of various electrical functions are plotted in the frequency domain. In Figure 2.20 it is possible view what said in this paragraph.
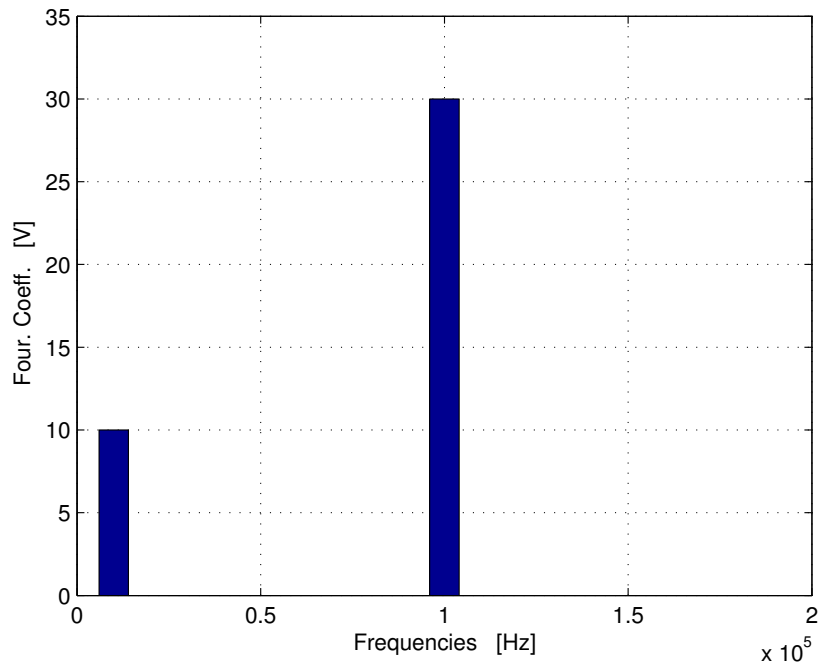
Figure 2.18: Voltage harmonic spectrum for the model developed in this paragraph $V_{hf} = 30$ and $V_{mf} = 10$ $[V]$.
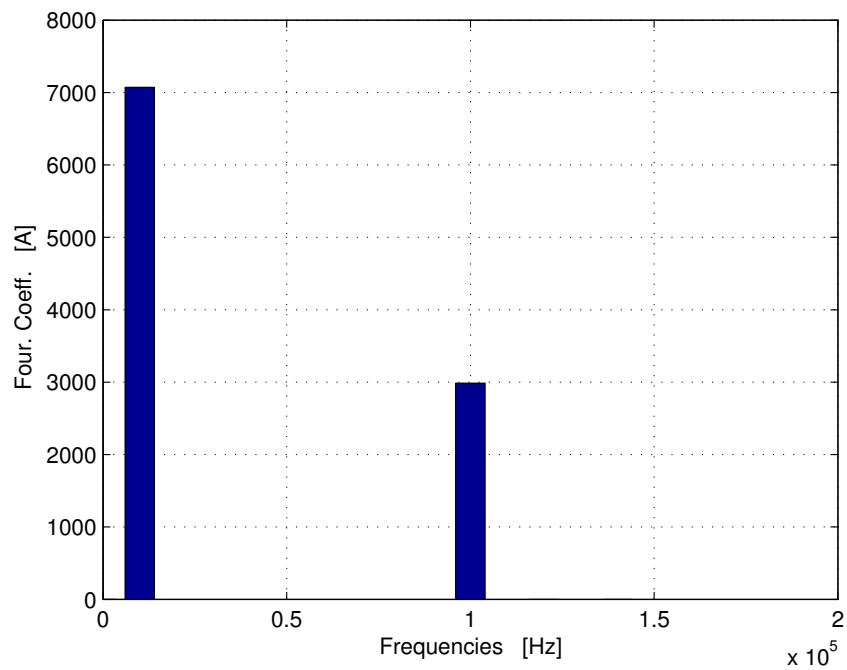
Figure 2.19: Curent harmonic spectrum for the model developed in this paragraph I_{hf} and I_{mf} $[A]$.
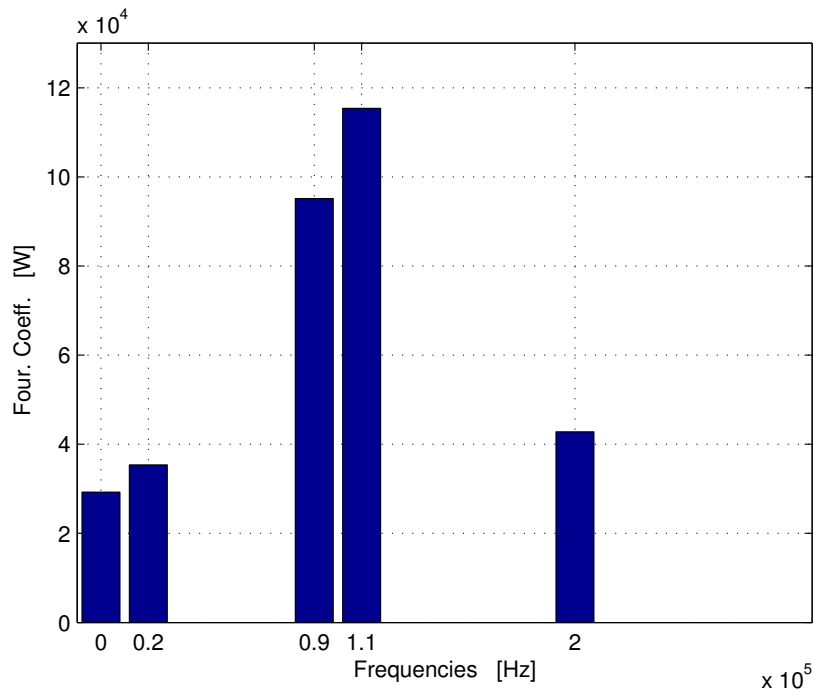
Figure 2.20: Power harmonic spectrum for the model developed in this paragraph.

It is also interesting imagine to vary the ratio $S = \frac{V_{hf}}{V_{mf}}$ and understand how it is possible to vary the harmonic spectrum, with a constant $V_{mf} = 10 \ [V]$.
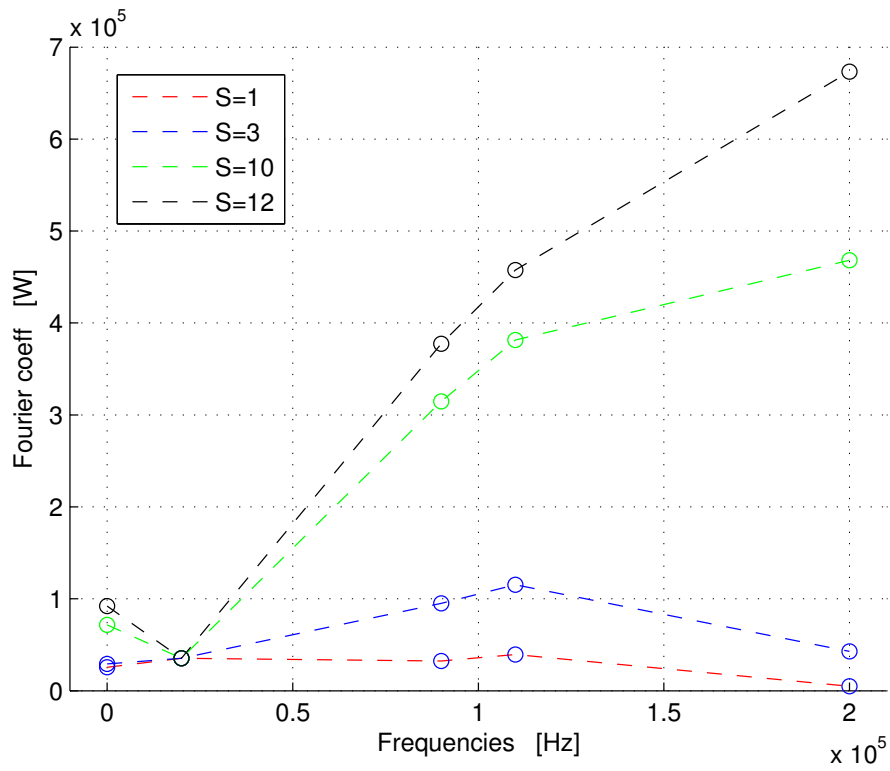
Figure 2.21: Power harmonic spectrum for the model developed in this paragraph varying S.

Chapter 3

FEM - Finite Elements Method

The model developed in this work, takes into account a system constituted by an inductor coupled with a workpiece. Tipically, inductors are toroidal passive electric components, consisting of a circular ring-shaped non ferromagnetic material, such as copper. An inductor with a closed-loop core can have a higher magnetic field and thus higher inductance, indeed the amount of magentic flux that strays outside the core (leakage flux) is minimum.

For heat treatment processes the inductor is necessary to induce Foucault currents into the workpiece. From an electric point of view, therefore it is possible to study that process with the model of the transformer, where the inductor is the primary of the transformer and the workpiece is the secondary. Advantages of this system is that, supplying the inductor with high frequency wave forms it is possible to transfer power in extremely thin layers inside the workpiece. This work considers afterwards an axial symmetric model. This means that must have

- Geometrical symmetry, in other words must be possible to describe the components in the $[r, z]$ plane of a r, z, φ coordinate system.

- Physical symmetry, that means some field spatial components can be neglected.

- Wymmetry of sources. This particularly for our models means that for example the current, that is imposed to enter in the inductor (for $r > 0$) must exit from the inductor (for $r < 0$).

This simplification of the problem is sufficiently in accord with a real component. Probably the main effects that are not take into account are the border effects that occur for the anisotropy due to the connection to the busbar.

Neglecting this effect, therefore it is possible to develope the MQS (magneto quasi static) formulation for an axial symmetrical model:

$$\nabla \times \nu \nabla \times \mathbf{A} + \sigma \frac{\partial \mathbf{A}}{\partial t} + \sigma \nabla V = 0 \qquad (3.1)$$

$$\nabla \cdot \frac{\partial \mathbf{A}}{\partial t} = -\nabla \cdot \nabla V \qquad (3.2)$$

where, as already seen, $\mathbf{A}$ is the magnetic vector potential, V is the electric scalar potential, σ is the electrical conducticity and $\nu = \frac{1}{\mu}$ is the magnetic reluctivity. Now
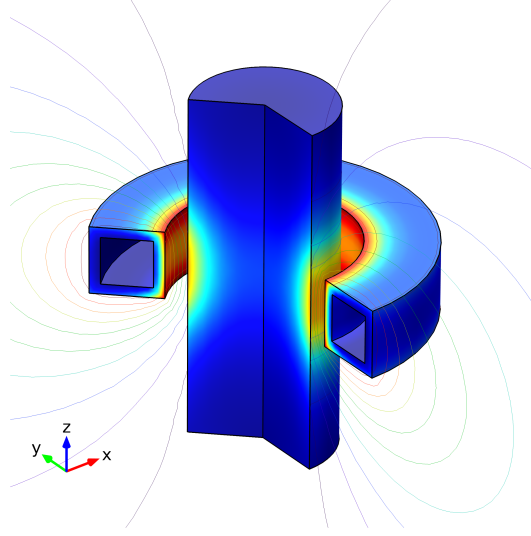
Figure 3.1: Example of an axial symmetric geometry. In figure is represented the coupled system of an rectangular copper coil inductor and a steel bellet. It is possible to view that this kind of system has also physical symmetry.

to develope the model it is important to understand the components of the fields that describe the problem. Thinking of supplying the inductor with a current density that is normal to the plane (r, z); magnetic field H may have only z-component, than in a interesting matematical form:

$$\mathbf{H} = [H_r, H_z, H_\varphi] = [H_r, H_z, 0] = H_r\mathbf{u_r} + H_z\mathbf{u_z}$$

$$\mathbf{J} = [J_r, J_z, J_\varphi] = [0, 0, J_\varphi] = J_{varphi}\mathbf{u_\varphi}$$

and $\mathbf{B} \nearrow\nearrow \mathbf{H}$, $\mathbf{E} \nearrow\nearrow \mathbf{J}$ because of magnetic permeability and electrical conductivity are isotropic.

Now there is the necessity of developing curl, divergence and gradient formulations for an axial symmetric coordinate system:

$$\nabla \times \mathbf{W} = (\frac{1}{r}\frac{\partial W_z}{\partial \varphi} - \frac{\partial W_\varphi}{\partial z})\mathbf{u_r} + (\frac{\partial W_\varphi}{\partial z} - \frac{\partial W_z}{\partial r})\mathbf{u_\varphi} + \frac{1}{r}(\frac{\partial rW_\varphi}{\partial r} - \frac{\partial W_r}{\partial \varphi})\mathbf{u_z} \quad (3.3)$$

$$\nabla \cdot \mathbf{W} = \frac{1}{r}\frac{\partial rA_r}{\partial r} + \frac{1}{r}\frac{\partial A_\varphi}{\partial \varphi} + \frac{\partial A_z}{\partial z} \quad (3.4)$$

$$\nabla f = \frac{\partial f}{\partial r}\mathbf{u_r} + \frac{1}{r}\frac{\partial f}{\partial \varphi}\mathbf{u_\varphi} + \frac{\partial f}{\partial z}\mathbf{u_z} \quad (3.5)$$

Now for what just seen, the formulation of the various terms that form the equation 3.1 can be rewritten as follows. Because of the curl of a vector must be normal to the vector: $\nabla \times \mathbf{A} \perp \mathbf{A}$ then as a consequence the magnetic vector potential must have only φ-component. This fact can be easily seen from the next equation, that is the first term of the general equation 3.1

$$\nabla \times \nu\nabla \times \mathbf{A} = -(\frac{\partial}{\partial z}\nu\frac{\partial A_\varphi}{\partial z} + \frac{\partial}{\partial r}\frac{\nu}{r}\frac{\partial rA_\varphi}{\partial r})\mathbf{u_\varphi}$$

$$\nabla \cdot \sigma \frac{\partial \mathbf{A}}{\partial t} = \frac{1}{r} \frac{\partial}{\partial \varphi} \sigma \frac{\partial A_\varphi}{\partial t} = 0$$

because the φ-component of the magnetic potential can not be function of φ, in other words $A_\varphi = f(r, z)$. Finally

$$\nabla V = -\mathbf{E} - \frac{\partial \mathbf{A}}{\partial t}$$

that means ∇V has only φ-component, than in cilindrical coordinates:

$$\nabla V = \frac{1}{r} \frac{\partial V}{\partial \varphi} \mathbf{u}_\varphi$$

Now putting togheter the three components of the main equation, we obtain the scalar formulation of the MQS formulation:

$$\frac{\partial}{\partial z} \frac{\nu}{r} \frac{\partial r A_\varphi}{\partial z} + \frac{\partial}{\partial r} \frac{\nu}{r} \frac{\partial r A_\varphi}{\partial r} - \frac{\sigma}{r} \frac{\partial r A_\varphi}{\partial t} = \frac{\sigma}{r} \frac{\partial V}{\partial \varphi} \tag{3.6}$$

And defining as new parameters of the model

$$\nu' = \frac{\nu}{r}$$

$$\phi = r A_\varphi$$

$$\sigma' = -\frac{\sigma}{r}$$

the final equation that full describe a magneto quasi static axial simmetric model is:

$$\frac{\partial}{\partial z} \nu' \frac{\partial \phi}{\partial z} + \frac{\partial}{\partial r} \nu' \frac{\partial \phi}{\partial r} + \nu' \frac{\partial \phi}{\partial t} = J_{s\varphi} \tag{3.7}$$

where the therm $J_{s\varphi}$ describes the source of the system.

$$J_{s\varphi} = -\sigma' \frac{\partial V}{\partial \varphi} \tag{3.8}$$

Coefficients of PDEs become function of the spatial coordinate r, that means materials, from a numerical point of view are not again homogeneuous. But what is the physical meaning of $\phi = r A_\varphi$? To understand whats is the meaning of ϕ we try to explicit the magnetic flux that is linked with the geometry obtained by the rotation around the point O in figure.

Γ is the boundary that $\mathbf{P}$ makes after a rotation. Σ is the surface generated by the boundary Γ.

$$\Phi = \int_\Sigma \mathbf{B} \cdot d\mathbf{S} = \int_\Sigma \nabla \times \mathbf{A} \cdot \mathbf{n} \, dS = \oint_\Gamma \mathbf{A} \cdot \mathbf{t} \, dl \tag{3.9}$$

Fot he axial model $\mathbf{A} = [0, 0, A_\varphi(r, z)]$. Than for a certain fixed point P for which its components are fixed, the magnetic potential can not vary along φ. This means it must be constant for a cartain couple of coordinates. Than the linked magnetic flux Φ is:

$$\Phi = \oint_\Gamma \mathbf{A} \cdot \mathbf{t} \, dl = A_\varphi(2\pi r) = 1\pi\phi \tag{3.10}$$
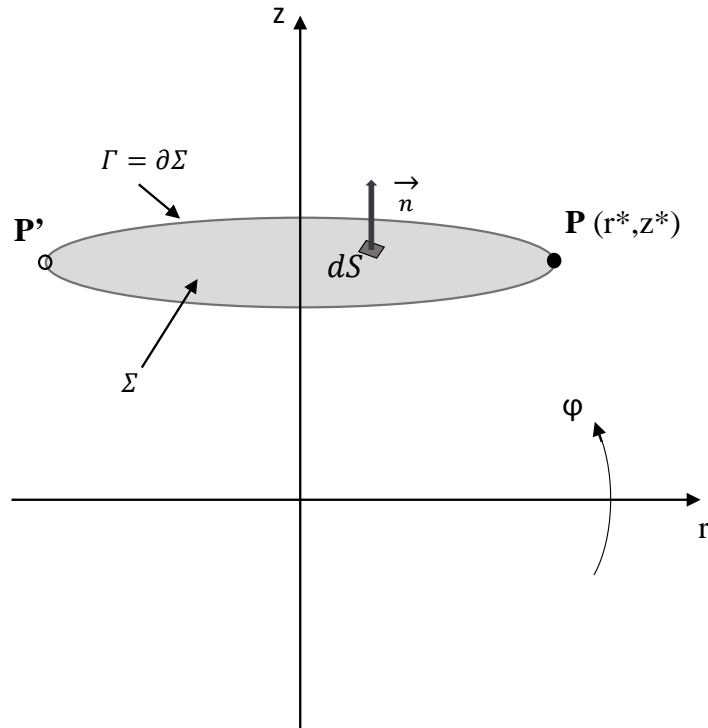
Figure 3.2: Magnetic flux linked with an axial simmetric geometry

3.1   Structure of a Finite Element Method

Finite elements method solves partial differential equations (PDEs), transforming them in linear systems of the type $A\mathbf{x} = \mathbf{b}$ where A is a matrix, typically extremely sparse, $\mathbf{x}$ is the unknown vector and $\mathbf{b}$ is the column of known terms. FEM more generally works with function $f(\mathbf{x})$ and want to find a solution that will be a function. With this approach is possible to solve problems that might be more generally time and space dependent. As already seen in Chapter 1 it is possible to write an electro-magnetic problem in a general form:

$$\nabla \cdot \alpha \nabla U + \delta \frac{\partial U}{\partial t} = \beta \qquad (3.11)$$

where the problem is defined in a domain Ω, in which we impose generally boundary conditions, that for example could be Dirichlet's conditions.

With this approach we want find a potential U that satisfyies simultaneously boundary conditions BC and the PDEs. The kernel of the FEM is that it splits the domain Ω in a finite number of elements. The geometry of elements depends from the space dimension. If for example the problem is a three dimensional model the elements that sets up the domain will be three dimensional, and for example tetrahedra and hexahedra. From an enggineering point of view there is typically the necessity of simplifying a general problem that could be extremely complex. Indeed the solution of very "weight" three dimensional problems, provided that it is possible, could need too much time. This means that for example if a 3D model
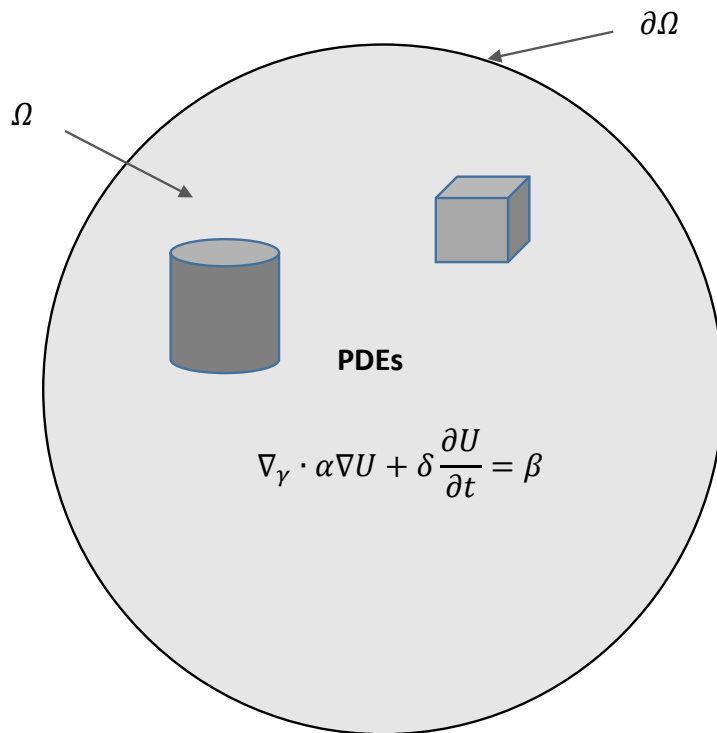
Figure 3.3: General model that a FEM may compute.

has obeyed the axial symmetry, it is strongly advised to study it in a simplyfied way. The next paragraphs will introduce the main points of a finite elements method and the software used to simulate the surface hardening process.

Main points of a FEMs are:

- Mesh

- Shape Function

- Solution

3.1.1   Mesh

Practically the mash is strictly connected with the freedom number of the problem. A domain Ω is splitted as already said in a finite number of elements, that can have an arbitraty dimension. Neglecting the mono dimensional case and focusing on a 2D formulation it is easy to understand that a plane domain cha be divided in a certain number of triangles or rectangles. To correctly mesh a model, elements must enjoy different properties, for example:

- $e_1 \cup e_2 \cup e_3 \cup \ldots = \Omega$. That means the union of all the elements must rebuild all the domain

- $e_i \cap e_j = 0$. Elements can not intersect each other
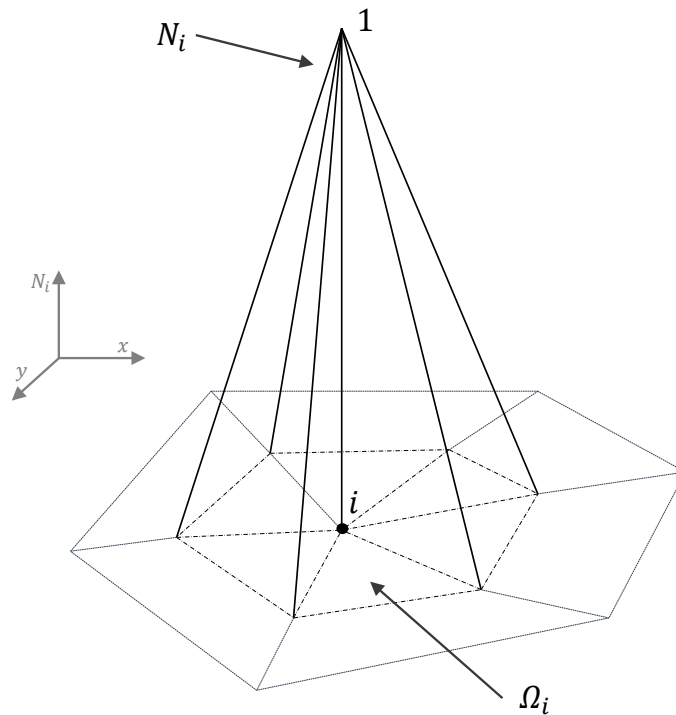
Figure 3.4: Typical shape function with k=1, that means it is linear. Note that out of the region Ω_i $N_i = 0$. i is a general point of the mesh.

- $e_i \not\subseteq e_j$. One element can not be included in one other.

It is clear that if we consider triangular elemets is possible to define for every one its vertices that are Lagrange points. Therefore if we consider a region setted up of a certain number of elements it is possible to find a certain Lagrange point that is surrounded of different elements. The set of elements that have the i-point as vertex is called support of the i-point Ω_i. This entity is extremely important to be able to define shape functions and write an approximate form of the problem that can be solved numerically.

3.1.2 Shape Function

$$
N_i^k = \begin{cases} 0 & \forall e_j \notin \Omega_i \\ 0 & \forall e_j \in \Omega_i \text{ and } r \neq i \\ 1 & \forall e_j \in \Omega_i \text{ and } r = i \end{cases} \tag{3.12}
$$

where r is the global number of the points. N_i^k is an interpolation polynomial which degree is k. The degree of the shape function can be chosen arbitrally, it is important to subline that increasing the degree k requires more points (the so called middle point of edges) and more time to the solver to compute the linear systems.

3.1.3   Global Interpolation

Where e is an element of the domain Ω and N_i^e is the shape function of each element. n_e is the total number of elements of the domain.

After have supposed to can completely solve a problem that can be written in a PDE form, than will exist a solution U for every element of the space. Than if we know the potential U_i for each points of Ω, an that fact in a mathematic way:

$$U_i \forall i \in \Omega$$

In this way it is possible to build a spatial profile U_h that is the approximate form of the potential U

$$U_h = \sum_{i=1}^{n_n} U_i N_i = \sum_{i=1}^{n_n} U_i \sum_{e=1}^{n_e} N_i^e \tag{3.13}$$

This is the approximation of the potential U, defined in each element and in each point of the domain Ω. It is important subline that the discretization of the space is strictly linked with the dimention of the elements. If a mesh was regular, than h would mean the distance between points like in a FDM. In this work it is developed and used the more known weighted residual approach.

3.2   Weighted Residual approach

This approach does not need to define the internal energy of the problem, that typically could be extreamely difficult for an electromagnetic coupled problem. This formulation instead takes into account a formulation like

$$L(U) = 0 \tag{3.14}$$

in addition with specifici boundary conditions (BC). The weighted residual approach defines an equivalence between the PDEs problem and another problem, that is:

$$\int_\Omega w \cdot L(U)\, dV = 0 \tag{3.15}$$

for all the test functions w that can be defined in a general domain Ω. This means that the same function U, that in an electromagnetic problem is the magnetic potential (that is the solution of PDEs), at the same time it is the solution of the integral problem). It could be possible to demonstrate this correlation in both the sense. To solve the weighted residual approach, as in the variational approach, it is necessary to give up to an exact resolution and introduce the approaximate form of the potential U:

$$U_h = \sum_{j=1}^{n_n} U_j N_j$$

This means that the domain that contains the solutions of the problem will be smaller than the domain that contains the exact solutions of the more general problem. And it will be a domain that contains only polinomial functions. At this point to solve the problem and obtain an unique solution it is necessary to introduce a choice: the

Galerkin Choice. This means to reduce the test functions to only particular cases: test functions must be polinomial functions such as shape functions, then:

$$w_i = N_i \tag{3.16}$$

Finally it is possible to write the problem as:

$$\int_\Omega N_i \cdot L(U_h) \, dV = 0 \forall i = 1, 2, ..., n_n \tag{3.17}$$

Particularly for the magneto quasi static problem (MQS), defined in an axial symmetric domain Ω, the residual is:

$$L(U_h) = L(A_{\varphi h}) = \nabla \cdot \nu \nabla \sum_{j=1}^{n_n} A_{\varphi j} N_j - \sigma \frac{\partial}{\partial t} \sum_{j=1}^{n_n} A_{\varphi j} - J_{s\varphi} = 0 \tag{3.18}$$

and finally the problem that might be solved, for all the points of the domain Ω, in its integral form is

$$\int_\Omega N_i \cdot (\nabla \cdot \nu \nabla \sum_{j=1}^{n_n} A_{\varphi j} N_j - \sigma \frac{\partial}{\partial t} \sum_{j=1}^{n_n} A_{\varphi j} - J_{s\varphi}) \, dV = 0 \tag{3.19}$$

Observing that the function that might be integrated, can't be a continuous function, it is necessary to define the multidimensional form of the INTEGRAZIONI PER PARTI:

$$\int_a^b f \cdot g' \, dx = f \cdot g(b) - f \cdot g(a) - \int_a^b g \cdot f' \, dx$$

and in our particular case:

$$f = N_i$$

$$g' = \nabla \cdot \nu \nabla \sum_{j=1}^{n_n} A_{\varphi j} N_j - \sigma \frac{\partial}{\partial t} \sum_{j=1}^{n_n} A_{\varphi j} - J_{s\varphi}$$

This means that the integration can be splitted in two different therms, having defined the initial integral as I, than:

$$I = -\int_\Omega N_i \cdot (\nu \frac{\partial A_{\varphi h}}{\partial t} - J_{s\varphi}) \, dV - \int_\Omega \nabla N_i \cdot \nu \nabla A_{\varphi h} \, dV + \oint_{\partial\Omega} N_i \cdot \nu \nabla A_{\varphi h} \cdot \mathbf{n} \, dS = 0 \tag{3.20}$$

Green integration law helps us to solve this extremely complex integration and obtain a more simple form. The last equation is the Weak form of the MQS problem. The last therm of the equation is computed on the boundary of the domain. It is called weak form because of it is necessary that is must be a continous and one time only derivable function. The kernel of the approach that it makes possbiel to transform a general partial differantial equation system into an algebrical equations system. Writing in a different way agein the integral, it is possible to subline the sources of the model and the time dependet therm:

$$-\int_\Omega \nabla N_i \cdot \nu \nabla A_{\varphi h} \, dV + \oint_{\partial\Omega} N_i \cdot \nu \nabla A_{\varphi h} \cdot \mathbf{n} \, dS = \int_\Omega N_i \cdot \nu \frac{\partial A_{\varphi h}}{\partial t} - \int_\Omega N_i \cdot J_{s\varphi} \, dV \tag{3.21}$$

To understand this formulation there is the necessity of develop the integral:
The first term in that case:

$$
\int_{\Omega} \nabla N_i \cdot \nu \nabla A_{\varphi h} \, dV = \int_{\Omega} \nabla N_i \cdot \nu \nabla \left(\sum_{j=1}^{n_n} A_{\varphi j} \cdot N_j \right) dV
$$
$$
= \sum_{j=1}^{n_n} \left(\int_{\Omega} \nabla N_i \cdot \nu \nabla N_j \, dV \right) \cdot A_{\varphi j} = \sum_{j=1}^{n_n} k_{ij} \cdot A_{\varphi j} \tag{3.22}
$$

where the coefficient k_{ij} is, as the variational approach did, the $i - j$ element of the stifness matrix $[K]$:

$$
k_{ij} = \int_{\Omega} \nabla N_i \cdot \nu \nabla N_j \, dV = \sum_{e=1}^{n_e} \int_{\Delta e} \nabla N_i \cdot \nu \nabla N_j \, dV \tag{3.23}
$$

with Δe the general element of the mesh (triangular or quadrilatera in an axial symmetric model).

The second term instead:

$$
\oint_{\partial \Omega} N_i \cdot \nu \nabla A_{\varphi h} \cdot \mathbf{n} \, dS \tag{3.24}
$$

This term represents the B-normal conservation condition. It is possible view that internal nodes do not give contribution to this integral. Assuming we can isolate each element of the mesh, than the integral computed on the line that divides two neighboring elements becomes:

$$
\int_A^B N_i^1 \nu^1 \frac{\partial A_{\varphi h}^1}{\partial n^1} \, dP + \int_B^A N_i^2 \nu^2 \frac{\partial A_{\varphi h}^2}{\partial n^2} \, dP \tag{3.25}
$$

Because on the boundary of each element shape functions must be equal than $N_i^1 = N_i^2$ on the boundary $\overrightarrow{AB}$. In adition to the conservation of the normal component of the magnetic induction field. Instead boundary nodes may have only three possibilities:

- Dirichlet. $A_{\varphi j} = A*_{\varphi j}$

- Homogeneous Neumann. $\frac{\partial A_\varphi}{\partial n_j} = 0$

- Not homogeneous Neumann. $\frac{\partial A_\varphi}{\partial n_j} = f_j$

3.2.1 Fourier's Equation

The develop of the method for the Fourier's equation is more simple:

$$
-\nabla \cdot \lambda \nabla T + C \frac{\partial T}{\partial t} = q \tag{3.26}
$$

where $C = \rho C_p$ is the thermal capacity and q are the heating sources of the model. Now it is possible integrate by Galierkin method as done for the electromagnetic

model.

$$\int_{\Omega} \nabla N_i \cdot \lambda \nabla T_h \, dV - \oint_{\partial \Omega} N_i \lambda \nabla T_h \cdot \mathbf{n} \, dS +$$
$$+ \int_{\Omega} N_i C \frac{\partial T}{\partial t} \, dV = \int_{\Omega} N_i q \, dV \tag{3.27}$$

At this point it is necessary to develop the integral on the boundary of the domain:

- An internal node does not contribute to this integral for the conservation of the thermal flow

- Neumann homogenous node. In other word $\frac{\partial T}{\partial n} = 0$ is the adiabatic condition. Then also in this case the integral is zero.

- Dirichlet node. We are imposing a temparture. The integral is zero because it is overwritten

- Robin node. This is the convective heat flow condition. In other words exists a convective flow towards the outside of the domain.

This means that the integral done on the edge $\partial \Omega$ is non zero only if a Robin boundary condition is imposed.

$$\lambda \nabla T \cdot \mathbf{n} = \alpha(T_0 - T) \tag{3.28}$$

and then

$$\oint_{\partial \Omega} N_i \lambda \nabla T \cdot \mathbf{n} \, dC = \oint_{\partial \Omega} N_i \lambda \frac{\partial T}{\partial t} \cdot \mathbf{n} \, dS \tag{3.29}$$

And the complete model now is:

$$\int_{\Omega} \nabla N_i \cdot \lambda T_h \, dV + \oint_{B_{conv}} N_i \alpha T_h \, dS + \int_{\Omega} N_i C \frac{\partial T_h}{\partial t} \, dV =$$
$$= \int_{\Omega} N_i q \, dV + \oint_{B_{conv}} N_i \alpha T_0 \, dS \tag{3.30}$$

It is finaly possible to write this equation with matrix, if it is possible to write thermal sources in the same way as shape functions, in other words:

$$\sum_{j} n_n \left(\int_{\Omega} N_i N_j \, dV \right) \cdot q_j \tag{3.31}$$

and also the temperature T_0 can be imagined as solution of a previous FEM solution, then we know one of its interpolation:

$$T_{0h} = \sum_{j} n_0 N_j T_j \tag{3.32}$$

then

$$\sum_{j} n_n \left(\int_{CONV} N_i \alpha N_j \, dV \right) T_j^0 \tag{3.33}$$

Instead other terms of the integral formulation can be computed as:

$$\sum_j n_n \left(\int_\Omega \nabla N_i \cdot \lambda \nabla N_j \, dV \right) T_j \tag{3.34}$$

$$\sum_j n_n \left(\int_{CONV} N_i \alpha N_j \, dS \right) T_j \tag{3.35}$$

and if it is possible also in this case write the temperature with an interpolation function:

$$T_h = \sum_j n_n N_j T_j \tag{3.36}$$

the last integral can be sobstituted with:

$$\int_\Omega N_i C \frac{\partial T_h}{\partial t} \, dV = \sum_j n_n \left(\int_\Omega N_i C N_j \, dV \right) \frac{\partial T_j}{\partial t} \tag{3.37}$$

And finally the matrix formulation of the FEM is:

$$[K] \cdot [T] + [B] \cdot [T] + [M] \frac{\partial}{\partial t}[T] = [M_s] \cdot [q] + [B] \cdot [T^0] \tag{3.38}$$

It is possible write again this alst equation, and show that it is possible to solve the DAEs with a general θ-method:

$$[K + B] \cdot [T] + [M] \frac{\partial}{\partial t}[T] = [S] \tag{3.39}$$

$$[M] \cdot \frac{\partial}{\partial t}[T] = [S] - [K + B] \cdot [T] \tag{3.40}$$

A time solution define a time step $\Delta t = t_{n+1} - t_n$ and then it is possible to use Theta Method to solve the equation for every time step.

$$[M]\left([X_{n+1}] - [X_n]\right) = \left(\theta f_{n+1} + (1 - \theta) f_n\right) \Delta t =$$
$$= \Delta t \left(\theta([S_{n+1}] - [K_{n+1} + B_{n+1}] \cdot [X_{n+1}]) + (1 - \theta)([S_n] - [K_n + B_n] \cdot [X_n]) \right) \tag{3.41}$$

and finally obtain the solution at next time step as:

$$([M] + \Delta t \theta [K_{n+1}] + B_{n+1}]) \cdot [X_{n+1}] =$$
$$([M] + \Delta t (\theta - 1)[K_n + B_n]) \cdot [X_n] + \Delta t \left(\theta[S_{n+1}] + (1 - \theta)[S_n] \right) \tag{3.42}$$

3.3   Newton-Raphson

To solve a general non-linear equation Newton-Raphson methos is used. This iterative scheme allows to obtain a solution to the problem $f(x) = 0$ by making a linearization of the nonlinear function. This means that instead of the problem $f(x) = 0$ NR method take into account the function $L(x) = 0$. In other words the method search the solution that make zero its linearization. The idea of the method is as follows: one starts with an initial guess which is reasonably close to the true

root, then the function is approximated by its tangent line (which can be computed using the tools of calculus), and one computes the x-intercept of this tangent line (which is easily done with elementary algebra). This x-intercept will typically be a better approximation to the function's root than the original guess, and the method can be iterated. Typically the NR iterative scheme is synthesized in this way, if $f : [a, b] \Rightarrow \mathbb{R}$ is a differentiable function defined on the interval $[a, b]$. Suppose we have some current approaximation x_n of the solution, then we can derive the formula for a better approaximation x_{n+1}.

$$x_{n+1} = x_n - \frac{f(x_n)}{f'(x_n)} \tag{3.43}$$

where, f' denotes the derivative of the function f. Nwton's method when converges it does it in a more than quadratic way. The iterative shceme used by FE method is developed here for the most simple case: the Fourier's equations supposed non-linear:

- T^k is an estimate of the initial temperature on an element.

- T^{k+1} is the new estimate of the temperature.

then it is possible define the gap between the two temperatures:

$$T^{k+1} = T^k + \delta T \tag{3.44}$$

$$\lambda(T^{k+1}) = \lambda(T^k) + \lambda'(T^k)\delta T \tag{3.45}$$

And finally it is possible to develop the PDEs as:

$$- \nabla \cdot \lambda(T)\nabla T = 0 \tag{3.46}$$

The PDE at step k+1 is then:

$$\begin{aligned}
&- \nabla \cdot \lambda(T^{k+1})\nabla T^{k+1} = 0 = \\
&= -\nabla \cdot \left(\lambda(T^k) + k'(T^k)\delta T \right) \nabla \left(T^k + \delta T \right) = 0
\end{aligned} \tag{3.47}$$

Then it is possible to neglect higher order therms and get the PDE that is again solvable with a finite elements approach.

$$- \nabla \cdot \lambda(T^k)\nabla \delta T - \nabla \cdot \lambda'(T^k)\delta T \nabla T^k = \nabla \cdot \lambda(T^k)\nabla T^k \tag{3.48}$$

At this point is possible to define a test function W' and define the weak form, by Green integration method:

$$\begin{aligned}
&- \int_\Omega W' \times (\nabla \cdot \lambda(T^k)\nabla \delta T) \, d\Omega - \int_\Omega W' \times (\nabla \cdot \lambda'(T^k)\delta T \nabla T^k) \, d\Omega = \\
&= \int_\Omega W' \times (\nabla \cdot \lambda(T^k)\nabla T^k) \, d\Omega
\end{aligned} \tag{3.49}$$

and after add the boundary conditions we obtain the following matrix writing:

$$[\lambda + N + B] \cdot [\delta T] = -[\lambda] \cdot [T^k] - [B] \cdot [T^k] + [b] \tag{3.50}$$

where $[K]$ is the stiffness matrix, defined by elements k_{ij}, $[B]$ is the boundary condition matrix, instead $[N]$ is a not symmetrical matrix defined by elements n_{ij}

$$n_{ij} = \int_\Omega \nabla N_i \cdot \lambda'(T^k) \nabla T^k N_j \, d\Omega \tag{3.51}$$

Nonlinearity of magnetic field are more complex, but the same approach can be done also for magnetic fields: It is possible to write induction magnetic field as $|\mathbf{B}| = function(|\mathbf{H}|)$. This means that it is possible to define a magnetic permeability for each value of the amgnetic field.

$$\frac{1}{\mu} = \nu(|\mathbf{B}|) = \nu(\nabla \times A_\varphi) \tag{3.52}$$

It is possible to define the partial derivative with induction field as:

$$\frac{\partial \nu}{\partial B} \approx \frac{\Delta \nu}{\Delta B} \tag{3.53}$$

but typically for an electromagnetic problem the unknown isn't B but A_φ this means that

$$\frac{\partial \nu}{\partial A_\varphi} = \frac{\partial \nu}{\partial B} \cdot \frac{\partial B}{\partial A_\varphi} \tag{3.54}$$

And this problem is resolvable because the first term $\frac{\partial \nu}{\partial B}$ is typically known through the magnetization curve, instead the last term $\frac{\partial B}{\partial A_\varphi}$ can be computed through shape functions.

Chapter 4

MODEL

In this chapter it is presented the model solved with a finite element technique. The core of this work is that both the electromagnetic and the thermal problem are solved in the time domain. The attempt to solve the electromagnetic problem in the time domain, should allow to evaluate more precisley the effect of magnetic non-linearity with respect to a computation in the frequency domain. In particular this fact should be even more true in the case of SDF hardening processes. In this case, because the superimposition of the effetcs is not possible, it should be considered for the two different frequencies, two different magnetization curves and different values of magnetic permability, and it is extreamely difficult to realize. Unfortunately, since the time constants with which the two physicals evolve are completely different it is possible to uncouple, at least numerically, the electromagnetic model from the thermal. Typically a process of surface induction hardening is extremely fast, as long as the power induced in the workpiece is concentrated in reduced thickness. Typically the frequency range is in the order of $10^1 - 10^2$ $[kHz]$. This means that the process time to be simulated at the computer, in the thermal model is

$$T_{therm} \approx 10^{-1} \ [s]$$

instead the magnetic period to be simulated in the electromagnetic model is for example

$$T_{em} = \frac{1}{f} \approx 10^{-5} \ [s]$$

where $f \ [Hz]$ is the frequency of electrical sources. Shennon's theorem says that to rebuild a wave with good accuracy, we need at least $N = 40$ samples per period. This means that a good time step to solve the problem is for example

$$dt = \frac{T_{em}}{N} \approx 2.5 \cdot 10^{-7};$$

Afterwards a surface induction hardening process, with an completely coupled (electromagnetic and thermal) model might need an extreamley large number of time steps to be numerically computed:

$$n_{steps} = \frac{T_{therm}}{dt} \approx 4 \cdot 10^5 \ [steps]$$

It's clear that this approach need too many iterations to be solved. Taking into account also the complications in the problem as nonlinearity of the PDEs, such as magnetic saturation and Curie's transformation, to obtain the convergence of the solution could be necessary to reduce the time step dt and increase the number of elements of the mesh. This means that also a simple geometry requires a long time to be solved, probably several weeks. This is not admissible from the point of view of the designer. This work solves this main problem, by decoupling the resolutions of the two transients , but without introducing excessive simplifications that could affect the adehesion to the physic of the model. Indeed, it is plausible to assume that in a time interval sufficiently small, the power induced in the workpiece is constant, and it is precisely the average value of the power induced. Moreover it can be assumed, if the temperature grows relatively few degrees during this time period, that the electromagnetic parameters, such as magnetic relative permeability and electrical conductivity do not vary with temperature. These observations imply that it is possible to solve first of all the EM transient with a certain temperature distribution inside the piece, then derive the average heating power distribution calculated in the EM period, and assume this power as time constant source in a time step of the thermal transient. Finally then obtain a temperature distribution which will be computed the subsequent EM transient, and so on unitl the end of the process.

Practically it is possible to do that assuming that for a certain integer number of EM periods N_{em}, the waves form of the electromagnetic phenomena (such as magnetic field, current, power ...etc) can't vary as long as the temperature does not change. This means that if t_k and t_{k+1} are the initial and the last points in time at which the thermal transient is solved,

$$dt_{therm} = t_{k+1} - t_k \ [s] \tag{4.1}$$

then the thermal time step must be an integer multiple of the electromagnetic period:

$$dt_{therm} = N_{em} \cdot T_{em} \ [s] \tag{4.2}$$

where the electromagnetic period is the period defined by the medium frequency, in a simultaneous double frequency method (f_{mf} and $f_h f$), instead in a single frequency induction hardening is the period defined by the chosen frequency.

$$T_{em} = \begin{cases} \frac{1}{f} & \text{with single frequency supply} \\ \frac{1}{f_{mf}} & \text{with SDF supply} \end{cases} \tag{4.3}$$

It is important to underline that the time step dt_{therm} must be chosen sufficiently small in order to have resonable temperature variation (about 40 [°C]) in a time step, because the surface will be characterized by the highest heating rate, at least for most of the process. The maximum acceptable temperature jump $\Delta\theta$ of a surface point between two magnetic periods T_{em}^k and T_{em}^{k+1} is in the order of [30-40] °C. This value is a good compromise between acceptable computation times and accuracy of the model.

The concept iterative scheme of the coupled model is sketched in Figure 4.2.

This kind of computation is the so called indirect coupling, but exist other method that are here discussed. Probably the simplest method is the so called Two-step coupling. Sure enough the electromagnetic problem is solved during the first
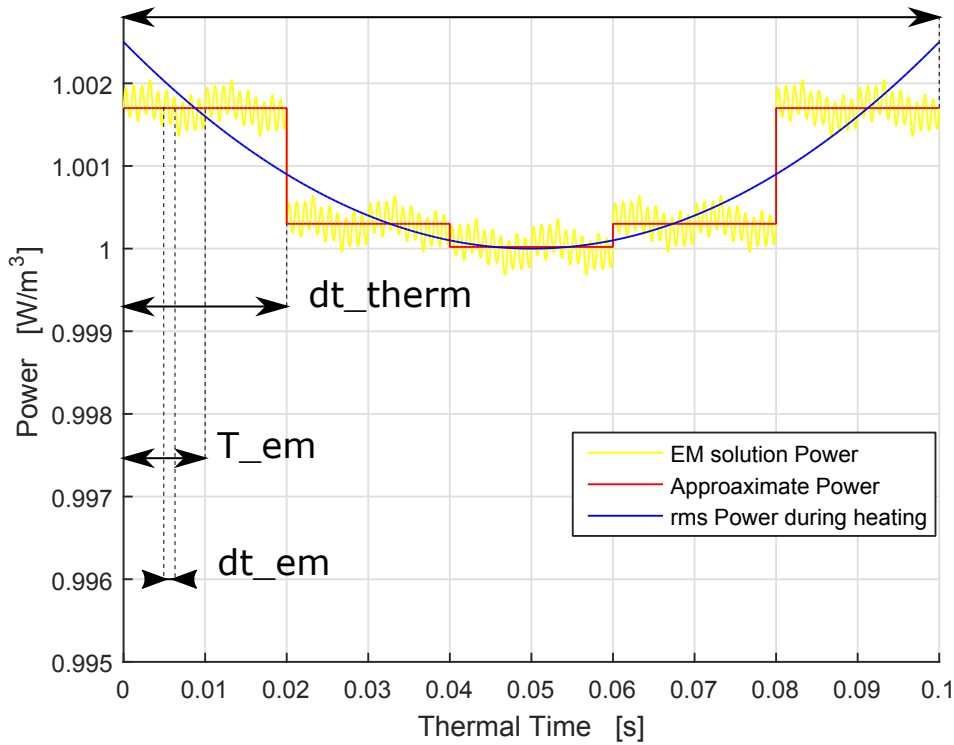
Figure 4.1: Qualitative consideration about the approaximations of the model. In particular for the power during the transient thermal solution.

computational step; then both obtianed current and power density distributions are used to determine the heat sources to be used for solving the thermal problem. The main advantages of the two-step procedure are its short execution time and moderate memory requirements in comparison to the direct coupling method that solves for each time step the global probelm simultaneously. Typically this approach does not take into account of the modifications of material properties in the course of heating. This work instead employs a suitable approach: the indirect coupling. This as seen before is an iterative process which consists of multiple times, iteratively exchanging the results calculations and accordingly updating material physical properties.

4.1 Description of simulation models

The numerical simulation of this work studies an extreamly simple geometry, like a billet coupled with a coil conductor. This assumption was done to solve in the time domain both the problems, avoiding extremely long times. As already said the core of this work is the attempt of understanding different effects such as the importance of the magnetic saturation during the thermal process. It is well known the effect of the temperature on the penetration of the magnetic field and on the distribution of the thermal sources. But it is extremely difficult to understand how much important might be the magnetic saturation during the process, and for example its effect in a simultaneous double frequencies process.
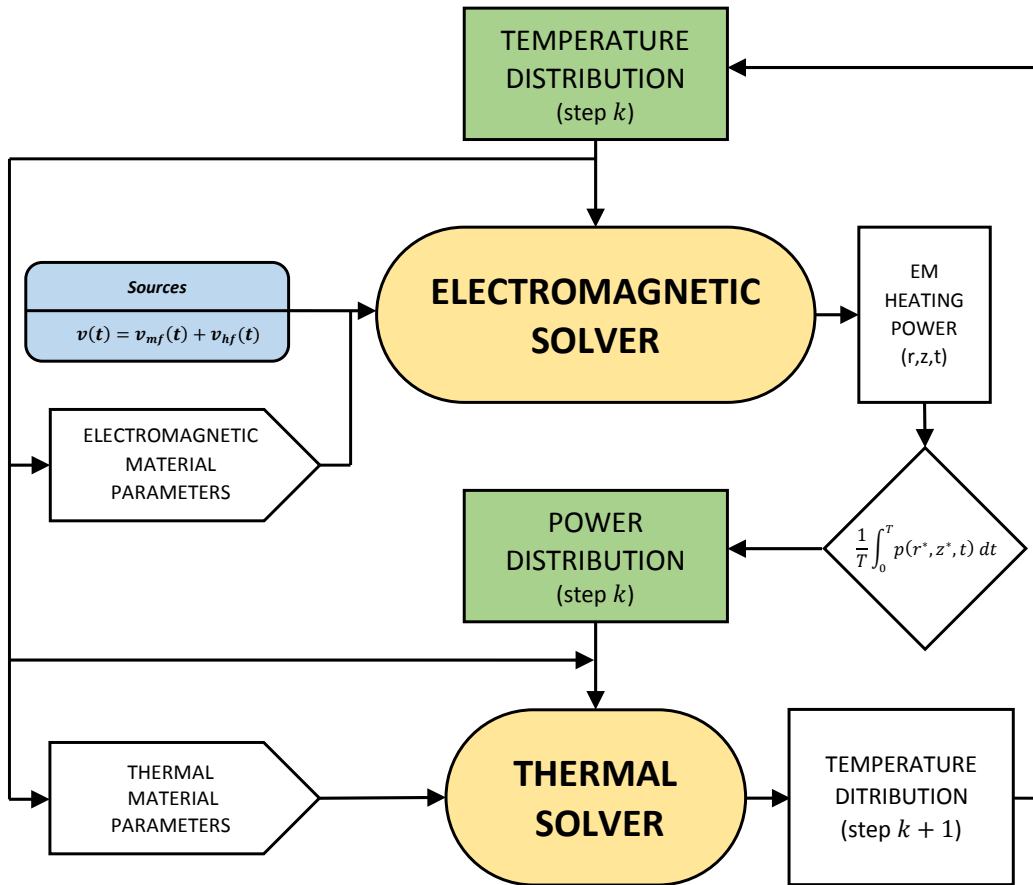
Figure 4.2: Flowchart of the FEM solution of the coupled problem. T is the electromagnetic period, that in our case is 10^4 [s], instead $T_{th} = t_{k+1} - t_k$ is the thermal periodi in which the thermal prblem is computed

4.1.1   The Component

The workpiece that must be hardened is a steel billet. It's characterized by its heigh thath is usually bigger 2-3 times than its radius. This kind of geometry is particularly well suited for mapped mesh-type. The lines of equipotential tend to concatenate the piece in a parallel manner with respect to the height of the billet. A good mesh should everytime respect skin depths of the problem. One of the main problems, from a point of view of the mesh, feeding the inductor with two different frequencies simultaneously, it is to define an unique penetretion depth of the problem. From the formulation of the skin effect:

$$\delta = \sqrt{\frac{\rho}{\pi f \mu_r \mu_0}} \ [m] \tag{4.4}$$

where $\rho = \frac{1}{\sigma}\ \Omega m$ is the resistivity of the domain in which the magnetic field exists. Skin effect is the tendency of an alternating electric current to become distributed within a conductor such that the current density is largest near the surface of the conductor, and decreases with greater depths in the conductor. The electric current flows mainly at the "skin" of the conductor, between the outer surface and a level called the skin depth δ. The skin effect causes the effective resistance of the conductor to increase at higher frequencies where the skin depth is smaller, thus reducing the effective cross-section of the conductor, in accord with the weel known realtion:

$$R = \rho\frac{L}{S} \approx \frac{\rho L}{\pi(D-\delta)\delta}$$

that means that the effective resistance, due to a current confined near the surface of a large conductor, (much thicker than δ) can be solved as if the current flowed uniformly through a layer of thickness δ based on the DC resistivity of that material. We can therefore assume a cross-sectional area approximately equal to δ times the conductor's circumference. Thus a long cylindrical conductor such as a wire, having a diameter D large compared to δ, has a resistance approximately that of a hollow tube with wall thickness δ carrying direct current. Using a material of resistivity ρ it is possible to find the AC resistance of a wire of length L. The skin effect is due to opposing eddy currents, induced by the changing magnetic field resulting from the alternating current. At 60 $[Hz]$ in copper, the skin depth is about 8.5 $[mm]$. At high frequencies the skin depth becomes much smaller. Increased AC resistance due to the skin effect can be used obviously in hardening heat treatment to heat only thin layer of material extreamly fast and with massive power concentration.

Taking advantage of the formulation 4.4, which originates for example from an analytical solution of electromagnetic through the Bessel functions for the eletromagnetic equation, we can define an unique mininum penetration thickness for the model. This consideration might not be the optimal solution from an engineering point of view, focused on the efficiency, but ensures that we do not take excessive errors in spatial discretization. The computation of the model with a mesh that does not respect the skin effect, could lead to unacceptable errors, that would make the model not reliable and not physical. For example numerical cancellation problems, typical of a magnetic potential/electrical potential formulation (AV formulation).

Therefore it is essential to understand during the process as vary the thicknesses of penetration. You see from the wording 4.4 that the skin depth is a function of the electromagnetic parameters and frequency. This means that sinusoidal waveforms, at different frequencies, are characterized by different thicknesses of penetration. But it's easy to understand that the relative permeability changes for the combined effect of the saturation and of the temperature, due to the Curie's phase transformation, affects the penetration thickness. Finally there is also to consider the linear dependence of electrical resistivity with temperature.

In summary, one can derive the following qualitative trends for the skin depth

$$\delta(\theta) = \left(\sqrt{\frac{\rho_0}{f\mu_0}}\right)\sqrt{\frac{1 + \alpha(\theta - \theta_0)}{1 + \mu_r(1 - \exp\frac{\theta - \theta_c}{C})}} \tag{4.5}$$

So if we consider different frequencies it is possible to understand how the skin depth δ changes during the heating process. In the first part of the heat treatment,

when there are not areas of the billet whom temperatures θ are over the Curie's Temperature θ_c the model should need smaller elements than in the last part of the process. However this is not true. As a result of the demagnetization of portions of space facing the inductor, the magnetic field and thermal sources tend to penetrate towards the center of the workpiece, but in these areas, the permeability is still very high. Therefore, it is necessary to consider an extremely dense mesh in all the thickness that must be hardened.
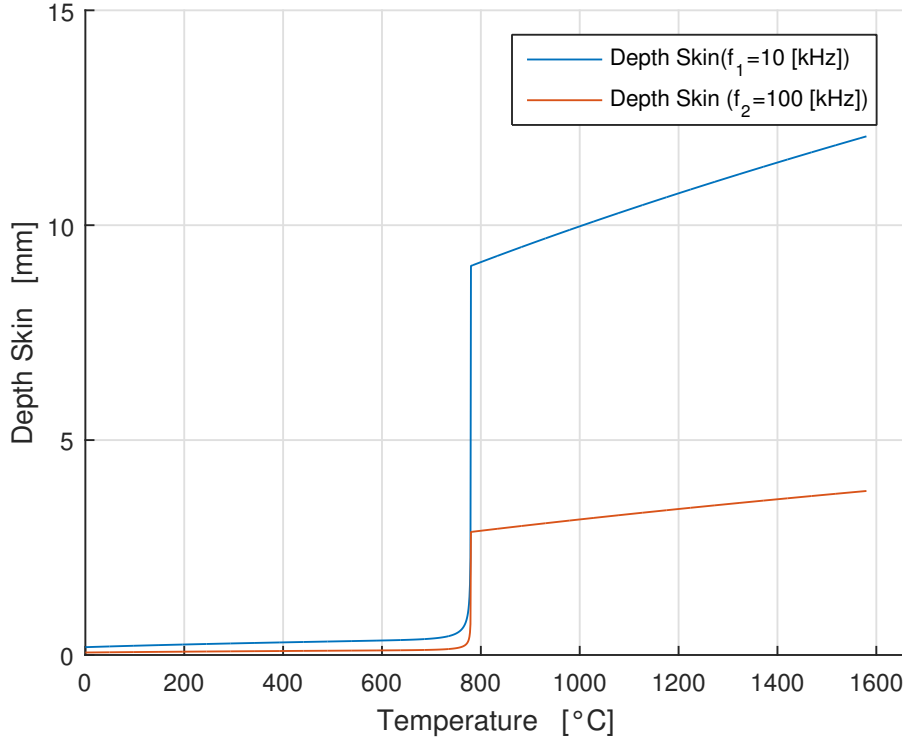
Figure 4.3: Behaviour of the penetration depth, as function of the temperature θ, during the heat process. The skin effect tends to be less marked on the surface during heating. Thus, distributions of current tend to penetrate to the heart of the billet. But still in accordance with the depth of penetration.

Similar considerations must be made instead to the effect of magnetic saturation. It is possible to explicit the behaviour of the skin depth with the value of the magnetic field and than with time.

$$\mu_r = \frac{|\mathbf{B}(|\mathbf{H}|)|}{\mu_0|\mathbf{H}|} = 1 + \frac{2B_s}{\pi}\frac{1}{|\mathbf{H}|}\arctan\left(\frac{\pi\mu_0(\mu_{r0}-1)|\mathbf{H}|}{2B_s}\right) \tag{4.6}$$

It is easy to understand that try to define a penetration depth for a time dependent model, and in which the relative permeability is strictly function of the magnetic field, and that it is function of time, could not have sense. Despite this could help to understand how the distribution of currents and power inside the billet varyes, this work tries to describe the behaviour of the skin depth with amplitude of magnetic field and time dependence. Using the formulation of the relative permeability seen

in the Equation 4.6 it is possible to write the penetration depth δ as function of the amplitutude of the magnetic field $|\mathbf{H}|$ under the hypotesis that the temperature does not change:

$$
\begin{aligned}
\delta(|\mathbf{H}|) &= \sqrt{\frac{1}{f}\frac{\rho_0}{\pi\mu_0}\frac{1}{\mu_r(|\mathbf{H}|)}} = \\
&= \sqrt{\frac{1}{f}\frac{\rho_0}{\mu_0}}\sqrt{\frac{|\mathbf{H}|}{\pi|\mathbf{H}| + 2B_s\arctan\left(\frac{\pi\mu_0(\mu_{r0}-1)|\mathbf{H}|}{2B_s}\right)}}
\end{aligned}
\tag{4.7}
$$
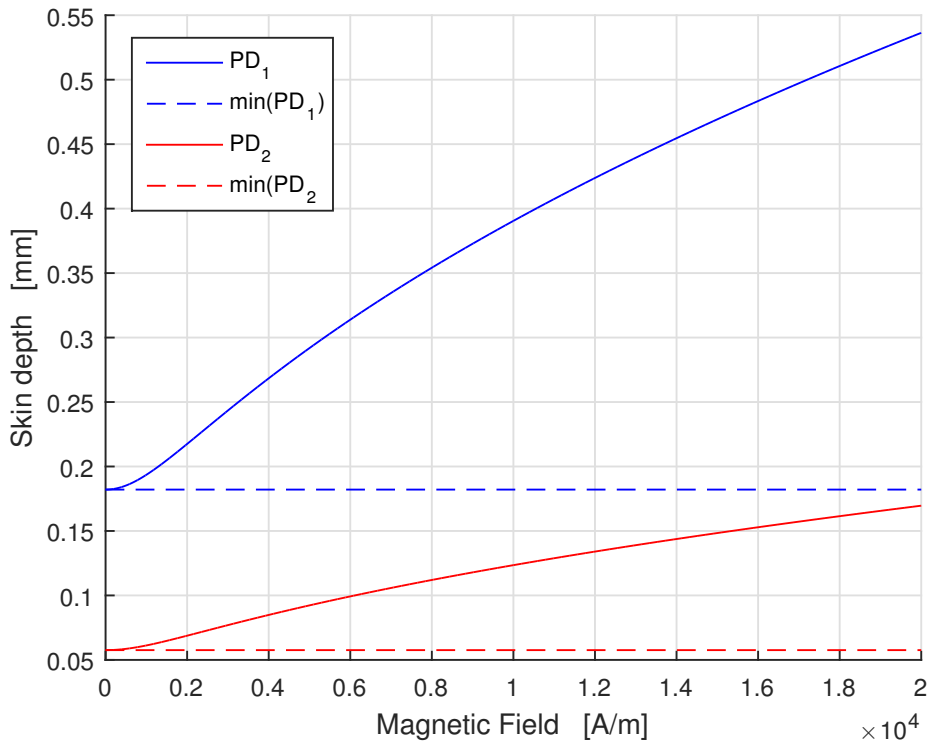
Figure 4.4: Behaviour of the penetration depth, as function of the magnetic field $|\mathbf{H}|$, this formulation is an attempt to consider the saturation effect. Later this work tryies to verify it with the results of simulations

Then the concept of penetration depth could again have sense also in a time dependent solution. Because eddy currents are still concentrated in thin regions, that vary for the effect of relative permeability and electrical conducitivity. At the end there is the necessity to define a minimum and a maximum dimension of the mesh. This work considers a mapped mesh for the steel billet as it is possible to see in Figure 4.7.

The geometry

The sizes of the steel billet modeled with a FEA software, and precisley the commercial software Comsol are:

Constant	Value	Unit
$radius$	10	$[mm]$
$height$	50	$[mm]$

Table 4.1: Dimensions of the billet.

The inductor that is taken into consideration is a typical geometry. It is water cooled in the center with a rectangular section cooling conduit. This is necessary because the currents that typically are used should heat too much the coil and the temperature might also melt it.   To obtain an acceptable solution of the

Constant	Value	Unit
$r_{int-ind}$	12	$[mm]$
h_{ind}	10	$[mm]$
s_{ind}	1.5	$[mm]$

Table 4.2: Dimensions of the water cooled coil.

electromagnetic problem it is good practice to define a region, that is called infinite box, in which the magnetic field goes to zero, in other words it is imposed what happens theorically to infinity. The infinite box, that in our case is a ring-shaped air region, is defined by an inner radius $r_{inf-int}$ and an outer radius $r_{inf-ext}$. This simplification, of course, introduces a no physicality, but if you choose relatively large size compared to the workpiece it is negligible. For example in this work I choose an internal radius that is ten times the height of the simlutaed system

Constant	Value	Unit
$r_{inf-int}$	150	$[mm]$
$h_{inf-ext}$	200	$[mm]$

Table 4.3: Dimensions of the infinite elements.

4.1.2   The mesh

The mesh of course must respect the geometry and the physic of the model. To save time and memory, it was chosen a mesh type mapped to the billet and the inductor. The billet was divided into four rectangles, respectively, in agreement with the distribution of the magnetic fields and of the thicknesses of penetration. As precautionary measures I choose to have 2-3 elements for depth of penetration to a depth of 4 mm from the surface of the billet. The two inner regions instead have a mesh, always mapped, but more relaxed. The inductor was always divided into rectangles, but with elements whose minimum width coincides with a third of
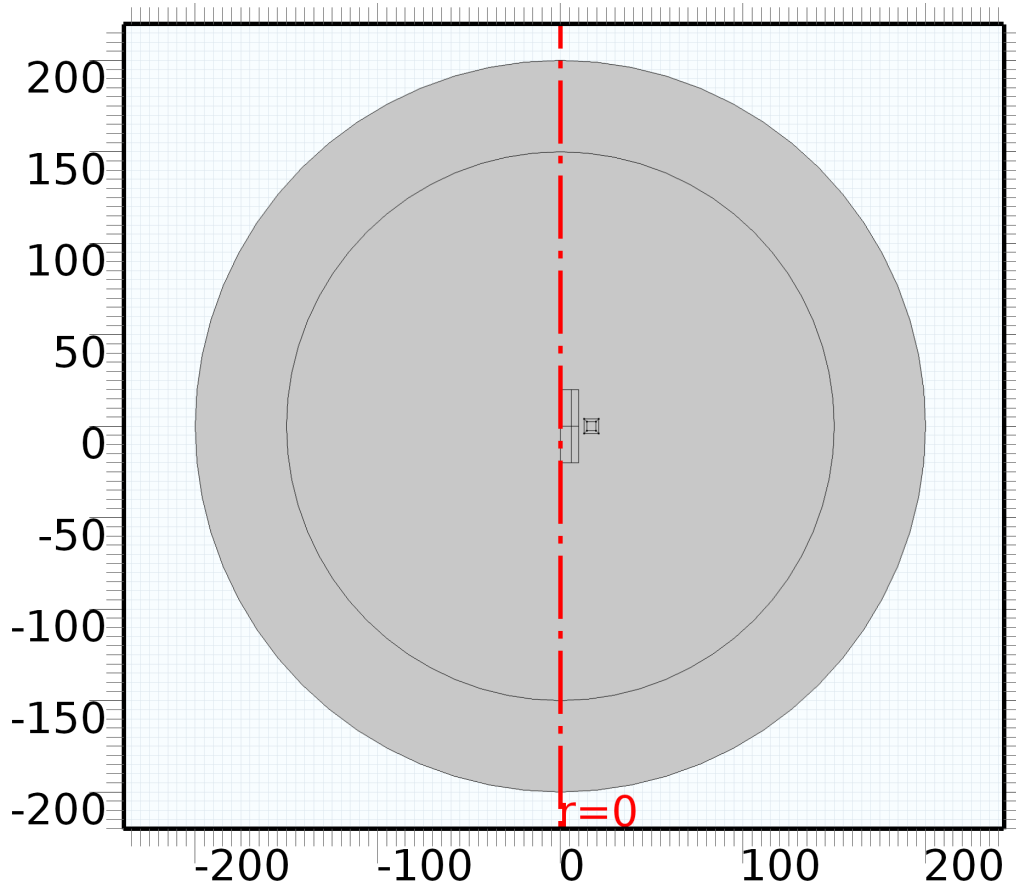
Figure 4.5: Overall view of geometry and physics of the problem

the thickness calculated depth with constant parameters of the copper and in high frequency (100 kHz). Instead the air and the inductor cooling was meshed with free triangular elements. Below are listed different penetration depths δ, they are combination of different values of the material parameters.

Penetration Depth	Frequency [kHz]	μ_r	ρ [Ωm]	Value [mm]
δ_{steel}	10	600	$2.5 \cdot 10^{-7}$	0.3
δ_{steel}	100	600	$2.5 \cdot 10^{-7}$	0.1
δ_{steel}	10	1	$2.5 \cdot 10^{-7}$	0.8
δ_{steel}	100	1	$2.5 \cdot 10^{-7}$	0.5
δ_{Cu}	10	1	$2.0 \cdot 10^{-8}$	1.0
δ_{Cu}	100	1	$2.0 \cdot 10^{-8}$	1.3

Table 4.4: Several penetration depth that describes the problem for a specific material and specific frequencies.

All these considerations involve the need to have a mesh extremely dense for good results, and to be certain that the method converges to a true solution, because of a time-dependet solver, and particularly of a non linear model, needs a certain
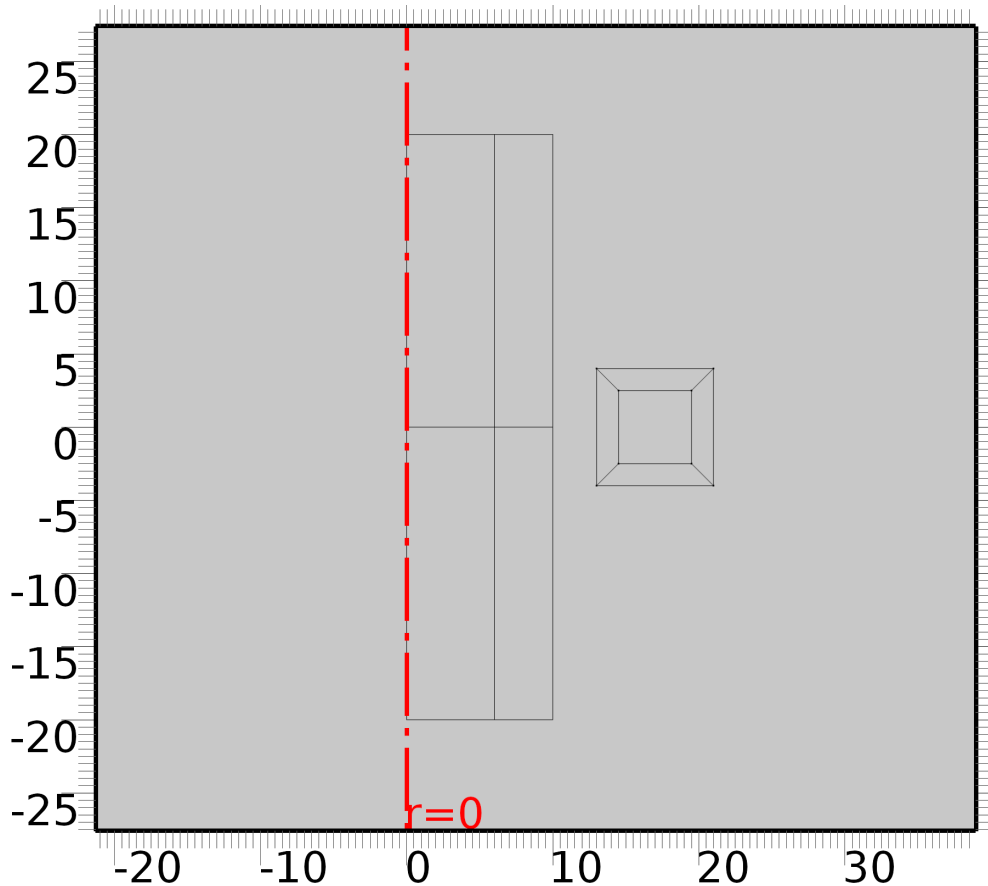
Figure 4.6: View of the steel billet and copper coil in the axially symmetric model.

time and space discretization.

The billet is meshed with rectangular elements. It is possible view that surface elements have smaller geometrical dimension. This is in accordance with the depth of penetration of the electromagnetic field and the direction of lines of equipotential. To obtain good results (with errors as low as possible) but to reduce calculation time and computational cost (in terms of memory required by the solver) the dimensions of elements are relaxed towards the heart of the billet and upward and downward. Also the inductor is meshed with mapped elements that are regular quadrilaterals. Because of penetration depths of the coil, that is built with copper, are much greater than those of steel, in the model are chosen bigger elements for the inductor.

4.2 Electromagnetic Model

The electromagnetic problem can be easily represented with a flowchart of the solution model, that is shown in Figure 4.9.

4.2.1 Power supply

The inductor is voltage supplied. In particular it was imposed to the inductor a voltage equal to the superposition of two sinusoidal wave form with two different
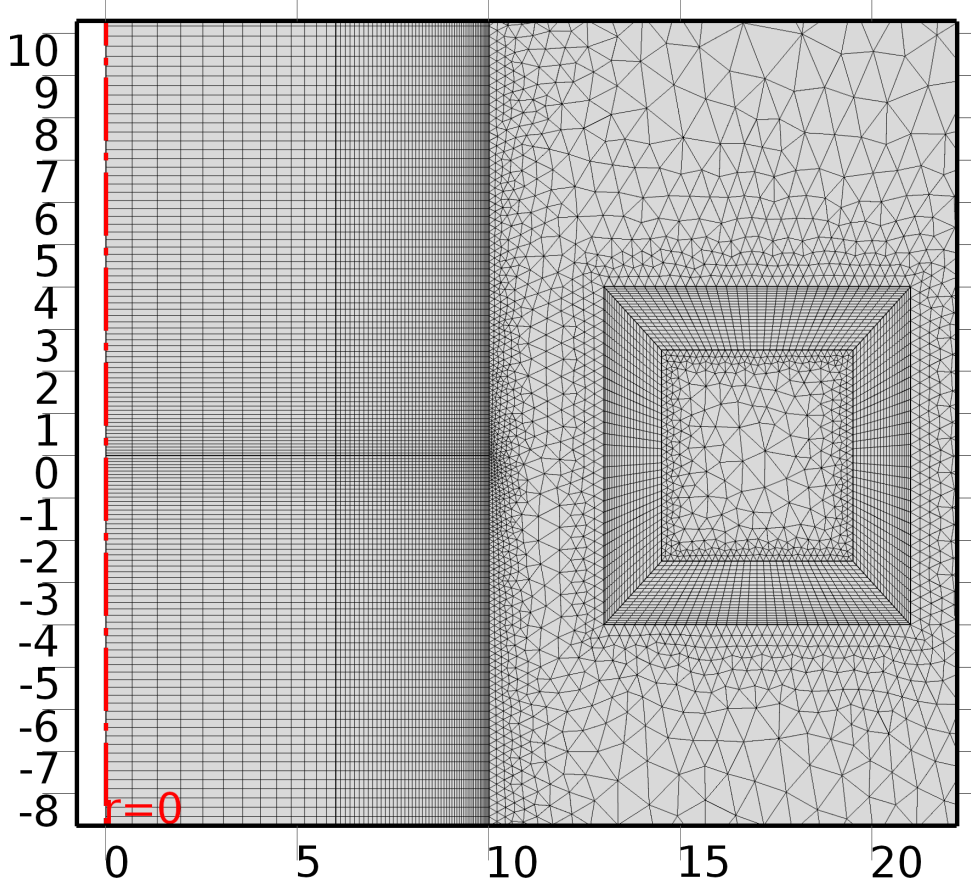
Figure 4.7: Mesh structure of the billet and of the coil.

frequencies. From an electrotechnical point of view this is equivalent to put in series two voltage generators independent of each other. As seen, to obtain a power that is the sum of different terms it is chosen an integer ratio between the two frequencies.

$$k = \frac{f_{hf}}{f_{mf}}$$

with $k \in \mathbb{N}$. Than if V_{hf} $[V]$ is the rms value of high frequency and V_{mf} $[V]$ the rms value of medium frequency.

$$v(t) = V_{mf} \cos(2\pi f_{mf}) + V_{hf} \cos(2\pi f_{hf}) \ [V] \tag{4.8}$$

The main motivation for which was chosen to supply the inductor with voltage instead of current is due to the fact that usually SDF generators are voltage-controlled inverter. Because as the inductor was modeled as a single turn coil, this means that the computation provides the evolution of distribution of current density of inductor coil. This is the best way to model an inductor to take into account many problems as edge effects, saturation and evolution of a wave form in time, particularly if penetration depth is smaller and smaller than the dimensions of inductor. This means that the voltage sorce is well known and imposed during all the electromagnetic period:

$$\mathbf{J_e} = \sigma \frac{v(t)}{2\pi r} \mathbf{e_{coil}} \tag{4.9}$$
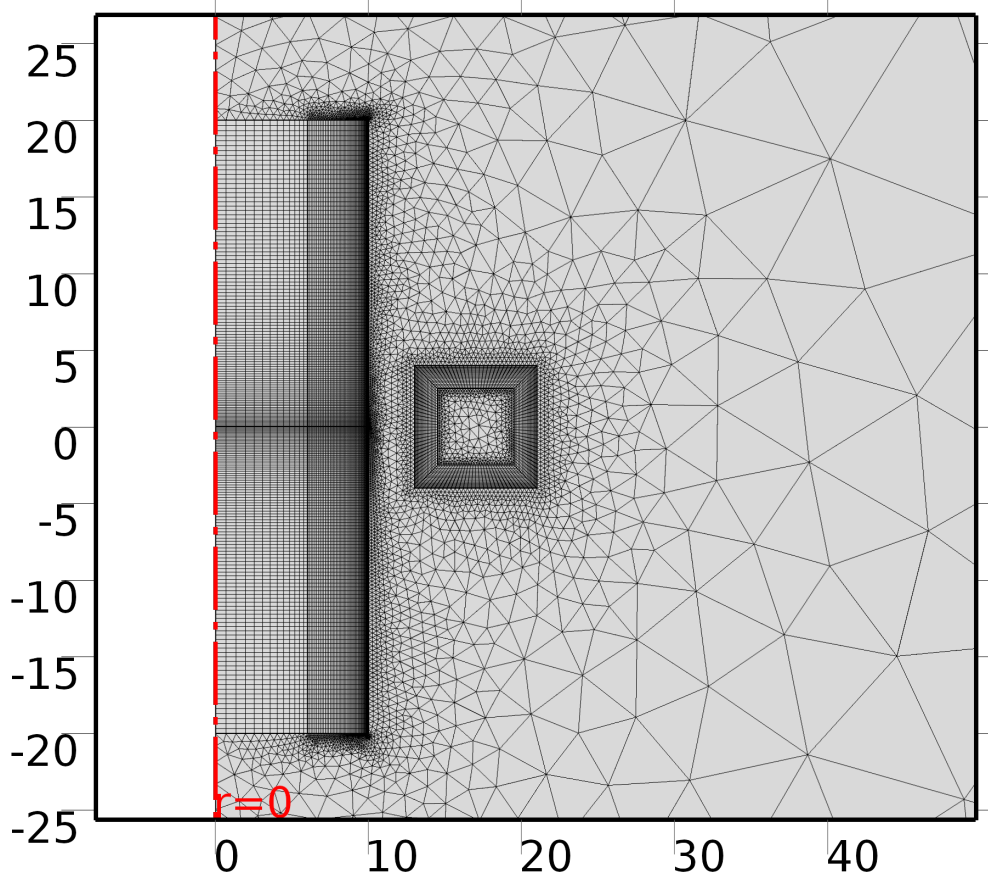
Figure 4.8: Overall mesh of the model

This means that the current density $\mathbf{J_e}$ $[A/m^2]$, imposed normal through the inductor section (it is weel known that for a 2D-Axial Symmetric model, current desities admit only φ-out-of-plane-component), can be computed for each element of the mesh. It is possible split the current density inside the coil inductor as two terms at different frequencies:

$$\mathbf{J_e} = \sigma \frac{V_{hf} \cos(2\pi f_{hf})}{2\pi r}\mathbf{e_{coil}} + \sigma \frac{V_{mf} \cos(2\pi f_{mf})}{2\pi r}\mathbf{e_{coil}} \qquad (4.10)$$

This means that for the single turn coil the superimposition of the effects is valid. This is even more true, if we consider that the metarial used for the inductor is copper. Now Maxwell's equations seen in chapter 1 makes possible the computaion of the problem. Because typically the inductors are current controlled, it is necessary to obtain also the currents and the absorbed power in the time. Thus:

$$i_{coil} = \int_{S_{coil}} \mathbf{J} \cdot \mathbf{e_{coil}} \, dS \qquad (4.11)$$

4.2.2   Steel Billet

This region is the workpiece that must be heated during the process. This physic region is characterized by initial high value of magnetic relative permeability. So we
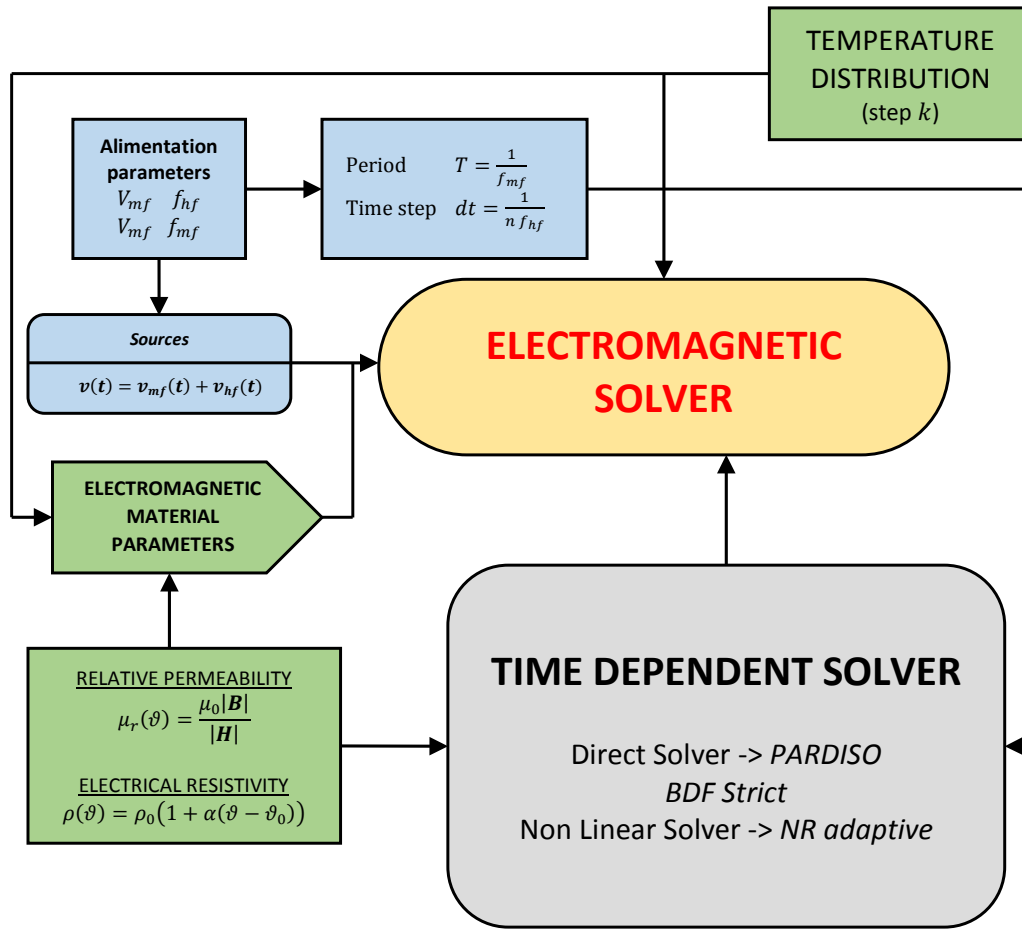
Figure 4.9: Flow chart of the electromagnetic model. The problem is solved in time domain, and the PDEs are characterized by non linear coefficients.

expect high values of magnetic flux inside. An ideal, linear region, with constant μ_r typically imposes B-normal component through interface between air and workpiece. Magnetic potential countour are typically perpendicular into interface of a material with very high μ_r. Instead during the time evolution of electromagnetic problem, steel saturates and magnetic potential equiflux lines are tangential to interface between air and steel billet. The system of equations for the billet is soved by the boundary element method with iterative correction of relative magnetic permeability and electric resistance, every time increment depending of temperature in the element. THe specific Joule heat sources $w(r,z)$ $[W/m^3]$ are calculated for each element, for each time step of the time-transient electromagnetic solver.

$$w(r,z) = \frac{1}{\sigma}|\mathbf{J}(r*,z*) \cdot \mathbf{J}(r*,z*)| \tag{4.12}$$

where the current density for each element of the mesh is:

$$\mathbf{J} = -\sigma \frac{\partial \mathbf{A}}{\partial t} = -\sigma \frac{\mathbf{A}(\mathbf{t_{k+1}}) - \mathbf{A}(\mathbf{t_k})}{t_{k+1} - t_k} \tag{4.13}$$

4.3   Thermal Model

The thermal problem is modeled by imposing a distribution of heating power in the billett. The model takes into account the heat loss during the process, by imposing Robin condition on the surface. Taking account of convective losses and radiative. The radiative lossed, when the temperature exceeds 800 [° C], become much more significant. The air temperature is set to 20 [° C] The thermal model , as already introduced takes into account the variation of the parameters during the process . In other words, the coefficients of the Fourier are a function of temperature . This means that the thermal model is solved through a non-linear solver. The inductor is not modeled in the thermal process. This simplification is a good hypothesis, as in practice the inductor is cooled. In other words the inductor is in thermal steady state during the entire hardening heat treatment.

4.3.1   Quenching

The quenching phase of the treatment follows the heat phase. After having turned off the inductor you may need a maintenance period to to allow diffusion of heat towards the interior of the workpiece (conduction due to the large gradient between the surface and the core of the billet) and to the environment for surface losses (convection with the surrounding air plus radiation: because several surface points are over 1000 ℃). After that short period, that usually does not exceed the order of the second the entire piece is subjected to quenching phase. To recreate carefully the step of quenching there is the need to describe the behavior of the cooling phase by means of suitable curves . These cooling curves have been obtained through experimental tests , carried out on test pieces . The cooling curves in particular examine the trend of cooling under the action of a fluid quenching . It is seen that experimentally the process is composed of three distinct phases :

- Vapor blanket phase

- Nucleate boiling phase

- Convective cooling phase

Vapour blanket phase

This phase is characterized by teh Leidenfrost effect, that is the event that happens when a fluid comes in near contact with a mass significantly hotter than the liquid's boiling point. The phase so is characterizeb by relatively little cooling rate, because the vapour blanket acts as an insulator, andly cooling occurs mainly by radiation than convection. To simulate numerically this stage , you can consider a dependency of the convection coefficient with temperature. So the initial stage of cooling , wherein the temperature of the surface is much higher than the boiling point

of the fluid, is characterized by convective heat transfer coefficients α $[W/m^2/C]$ extremely low.

Nucleate boilng phase

This step is the most interesting for cooling. In fact, the layer of vapor disappears but manifests a strong agitation of the fluid. This means that the convective coefficient is extremely high. It is possible view that for the considered quenchant (PAG quenching fluid with 10 % polymer concentration at 25 [°C]) the convective coefficient is also 3-4 more times greather than in the preovious phase.

Convective cooilng phase

The temperature of the surface is not enough high to boil the fluid . This phase is characterized by simple conduction and convection between the body and the fluid.

The interface heat transfer coefficient (HEC) is defined as follows:

$$h = \frac{q}{A(\theta - \theta_{amb})} \ [W/m^2/C] \tag{4.14}$$

where h is the heat transfer coefficient, q is the heat flow, A is the surface of the workpiece in contact with the quenchant, θ is the surface temperature vector and θ_{amb} is the uniform homogeneous external temperature, typically assumed as 25 [°C].

All these considerations can be summarized in a cooling diagram HEC-temperature that takes into account all these phenomena.

4.4 Coupling

The coupling between the two physical is performed, respectively, through the temperature distribution in the billet and through the heating power. The numercial computaion of the EM problem has as solution the magnetic scalar potential. From the latter can easily be obtained the trend in time (in the magnetic period) of the induced power: where the thermal conductivity in each element of the mesh of the billet is a distribution function of the temperature distribution computed in the previous thermal step. Obviously the model must start from an initial condition of uniform distribution of temperature $\theta_0 = 20$ [°C]. At this point, the coupling with the thermal modell is carried out thanks to the integration of the distribution of electromagnetic power in the period. The result is then the average value of the heating power for each element that constitutes the mesh. In practice from electromagnetic solution are pulled out all the Lagrange points constituting the mesh, and are integrated through an appropriate numerical integration method. Because as written, the electromagnetic model was solved considering linear shape functions, simple integration via method of trapezoids provides excellent results in low-cost computing. This is even more true when you consider that every electromagnetic period is sampled with 401 points, that means in our case a time step of $2.5 \cdot 10^{-7}$
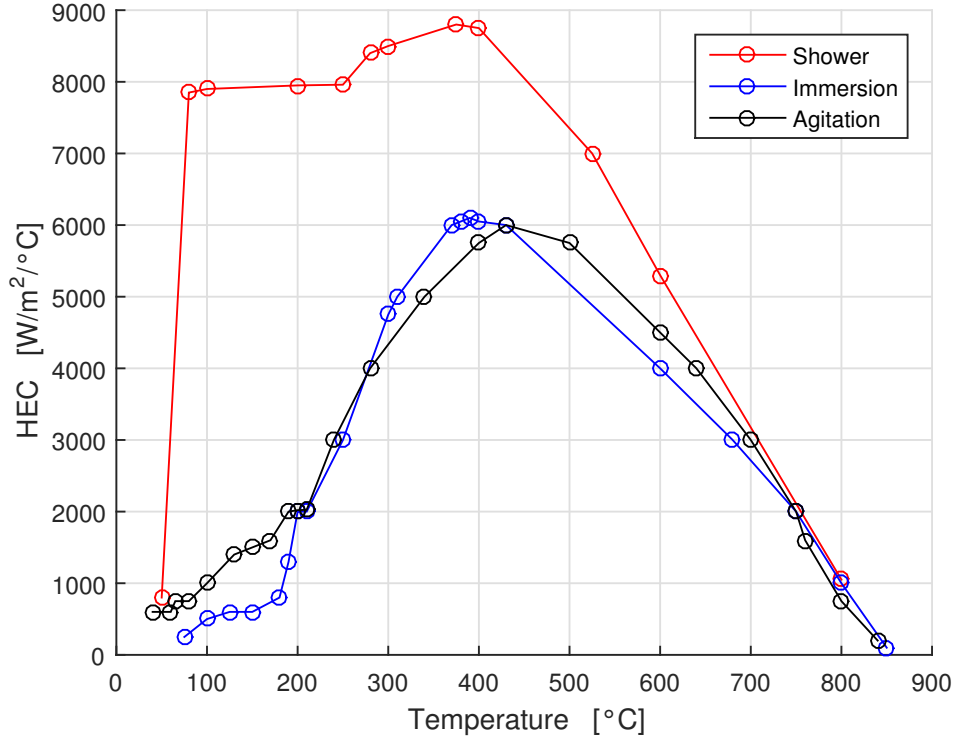
Figure 4.10: HEC for different quenching methods.

$[s]$.

$$w(\mathbf{P}, t) = \begin{bmatrix} w(\mathbf{P_1}, t_1) & w(\mathbf{P_1}, t_2) & ... & w(\mathbf{P_1}, t_{n-1}) & w(\mathbf{P_1}, t_n) \\ w(\mathbf{P_2}, t_1) & w(\mathbf{P_2}, t_2) & ... & w(\mathbf{P_2}, t_{n-1}) & w(\mathbf{P_2}, t_n) \\ ... & ... & ... & ... & ... \\ w(\mathbf{P_m}, t_1) & w(\mathbf{P_m}, t_2) & ... & w(\mathbf{P_m}, t_{n-1}) & w(\mathbf{P_m}, t_n) \end{bmatrix} \tag{4.15}$$

where n is the number of samples in a period, and m the number of Lagrande points, that depends from the quality of the mesh. A Lagrange point in an axial symmetric model is univocally defined from its coordinates: $\mathbf{P} = [x, y]$. To obtain the avarage power in a period:

$$< w(\mathbf{P}) >= \frac{1}{T} \int_{t_0}^{t_f} w(\mathbf{P}, t) \, dt = \frac{1}{T} \int_0^T w(\mathbf{P}, t) \, dt \tag{4.16}$$

Than for the Stevin law, it is possible to approaximate the Integral 4.16, in other words the area below the power function, with the area of the trapezoid. Because of the magnetic potential is linear, and the time discretization is constant, it is also the exact integral, than:

$$< w(\mathbf{P}) >\approx \frac{dt}{T} \left(\frac{w(\mathbf{P}, 0) + w(\mathbf{P}, T)}{2} + \sum_{i=2}^{n-1} w(\mathbf{P}, t_i) \right) \tag{4.17}$$

So you get the distribution of the average power inside the billet . This distribution is then the only heat source in the thermal problem, assumed constant over the period

of the thermal solver. At the end of electromagnetic solving it reaches a certain temperature distribution in the billet to step k. This distribution is set as input to step $k + 1$ of the electromagnetic model . The computation of the thermal problem has as ouput a temperature distribution, that is the input of the next electromagnetic problem.

$$\theta_k (\mathbf{P}) \to \theta_{k+1} (\mathbf{P})$$

While for the electrical resistivity is very easy to define a linear function with temperature, for the relative magnetic permeability was necessary to define a curve function of both temperature , that of the magnetic field (or magnetic induction) . To do this , to lighten level computational software , the curve $|\mathbf{B}(|\mathbf{H}|, \theta)|$ has been modeled with a piecewise function . In taking into account thebehaviour of magneic field with temprature (equzione magn sat). Instead of describing the behavior as a function of the temperature of the induction field with an exponential function , it is possible to define a piecewise defined function:

$$F(\theta) = \begin{cases} 0 & \theta \leq \theta_i - \Delta\theta \\ 1 - \exp\left(\frac{\theta_i - \theta_c}{C}\right) & \theta_i - \Delta\theta \leq \theta \leq \theta_i + \Delta\theta \\ 0 & \theta \geq \theta_i + \Delta\theta \end{cases} \tag{4.18}$$

In this way it possible to obtain a shape function piecewise that is represented for certains temprature range in figure 4.11. It is important remeber that the behaviour of the induction magnetic field is again:

$$|\mathbf{B}(|\mathbf{H}|, \theta)| = \mu_0 |\mathbf{H}| + \frac{2B_s}{\pi} \arctan \frac{\pi \mu_0 (mu_{r0} - 1)}{2B_s} |\mathbf{H}| \cdot F(\theta)$$

Finally, with the same temperature distribution are updated as seen all electromagnetic parameters for each element constituting the mesh of the billet.

4.5 Solver

4.5.1 Electromagnetic Solver

The resolution of the electromagnetic problem is the more time consuming part of the solution of the model . In fact the non-linearity magnetic (ie the correlation between the magnetic field $\mathbf{H}$ $[A/m]$ and the magnetic flux $\mathbf{B}$ $[T]$ through a feature typically highly non- linear, makes it very slow and costly resolution. The commercial software Comsol makes possible to define with reasonable freedom Magnetic feature through a map [magnetic field-magnetic flux]. In practice the software after the resolution of the rotor of the magnetic potential, obtains the magnetic flux $\mathbf{B}$, then it calculates the module at a specific element and for that value of magnetic flux goes through linear interpolation to derive the relative value of the magnetic field $|\mathbf{H}|$ $[A/m]$. The model is developed in the time domain , so it is necessary to use as a resolver a TIME-DEPENDENT SOLVER. To ensure a convergence of the method and the obtaining of a solution, it was chosen as the direct solution method: PARDISO.
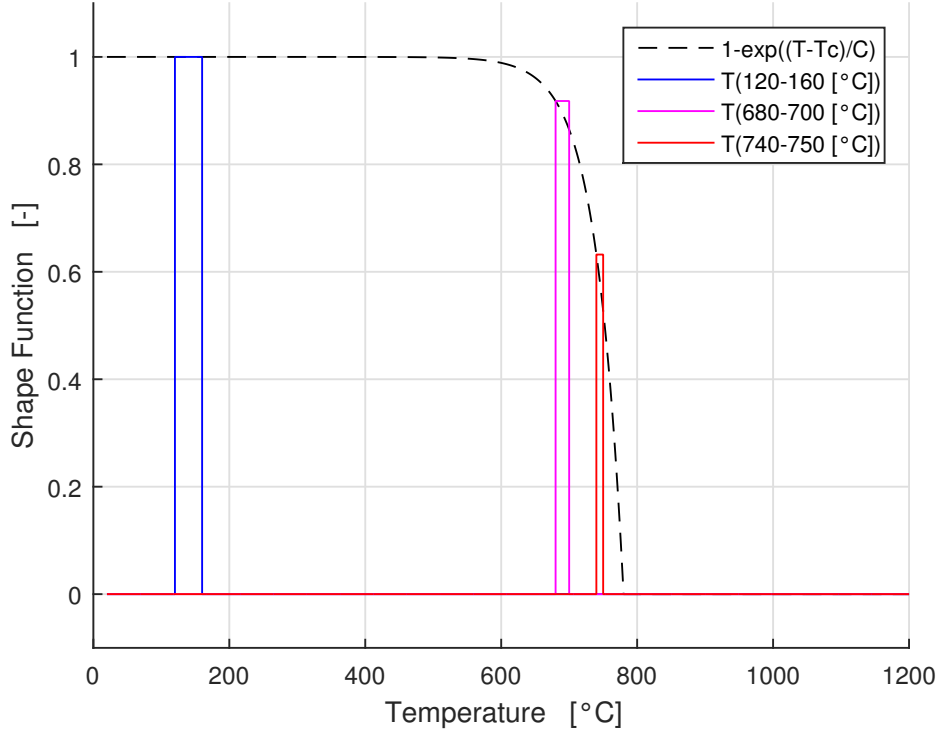
Figure 4.11: Example of different piecewise functions that sobstitute the more general analytic formulation of the temperature exponential function.

Time dependent solver	$dt = 2.5 \cdot 10^{-7}$ $[s]$	$t_i = 0$ $[s]$	$t_f = 2.0 \cdot 10^4$ $[s]$
Direct Solver	PARDISO		
BDF-Strict	$t_{min} = 1 \cdot 10^{-8}$ $[s]$	$t_{max} = 1 \cdot 10^{-8}$ $[s]$	
Non Linear Method	Newton-Raphson	Authomatic	

Table 4.5: Electromagnetic time dependent solver configuration

4.5.2   Thermal problem Solver

The resolution of the thermal problem has less difficulties than the computational problem of the electromagnetic model. The difference in complexity was so great that the time for a resolution of the thermal equations were negligibile. However the thermal model presents nonlinearity in coefficients so it was set a resolution in the time domain with a suitable non-linear solver. It is important remember that for the thermal model, for each time step the distirbution oh the heating power is supposed constant in an interior computation period. The heating power $w(r, z)$ $[W/m^3]$ is the avarage induced power in an electromagnetic period, so it is possible to solve the Fourier's equation with a more large time step, because it is supposed constant. The quenching phase instead is modeled with an HEC(θ) behaviour imposed on the surface of the billet. The time step is the same of the heating phase, because

parameters are non-linear. The quenching is solved in a time rage of 1 [s].

Time dependent solver	$dt = 1 \cdot 10^{-4}$ [s]	$t_i = 0$ [s]	$t_f = 5.0 \cdot 10^3$ [s]
Direct Solver	PARDISO		
BDF-Strict	$t_{min} = 1 \cdot 10^{-4}$ [s]	$t_{max} = 1 \cdot 10^{-4}$ [s]	
Non Linear Method	Newton-Raphson	Authomatic	

Table 4.6: Thermal problem time dependent solver configuration

Chapter 5

Simulation Results

In this chapter the results of the numerical computation of the finite elements model described in Chapter 4 are illustrated . The first part of the chapter describes the process of surface hardening with the use of simultaneous dual frequency from the thermal point of view. This section shows the most important results of the hardening process, such as:

- powers involved

- thicknesses hardened

- zones of overheating

- efficiency of the method

- process times

- considerations about quenching

The second part is aimed to describe from an electromagnetic point of view this innovative technique, with particular attention to the effect of the use of a second frequency, in particular to the effect that this has on saturation of the treated piece. Specifically it focuses on:

- induction field behaviour in time

- eddy currents distribution in time

- effect of the sudden variation of the relative permability in time

- behaviour of the electromagnetic heating power inside the billet during the electromagnetic period

- behaviour of the absorbed power from the coil

Before taking a careful analysis of the results is convenient to define first of all points, cut lines and surfaces on which the results were plotted.

5.1   Hardening Process

The effective value of the power, and the current during the heating phase are storngly time varying. It would be interesting to be able to express an analytical formulation of the rms power as a function of the relative permeability and resistivity. From this it would be able to express an analitical formulation of the RMS value of the power as function of the temperature. It's also interesting to see the influence of the surface on which you concatenate the magnetic field, which is seen to change during the process. The surface S_1 $[mm^2]$ is a function of the thickness of penetration. In fact it can be assumed (at least initially for a linear model and in single frequency) that the surface S_1 is the only surface on which the magnetic field is concatenated.

$$S_1 = \pi\delta(2r_{ext} - \delta^2) \tag{5.1}$$

$$\Phi = \int_{S_1} \mathbf{B} \cdot \mathbf{n}\, dS \tag{5.2}$$

And it is possible to define for a magnetic model the induction coefficient:

$$L = \frac{N\Phi}{I_{rms}} \tag{5.3}$$

For an axial symmetric model:

$$L \propto \mu_r(\theta)\delta(\theta) \tag{5.4}$$

Instead it possible to view the resistence as:

$$R = \rho_0 \frac{lungh}{S_2} \tag{5.5}$$

Also for this case it can be understood that the Resistance tends to increase with the frequency due to the diminuation of the penetration depth. So if δ determines the effective area S_2 $[mm^2]$ on which there is a current density not equal to zero, then it is interesting to see the effect of temperature on the surface S_2 and then the resistance R. So it possible to describe the resistence as:

$$R \propto \rho(\theta)\frac{1}{\delta(\theta)} \tag{5.6}$$

Then combining all hese considerations:

$$\delta = \sqrt{\frac{2\rho(\theta)}{\omega\mu_0\mu_r(\theta)}} \ [mm^2] \tag{5.7}$$

And finally the Impedence Z $[\Omega]$, function of Resistance R $[\Omega]$ and Reactance X $[\Omega]$:

$$Z = \sqrt{R^2 + X^2} = \sqrt{R^2 + (\omega L)^2} \tag{5.8}$$

It is possible try to explain the behaviour of impedance with temperature θ:

$$Z \propto \sqrt{(\frac{\rho(\theta)}{\delta(\theta)})^2 + (\omega\mu_r(\theta)\delta(\theta))^2} \tag{5.9}$$

where the behaviour of magnetic relative permeability, electrical resistivity and penetration depth are already discussed. This means that the impedence Z is strictly dependent with temperature:

$$Z \propto \sqrt{(\exp(\Delta\theta)^2 + (\theta)^2}$$ (5.10)

This means that the impedance is strongly decreasing for relatively low values of temperature. Then, when the average temperature of the surface becomes sufficiently high, in practice above about 600 ° C, the relative permebaility begins to collapse. The first derivative of the impedance changes sign and begins to grow strongly.
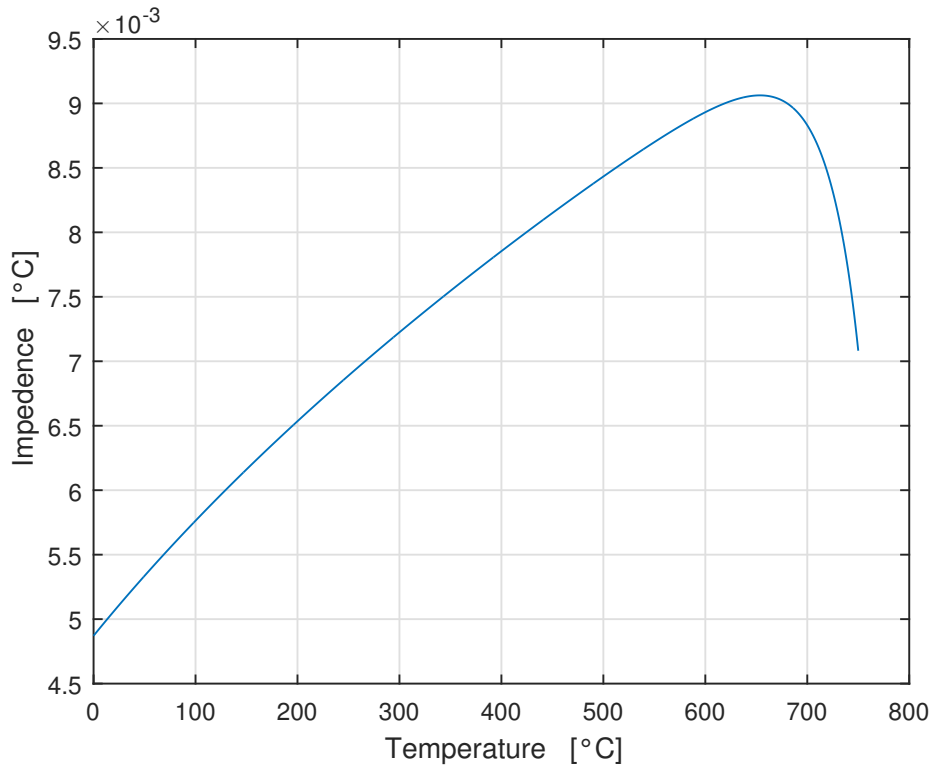
Figure 5.1: Behaviour of impedence Z $[\Omega]$ with temperature θ $[C]$

The root mean square of the current:

$$I_{rms}(\theta) = \frac{V_{rms}}{Z(\theta)} \ [A]$$ (5.11)

and the root mean square of the power is:

$$S_{rms}(\theta) = \frac{V_{rms}^2}{Z(\theta)} \ [VA]$$ (5.12)

In the Figure 5.3 you can see this trend as a function of time. The trend qualitative difference between the two graphs is due to the variation of the heating rate in the last phase of the thermal process.
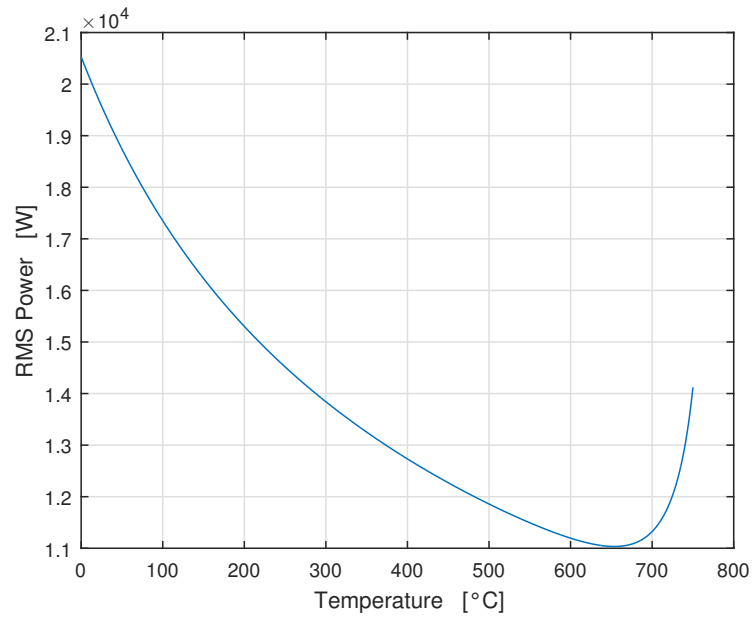
Figure 5.2: RMS Power function of temperature θ. This plot takes into account a linear evolution of the average value of the temperature of the surface
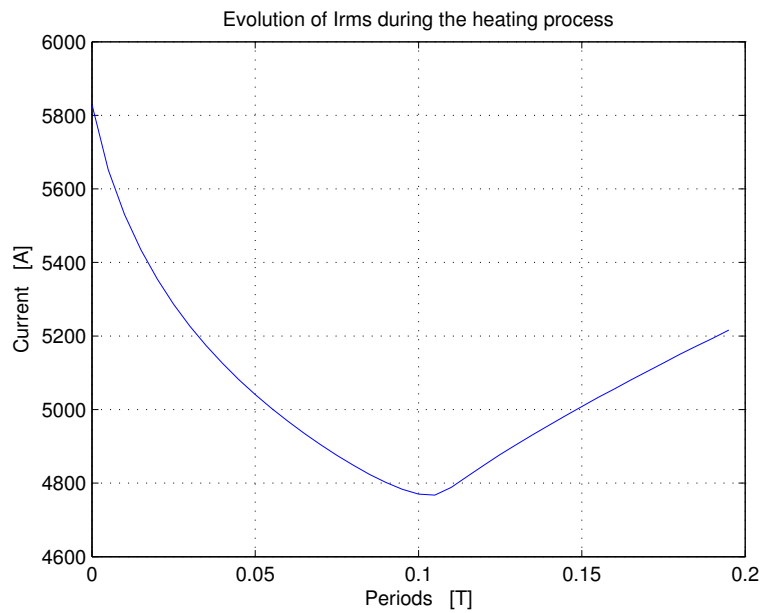

Figure 5.3: RMS Current function of temperature θ. This plot takes into account a linear evolution of the average value of the temperature of the surface

From the electrical point of view it is extreamelt interesting also try to understand how evolves the active power absorbed by the sysyem during the process. So it is possible to define for each thermal step the average value of the power absorbed, that is the total active power of the load. This is plotted in Figure 5.4. It is clearly

possible view that it varies non linearly during the SDF hardening process.
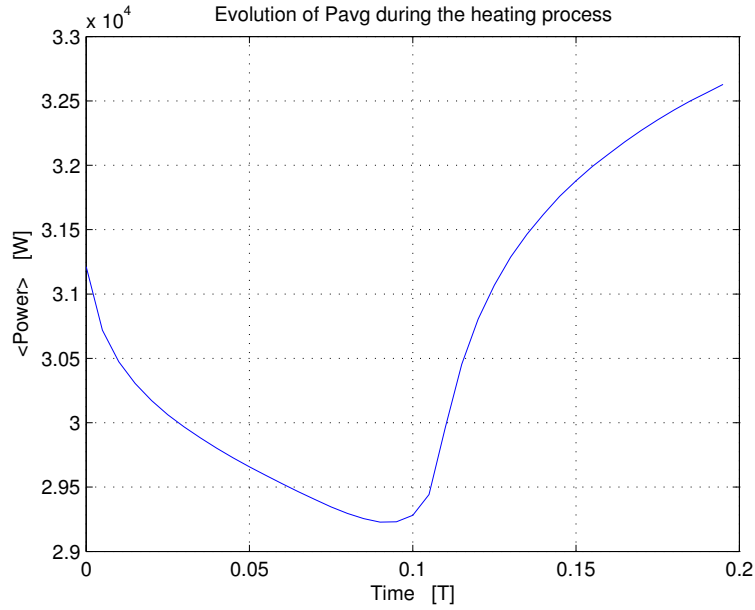
Figure 5.4: Avarage value of the power P_{AVG} as function of process time.
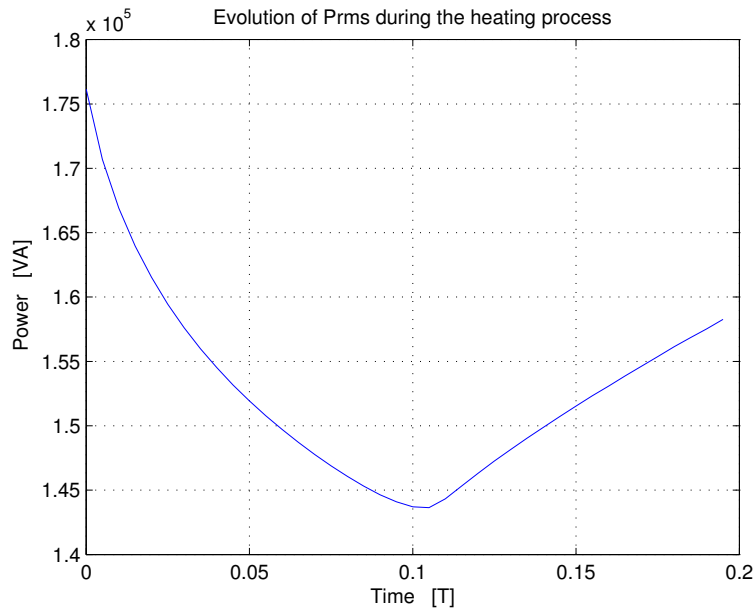
Figure 5.5: RMS value of the power P_{RMS} as function of process time.

It is possible now to obtain the value of the series resistance as:

$$P_{AVG} = R \cdot I_{RMS}^2 \qquad (5.13)$$

where R [Ω] is the equivalent resistance value. It is clear that the load resistance is the series of two resistance, the first is the inductor resistance, and the second the

workpiece resistance bring back to the inductor. This means that the load resistance
viewed from the feed is:

$$R = R_{ind} + R_{bill-ind} \tag{5.14}$$

This means that it is possible define a value of the resistance for each thermal
time step. In Figure 5.6 it is possible to view the trend of the resistance during the
heating process.
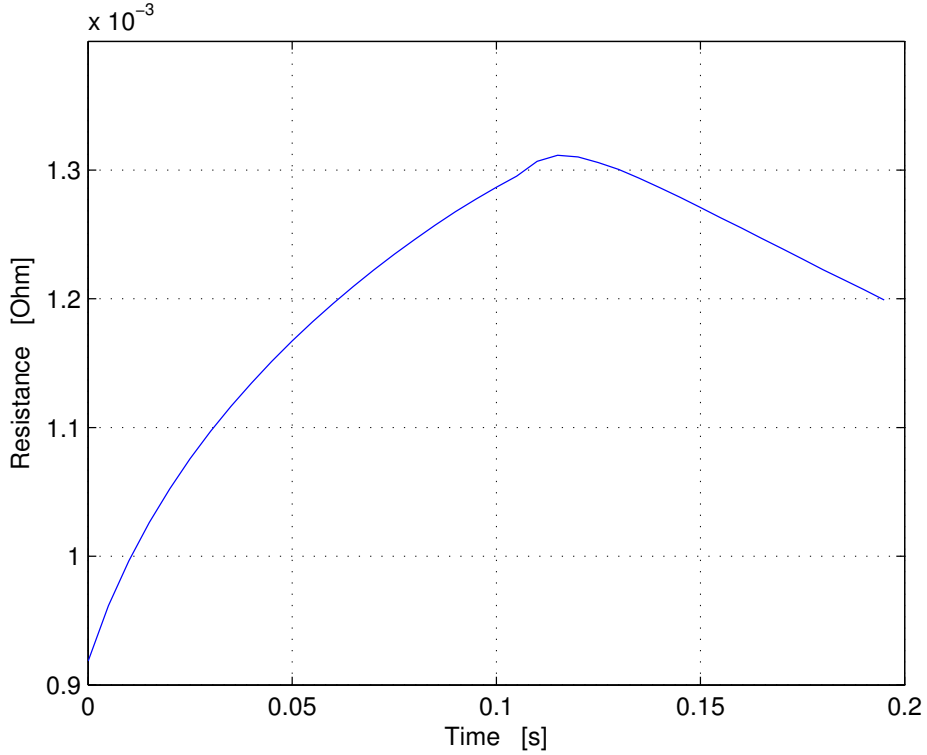
Figure 5.6: Value of the equivalent resistance viewed from the feeding.

After having defined avarage power, in the same way it is possible to define
reactive power and power distortion. In this case, because of both high and medium
frequency are extreamely important, it is difficult define these two different values.
But it is clear that both of them are important from an electrical point of view. Then
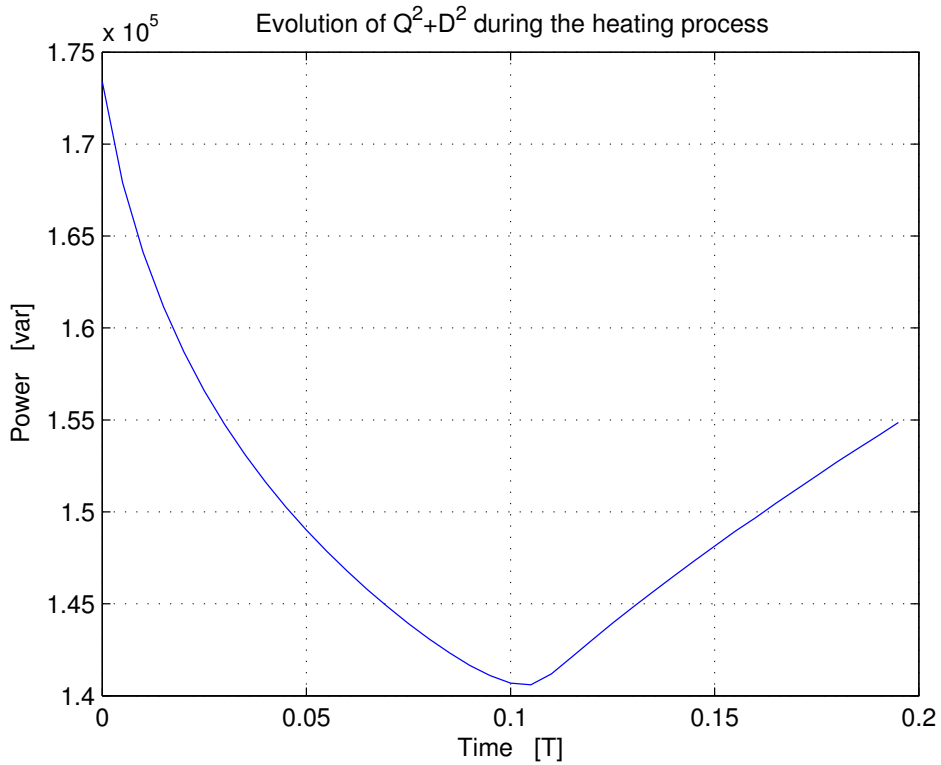the two terms can't be easily divided. But however without loss of generality it is
possible write:

$$P_{RMS} = \sqrt{P_{AVG}^2 + Q^2 + D^2} \tag{5.15}$$

then because of P_{AVG} and P_{RMS} are known, it is possibile to compute the sum

$$Q^2 + D^2 = \sqrt{P_{RMS}^2 - P_{AVG}^2} \tag{5.16}$$

And finally its value during the heating process is plotted in Figure 5.7

Figure 5.7: Trend of the term $Q^2 + D^2$ during the heating process.

It's possible also define the concept of efficiency of the process. Electromagnetic efficiency is defined as usuful power output divided by the total electrical power consumed, typically denoted as η_{el}:

$$\eta_{el} = \frac{Useful power output}{Total power input} \tag{5.17}$$

In this case the efficieny is the ratio between the avarage value of the total induced power inside the billet and the total active power supplied by the generators. This means that in this case:

$$\eta_{el} = \frac{< P_{billetta} >}{< P_{gen} >} \tag{5.18}$$

then it is possible to compute the total power transferred to the billet as:

$$\int_{\Sigma} \left(\frac{1}{T} \int_{T} w(r, z, t) \, dt \right) dV = \int_{\Sigma} P_{AVG} \, dV \tag{5.19}$$

where Σ is the volume of the billet. Instead the total power absorbed by the inductor is the avarage value of the istantaneous power computed in an electromagnetic period. The behaviour of the efficieny during the process is plotted in Figure 5.8, instead the behaviours of induced power to the load and total power absorbed by the inductor are plotted in Figure 5.9.
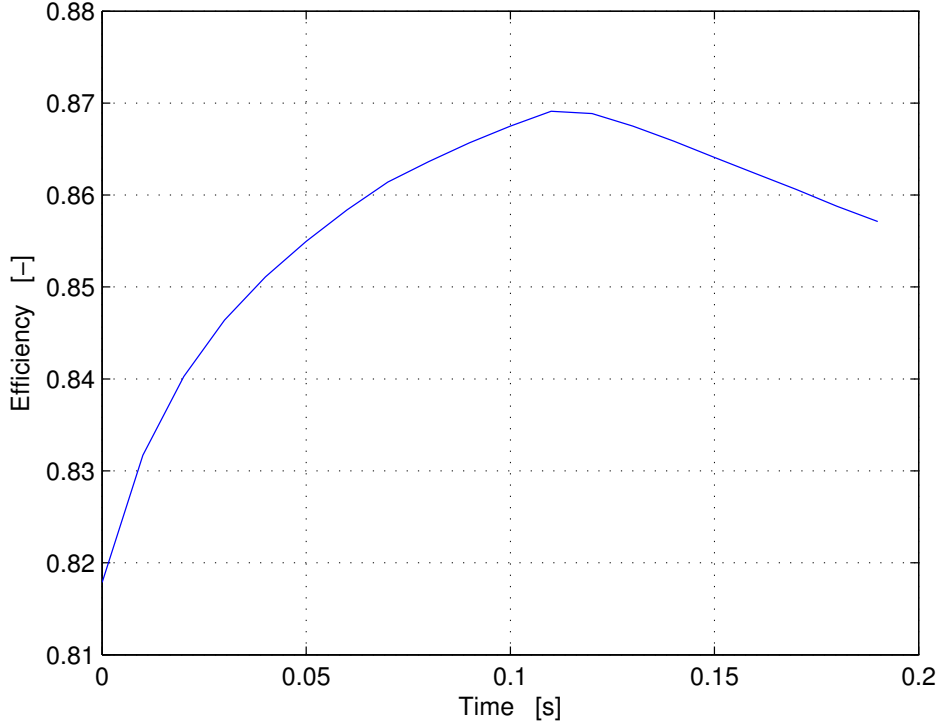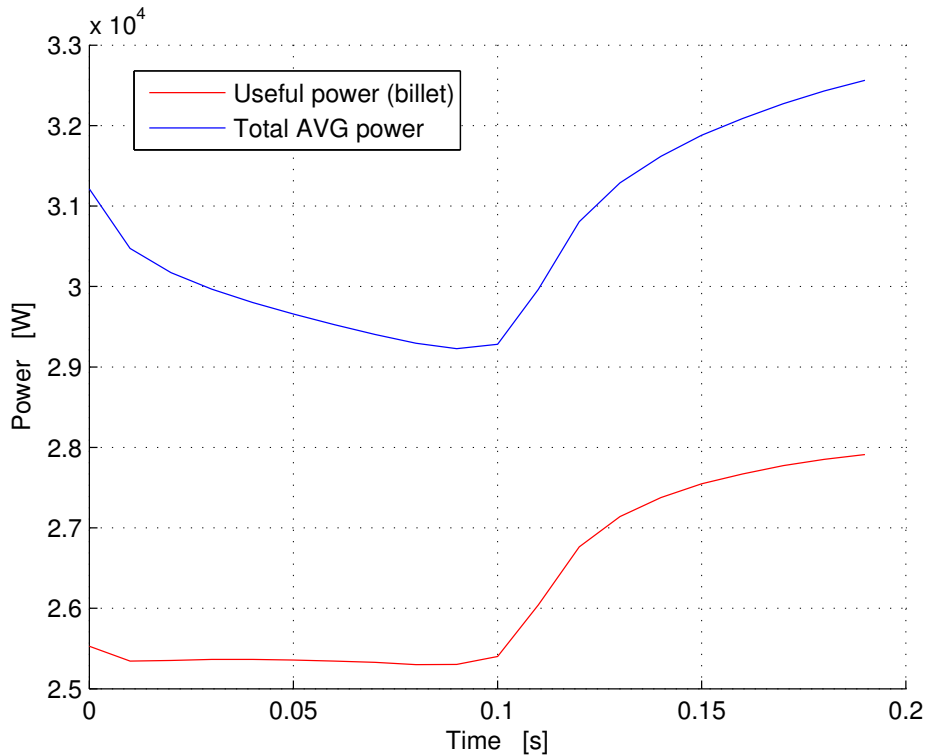
Figure 5.8: Efficiency during the heating process.

It is clear from Figure 5.8 that electromagnetic efficiency is extreamely high for this process, this is an accord for what is possible to see in an theorical approach as done in [18]. The figure shows also the efficiency reduction for a time that is over 0.11 [s] this phenomenon is the effect of the temperature. It is possible to obtain an analytical formulation for the efficiency as function of magnetic permeability, resistivity and frequency. It is clear that in this model the system is fed with two different frequencies, this means that showuld be possible to define the efficieny for each frequency. instead is possible to obtain a semplyfied relation that is true for frequency values sufficiently high:

$$\eta_{el} \approx \frac{1}{1 + \alpha\sqrt{\frac{\rho_i}{\rho_b\mu_b}}} \tag{5.20}$$

where α is the coupling coefficient inductor-load. Then because of the magnetic permeability varies during the process is possible to write a behaviour of efficiency with temperature θ or time t. This behaviour shows that the global electromagnetic efficiency is high for all the process and is higher than 80 % for all the time process and tends to increase (for the effect of resistivity that is proportianl with the temperature) untill the temperature is close to θ_c in a large portion of the billet.

$$\eta_{el} \approx \frac{1}{1 + \alpha\sqrt{\frac{\rho_i}{\rho_b(\theta)\mu_b(\theta)}}} \tag{5.21}$$

Figure 5.9: Powers during the heating process. Useful power and total absorbed power.

It is possible to define instead in the same way the istantaneous power transferred to the billet. Particularly in Figure 5.10 the heating power is plotted. It is computed by integration in the total volume of the billet. It is possible view that its avarage value is exactly the avarage value computed for $t_{th} = 0 - 0.005$ $[s]$. This power causes the heating in the billet. It is extreamely variable in the electromagnetic period, in accordance with the behaviour of the relative permeability and the resistance and with the two frequecies of the source.

5.2 Numerical thermal results

The analysis of post-processing was done with the help of commercial software MATLAB . The resolution FEM fact allows you to export files containing solutions . These were then reworked by MATLAB and plotted in the regions of interest. First of all it is important to define a map of the points which the figures refer to. The points selected for the analysis of the data are, in my opinion, the points of greatest interest from the point of view of the elettromagnetic and thermal process. The process of induction hardening in dual frequency typically want as output data (or specific process) parameters such as temperature differencies in the directions x,y (r , z in the model). Of non-negligible interest in this work were also analyzed parameters such as the rate of heating, the distribution of the power induced and the values of the electromagnetic fields inside the billet.
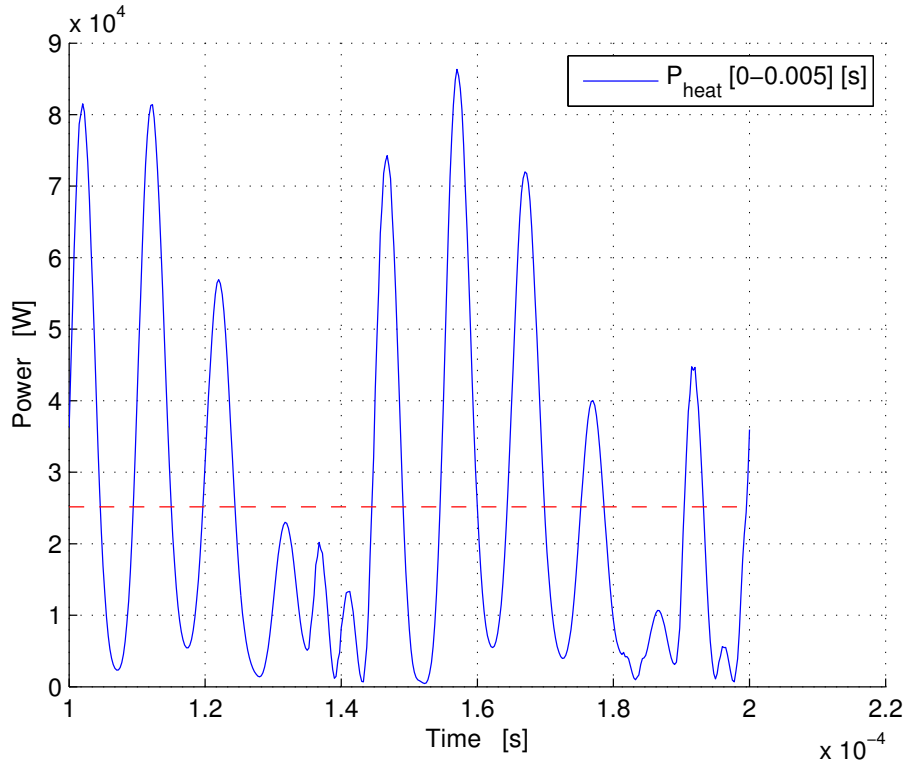
Figure 5.10: Istantaneous heating power in the billet, computed for the period $\Delta t_{th} = 0 - 0.005 \ [s]$

Point	r-coordinate [mm]	z-coordinate [mm]
A	10	0
B	0	0
C	5	0
D	7.5	0
E	10	2
F	10	5
G	10	20
H	8	0

Table 5.1: List of the points analyzed in the results

In detail it is also possible to analyze what happens on the main points of interest. For example in order to hard a layer of 1 [mm] you can plot trends from different points with a better detail . In Figure 5.11 you can see that for example after a heat treatment of 0.2 [s] there exists a strong thermal gradient to a depth of 2 [mm] . In fact, the points of the surface in a section transverse to the billet to the coordinates z = 0 [mm] are at a temperature of about 1100 [°C] , while already one millimeter the temperature is slightly higher than the Austenitizing temperature od steel. A 2 [mm] the temperature falls to about 580 [°C]
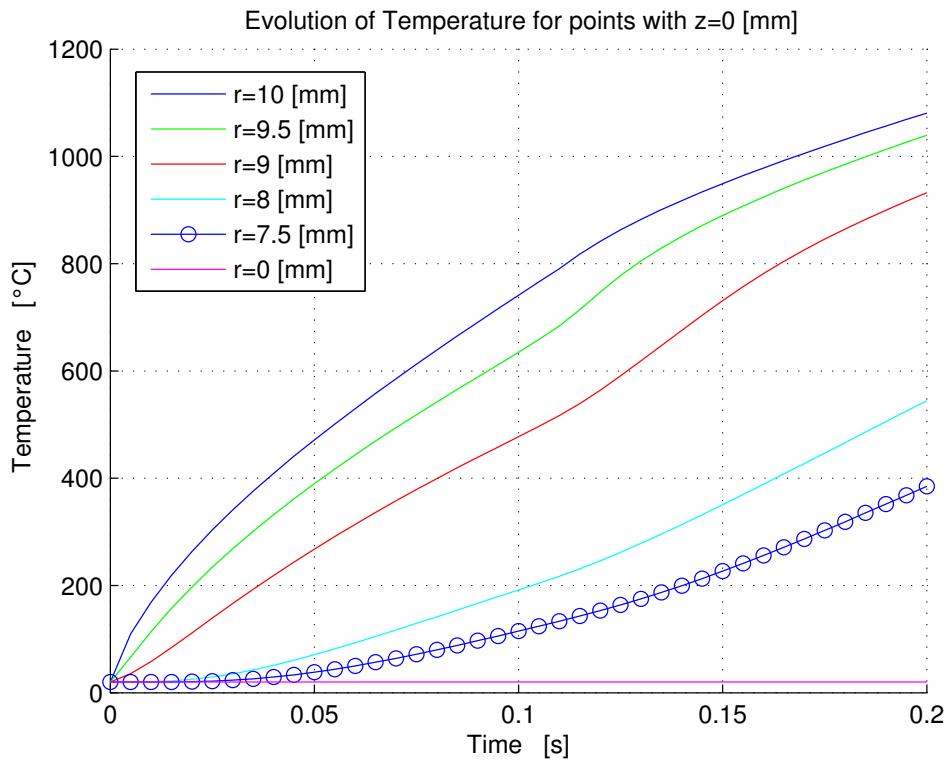
Figure 5.11: Temperature evolution in time of main points at 0 [mm] z-coordinate

It is possible to see from the geometry analyzed that the inductor is much smaller than the billet heated . This means that only a small band of billet is well coupled with the inductor itself. So the distribution of the heating power is confined in a central band with respect to the inductor. During the heating in fact temperature gradients along the z-coordinate are very intense . From Figure 5.12 you can see the evolution on the most interesting points of the surface of the billet.
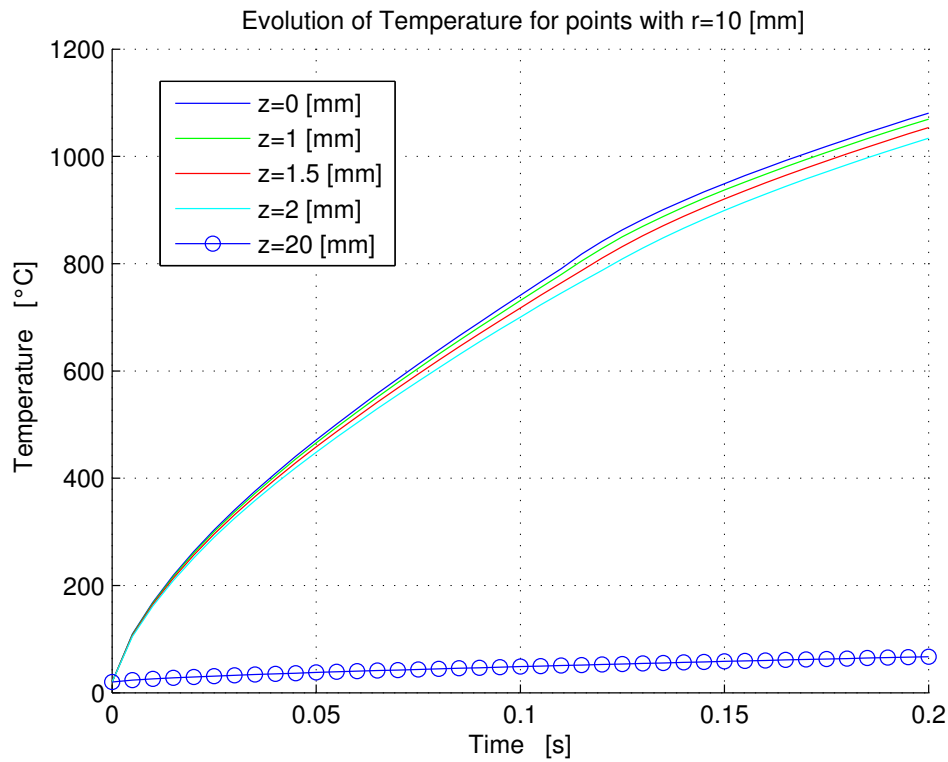
Figure 5.12: Temperature evolution in time of main points at 10 [mm] r-coordinate

It is clear that with the inductor chosen becomes very difficult to hard the edges . But in practice the inductor has dimensions comparable with that of the height of the toothed wheel to be hardened . The objective of this work was not achieve uniform distribution along the height , but to see in detail the phenomena of interest. To understand the temperature trend, for example some distributions of temperature have been also plotted , in sections parallel to the height of the billet in two different time instants , before the demagnetization effect the Curie and at the time of 0.1 [s] when a good portion of the billet has passed the critical temperature.
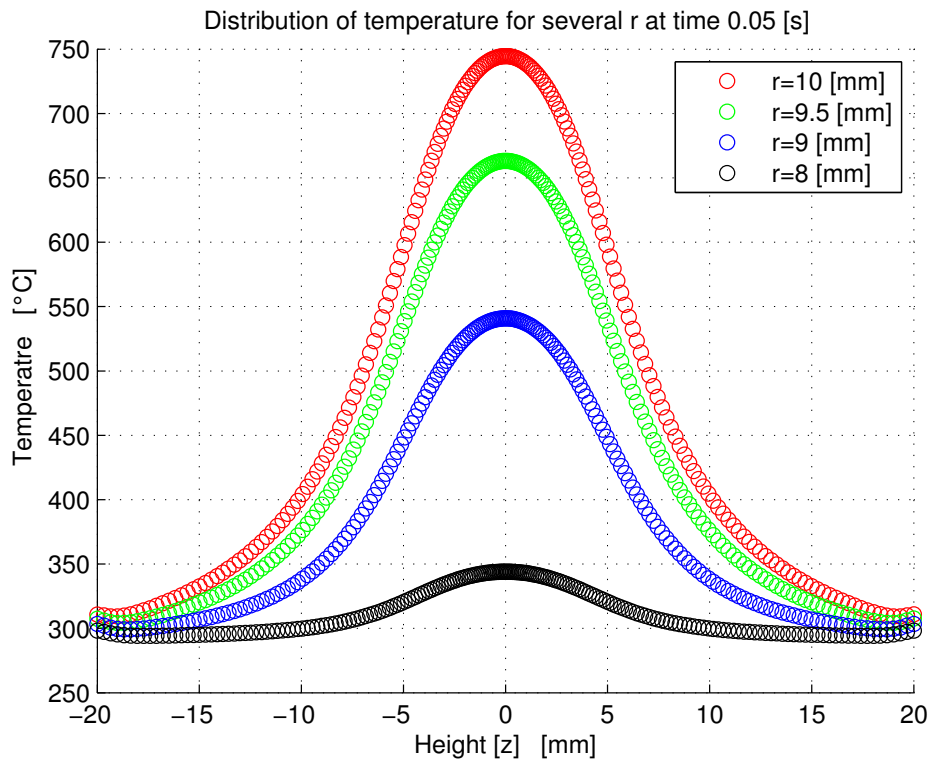
Figure 5.13: Temperature ditribution for different r values at process time of 0.05 [s]
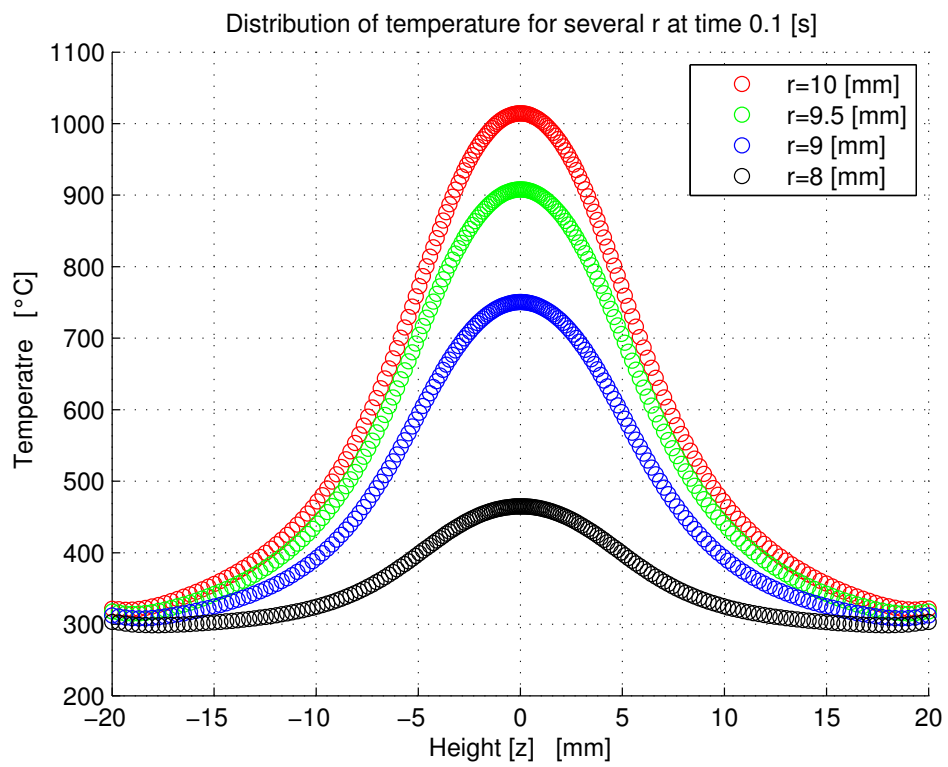
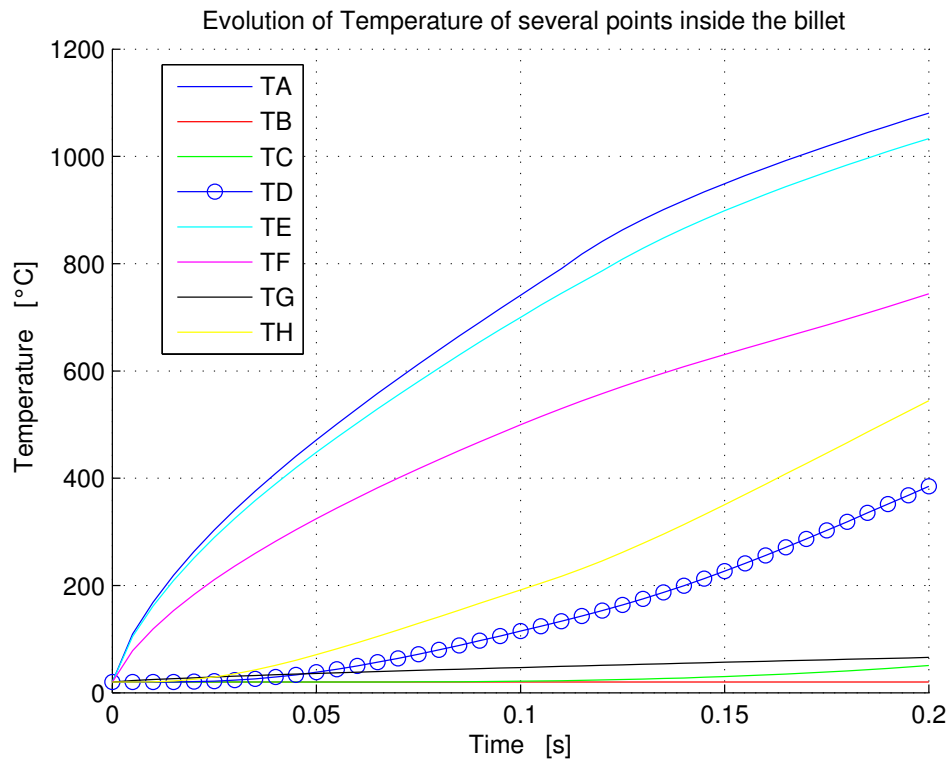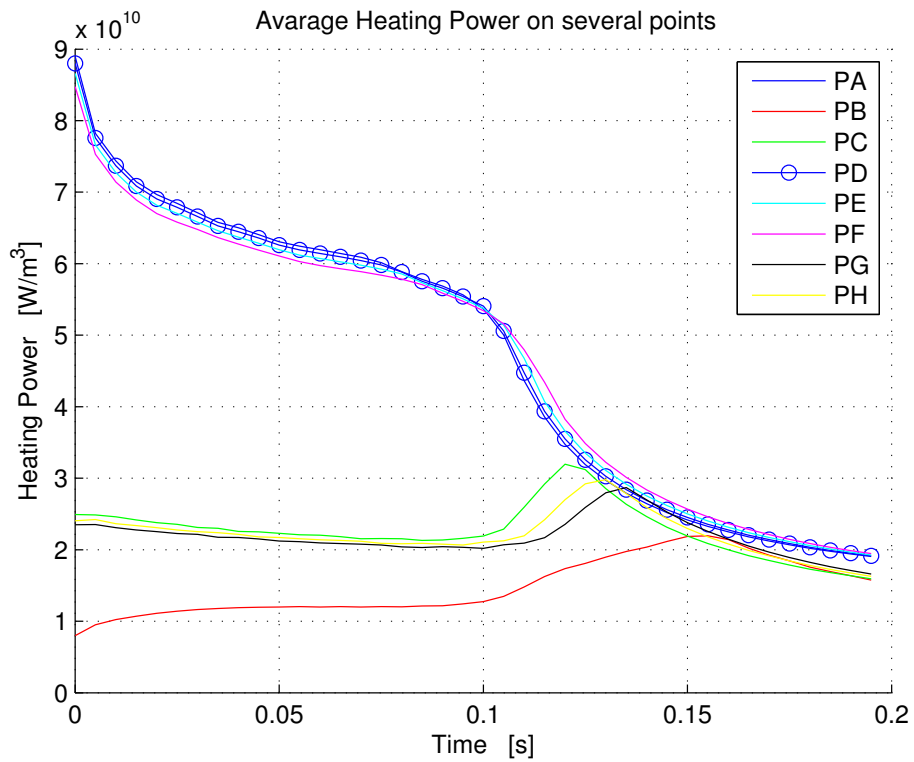**Figure 5.14:** Temperature ditribution for different r values at process time of 0.1 [s]

Figure 5.15: Temperature evolution in time of several points indisde the billet.

Figure 5.16: Heating rates evolution in time od several points indisde the billet.

From the Figure 5.17 it is clear how much important is the rate changes during the heating process. There is a strong thermal inertia of the layers of material that in the first steps of the process do not undergo by induced powers. From hardening point of view, an extremely important parameter is heating rate, that qualitatively expresses the theoretical times necessary for hardening.
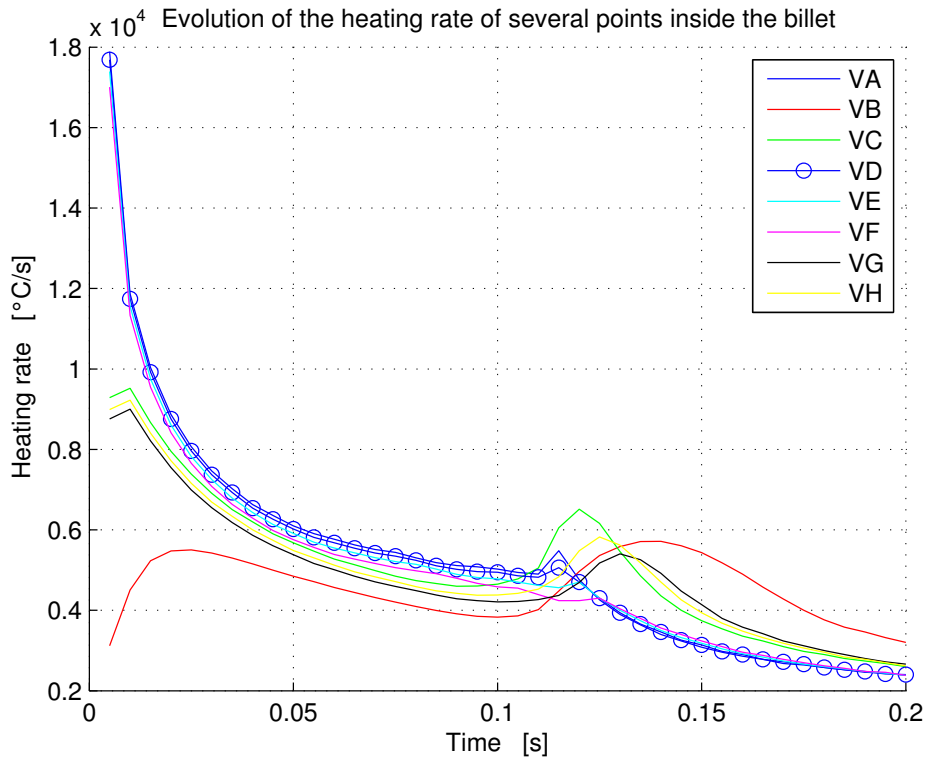
Figure 5.17: Heating rates evolution in time od several points indisde the billet.

From the theory it is also known that the rate of heating is useful for defining the temperature A_{c3} $[C]$, which is known to be a function of the heating rate. Because of induced power is not constant inside the billet, also heating rate will be not constant inside the billet. This means that the transformation to austenite begins at different temperatures, and is not simultaneous in to the workpiece. The results subline that heating rate are extreamely strong all along the process. Figure 5.17 shows a sharp drop of the heating rate of the points nearest to the inductor already from earliest moments of the process. This is caused by the reduction of the induced power, by the effect of the losses by convection, and above 700 [°C] also by the radiative losses. Another extremely interesting phenomenon is the increase of the heating rate of thedeepest points of the billet. This is caused by Curie transormation. Induced power drifts to penetrate inside the billet. This means that austenization is not simultaneous during the process.

This section presents the results of the study of the electromagnetic problem, solved in the time domain. In particular way it focuses on the effects of temperature on the magnitudes electromagnetic oscillating in time. Also a numerical solution, with a time-dependent solver allows to reconstruct with extreme accuracy (at least in theory) the effect of magnetic saturation.

The results in this section are presented for different periods of the heat treatment: ie for different distributions of temperature, as each electromagnetic period has been solved assuming a temperature distribution constant in the related period. I've decided to present several interesting cases, particularly:

- Initial condition of constant temperature distribution inside the billet. This means the thermal time range: 0 to 0005 [s]

- Thermal time range 0.2-0.205 [s] at this time the electromagnetic phenomenon is not affected by the temperature, because temperature is everywhere inside the biller under 600 [°C] which is temperature at which starts the fall of relative permeability.

- Thermal time range 0.1-0.105 [s]: at this point of heating process there are not points that have exceed Curie tememprature, but the maximum temperature in the billet is 600 [°C], this means that relative permeabilty is decreasing.

- Thermal time range 0.12-0.13 [s]: in this situation there is a small area, whose points have exceeded Curie.

- Thermal time range 0.15-0.16 [s]. At this point, a large portion of the billet has eclipsed Curie.

After the instant $\theta = 0.05$ $[s]$ exists a small portion of space whose temperature has exceeded the critical temperature of Curie. This means that there are points with unitary relative permeability, ie the steel in this portion of the space has lost its magnetic properties. This means heating sources tend to penetrate in the billet in a layer that is larger than initial skin depth (computed with a temperature of 20 [°C]).

Similarly you can imagine to consider an average temperature of the sourface that has a non-zero magnetic field, and also an average relative permeabilty of it. During the process of austenitizing, the temperature increases and a greater portion of the surface exceeds the critical temperature. This from an electrical point of view is manifested by the collapse of the inductance seen from the generator. This trend follows the exponential function viewed in Chapter 1. Similar observations can be done for the resistance of the billet. It is proportional to the resistivity which instead evolves with a nonlinear function of temperature. These considerations can be put together and obtain a qualitative behavior of the power absorbed by the inductor during the process. So during the process the induced power tends to penetrate to the heart of the billet, into a layer also superior compared to the desired thickness of quenching. This phenomenon, however, is mitigated by the fact that the total power consumption was collapsed due to the increase of the resistivity. Instead, when the avarge temperature of a portion S $[mm^2]$ is higher than 650 [°C] the power consumption tends to increase again. So there is the need to obtain short heating time, otherwise you may hard too much material. It is also important to note that this phenomenon also has its positive sides: it is almost impossible to avoid that the area closed to the inductor exceed the temperature A_{c3} (maximum final temperature above 1100 [°C]), and this causes the magneto-phase transformation of the steel. This phenomenon cuause the reduction of surface heating, and therefore it reduces the heating rate in these areas and this practically means that the overheating, that causes the reduction of hardness, is not too much intense. As already seen the distribution of the average heating power varies strongly during the electromagnetic process. As the aim of the process is to get a heating as possible superficially (reduced thickness hardening) it is very useful for example to plot the trends of power induced in different depths, and try to understand how they change over process time. To do

this, because the temperature does not follow a linear trend with time, as the heating rates are not constant during the process, it is useful for example to try to plot the distribution of Heating Power w $[W/m^3]$ for all periods of the thermal simulation. From 3D figures that express these trends it is easy see how the heating power penetrates deeply toward the center of the billet. This phenomenon can be easily verified experimentally and explains the difficulties of effective hardening process. The non-linearity (and non-ideality) of the material involve phenomena in contrast with the goal of the process. In fact, at least theorically, surface hardening would induce power only on the surface of the workpiece and it would raise the temperature to the desired oin a specfic layer only for conduction . This practically is impossible, beacuse heating sources are not spatially fixed during the heating process.

Evolution of heating power on 10 [mm]
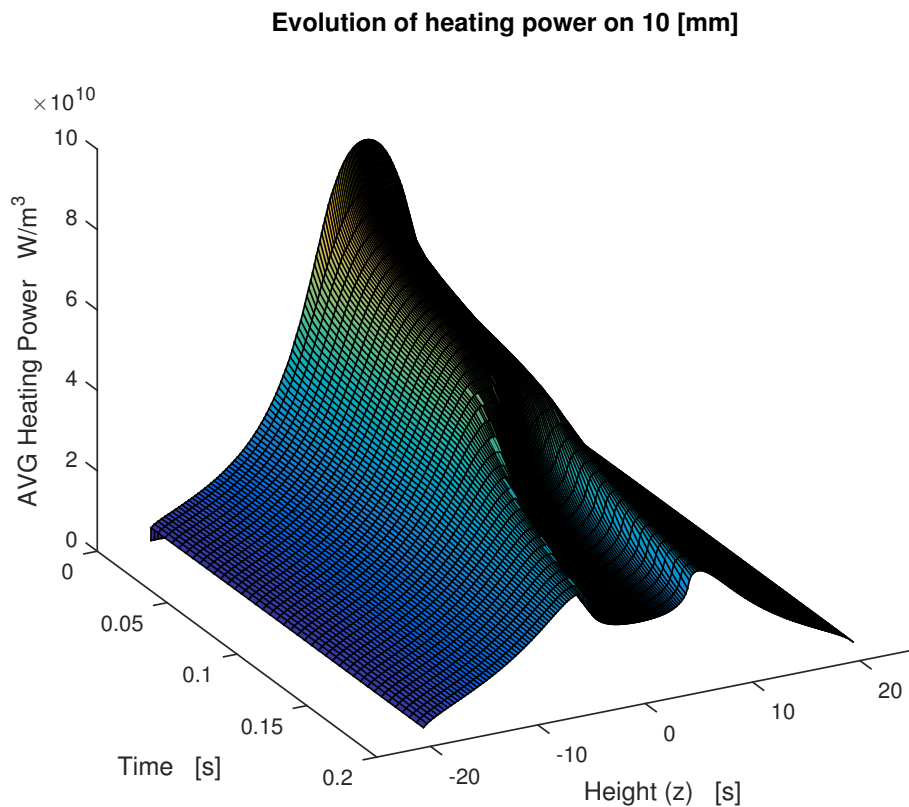
Figure 5.18: Evolution of surface heating power $w(r = 10[mm])$ $[W/m^3]$

Evolution of heating power on 9.9 [mm]
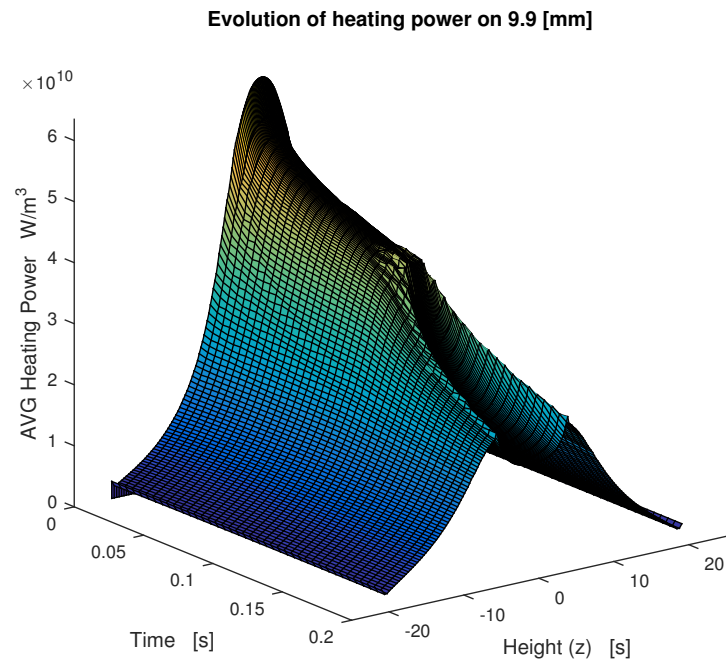
Figure 5.19: Evolution of heating power $w(r = 9.9[mm])$ $[W/m^3]$

Evolution of heating power on 9.8 [mm]
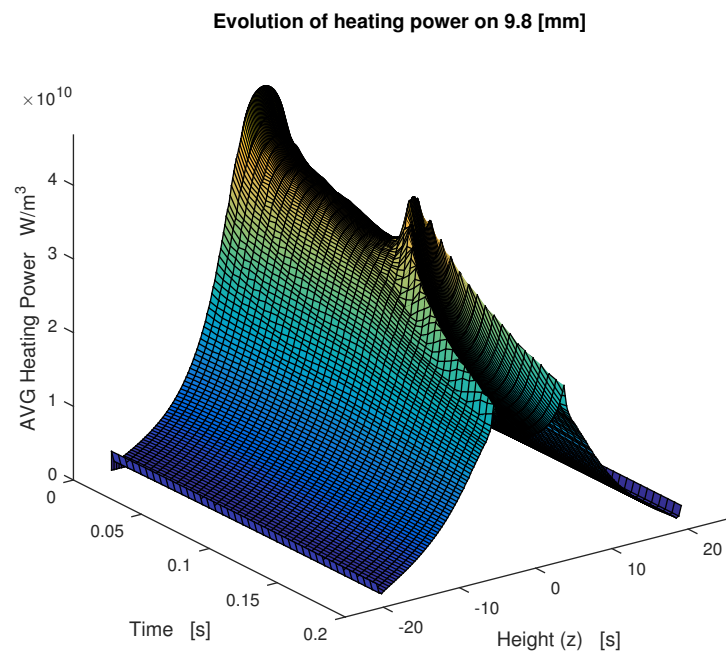
Figure 5.20: Evolution of heating power $w(r = 9.8[mm])$ $[W/m^3]$

Evolution of heating power on 8.5 [mm]
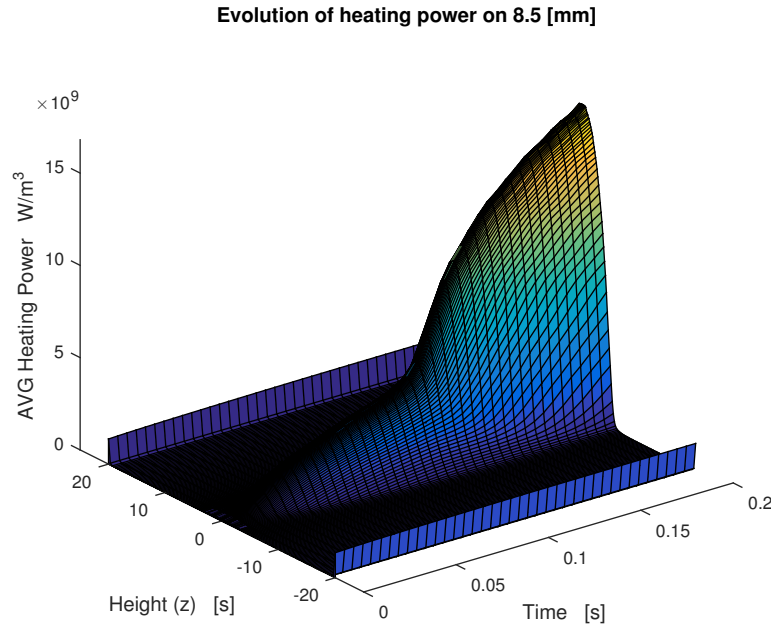
Figure 5.21: Evolution of heating power $w(r = 8.5[mm])$ $[W/m^3]$

5.2.1 Magnetic Saturation

Before starting the discussion of the results, we try to understand what is the effect of the saturation of magnetic field on distributions of heat sources inside the piece. It is clear that the saturation consists in the collapse of the derivative of the induction field with respect to the magnetic field. Since there is an explicit relationship between the magnetic field and the current, that generates it, it is easy to see that in a time dependent domain exists explicit relationship between time and the magnetic field. Then we can express the effect of the saturation as function of time, namely during the electromagnetic period. As already I have already shown, from a computational point of view it is necessary, to use extremely small time steps, as the derivative of the induction field with respect to time can be extremely sharp, if the frequencies involved are high. Then follow this road you can try to put together the characteristics of magnetization and the formulation of the magnetic field over time, and eventually try to define a time derivative of the induction field, which we know is tied to the rotor of the electric field, or to the distribution and the intensity of the induced currents inside the billet.

$$\mathbf{B}(t) = \mu_0 \mu_r(|\mathbf{B}(t)|)\mathbf{H}(t) \tag{5.22}$$

The main complication of this formulation is based on both magnetic field, both magnetic permeability are function of time, because current, that generates magnetic is function of time.

Assuming for now a simplified model, in which the magnetic field is created for example by a filiform source on which circulates a current $i(t)$, and is assessed in a point of the domain $\mathbf{P}(x, y, z)$, it is possible to see the magnetic field $H(t)$ as a

superposition of two currents that evolves with two different frequencies. Then you can write:

$$H(t) = H_1 \sin(\omega_1 t) + H_2 \sin(\omega_2 t) \tag{5.23}$$

that means the induction field is characterized by a behaviour in time, shown in the Figure 5.22.

The saturation tends to cut out the higher frequency components when the magnetic field at medium frequency is very intense and with equal sign, ie is distant from zero. When the field at a lower frequency passes near zero, the magnetic field varies very wildly, as the magnetic field is sufficiently small as to have a linear behavior with the permeability, equal to the maximum.

The same is true when the two components of the magnetic field are in phase opposition, the resulting magnetic field in these cases is equal to zero, and then the mangetic induction field changes the sign impulsively. This behaviour is plotted in Figure 5.23. This behavior is fully described by the trend over time of magnetic relative permability. It is extremely interesting to note that for extreamely high values of magnetic field (several hundreds of thousands of [A/m]) the saturation limits the relative permeability to very low values. This occurs for most of the magnetic period. So neglecting, or better simplifying this very important behaviour, could result in erroneous assessment of induced current densities (also important), and it does not fully describe, from a physical point of view, this problem. In particular way when the coil is supplied with two superimposed waveforms. What causes the heating of the billet are the eddy currents. This means that what it is necessary try to describe are the time derivatives of the induction field, because $\nabla \times \rho \mathbf{J} = -\frac{\partial \mathbf{B}}{\partial t}$ Now it is possible, as already done, develops the derivative of induction magnetic field with respect to time:

$$\frac{\partial B}{\partial t} = \mu_0 \frac{\partial H(t)}{\partial t} \left(1 + (\mu_{r0} - 1) \cdot \frac{1}{1 + G^2(t)} \right) \tag{5.24}$$

$$G(t) = \frac{\pi \mu_0 (\mu_{r0} - 1)}{2 B_s} H(t) \tag{5.25}$$

The formulation of the partial derivative with respect respect to time of induciton magnetic field is highly impulsive. This means that when the total magnetic field (or the coil current) goes to zero, the derivative explodes. The last equation can be viewed as the sum of two terms, one that is characterized by a sinusoidal wave form, and a second that is more complicated. For a system powered wth a voltage that is the sum of two waves that evolvew with two different frequencies are extreamely important the values of the permeability. It is possible try to understand the evolution of the magnetic field in time at a point P (r=2 [mm]), assuming an ideal inductor, infinitely long, powered with a specific current, that is the current define analitically in the Chapter 2. In FIgure 5.23 is plotted the magnetic flux of this that takes into account the magnetic saturation. This model consider a magnetic field $H(t)$ $[A/m]$ that is generated by a current that is the sum of two frequencies components.
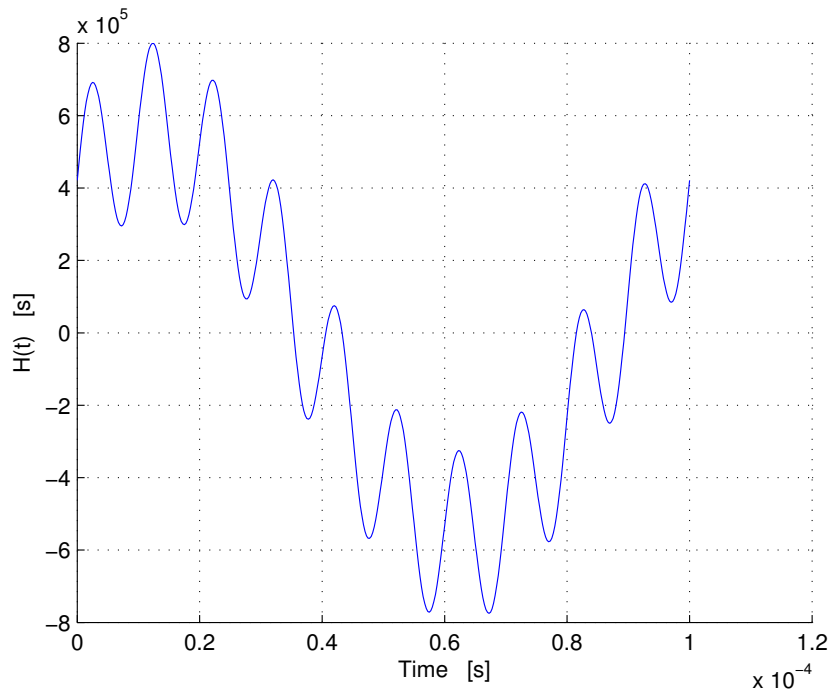
Figure 5.22: Magnetic Flux amplitude $norm\mathbf{H}$ $[A/m]$ generated by an ideal inductor.
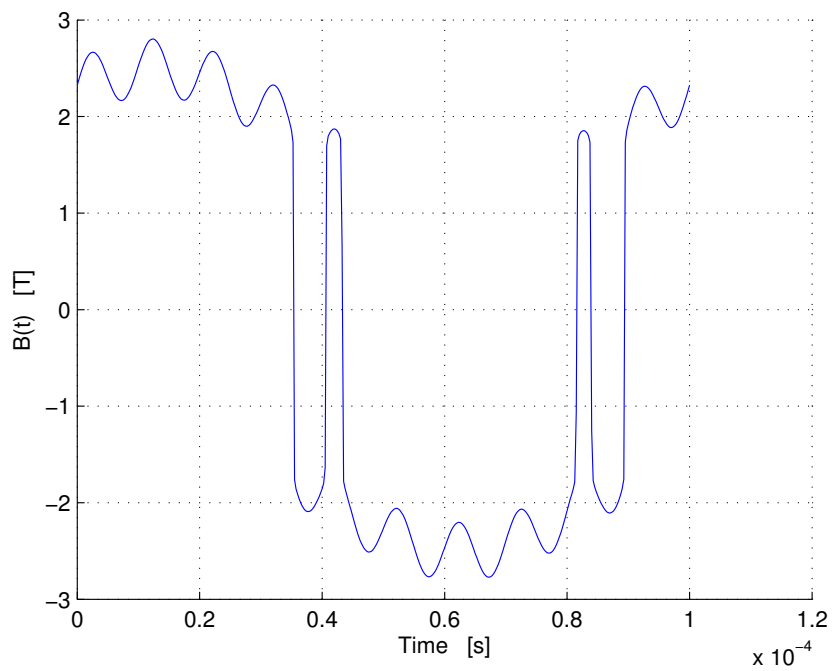
Figure 5.23: Magnetic Flux amplitude $norm\mathbf{B}$ $[T]$ that takes account of the magnetic saturation.

It is possible now to apply the Poynting vector, if the amplitude of electric field

is defined in time, and assuming that the electric field is perpendicular to mnagnetic field:

$$s(t) = E(t) \cdot H(t) \tag{5.26}$$

With the help of Poynting vector it is possible to represents the directional energy flux density (the rate of energy transfer per unit area) of an electromagnetic field.

$$\mathbf{S} = \mathbf{H} \times \mathbf{E} \tag{5.27}$$

This form is often called the Abraham form. Occasionally an alternative definition in terms of electric field $\mathbf{E}$ and magnetic flux density $\mathbf{B}$ is used. The Poynting vector represents the particular case of an energy flux vector for electromagnetic energy. However, any type of energy has its direction of flow in space, as well as its density, so energy flux vectors can be defined for other types of energy as well, e.g., for mechanical energy. The Poynting vector appears in Poynting's theorem, that is energy-conservation law:

$$\frac{\partial u}{\partial t} = -\nabla \cdot \mathbf{S} - \mathbf{J_f} \cdot \mathbf{E} \tag{5.28}$$

It is clear that saturation is one of main phenomena that occurs during this treatment. From an electrical point of view it changes the value of the inductance during the heating process. But is more important the saturation of the magnetic field for the high of for the medium frequency. From the calculation of the flux linked by the inductor, it is possible to calculate an equivalent inductance.

$$\Phi = L(i(t)) \cdot i(t) \tag{5.29}$$

For an axial symmetric model the circuitation of the magnetic scalar potential A_φ build integrally the magnetic flux linked with the workpiece. Than:

$$\Phi = 2\pi r \cdot A_\varphi \tag{5.30}$$

From a numerical point of view it possible to consider the total magnetic flux linked with the workpiece by an integration of it through the radius of the billet, than:

$$\Phi_{z=0} = \int_\Omega \mathbf{B} \cdot d\mathbf{S} = \oint_{\partial\Omega} \mathbf{A} \, dl \tag{5.31}$$

This means that the total magnetic flux, for an A-Sym model is:

$$\Phi_{tot} = \sum_{i=1}^{n_z} \Phi_i = \sum_{i=1}^{n_z} 2\pi r_{bill} \cdot A_{\varphi i} \tag{5.32}$$

This is the total linked magnetic flux with the billet. Obviously it is possible to define it for each time steps of the electromagnetic solution, and find a behaviour of the magnetic flux $\Phi(t)$ during the electromagnetic period. Analyzing the wave form in the Figure of the magnetic flux is possible to understand that the saturation tends to cut the high frequency, because the reduction of the the relative permeability is extreamely strong. This phenomenon is clearer if we compare the curves at different temperature distribution, where the magnetic relative permeability is already collapsed to 1. When the temparature of a non neglegible surface of the billet is over Curie temperature,

its magnetic relative permabily is collapsed to 1. This phenomenon is very similar to the effect of magnetic saturation. If a large section of the billet is exposed to an extremely high magnetic field, it certainly will saturate. Comparing the two behaviours at different temperatures, the effect of the fail of the relative permability is more enhanced in the case of many portion of surface over θ_c, because the wave form (that theorically, with a constant relative permeability (linear model), should be a perfect sinusoidal high frequency wave form superimposed to a medium frequency sinusoidal wave form) seems almost a medium frequency sine wave, with a mich reduced content of high frequency component. For this work this was done for different temperature distirbutions. This means that the Flux was evaluated in a magnetic period for each time step, and because it is possible to define a relationship between magnetic flow and current, than could be interesting try to define the concept of inductance, function of time, that the inductor views from its feeding.

$$L(t) = \frac{\Phi(t)}{i(t)} \tag{5.33}$$

For example for the initial temperature condition, the linked magnetic flux is represented in Figure 5.63.

5.3 Electromagnetic period analysis

It is particularly interesting to analyze what happens electromagnetically when the current passes through zero. In fact in this instant the power delivered by the inductor is zero, nut the time derivative of the magnetic field is very high. The magnetic field produced by the inductor is zero. So the inductor does not generate any current in the billet. The current density on the surface of the current can not instantaneously go to zero, however. Thus there is a current density, the sign of which depends on the supply current of the inductor at the previous instant. This surface current density then generates a magnetic field inside the piece of opposite sign, which generates opposite currents than those that the year product. In the simulations we see in fact the inversion of the sign of the current density along the radius of the workpiece, there are points where the current density goes to zero. This phenomenon from an electromagnetic point of view is extremely interesting. One understands that there are streams that do not concatenate with the inductor, but whose lines are closed again inside the billet, or in the air. There is therefore a sort of donut of magnetic energy which surrounds the billet. It is possible to view this phenomenon for different temperature distributions, this means for different istants of the heating process.
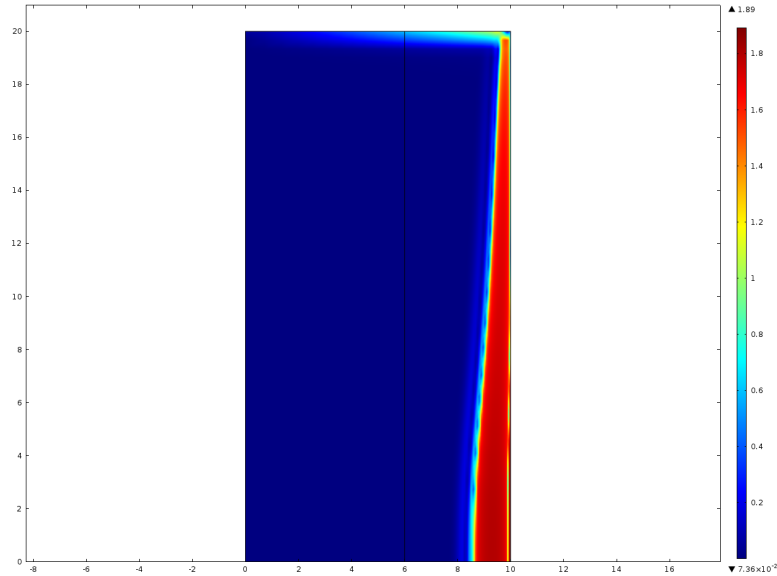
Figure 5.24: Magnetic Flux amplitude $norm\mathbf{B}$ $[T]$ plotted at time $t_0 = 1.3664 \cdot 10^{-4}$ $[s]$ in the first period of heating process.

In Figure 5.24 is represented the amplitude of magnetic flux when the current goes to zero and for an uniform temperature distribution, that means the temperature is everywhere equal to 20 [°C]. It is possibile view that magnetic flux inside the billet goes to zero. This phneomenon is more clear if it is considered the z-component of Magnetic Flux: B_z that for the geometry of the model is the most relevant. It is possible view that the z-component changes the direction along the radial coordinate of the workpiece. From the Figure 5.25 it is possible view that B_z plotted in a cutline parallel to r-direction and in the center of the billet B_z is extremely intense and with a negative sign on the surface of the billet, instead at 9.9 [mm] it changes sign and it maintains a very high and positive value for a thickness $\delta = 1.3$ $[mm]$. This effect can be explained by the fact that the inductor current at that instant is zero, then there is no magnetic field from the inductor. But all the magnetic field generated
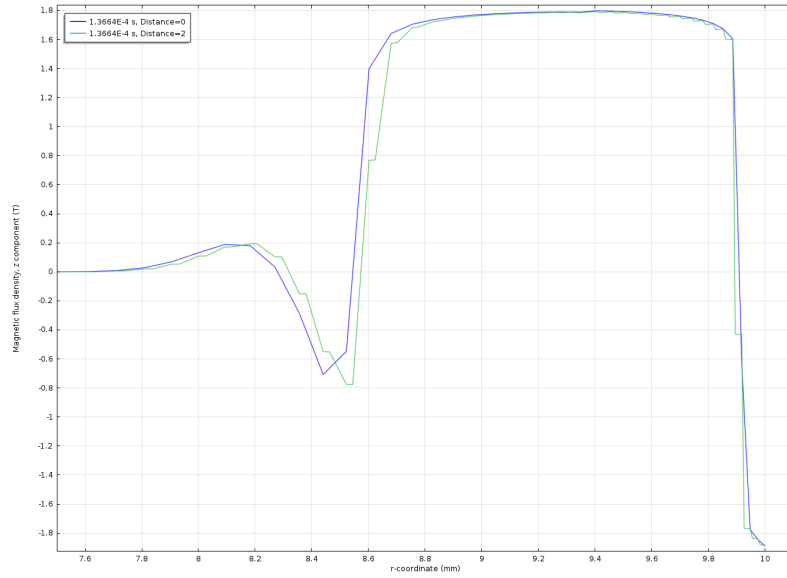
Figure 5.25: z-component of Magnetic Flux B_z $[T]$ plotted at time $t_0 = 1.3664 \cdot 10^{-4}$ $[s]$ in the first period of heating process, for two different cutlines.

In the same way it possible to plot the behaviour along the r-coordinate of the current density J_φ that of cours must changes sign in accord with what happens in Figure 5.25.
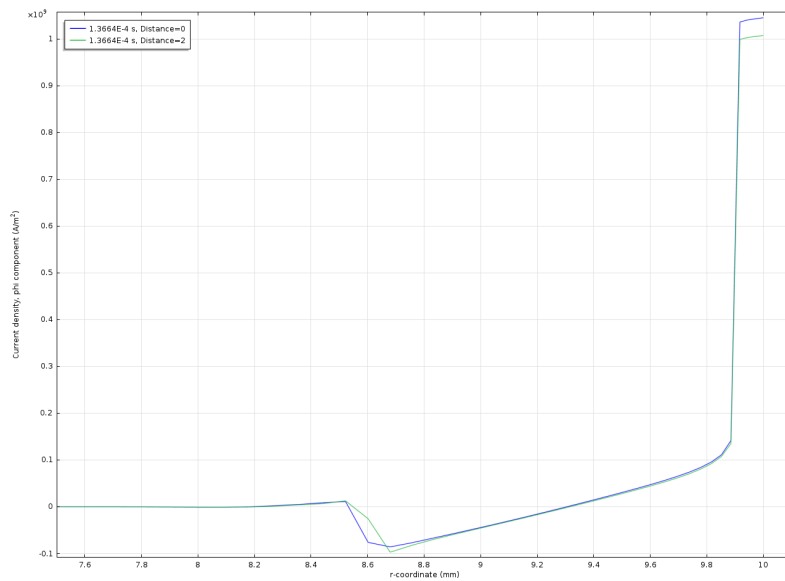
Figure 5.26: φ-component of Current density J_φ $[A/m^2]$ plotted at time $t_0 = 1.3664 \cdot 10^{-4}$ $[s]$ in the first period of heating process, for two different cutlines.

For this time step it is interesting also to analyze the induced power and relative permeability along the central cutiline. These two quantities are in fact the two most interesting variables of the problem, the first from a thermal point of view and the last from a purely electromagnetic point of view. It is evident that the induced power,

when the current passes through zero, remains confined in an extremely reduced thickness, when the temperature is far below the Curie point. Instead because of the magnetic field **H** is however very intense, a large portion of space is satured, that means the relative magnetic permeability is extreamely small.
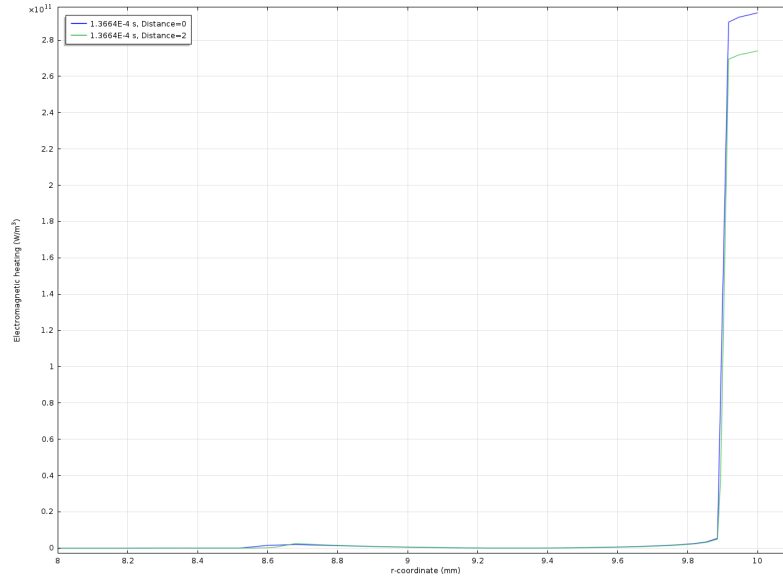
Figure 5.27: Specific heating induced power w $[W/m^3]$ plotted at time $t_0 = 1.3664 \cdot 10^{-4}$ $[s]$ in the first period of heating process, for two different cutlines.
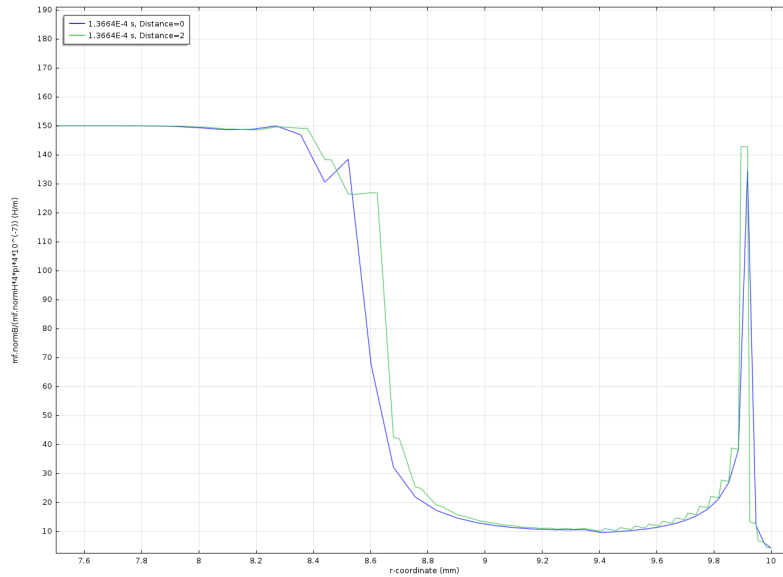
Figure 5.28: Relative magnetic permability μ_r $[-]$ plotted at time $t_0 = 1.3664 \cdot 10^{-4}$ $[s]$ in the first period of heating process, for two different cutlines.

Increasing the treatment, the temperature on the workpiece surface increases, and more and more points exceed the Curie transition zon , for example to the condition of temperature instantly heat of 0.1 [s].
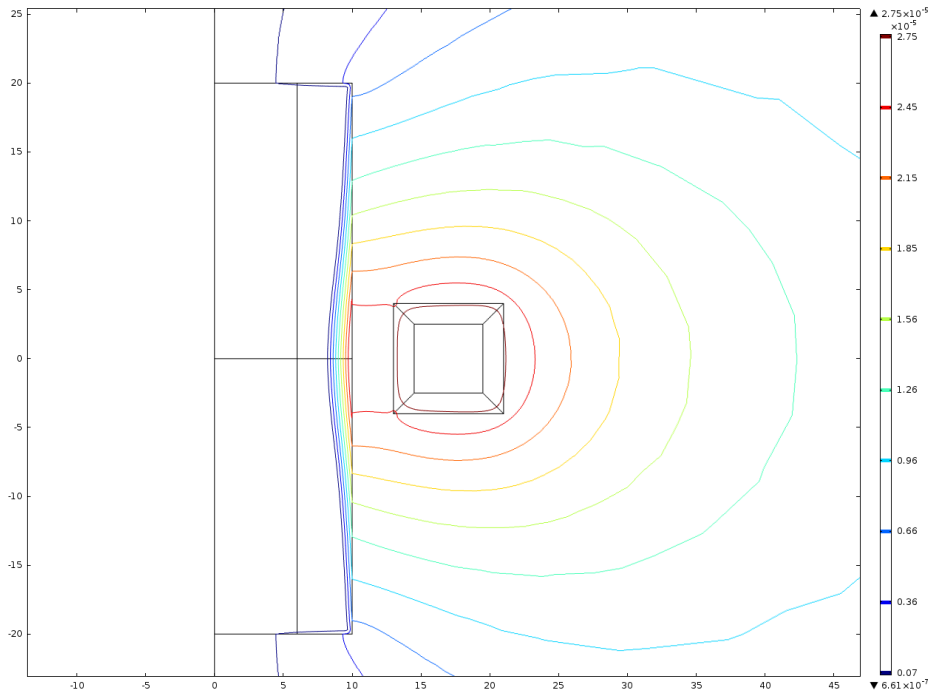
Figure 5.29: Behaviour of $2\pi A_\varphi$ at magnetic time $1.2225 \cdot 10^{-4}$ $[s]$ for the temperature distribution at process time 0.1 $[s]$
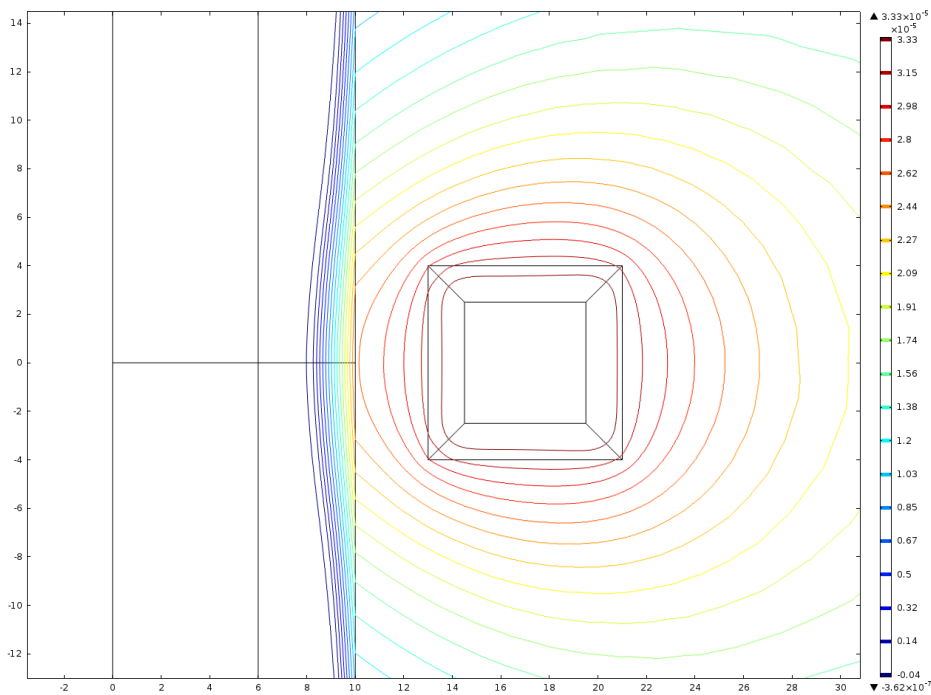
Figure 5.30: Behaviour of $2\pi A_\varphi$ at magnetic time $1.3 \cdot 10^{-4}$ $[s]$ for the temperature distribution at process time 0.1 $[s]$
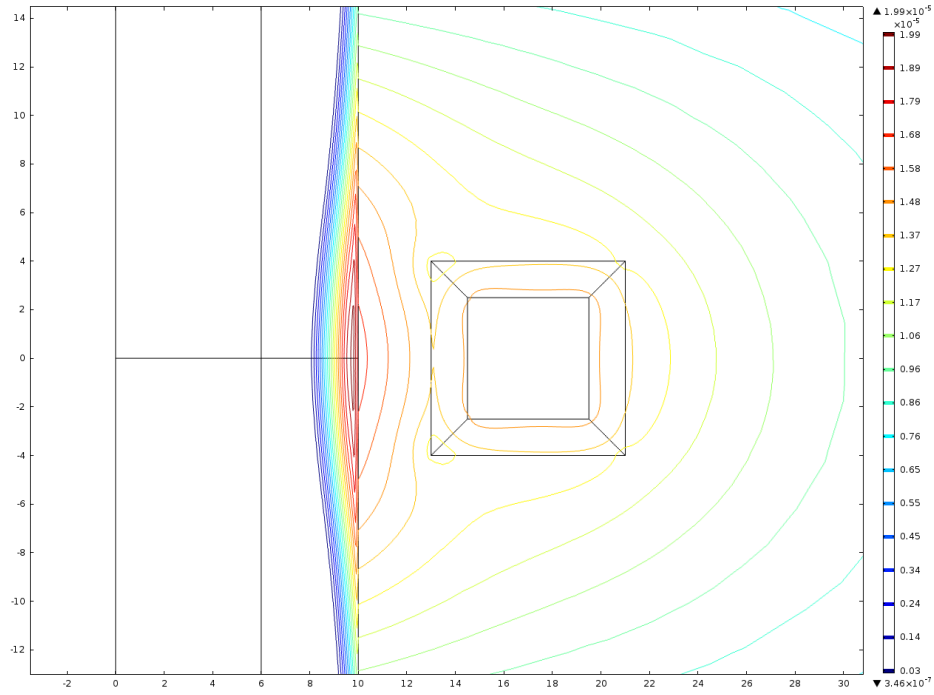
Figure 5.31: Behaviour of $2\pi A_\varphi$ at magnetic time $1.445 \cdot 10^{-4}$ [s] for the temperature distribution at process time 0.1 [s]
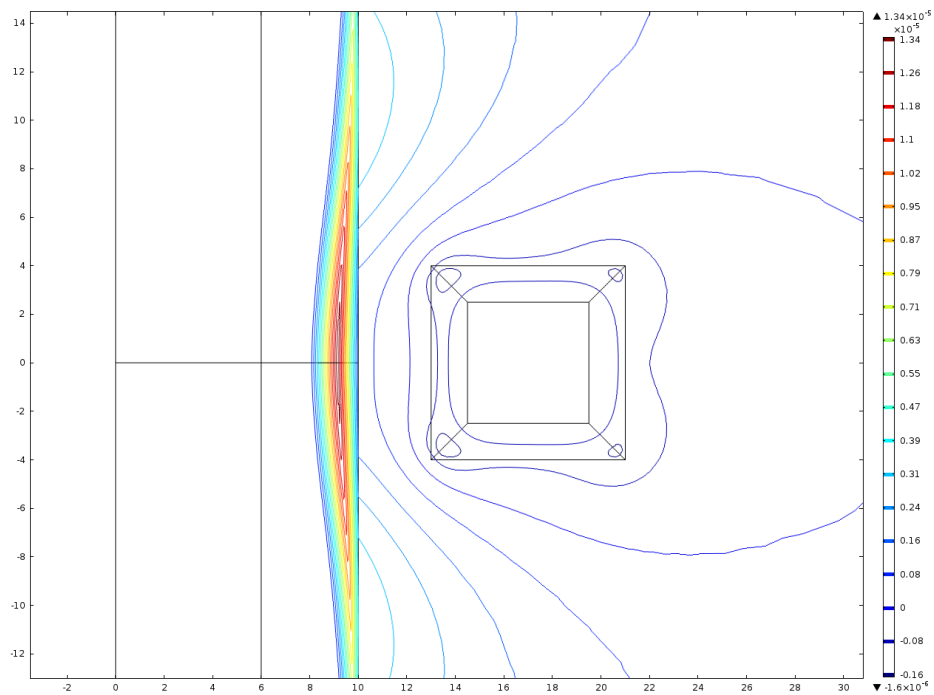
Figure 5.32: Behaviour of $2\pi A_\varphi$ at magnetic time $1.5 \cdot 10^{-4}$ [s] for the temperature distribution at process time 0.1 [s]

Figure 5.29 shows that when the current assumes its maximum value, the inductor

is fully coupled with the billet. Instead when the current falls to zero, Figure 5.31 shows a toroidal structure of magnetic energy in the airgap between inductor and billet. This means that the surface current density that exists on the billet generates itself a strong magnetic field that induces current inside the inductor. Than when the coil current become negative the situation is changed as shows Figure 5.32.

It is also interesting to plot the same trends for different temperature distributions. For example, with reference to Figure 5.33, it is clear, that when a very large portion of the billet is characterized by temperatures higher than Curie Temperature, the material changes its magnetic properties and becomes diamagnetic. If you combine this phenomenon with the passage by zero of the current, you get an even more complex behaviour with respect to that discussed previously.
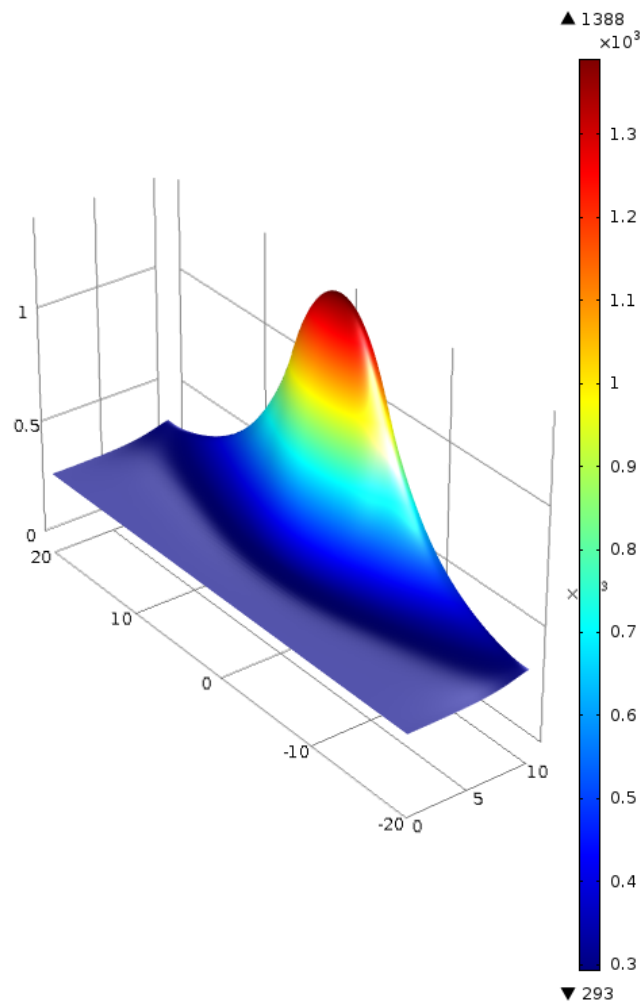
Figure 5.33: Temperature distribution [K] at heating time $t_{ht} = 2.15 \cdot 10^{-1}$ [s]
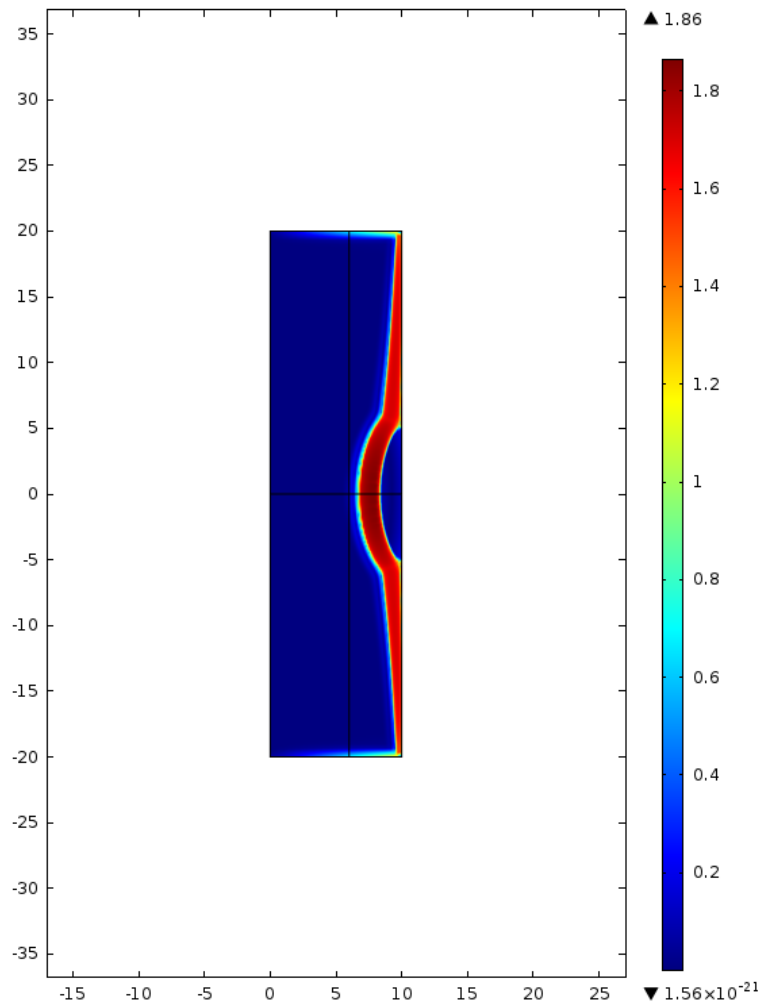
Figure 5.34: Amplitude of Magntic Flux $norm\mathbf{B}$ $[T]$ plotted at time $t_0 = 1.3618 \cdot 10^{-4}$ $[s]$ for a temperature distribution with many points over T_c.

From Figure 5.34 we see that the magnetic field penetrates very deeply into the piece. So the overcoming of the critical temperature, causes the penetration of the magnetic flux $\mathbf{B}$ towards the axis of the billet. This is the most interesting phenomenon of the heating process. It causes during the last part of the process the displacement of the thermal sources to different areas that one would expect if they did not take into account the effect of Curie transition. This means that overall electromagnetic periods, heat sources are located very deeply. This causes a heating much more intense in innermost zones. It results in a Austenite thickness wider than presumed. You can compensate for this by choosing power supply inductor extremely great, and quickly heating phases.
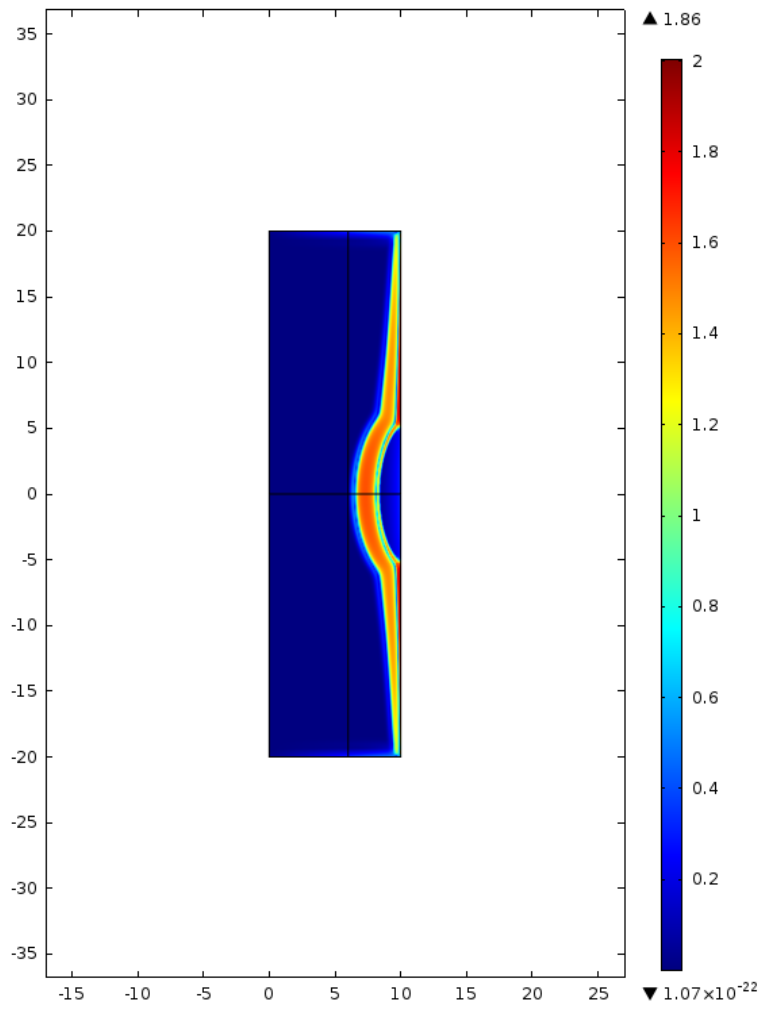
Figure 5.35: Amplitude of Magnetic Flux $norm\mathbf{B}$ $[T]$ plotted at time $t_0 = 1 \cdot 10^{-4}$ $[s]$ for the temperature distribution at heating time $t_{hf} = 0.215$ $[s]$
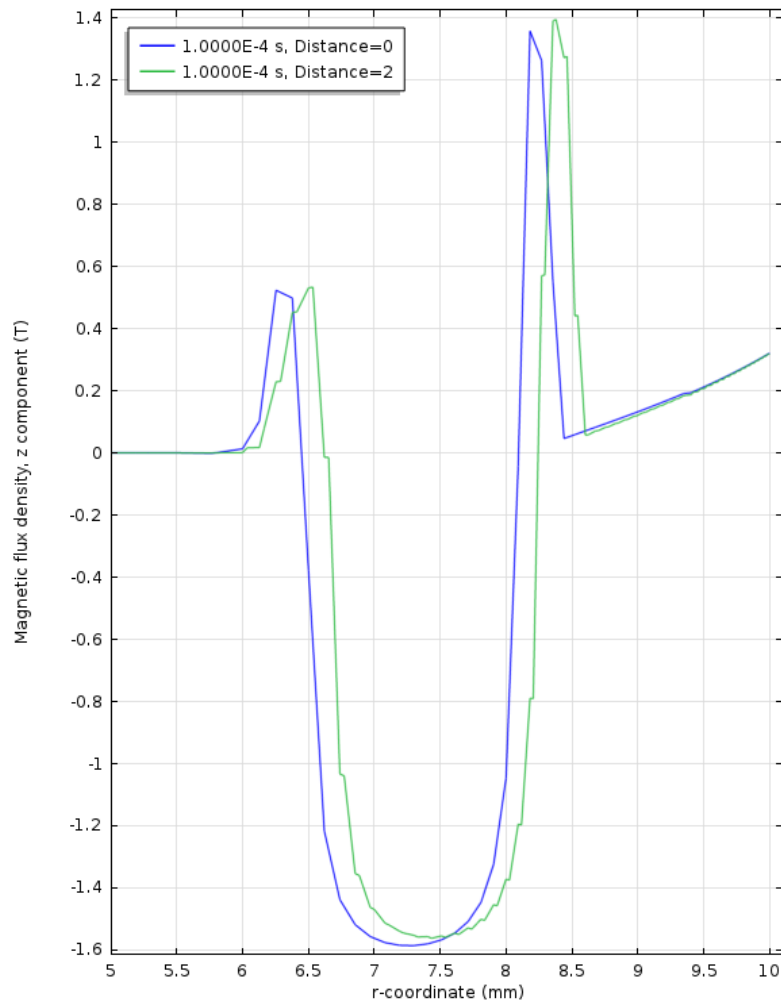
Figure 5.36: z-component of Magnetic Flux B_z $[T]$ plotted at time $t_0 = 1 \cdot 10^{-4}$ $[s]$, for the temperature distribution at heating time $t_{hf} = 0.215$ $[s]$ for two different cutlines.

In the same way it possible to plot the behaviour along the r-coordinate of the current density J_φ that of cours must changes sign in accord with what happens in Figure 5.25. it is clear that if the current density is proportional to the time derivative of the magnetic flux **B**, the distribution of induced currents is closely related to the distribution inside the piece of relative permeability. We see in fact from the figure of the distribution of the φ-component of the current density that it penetrates very deeply into the piece.
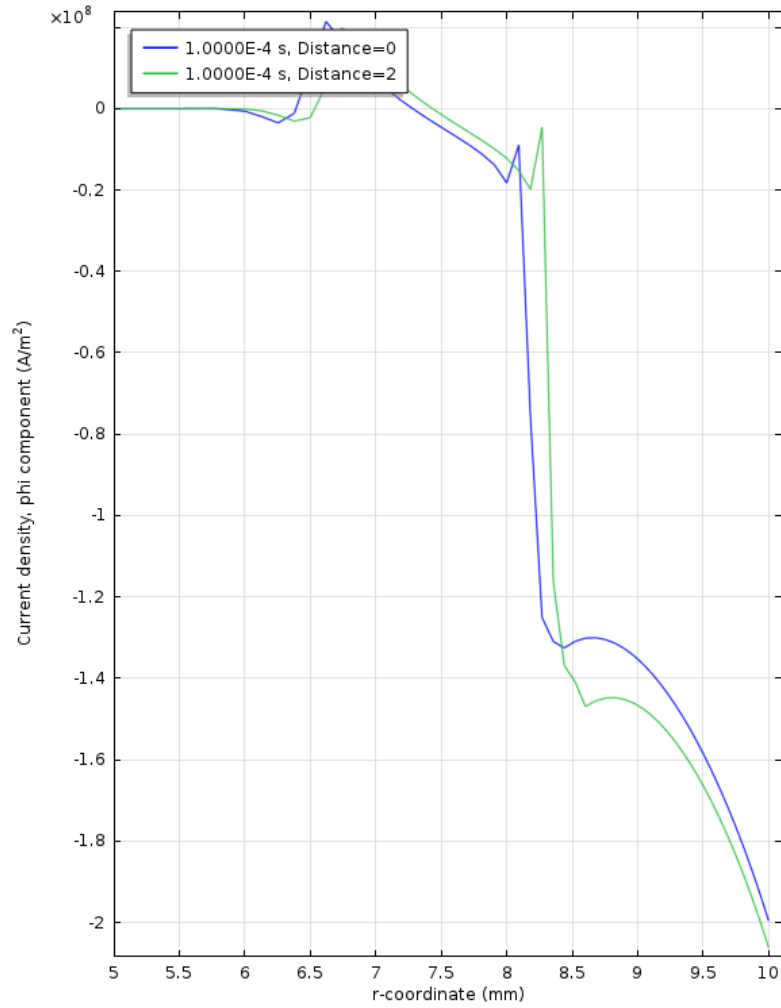
Figure 5.37: φ-component of Current density J_φ $[A/m^2]$ plotted at time $t_0 = 1 \cdot 10^{-4}$ $[s]$, for the temperature distribution at heating time $t_{hf} = 0.215$ $[s]$ for two different cutlines.

In the same way that was done for the heating power, it is possible to derive the average distribution of the current density, in a electromagnetic period. It is interesting to consider how most important electromagnetic parameters vary with temperature distribution. We observe a similar phenomen that occurs for avarage heating power. It means that don't consider a behaviour of electromagnetic phenomena as function of temperature could involve not acceptable errors, and than not acceptable heating profiles.
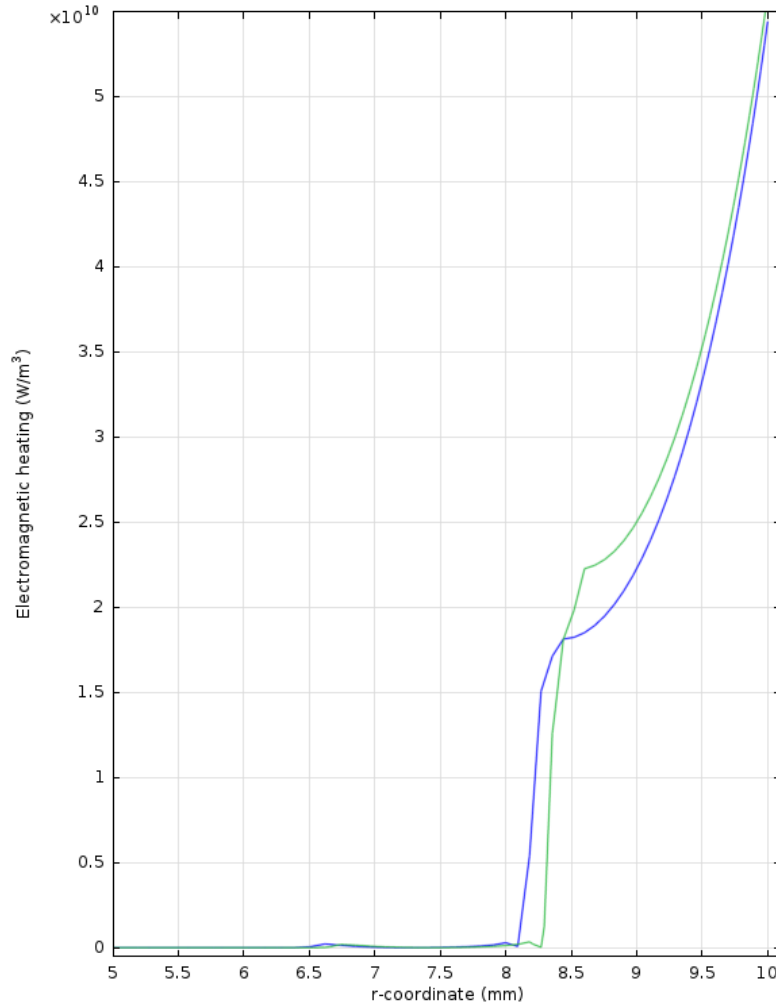
Figure 5.38: Specific heating induced power w $[W/m^3]$ plotted at time $t_0 = 1 \cdot 10^{-4}$ $[s]$, for the temperature distribution at heating time $t_{hf} = 0.215$ $[s]$, for two different cutlines.

Figure 5.60 shows that effectively when many points of the billet exceeds the critical temperature of Curie actually it occurs a shift of the current density towards the axis of the workpiece, not only for different instants of the period, but actually also in terms of average values. This behavior is also increased by the effect of saturation. it is also interesting to analyze the distributions of the magnitudes elettromangetiche for example when the current assumes the maximum value within the period electromagnetic. This occurs when the derivative with respect to time of the current assumes the zero value. Because the current assumed at this instant the maximum value, then the magnetic field generated by the inductor is maximum. Magnetic flux has already satured, so the magnetic permability is minimum. As was done for other electromagnetic quantities it is useful and interesting plot developments for different temperature distributions.
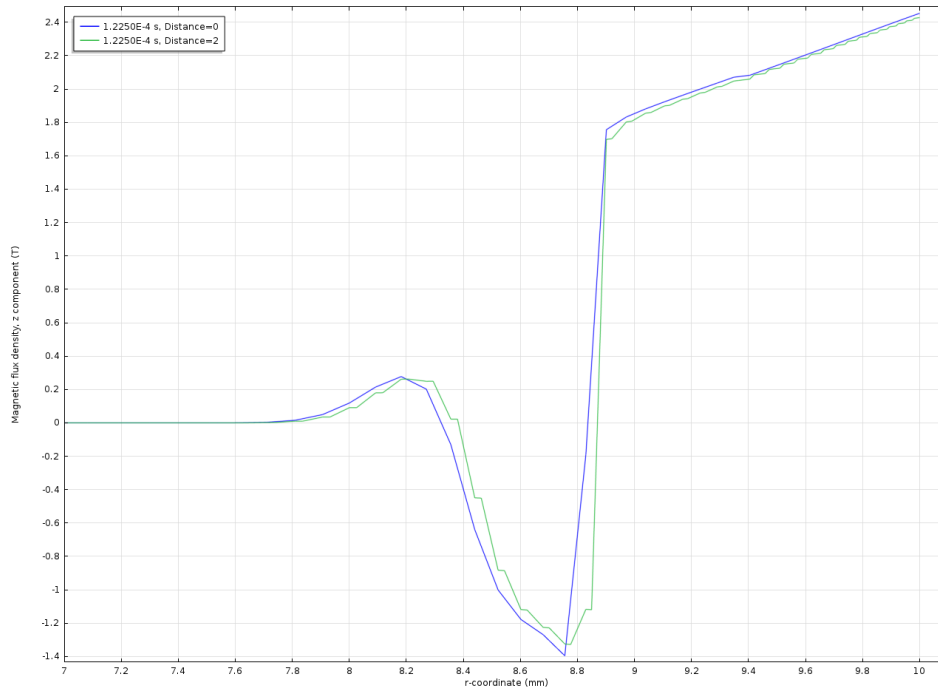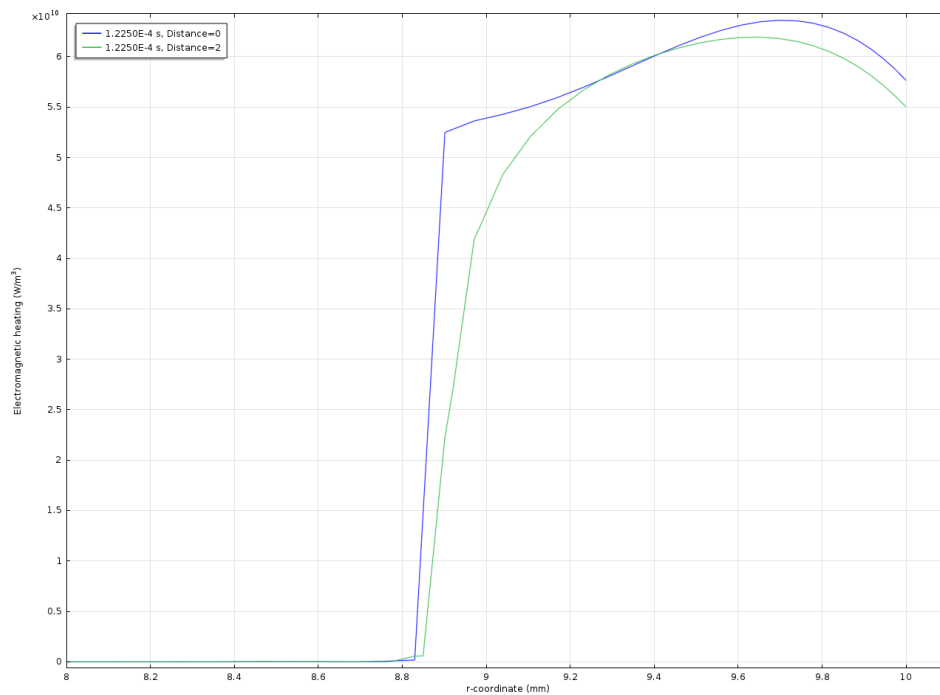
Figure 5.39: z-component of Magnetic Flux B_z $[T]$ computed for the temperature distribution at initial condition for two different cutline along r-coordinate.
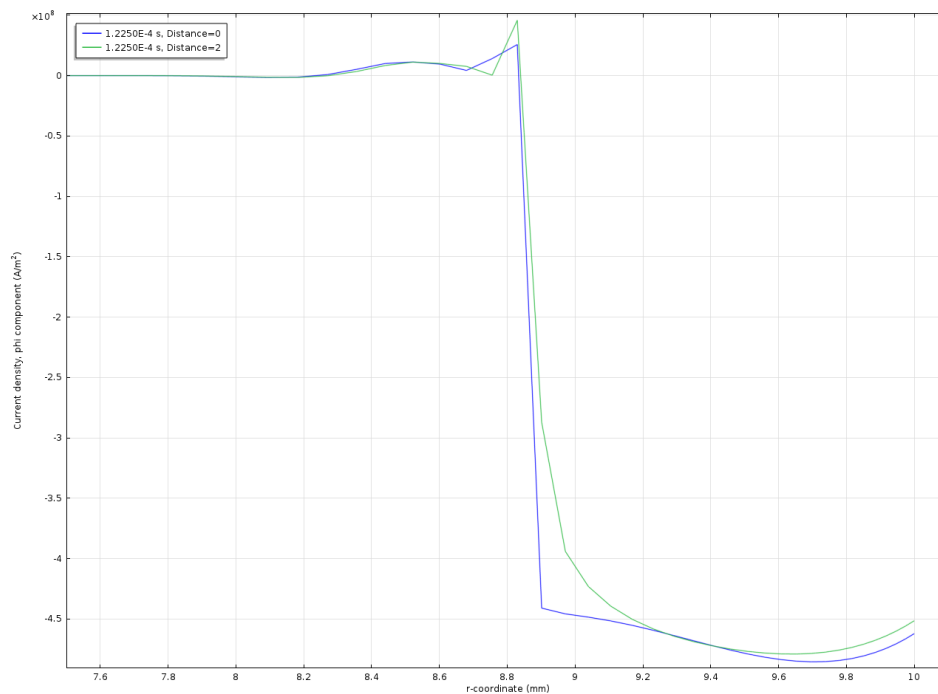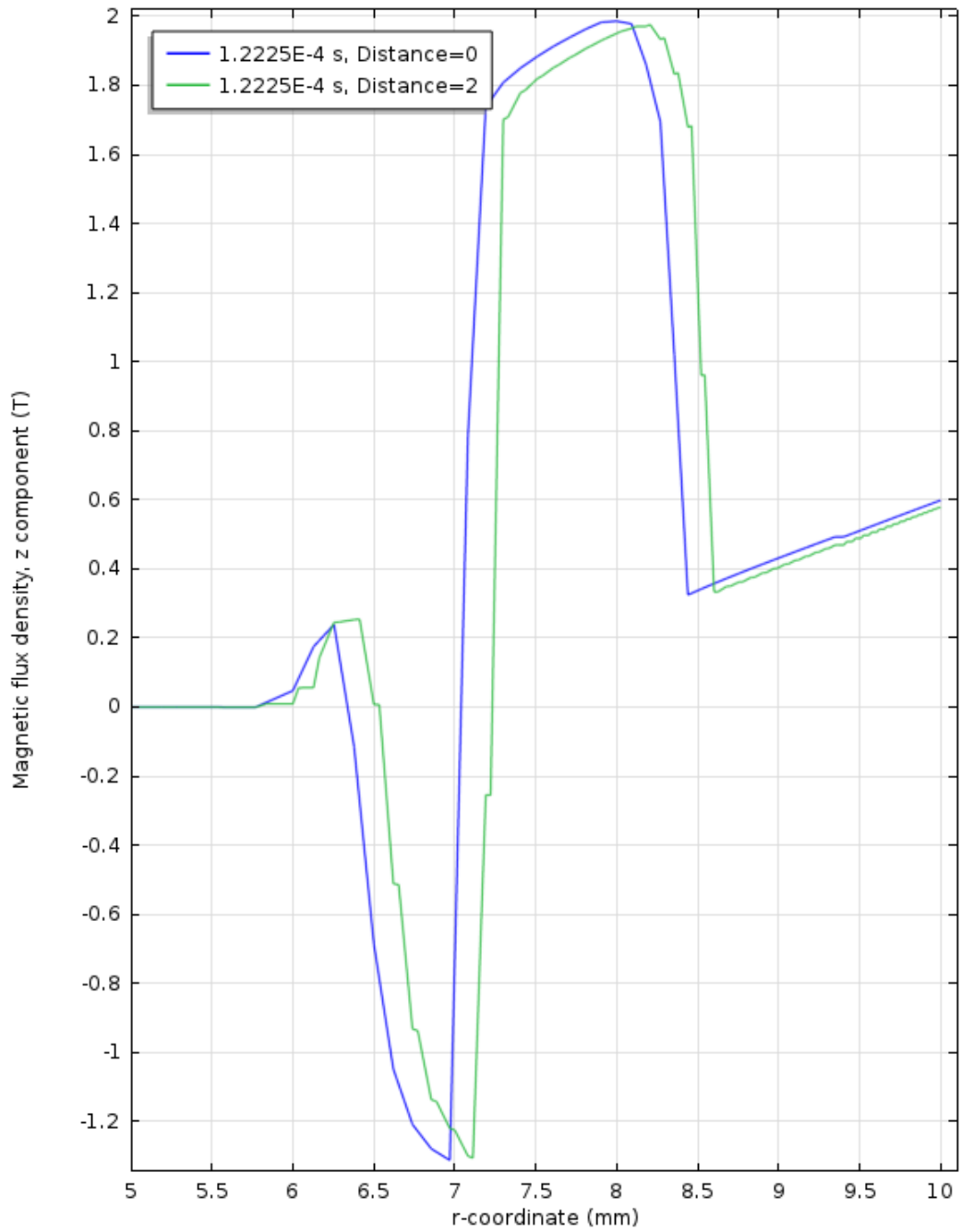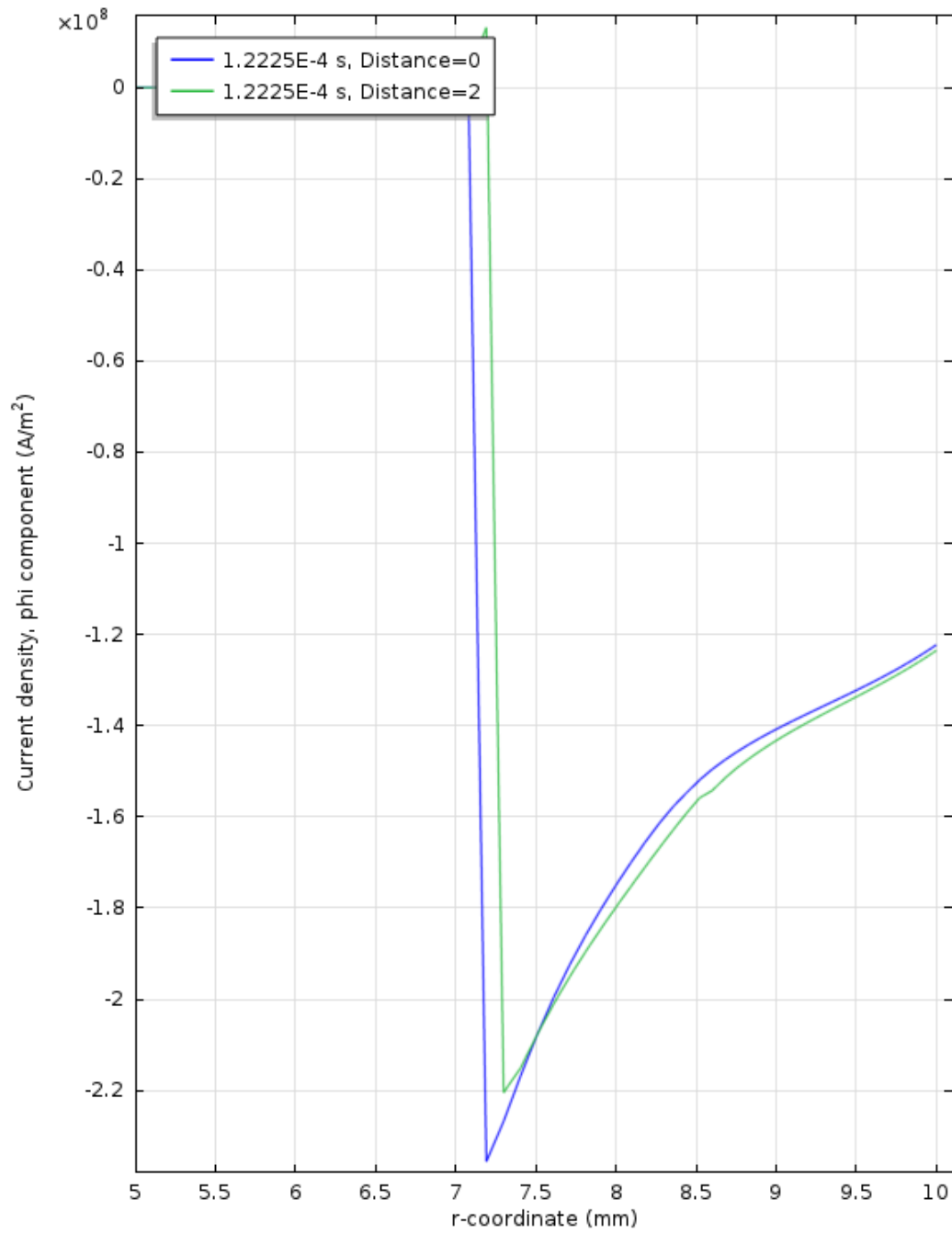

Figure 5.40: φ-component of current density J_φ $[A/m^2]$ computed for the temperature distribution at initial condition for two different cutline along r-coordinate.
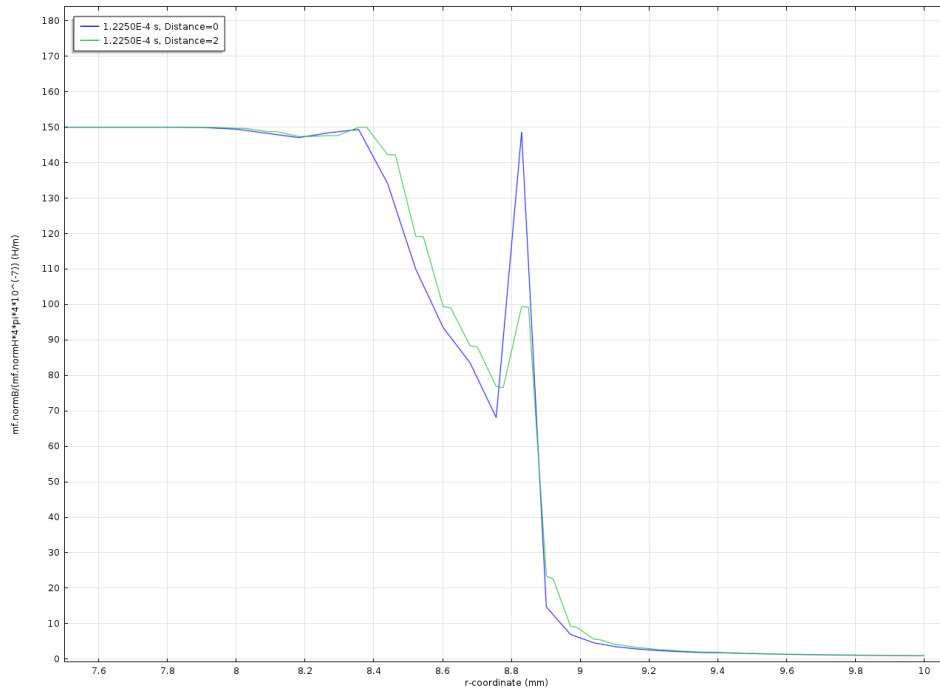
Figure 5.41: Relative permeability distribution μ_r $[-]$ computed for the temperature distribution at initial condition for two different cutline along r-coordinate.

Figure 5.42: Specific heating power distribution w $[W/m^3]$ computed for the temperature distribution at initial condition for two different cutline along r-coordinate.

In Figure 5.39 it is clear that a large portion of space is satured. In fact the

magnetic flux **B** remains almost constant for about $\delta = 1 \ [mm]$ and then collapses in value. Also relative permability shows this behaviour. Extremely interesting is the distribution of heating power into the workpiece (Figure 5.42, although the temperature is well separated from the critical temperature, the saturation tends to push the distribution of the thermal power at greater depth from the surface. Finally in this section are reported the trends for the final temperature distribution. In addition there are also the distributions of the electromagnetic quantities along the surface of the workpiece. In fact, in the final stages of the piece there was a large portion (a semi ellipse) in relative permeability unit. We see that the corners are concentrated strong current densities and thus strong heating powers that cause a localized overheating (in distributions are seen two peaks). This behavior is increased for example when the current assumes the maximum value, namely for the time instant $t_0 = 1.225 \cdot 10^{-4}$, in other words when the piece is in condition of maximum saturation. For this reason here are reported plots on the billet surface and on a cutline parallel to the first, but spaced 1 [mm].
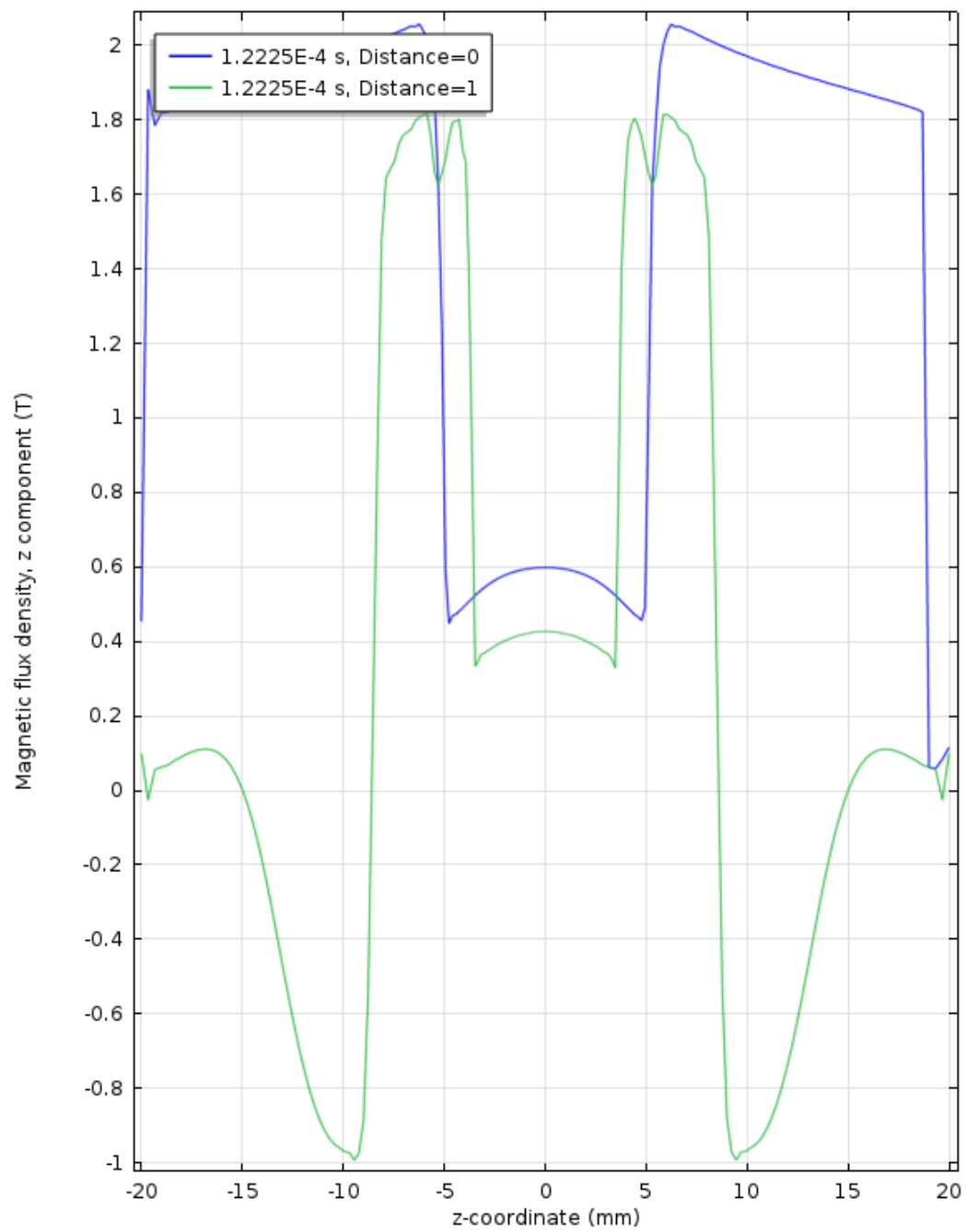
Figure 5.43: z-component of Magnetic Flux B_z $[T]$ computed for the temperature distribution at initial condition for two different cutline along r-coordinate.
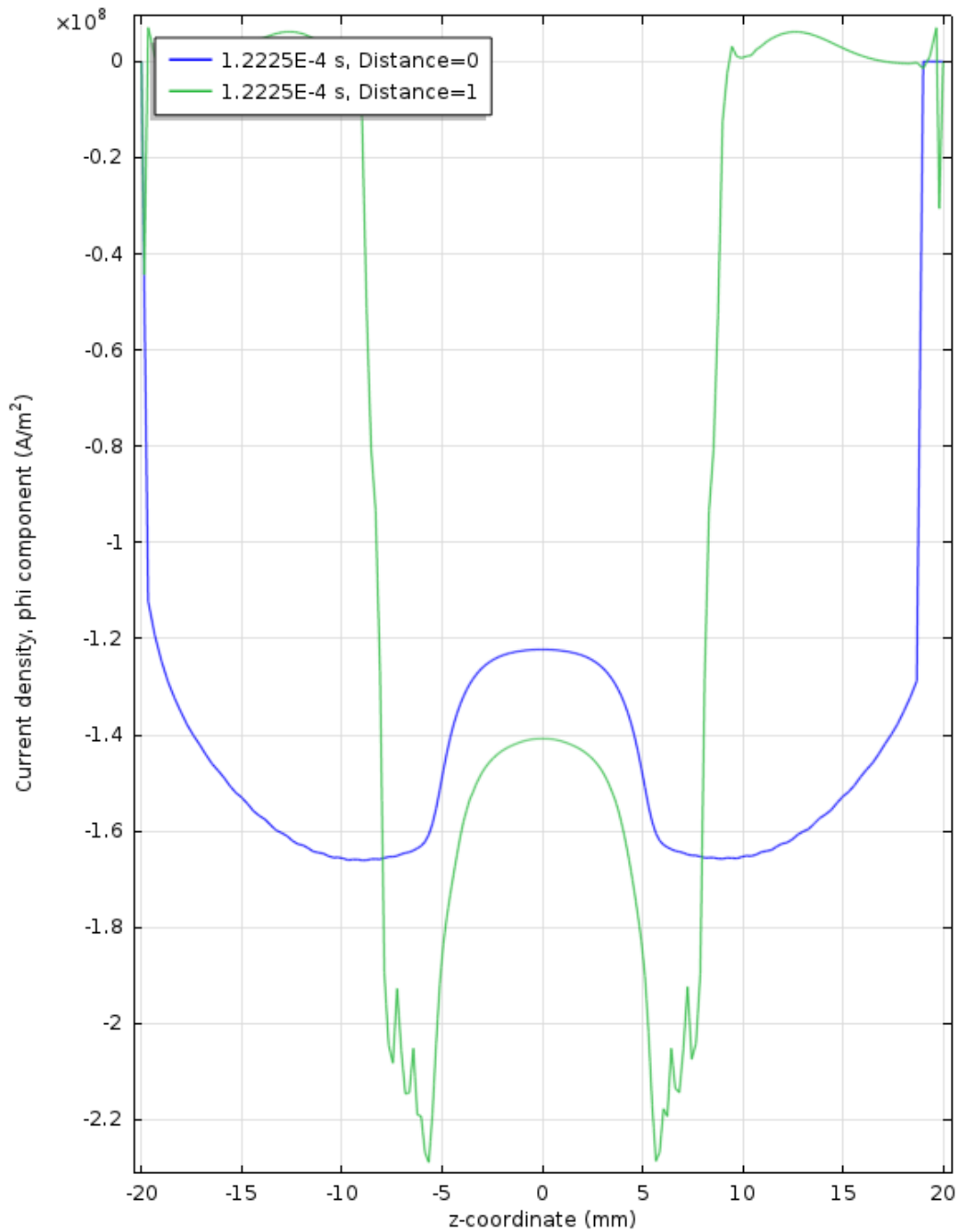
Figure 5.44: φ-component of current density J_φ $[A/m^2]$ computed for the temperature distribution at initial condition for two different cutline along r-coordinate.
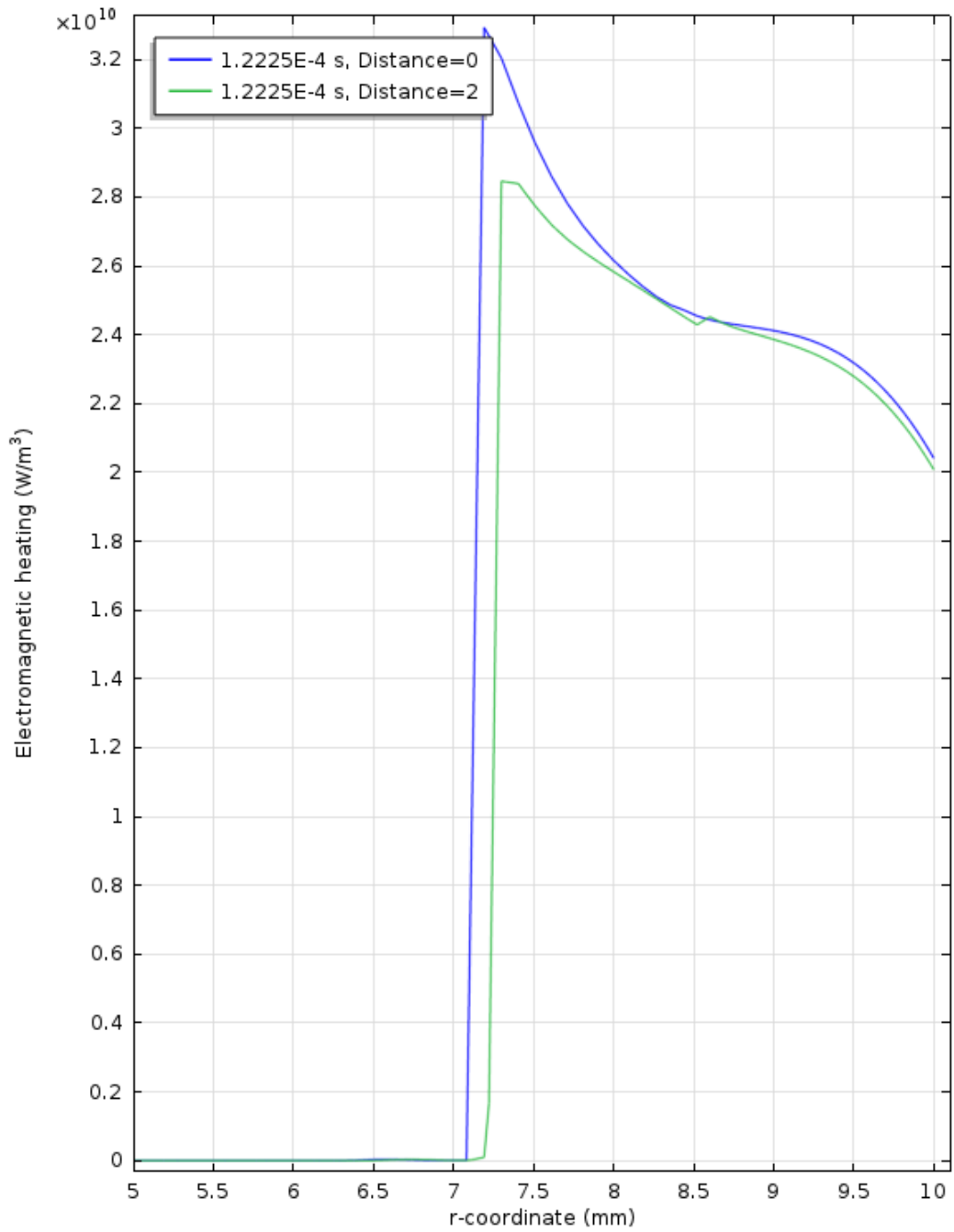
Figure 5.45: Specific heating power distribution w $[W/m^3]$ computed for the temperature distribution at initial condition for two different cutline along r-coordinate.

Figure 5.46: z-component of Magnetic Flux B_z $[T]$ computed for the temperature distribution at initial condition for two different cutline along z-coordinate.

Figure 5.47: φ-component of current density J_φ $[A/m^2]$ computed for the temperature distribution at initial condition for two different cutline along z-coordinate.

From an electromagnetic point of view it is interesting to try to understand as evolve the electromagnetic field for points of interest in the billet . The resolution of a model electromagnetically saturated, allows you to understand differences of current densities and power for different depths in the billet. In fact the magnetic field **H** $[A/m]$ decays with the distance from the source , this means that multiple areas in the surface of the billet will essentially be highly saturated , therefore characterized

by a very sudden trend of the magnetic field , while the areas more in depth feel less the decrease of magnetic relative permeability. This behaviour is shown in Figure 5.49 for points ad different depths. In addition it was also decided to plot the progress always in the period of the same electromagnetic magnitudes for a distribuzioen temperature in which there are areas at temperatures higher than the critical one. In this case we see how the magnetic flux $\mathbf{B}$ $[T]$ is lower in the surface than in areas with a greater depth.
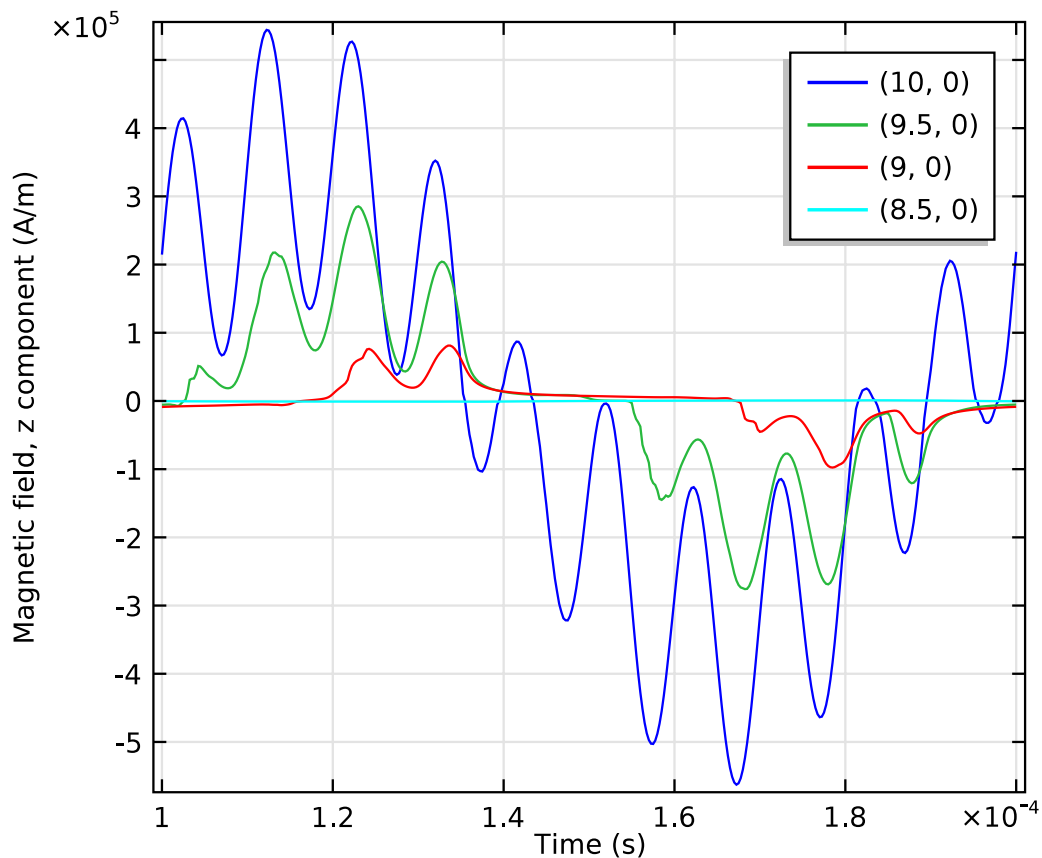
Figure 5.48: Behaviour in time of z-component of magnetic field H_z in the initial temperature distribution for four different points at $z = 0$ [mm]
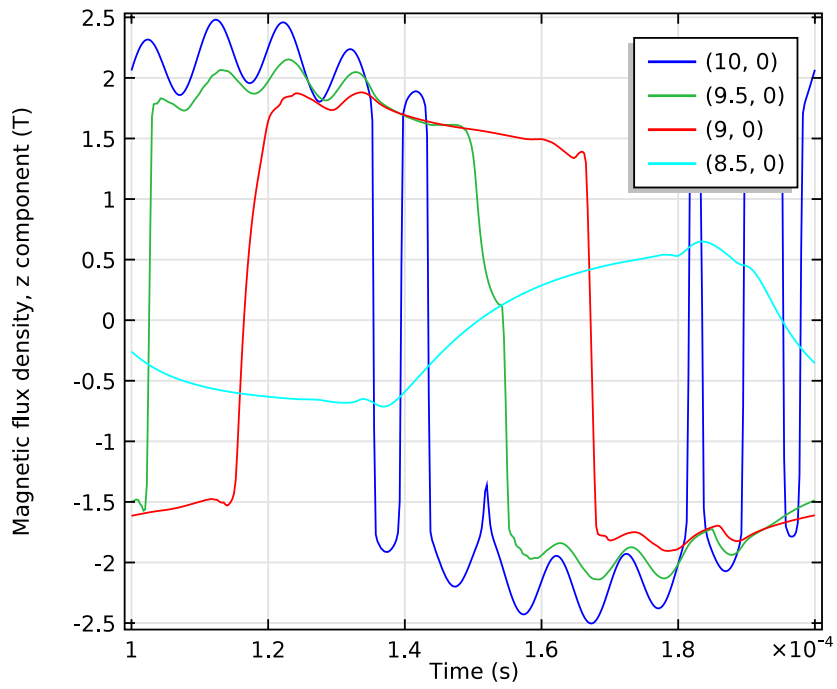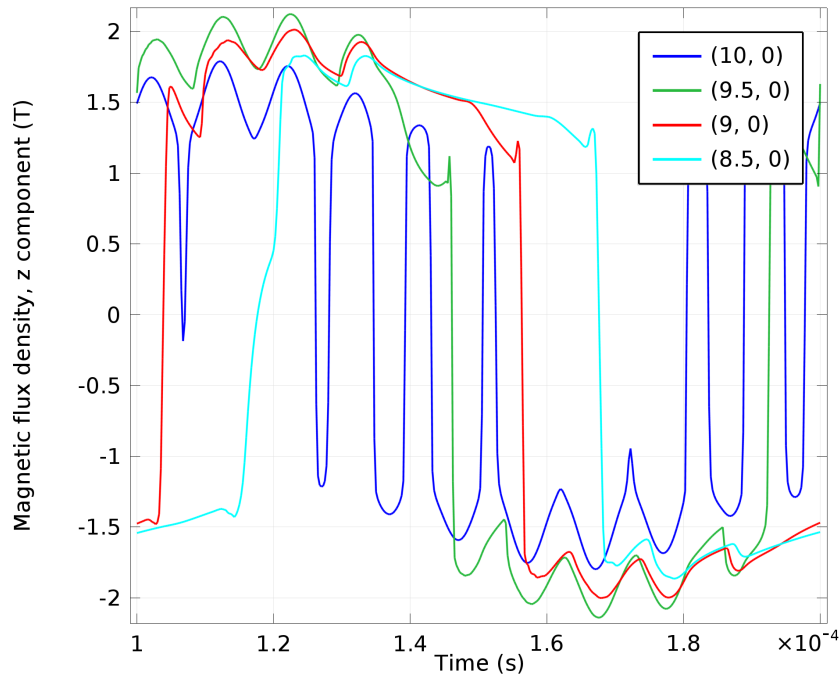
Figure 5.49: Behaviour in time of z-component of induction field B_z in the initial temperature distribution for four different points at z=0 [mm]
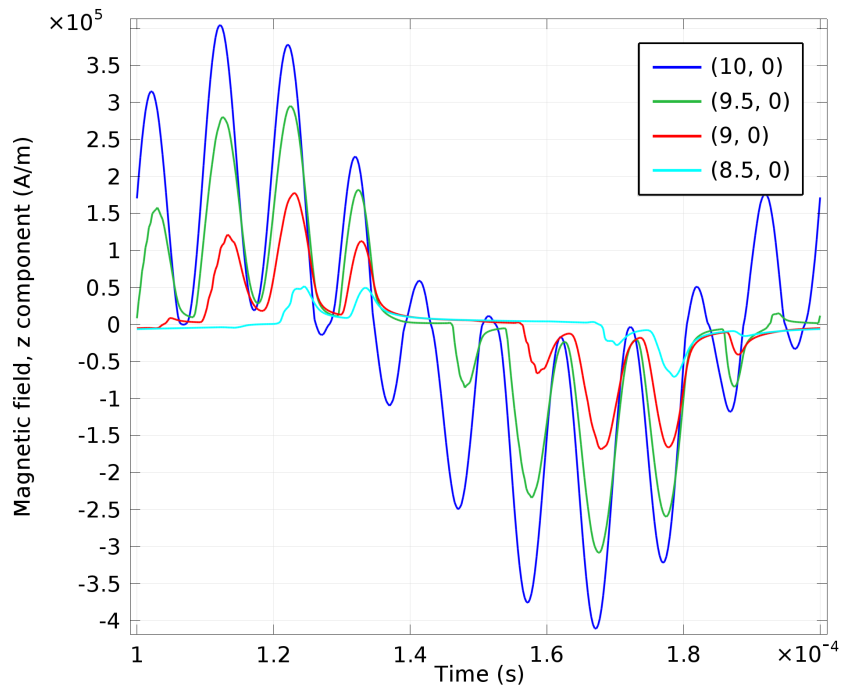
Figure 5.50: Behaviour in time of z-component of magnetic field H_z in the thermal period [0.1-0.105] [s] for four different points at z=0 [mm]

Figure 5.51: Behaviour in time of z-component of induction field B_z in the thermal period [0.1-0.105] [s] for four different points at z=0 [mm]

5.4 Electromagnetic avarage values during the process

It is also interesting to analyze the effect of temperature on the distribution of the induced currents, powers and magnetic fields inside the billet. From a computational point of view, it makes sense, at least mathematically, to try to define the average values of the main electromagnetic quantities: magnetic flux, current density, and relative permeability induced powers. it is possible , as done in the process of coupling between the two models , define the average values of these quantities , via a simple integration by trapezoid rule. Distributions presented on the following pages , we see the full effect of temperature on distributions of electromagnetic . The phase change of the steel, non-magnetic steel because , as already seen the displacement of the average distributions on the initial condition . In particular, the magnetic field now no longer follows the trend starting with the distance (that is attenuated as $\frac{1}{r}$) but now is attenuated also due to the decrease in permeability temperature , which instead now become function temperature , we know to be higher towards the surface of the billet . This means that the induction field tends to penetrate toward the center of the piece, just like the induced power (heating power) So it is interesting to analyze the variation of electromagnetic magnitudes for different temperature distributions. Obviously, as the process is also analyzed by a thermal point of view in the time domain , and having regard to the differences in time scales between the thermal process and the electromagnetic one , it is possible to plot the trend for example of the power induced on the surface of billet during the heating process. In Figure 5.36 is possible to view the behaviour of magnetic flux with temperature and

saturation. In the same way that was done for the heating power, it is possible to derive the average distribution of the current density, in a electromagnetic period. It is interesting to consider how most important electromagnetic parameters vary with temperature distribution. We observe a similar phenomenon that occurs for avarage heating power. It means that not considering a behaviour of electromagnetic phenomena as function of temperature leads to not acceptable errors, and than not realistic heating profiles. During heating they change for the effect of Curie's transaction. This means that the variations of the distributions of the electromagnetic quantities are observable only after a portion sufficiently wide of space has exceeded the critical temperature T_c $[C]$. First of all it is important to plot the different temperature distribution on which are computed the electromagnetic problems.
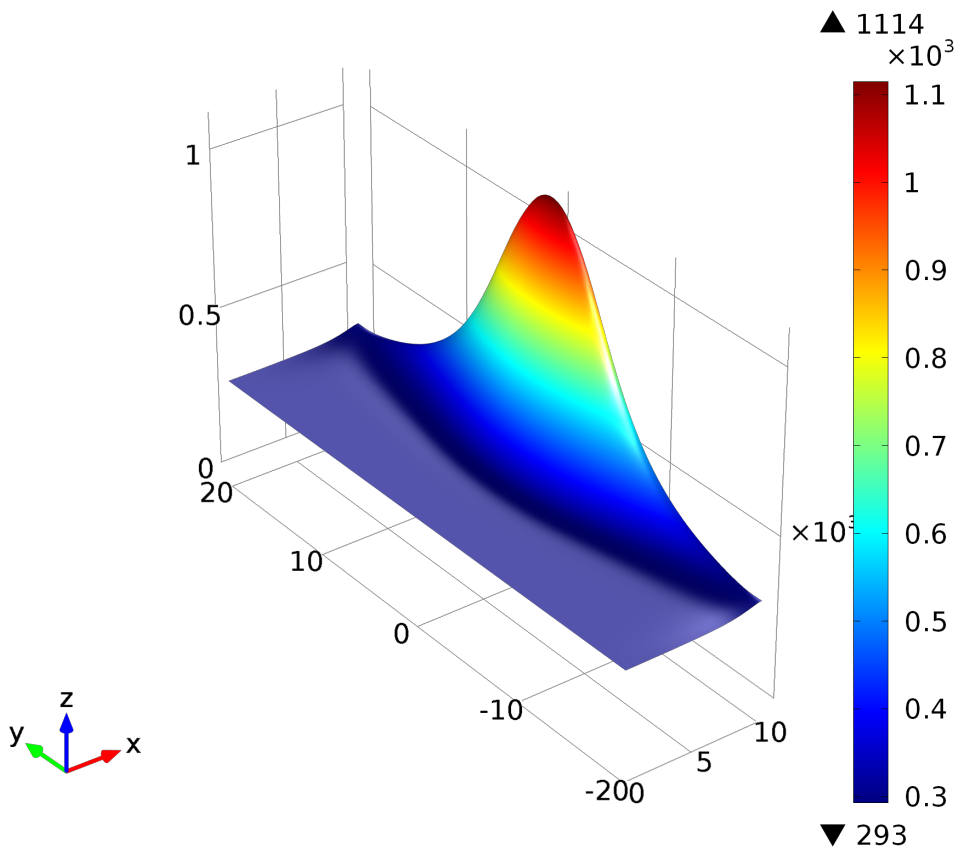
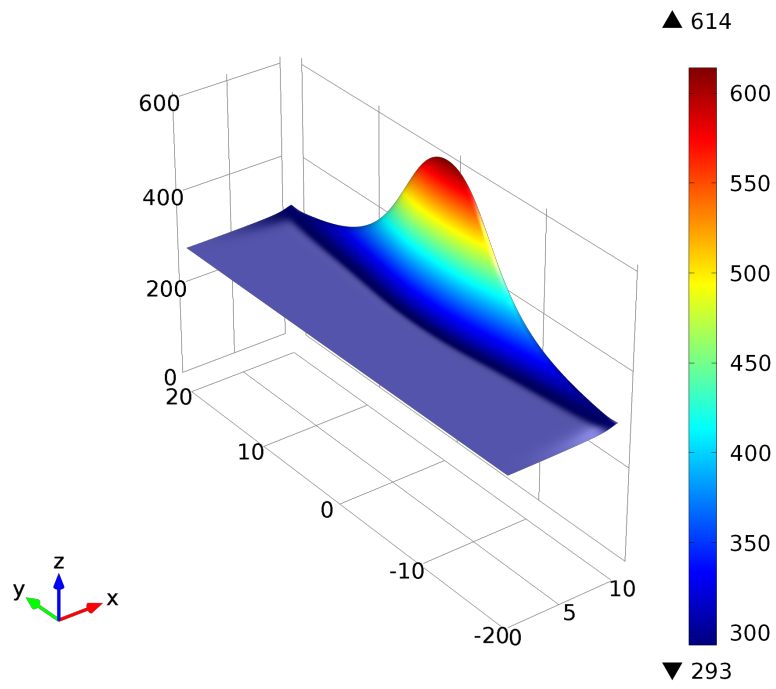**Figure 5.52:** Temperature distribution [K] computed at time 0 [s]

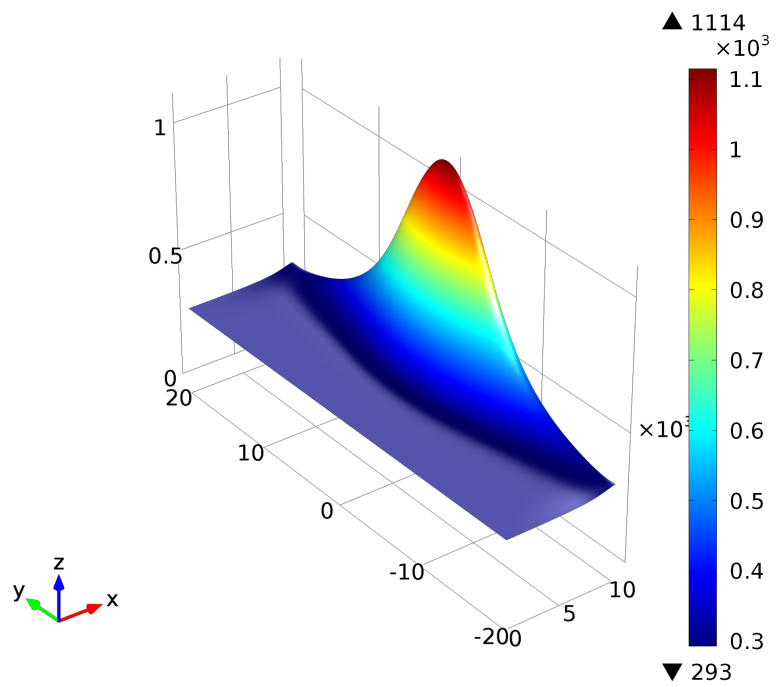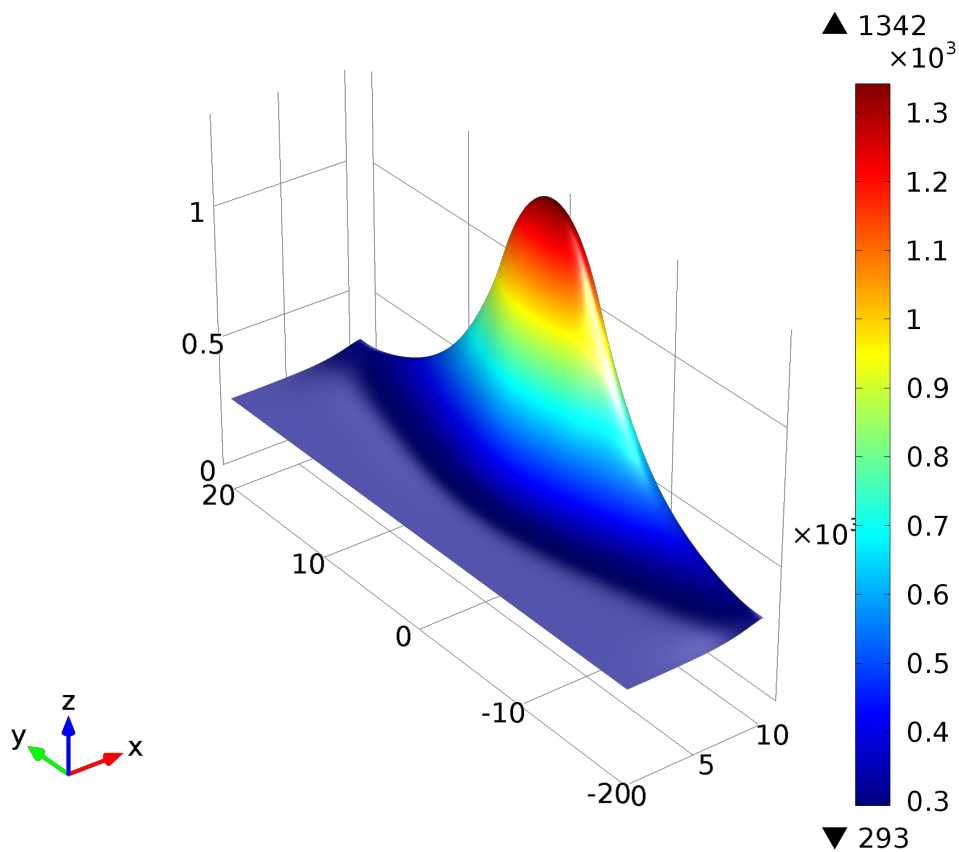**Figure 5.53:** Temperature distribution [K] computed at time 0.03 [s]

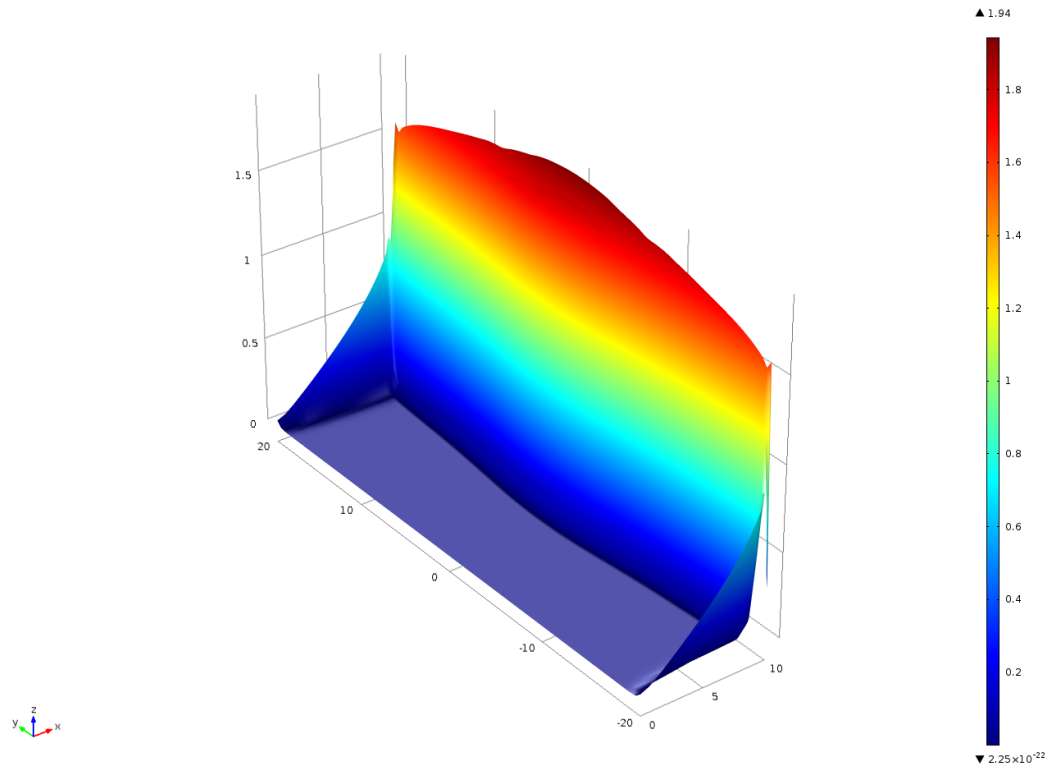**Figure 5.54:** Temperature distribution [K] computed at time 0.12 [s]

Figure 5.55: Temperature distribution [K] computed at time 0.2 [s]

A time domain solution makes possible to better undertand all these phenomena that occur during the process. For example it is interesting to view how electromagnetic wave penetrates in time through the workpiece. Saturation in fact tends to cut more high frequency than medium frequency. This means that if the core of the treatment is to more precisley control the heating profile, it is necessary to choose suitably the voltage supply, if the frequency is fixed. Induction hardening in SDF makes possible to play on the supplying power. In other words to play on heating sources, that have specific waveforms in time as seen in the second chapter.
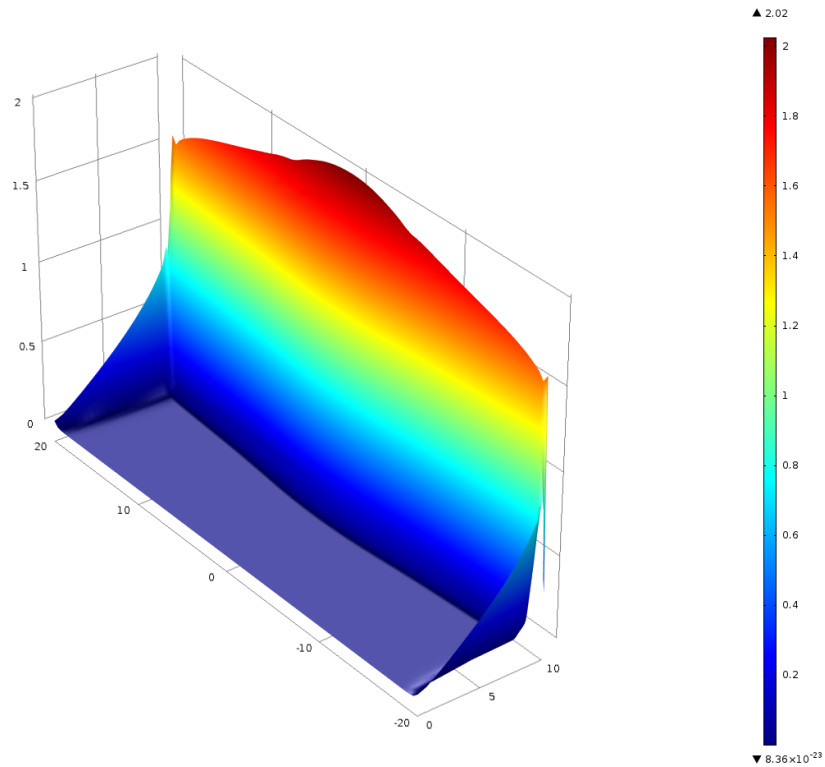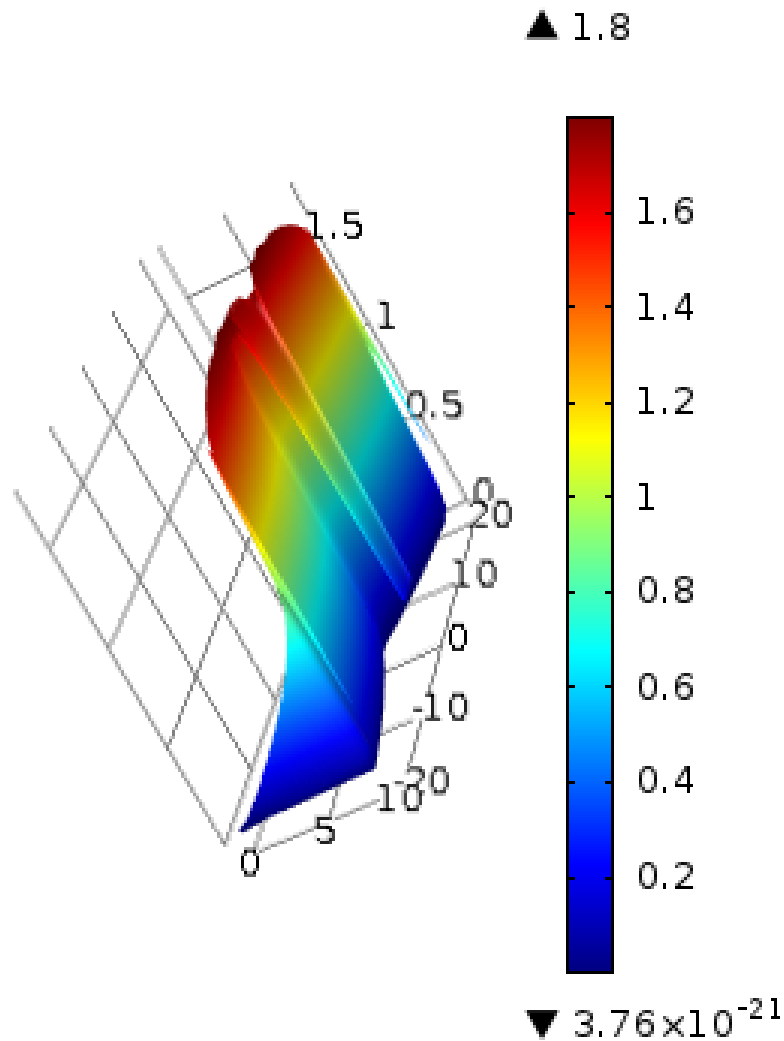
Figure 5.56: Avarage amplitude of magnetic flux **B** $[T]$ for initial temperature condition $\Delta t_{th} = [0]\ [ms]$.

In first time steps, in other words, from a thermal point of view when the temperature is not sufficient to to demagnetize the piece, the maximum values (for magnetic field and inudction field) are on the surface of the billet. When temperature is sufficient insted to change magnetic characteristics of steel, the distirbution of the magnetic flux changes. Avarage values of them shows that the maximum are not on the surface, but tend to penetrate the workpiece. It is possible view that also the induced powers and current densities change.

Figure 5.57: Avarage amplitude of magnetic flux **B** $[T]$ for temperature distribution at time $(\Delta t_{th} = [20]\ [ms])$.

Figure 5.57 shows a similar magnetic flux distribution as in the condition of uniform temperature, the distirbution of the avarage permeability, computefd in the electromagnetic period is extreamely similar as in condition of uniform temeprature distribution, it is interesting that the only phenomena that occur during this period are the reduction of the relative permeability for the effect of the saturation of magnetic field and the variation of the electrical conductivity for the increasing of the temperature in areas extreamely closed to the surface coupled with the inductor.
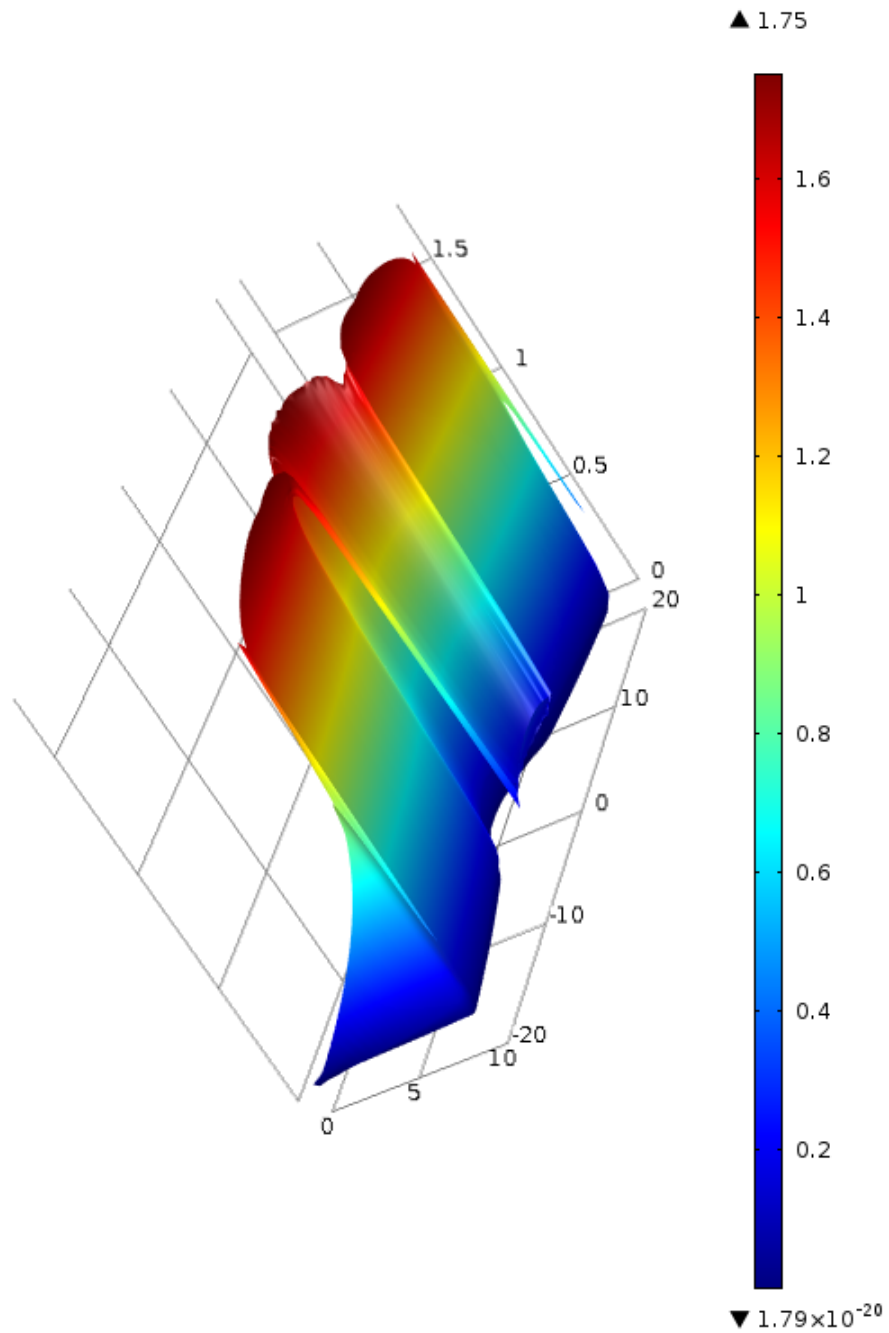
Figure 5.58: Avarage amplitude of magnetic flux **B** $[T]$ for temperature distribution at time $(\Delta t_{th} = [120] \ [ms])$.

The final temperature distribution sublines the reduction of the magnetic fields on the surface. it is evident that the magnetic field is much more intense towards the heart of the piece, than on the surface. It is possible to explain this phenomen if we consider the behaviour of current density. Indeed the curl of elecric field is strictly function of time derivative of magnetic flux. This means that it is possible write for example that:

$$\nabla \times \mathbf{E} = -\frac{\partial \mathbf{B}}{\partial t} = -\frac{\partial \mu(t)}{\partial t}\mathbf{H}(t) - \mu(t)\frac{\partial \mathbf{H}(t)}{\partial t} \tag{5.34}$$

and it is clear that temperature is extreamely important to undesrtand this phenomenon. Temperature tends to increase with time, this mean that the first term of this last equation tend to decrease with temperature. Instead areas towards the center are characterized by lower temperatures, this means that relative permeability is greater than on the surface of the billet. Then heating power density is greater in

greater depth. This phenomen become extreamley pronounced when temperature of a large area is over Curie's temperature θ_c [°C].

Figure 5.59: AVG distribution of amplitude of magnetic flux $norm\mathbf{B}$ $[T]$ computed for the temperature distribution at heating time $t_{hf} = 0.215$ $[s]$.
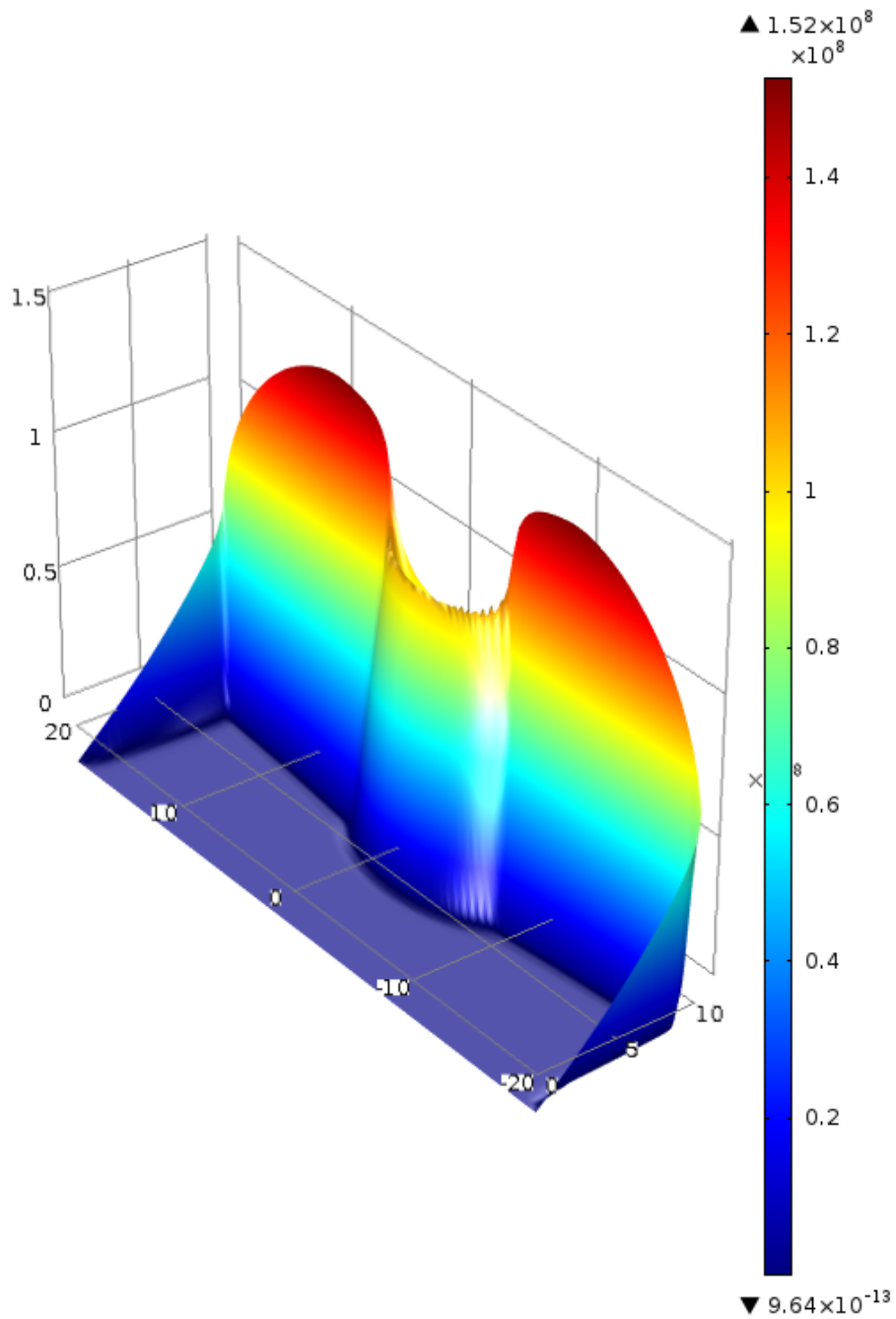
Figure 5.60: AVG distribution of amplitude of current density *norm***J** $[T]$ computed for the temperature distribution at heating time $t_{hf} = 0.215$ $[s]$.

To better understand the effect of saturation are plotted in the graphs of the main magnetic characteristics, in different periods with different temperature profiles. From these figures it is clear how magnetic saturation and temperature changes the distribution of the magnetic field inside the piece.

5.5   FEM Results

The resolution of the problem in the time domain electromagnetic also enables instant draw and plot trends that characterize the electrical power. In the chapter on electrical analysis, was carried out a simple and very general analytical explanation of electrical quantities through the resolution of a simple ideal model. It consists of an inductance and a resistance. The resolution of the FEM model allows you to query physical entities such as the induction coil and and derive the trends of their electrical parameters characterizing the power supply. It is clear that the software integrates the current density obtained on the section of the inductor with the FE approach, and so obtain the total current consumption for each time step. It may be noted that the trends obtained the power and current are in complete agreement with those obtained by the resolution of the related simplified model. This means that the model is correct and the model solution is valid. Comsol also allows also through postprocessing, to analyze the wave forms for example in the frequency domain. This tool is extreamely useful for this work because is possible to have a look of what are the main components of the power and the current. From the results it is clear that the voltage has only iwo frequency components. One evolves in time with the medium frequency $f_{mf} = 10 \ [kHz]$ and one evolves in time with the high frequency $f_{mf} = 100 \ [kHz]$. The current instead, although has two fundamental frequencies, always equal to the first two (10 [kHz] and 100 [kHz]) also shows different frequencies, respectively at frequencies intermediate between the two and further. This is phenomenon is the effect of the saturation. Indeed the saturation field of the magnetic field would result in a change in the value of the inductance from instant to instant and consequently causes the appearance of components at different frequencies. Compleately different however is the behaviour of the istantaneous power and its harmonic content. From the plots it is possible see well the four frequency components introduced in the section of the electrical model of the problem, plus the DC content. In this chapter we are plotted different harmonic contents for different temperature profiles . It is important to remember that during the process, due to the change of the electromagnetic parameters, the value of the power and current consumption in the period varies in a highly non- linear with the process time.

From the electrical point of view it is interesting, as already introduced at the beginning of the chapter, analyzing the variation in the thermal time of electrical quantities . Since for each period of electromagnetic simulation of the temperature distribution of the billet is assumed constant, it is possible to analyze, at least qualitatively, the effects which the temperature has on waveforms of the electromagnetic phenomenon. The model is developed to set voltage from an external source unchanging over time . This means that the waveform of the voltage (in any case variable during the period electromagnetic) does not vary with the tempetura . In other words, the waveform of the voltage is always the same for each step heat . As already seen instead current and power are strongly affected by temperature. Upon variation of this fact on the one hand, the resistivity increases in a linear fashion , of the other instead the relative permeability follows a trend strongly non-linear, making it very difficult to electromagnetic coupling. In Figure 5.61 are plotted three different behaviour of current for three different temperature distributions, respectively at the beginning of the process, when the temperature is uniform inside

the billet and two different temperature conditions (in the period [0.1-0.105] [s] and in the period [0.195-0.22] [s]). These two curves show as the average temperature of the surface electromagnetically coupled with the inductor plays the key role. In fact, although the resistivity is increased (which causes the collapse of the RMS value of the current) the value of the equivalent permeability feels mostly at greater heating time because the average temperature of the coupled surface is much higher than the temperature at which it begins to collapse the relative permeability, or in other words $\theta > 650$ [C].
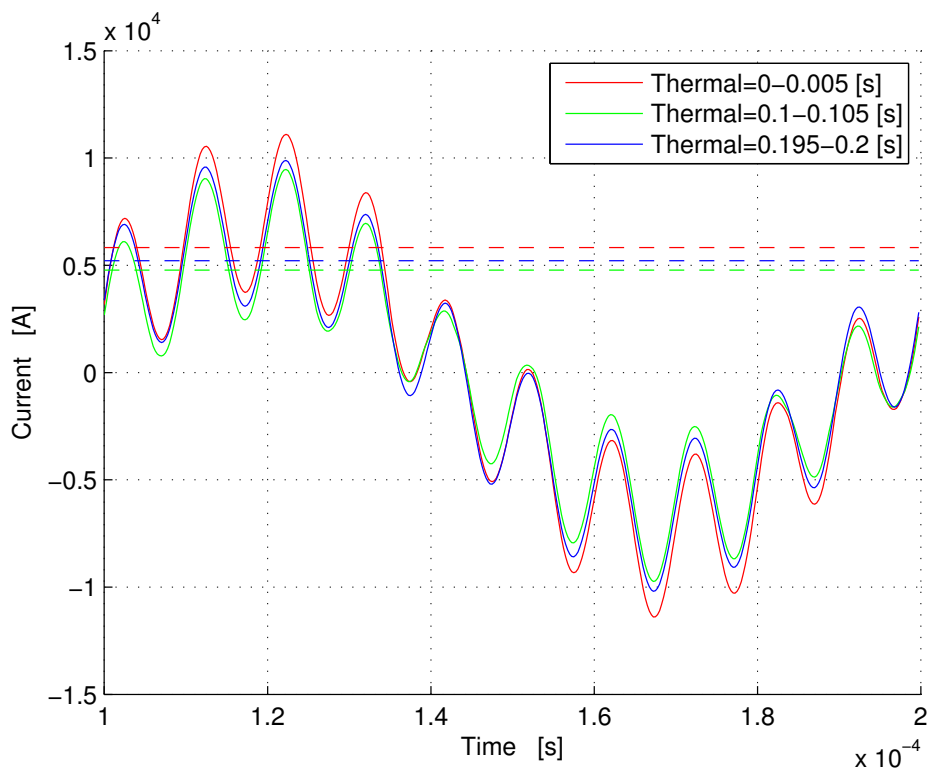
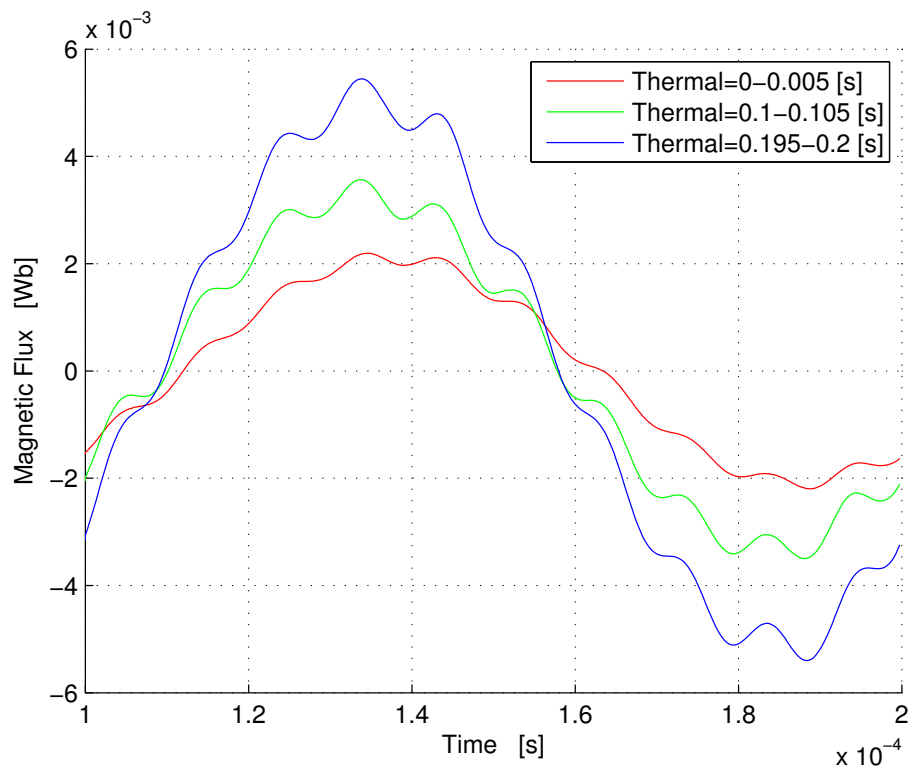**Figure 5.61:** Current evolution in several electromagnetic periods.
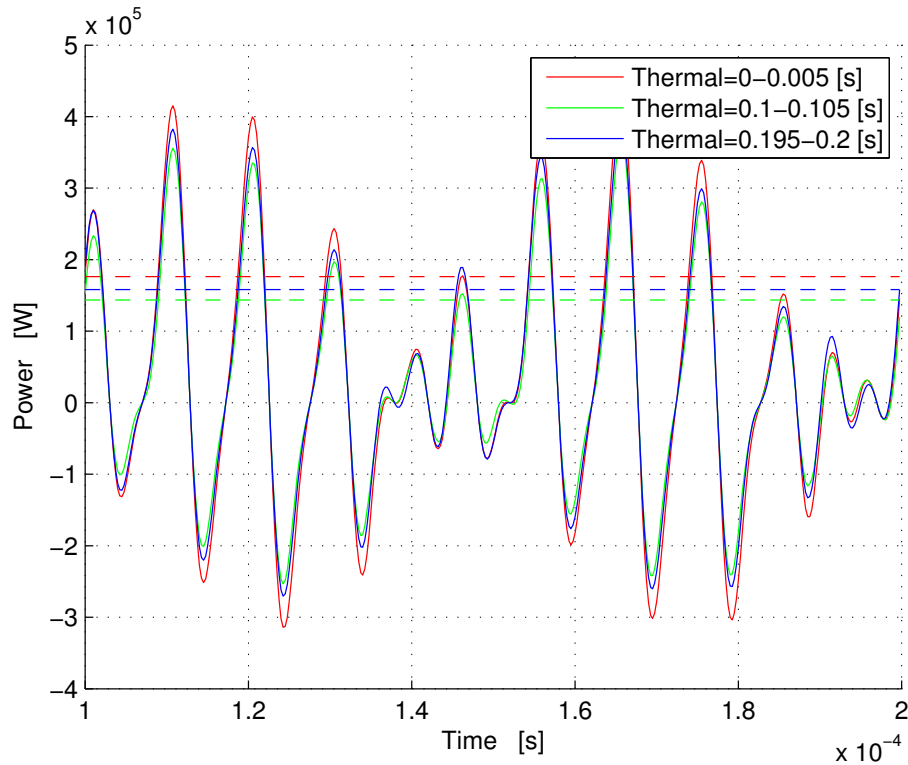
Figure 5.62: Power evolution in several electromagnetic periods.

The same approach can be done for the magnetic flux. Recalling that the latter can be made with high quality from the magnetic vector potential (in the model developed, remember to be a scalar quantity).

$$\Phi_{bill} = A_\varphi \cdot 2\pi r \tag{5.35}$$

where r is the geometrical coordinate. As seen previously , you can plot different values of magnetic flux obtained for different temperature profiles . In this case you see with the magnetic flux tends to increase with temperature. This phenomenon can be explained precisely with the temperature . In fact, the equipotential lines tend to penetrate toward the workpiece , this provoke an increase of the magnetic flux as more and more surface is affected by the magnetic flux. Figure 5.63 shows this behaviour.

Figure 5.63: Magnetic flux evolution in several electromagnetic periods, characterized by different temperature distributions.

Finally here are plotted the Fourier's distribution for several temperature distributions. It is possible to understand that the harmonic spectrum of power is qualitatively similar to one defined in the Chapter 2.
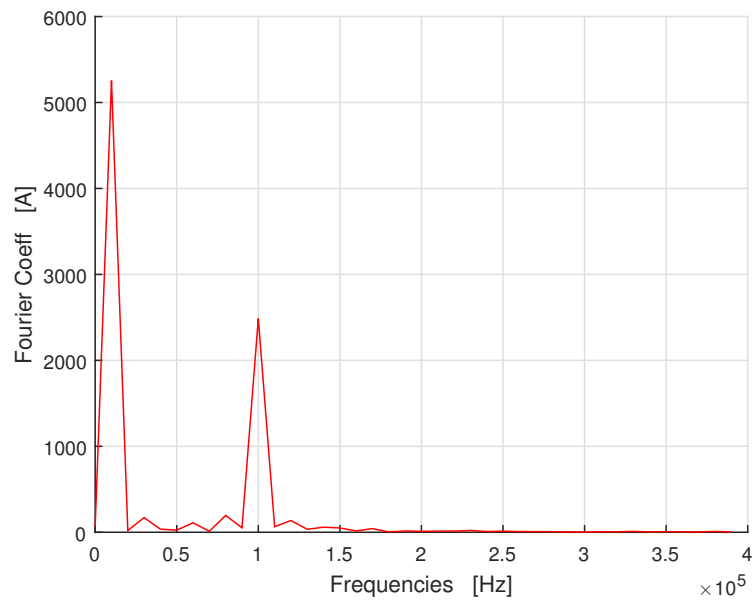
Figure 5.64: Current harmonic spectrum for the initiial temperature distribution.
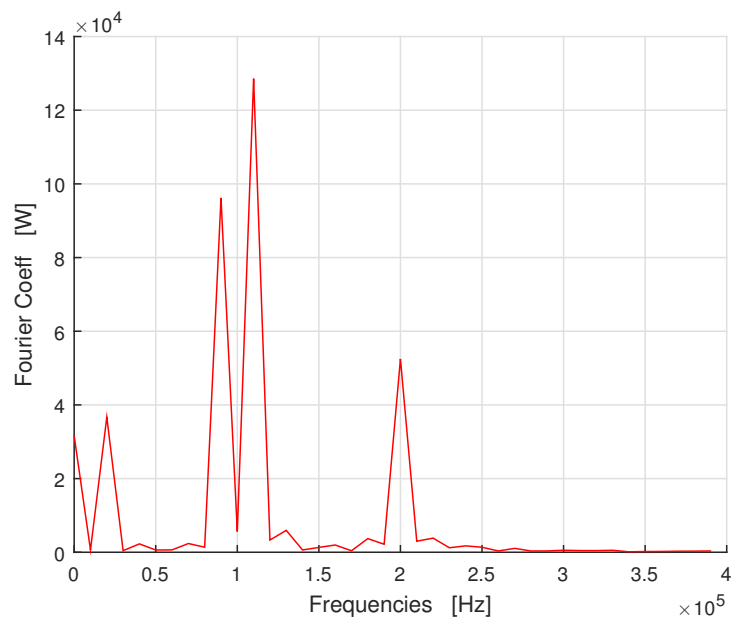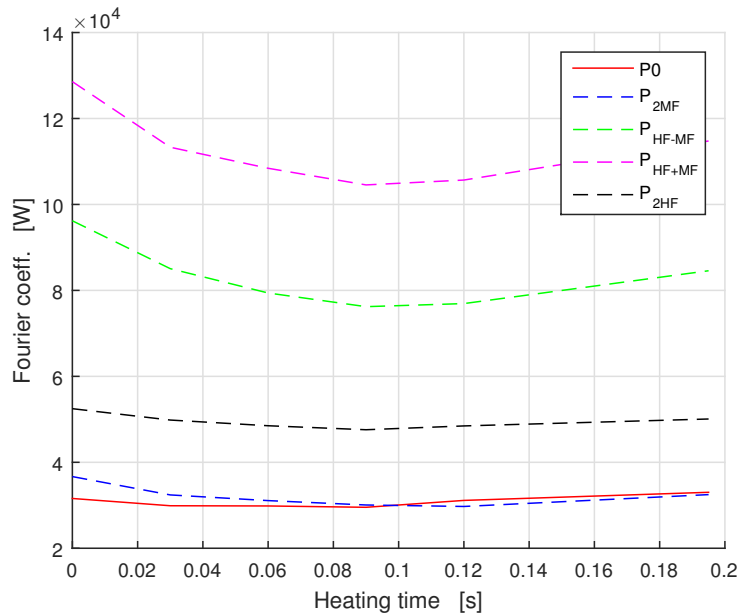

Figure 5.65: Power harmonic spectrum for the initiial temperature distribution.
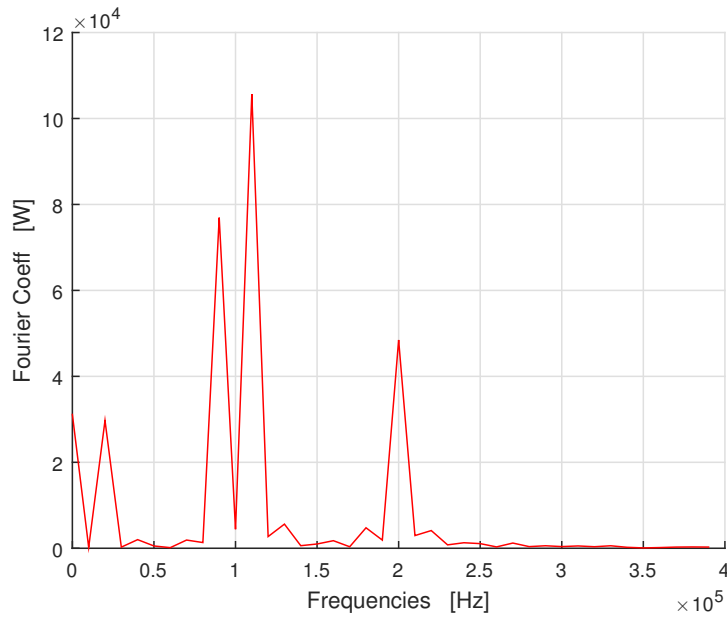
Figure 5.66: Power harmonic spectrum for temperature distribution at time $t_{th} = 0.12 \ [s]$.

Finally it is plotted the evolution of harmonic spectrum components (current and power) as function of heating time. It is clear that they aren't constant during the process, but they vary in accord with what already said in the second chapter.

Figure 5.67: Evolution of power harmonic spectrum with the heating time $[0 - 0.2] \ [s]$.
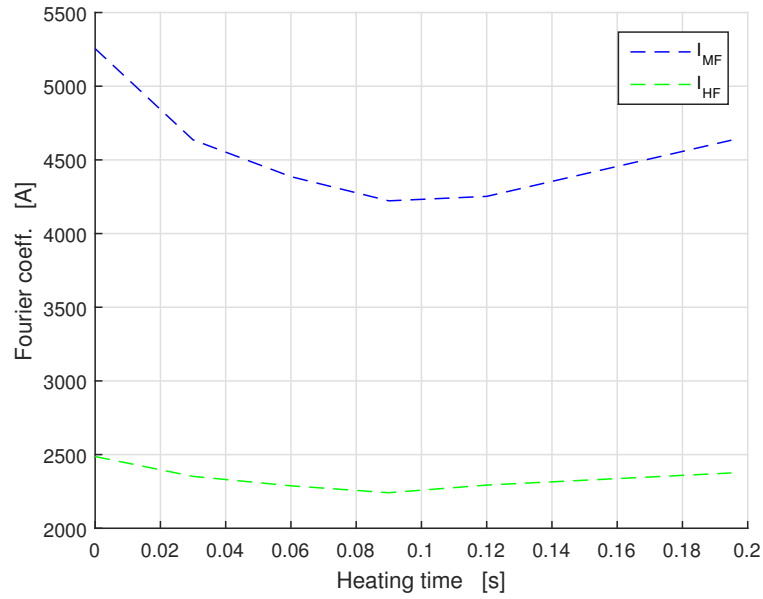
Figure 5.68: Evolution of current harmonic spectrum with the heating time $[0 - 0.2]$ $[s]$.
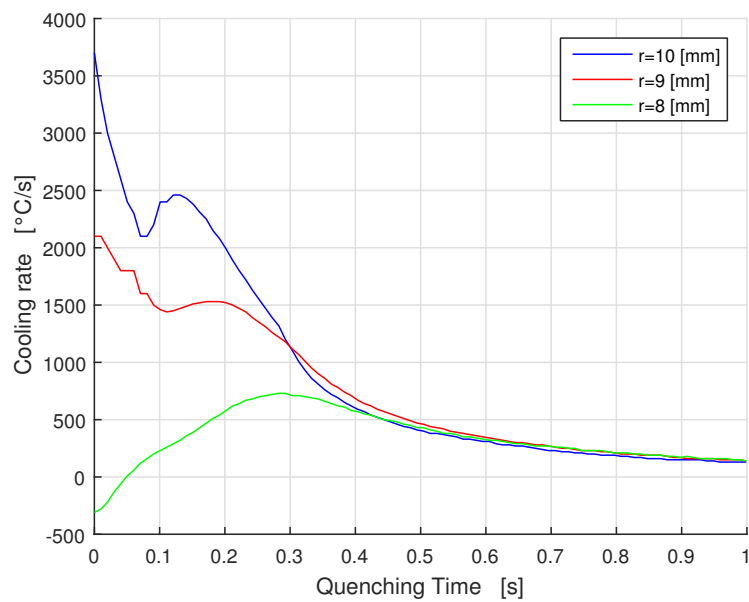
5.6   Quenching phase

The last process phase is the quenching of the billet. As desctribed in chapter 4 the quenching is the process in which the austenite transforms to martensite. This is done with a fast cooling. Here are presented the results for a specific HEC behaviour (Chapter Model), that takes into account of the main thermal phenomena, such as the changig of the coefficients α during the process. For this steel the quenching starts when the temperature of a region with a thickness of 1 [mm] is over the temperature $A_{c3} = 911$ $[C]$. In the same way it is possible to change this value for every kind of steel. Figure 5.69 shows the hardened thickness that can be obtained with the process and the evolution in time of temperature inside the billet in several points. The quenching is computed also with a time-dependet solver in the time range $[0 - 1]$ $[s]$, this because tipicallyt also this phase of the treatment is fast, indeed it needs only 1 [s] to fully cool down the desired thickness. Figure 5.70 is extreamely important in this process because the cooling rate must respect specific values to fully transform austenite to martensite.
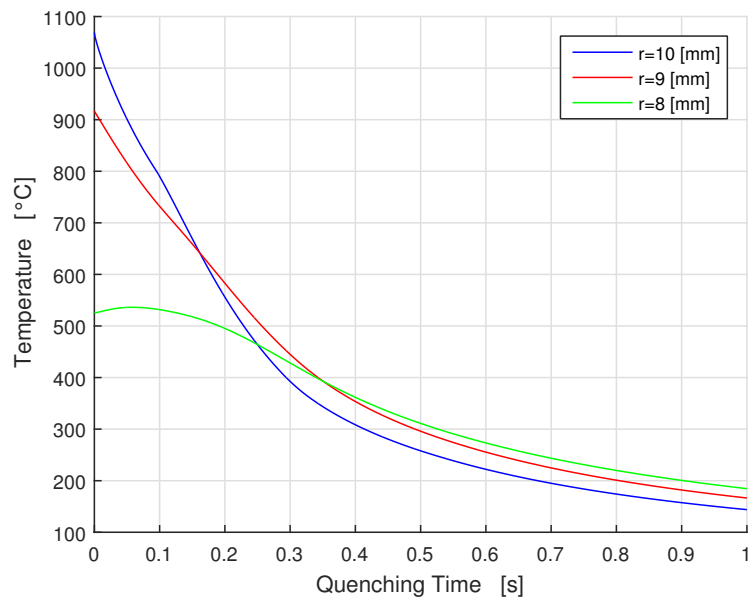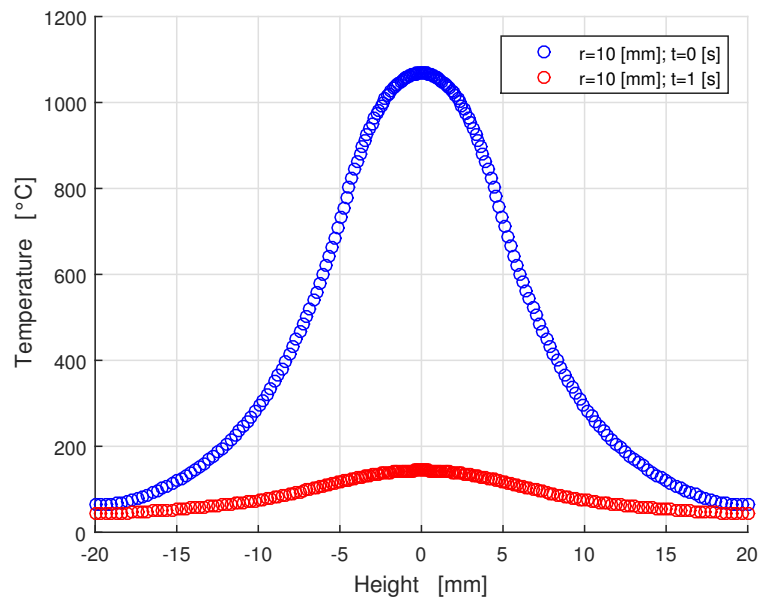
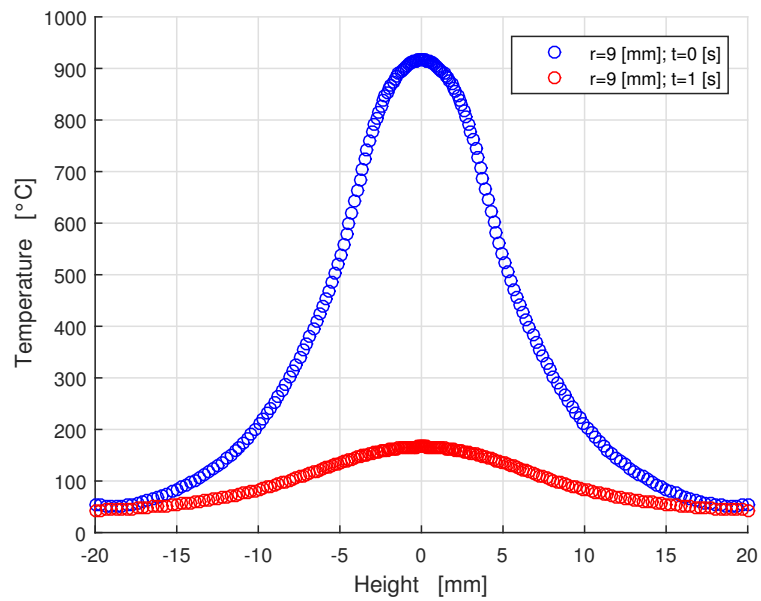**Figure 5.69:** Behaviour of temperature for several points during the quenching phase.

Figure 5.70: Behaviour of cooling rate for several points during the quenching phase.

Figure 5.71: Temperature distribution before and after the quenching for a cutline with $r = 10 \ [mm]$

Figure 5.72: Temperature distribution before and after the quenching for a cutline with $r = 9 \ [mm]$

Bibliography

[1] Barglik, Jerzy, Smalcerz, Albert, Przylucki, Roman, Dolezel, Ivo, "3D modeling of induction hardening of gear wheels", *Journal of Computational and Applied Mathematics. 270 (2014) pp. 231-240*

[2] Candeo, Alessandro, Ducassy, Christophe, Bocher, Philippe, Dugiero, Fabrizio, "Multiphysics Modeling of Induction Hardening of Ring Gears fro the Aerospace Industry", *IEEE Transactions on Magnetics. 47(5) (May 2011)*

[3] Homberg, Dietmar, "A mathematical model for induction hardening including mechanical effects", *Nonlinear Analysis: Real World Applications. 5 (2004) pp. 55-90*

[4] Homberg, Dietmar, Petzold, Thomas, Rocca, Elisabetta, "Analysis and simulations of multifrequency induction hardening", *Nonlinear Analysis: Real World Applications. 22 (2015) pp. 84-97*

[5] Homberg, Dietmar, Fuhrmann, J., "Numerical simulation of the surface hardening of steel", *Omternat J. Numer. Methods Heat Fluid Flow 9 (1999) pp 705-724*

[6] Cajner, F., Smoljan, B., Landek, D., "Computer simulation of induction hardening", *Journal of Materials Processing Technology 157-158 (2004) pp. 55-60*

[7] Karban, P., Donatova, M., "Continual induction hardening of steel bodies", *Mathematics and Computers in Simulation 80 (2010) pp. 1771-1782*

[8] Rodriguez, A. A., "Fortmulation via vector potentials of eddy current problems with voltage or current excitation", *Communications in Applied and Industrial Mathematics*

[9] Bermudez, A., Rodriguez, R., Salgado, P., "Numerical solution ef eddy current problems in bounded domains using realistic boundary conditions", *Comput. Methods Appl. Mech. Engrg. 194 (1996) pp. 159-178*

[10] Rodriguez, A. A., Valli, A., "Eddy Current Approximation of Maxwell Equations", *Modeling, Simulation and Applications. 4 (2010)*

[11] Sackl, S., Leitner, H., Zuber, M., Clemens, H., Primig, S., "Induction Hardening vs Conventional Hardening of Heat Treatable Steel", *Metallurgical and Materials Transactions A. 45 A (Nov. 2014) pp.5657-5666*

[12] Schwenk, Maximilian "Numerische modellierung der induktiven ein-und zweifre-quenzrandschichthartung", *Schrriftenreihe des instituts fur angewandte materi-alien, Band 10, KIT, 2012*

[13] Brooks, Charlie R "Principles of the austenization of steels", *London, Elsevire Applied Science, 1992 - ISBN 1-85166-770-9*

[14] Barglik, Jerzy, Dolezel, Ivo, Karban, Pavel, Ulrych, Bohus "Modelling of continual induction hardening in quasi-coupled formulation", *The international journal for computation and mathematics in electrical and electronic engineering 24 (2005) pp. 251-260*

[15] Matsui, Katsuyuki, Hata, Hiroyuki, Kadogawa, Hideyuki, Yoshiyuki, Koji "Research on practical application of dual frequency induction hardening to gears", *JSAE Review 19 (1998) pp. 351-371*

[16] Petzold, Thomas "Modelling, Analysis and Simulation of Multifrequency Induc-tion Hardening", *Von der Fakultat II - Mathematik und Naturwissenschaften der Technischen Universitat Berlin zur Erlangung des akademischen Grades Doktor der Naturwissenschaften (Dr. rer. nat.), Epubli, Berlin, 2014 - ISBN 978-3-7375-0087-6*

[17] Lupi, Sergio "Appunti di Elettrotermia", *Università degli studi di Padova (2005)*

[18] Cibaldi, Cesare "I criteri di scelta e di trattamento degli acciai da costruzione e da utensili. Vol. 1", *(2012) AQM*

[19] Davies, E.J. "Conduction and induction heating", *IEE Power engineering series 11 (1990) Peter Peregrinus - ISBN 0 86341 174 6*